Physicochemical Properties of Protein Inclusion Bodies

by

Norbertus Djajasantosa Wangsa-Wirawan

Thesis submitted to the degree of
Doctor of Philosophy

in

The University of Adelaide
Department of Chemical Engineering
Faculty of Engineering

December 1999

This work contains no material which has been accepted for the award of any other degree or diploma in any university or any other tertiary institution, and to the best of my knowledge and believe, contains no material previously published or written by another person, except where due reference has been made in the text.

I give consent to this copy of my thesis, when deposited in the University Library, being available for photocopying and loan.

SIGNED : _____ DATE : 17 December 1999

ACKNOWLEDGEMENTS

I would like to thank several individuals and organisations for their contribution to this thesis. First of all, my sincere appreciation for the provision of financial support in the form scholarships from the Department of Employment, Education, Training and Youth Affairs, the University of Adelaide and the Cooperative Research Centre for Tissue Growth and Repair. Additional financial support in the form of Travel Grants from the University of Adelaide Alumni Association, the University of Adelaide, and the Cooperative Research Centre for Tissue Growth and Repair are also greatly acknowledged.

My supervisors Dr. Brian O'Neill and Dr. Anton Middelberg deserve significant recognition for their guidance and inspiration. I would like to especially thank Dr. Brian O'Neill for his continuing support and encouragement in the final stages of this work and invaluable editorial assistance of this thesis. I also would like to thank Prof. Atsushi Ikai at the Tokyo Institute of Technology, Japan for providing Atomic Force Microscope and offering guidance and assistance during my stay at his laboratory.

The electrophoretic mobility study was performed within several laboratories which I am indebted to Dr. David Chittleborough and Ala Baklan of the Soil Science Department for providing equipment and technical assistance, and Dr. Brian Saunders of the Chemistry Department for his valuable discussion. My great appreciation to CEMMSA staff, particularly John Terlet for his assistance in the early stage of Atomic Force Microscopy study and Lyn Waterhouse for her guidance in the Scanning Electron Microscopy imaging. I also thank the Department of Microbiology for sharing their facilities.

I sincerely appreciate Chris Mansell and the Chemical Engineering Workshop team for their technical assistance and Mary Barrow, Elaine Minerds and Lynette Kelly for their secretarial support. My special thanks to Lynette Kelly for her editorial help and forwarding correspondence during my stay in Japan. My gratitude go toward the staff

and colleagues in the Department of Chemical Engineering for providing a pleasant environment and their friendship during the course of my study.

I would like to thank my friends who have helped to make Adelaide feel like home, particularly my house-mates Graham Thompson and Peter Harland. Thank you for your friendship and support. For Peter, may you rest in peace. My sincere appreciation to Yutaka Kido for his support and help, particularly in compiling my thesis. My deep appreciation also, to several individuals in Prof Ikai's laboratory, in particular Wang Tong, I thank you for your help and for welcoming me to your group.

At last, my family have always been my inspiration. I am grateful for their continuing support, love and encouragement, particularly my mother and sisters, Joana and Fransisca.

For my beloved mother

SUMMARY

An insulin-like growth factor 1 analog, termed LR^3-IGF-1 is normally obtained as a solid inclusion body when expressed at high level in recombinant *E. coli*. It is produced using fed-batch fermentation using a conventional feeding strategy then harvesting by centrifugation following homogenisation. The demand for this protein is expected to increase to satisfy the cell culture market. Clearly, improvements in the current production system and the downstream processing sequence are essential to maintain a competitive advantage in the market place. This work is focussed on achieving such improvements. First, optimisation of fermentation was considered to improve production yield and then flotation is considered as a possible inclusion body recovery method.

The production of inclusion bodies is currently performed using fed-batch fermentation using a constant rate feeding. This conventional feeding mode causes excessive accumulation of glucose and acetate which limit higher production yields. A novel 3-stage feeding strategy is proposed to overcome these limitations. A significant decrease of glucose and acetate accumulation has been achieved using the proposed feeding strategy. It doubles the final recombinant protein concentration.

As a precursor to considering flotation for inclusion bodies recovery, the physicochemical properties of the inclusion bodies have been measured. Despite the importance of such properties, they are not readily available in the literature. Therefore, physicochemical properties, such as electrophoretic mobility, particle characteristics, and the interactions forces between inclusion bodies and an air bubble, have been studied using a variety of methods including micro-electrophoresis, sodium dodecyl sulphate polyacrylamide gel electrophoresis (SDS-PAGE), scanning electron microscopy (SEM) and atomic force microscopy (AFM).

The electrophoretic measurement provides a map of net surface charge of the inclusion bodies and cell debris. Both cations and anions affect the electrophoretic

mobility of the inclusion bodies and the cell debris but as expected divalent ions produce more profound effects. The isoelectric point of cell debris is significantly lower than that for the inclusion bodies. This suggests that they may be separated by flotation techniques. As well, experimental work on electrophoretic mobility indicates that the isoelectric point (electrophoretic mobility) provides a qualitative measure of inclusion body purity, as the isoelectric point increased for cleaner inclusion bodies.

Particle characterisation using scanning electron microscopy and atomic force microscopy has shown that inclusion bodies posses an irregular shape and a rough surface, and have a mean particle size of 0.3 microns. This small particle size suggests either dissolved-air flotation or electroflotation as potential method for fractionation as both provide fine air bubbles. Agglomeration of the particles to increase particle size prior to flotation needs to be encouraged.

Interactions between the inclusion bodies and an air bubble dictate the elementary process of bubble-particle attachment. The interaction forces are evaluated using atomic force microscope (AFM) at various conditions, in particular at differing pH and solution concentrations. Variation in the interaction forces measured under various conditions indicates that electrostatic and hydrophobic forces provide significant contributions to the bubble-particle attachment process. This study provides fundamental information for rational design of a flotation recovery system. The atomic force microscope has been shown to be a reliable tool for measurement of interaction forces and has great potential for use in biotechnological research.

Dissolved-air flotation (DAF) is considered as a potential fractionation method for inclusion body recovery. A DAF mathematical model has been derived and proposed for inclusion body recovery. Physicochemical characteristics of inclusion bodies have been taken into account in the development of this model. This may provide an impetus for the application of DAF in biotechnology as a possible fractionation tool.

TABLE OF CONTENTS

LIST OF FIGURES

LIST OF TABLES

Chapter 1

INTRODUCTION

Advances in recombinant DNA technology have provided us with numerous high value biological materials (eg. proteins) normally expressed in foreign hosts, for example *Escherichia coli*. Numerous recombinant proteins have been produced and accumulated intracellularly as insoluble protein aggregates known as inclusion bodies. Increasing demand for biologically active proteins has forced biotechnology industries to scale up protein production. In these processes, a clear goal is to minimise the overall production cost to provide inexpensive products which are attractive in the market place. As a consequence, efficient large scale production system and downstream processing sequences are required. Physicochemical properties may potentially be exploited to improve separation/purification methods or to develop new techniques. Unfortunately, such properties of inclusion bodies are seldom available. Hence, a key aim of this thesis is to study the physicochemical properties of inclusion bodies with a view to improve production system using fed-batch fermentation.

1.1 BACKGROUND

Recombinant proteins expressed at high level in *E. coli* are normally accumulated within cells as an insoluble particulate known as an inclusion body. Production of protein inclusion bodies, for example insulin-like growth factors (IGFs), using recombinant *E. coli* can be split into two main streams, namely upstream processing (including fermentation) and downstream processing. In the upstream processing, natural *E. coli* is genetically manipulated to express foreign proteins and/or to increase the level of protein expression. The recombinant *E. coli* produced is first evaluated to examine the efficiency of the recombination process, using measures such as its stability and the level of protein expression. During fermentation, the recombinant *E. coli* grows and protein inclusion bodies are produced following the addition of an inducer. Inclusion bodies are accumulated inside the cells as granules with a diameter in the size range from a submicron particle to few microns. Clearly, the first step in the downstream processing sequence is cell breakage. The most common method in a large scale operation is high pressure homogenisation. A suspension of inclusion bodies, cell debris, and other contaminants (such as DNA, RNA, and fermentation substrate) is obtained following homogenisation.

The next step in the process is recovery of protein inclusion bodies from suspension or contaminants using a variety of solid-liquid separation methods. Centrifugation, filtration (microfiltration and ultrafiltration), precipitation, and flocculation are the current methods available. Filtration is often ineffective for this purpose as clogging of the filtration medium often occurs. This method also results in poor separation of inclusion bodies from cell debris due to their similarity in size. Additives are required for precipitation and flocculation. These compounds may create problems for subsequent purification steps. Furthermore, the additives themselves may cause contamination (eg. in a product intended for human therapeutic purposes). At present, centrifugation is the most commonly used method. It is effective and it provides excellent separation. However, centrifugation is highly capital intensive.

Recovery and purification of recombinant products are normally the most expensive steps in the whole production process of biological materials in modern biotechnology industries. These steps typically account for 50-80% of the total production cost (Gupta and Mattiasson, 1994). The higher the required product purity the higher the cost of downstream processing steps. Hence, it is essential to find effective separation methods which provide effective separation, high yield and low cost. This can reduce the total production cost significantly.

Flotation provides a possible alternative recovery process for protein inclusion bodies. It is a simple and economic solid-liquid separation method. Flotation has been widely used in mineral processing, and waste and water treatment industries for decades. However, flotation is seldom applied to protein separation. This method exploits physicochemical properties of particle surfaces, such as hydrophobicity. Unfortunately, such properties of inclusion bodies are poorly characterised in the literature.

This thesis proposes a study of the physicochemical characteristics of protein inclusion bodies and attempts to improve their production using fed-batch fermentation. Physicochemical properties including electrophoretic mobility, particle characteristics and interaction forces between the inclusion body and an air bubble were studied using a variety of methods, such as scanning electron microscopy (SEM), electrophoresis and atomic force microscopy (AFM). This physicochemical study is expected to provide a fundamental basis for rational design of inclusion body recovery by flotation. A new feeding system for fed-batch fermentation is also proposed to improve production yield.

1.2 PROTEIN INCLUSION BODY

1.2.1 Formation of Inclusion Bodies

Many eukaryotic polypeptides have been successfully expressed in genetically engineered *E. coli*. Generally, these proteins are highly expressed compared to their native sources. However, these are normally produced in an inactive form as an insoluble aggregate known as an inclusion body (Figure 1.1). Inclusion bodies can be located in either the cytoplasm or the periplasmic space, depending on the mode of gene expressions (Marston, 1986). The inactivity of these proteins implies that additional steps are required in downstream processing. Solubilization and refolding are required to produce the proteins in their active form. These steps incur a necessary additional production cost. However, expression of proteins as inclusion bodies is also advantageous. Expression of small proteins as inclusion bodies (for example insulin) is beneficial as the inclusion bodies are more resistant to the intracellular proteolytic degradation than soluble proteins (Kane and Hartley, 1991; Wei and Tang, 1995). In some cases, production of proteins as inclusion bodies favours recovery and purification processes. The inclusion bodies are produced in a relatively pure state and a highly concentrated form following disruption and centrifugation (Kane and Hartley, 1991). The product in the inclusion bodies can exceed fifty percent of the total fusion protein (Kane and Hartley, 1991). For example, in our expression system, the insulin-like growth factor 1 analog (LR^3-IGF-1) produced as inclusion bodies constitutes 85 % of the total fusion proteins (inclusion bodies).

Recombinant proteins can be expressed in either of two modes, i.e. fusion and direct modes. In the fusion mode, the eukaryotic protein gene is incorporated with a bacterial protein gene to form a fused protein with improved expression levels (Marston, 1986). The fusion mode is applied especially for small polypeptides since these polypeptides are recognised as foreign proteins and are degraded rapidly following formation (Wetzel & Goeddel, 1983). In the direct mode, the protein gene is cloned into a bacterial cell and recombinant proteins are produced as insoluble

aggregates. The main disadvantage of this mode is the difficulty in releasing of the product from aggregates into stable, active and soluble forms (Marston, 1986).

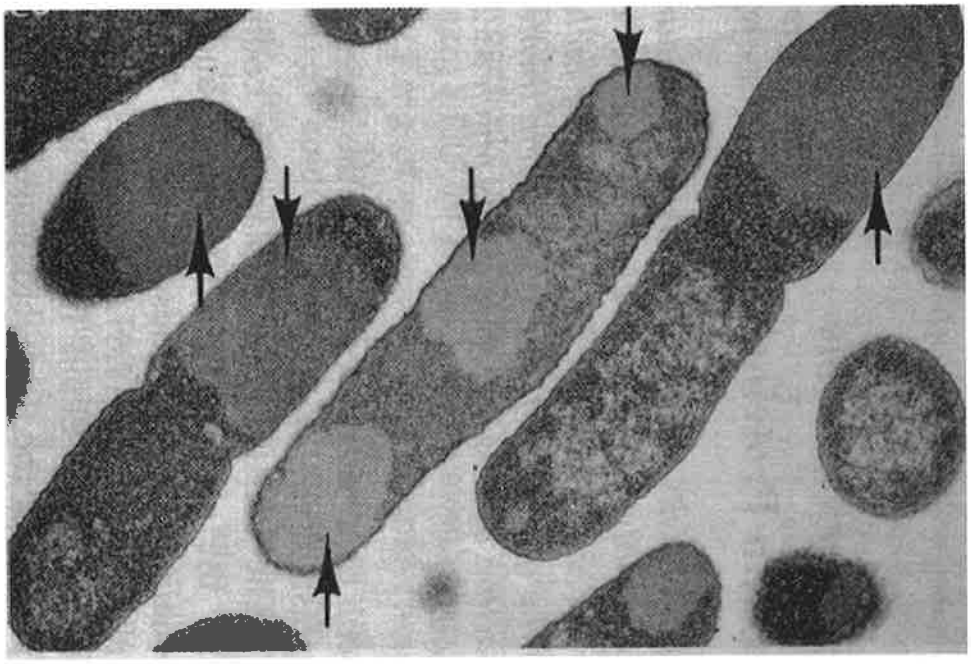

Figure 1.1 Recombinant *E. coli* producing β-gal-insulin A chain chimeric protein as inclusion bodies, shown by arrows (after Williams *et al.* 1982).

1.2.2 Properties and Structure of Inclusion Bodies

Inclusion bodies produced in the periplasmic space are amorphous, whereas those produced in the cytoplasm are highly regular (Bowden *et al.*, 1991). For example, the inclusion bodies of β-lactamase located in the cytoplasm are highly regular and cylindrical in shape, with an average length of 1.5 μm (Bowden *et al.*, 1991). Highly irregular shapes have also been found in inclusion bodies of human growth hormone (hGH) and in the β-subunit of human chorionic gonadotropin (βhCG) hormone (Mukhopadhyay, 1997). The size range of inclusion bodies ranges from submicrons to a few microns and differs from one inclusion body to others. For example, γ-interferon and prochymosin have a particle diameter of 0.81 μm ± 0.17 μm, and 1.28

μm ± 0.46 μm, respectively (Taylor *et al.*, 1986). Therefore, the size and shape of inclusion body particles could vary over a wide range (Mukhopadhyay, 1997). Bowden *et al.* (1991) suggested that the polypeptide sequence and cellular factors determine the size of the inclusion bodies. However, there was no further evidence to confirm this suggestion and this issue remains unclear. Furthermore, the density of inclusion bodies varies depending on the structure of inclusion bodies, for example amorphous or crystalline structures.

The composition of inclusion bodies is affected by various factors including cellular location (Bowden *et al.*, 1991) and both the expression mode and the growth condition (Valax & Georgiou, 1993). Inclusion bodies consist of the recombinant protein and contaminants, such as other proteins (for example membrane proteins), plasmid encoded proteins, phospolipids, polysaccharides, and nucleic acids (Kane and Hartley, 1991). The mechanism of contaminant incorporation into the inclusion body aggregates is poorly understood. It has been argued that contaminants attach to the various surfaces of aggregate particles by a variety of attractive forces, eg. ionic and hydrophobic interactions (Kane and Hartley, 1991). Another suggestion is that contaminants are entrapped when the over-expressed proteins aggregate (Paul *et al.*, 1983). Some contaminants can be removed easily by washing inclusion bodies using a detergent solution (Kane and Hartley, 1991). However, other contaminants are tightly incorporated with the aggregates and cannot be removed by a simple detergent wash.

1.2.3 Purification of Inclusion Bodies

The first step for inclusion body purification is cell disruption to release protein aggregates from the cells. This is normally performed by a high pressure homogeniser, especially for large-scale operations. The next step is recovery of the inclusion bodies from homogenised fermentation broth using some forms of solid-liquid separation, such as filtration and centrifugation. For example, cross-flow filtration has been used for extraction of rIL-2 inclusion bodies from *E. coli* (Meagher

et al., 1994). Centrifugation is the most commonly employed method at commercial scales. Other alternative methods have been developed to recover inclusion bodies, for example aqueous two-phase extraction system for direct recovery of inclusion bodies (Walker and Lyddiatt, 1996) and *in-situ* dissolution of inclusion bodies using chemical treatment (Hart *et al.*, 1994; Falconer *et al.*, 1996).

Further washing treatment may be conducted as the recovered inclusion bodies still contain contaminants. Solubilization (dissolution) is then performed to totally unfold protein inclusion bodies using chaotropic reagents, such as urea and guanidine HCl. The next step in a typical process sequence is refolding of the single protein into its native conformation thereby forming active proteins followed by purification of active proteins from existing contaminants. The final step is a further purification and/or a concentration to achieve the required product purity. These are usually performed using multi-step of chromatographic techniques.

1.2.4 Insulin-like Growth Factors

There are two types of Insulin-like growth factors (IGFs): IGF-1 and IGF-2. Both IGF-1 and IGF-2 are single-chain polypeptides (Humbel, 1990). The IGF-1 consists of 70 amino acid residues and the IGF-2 consists of 67 amino acid residues (Humbel, 1990; Van den Brande, 1992). These IGFs are present in blood plasma at a concentration of 20 - 80 nM and in most tissue of the body at a lower concentration (Humbel, 1990). So far, the IGFs of six species (human, bovine, porcine, ovine, rat, and mouse) have been extensively studied (Humbel, 1990).

Human insulin-like growth factors have been successfully cloned and expressed in *Escherichia coli*. Recombinant IGF-1 expressed in *E. coli* as fusion proteins have been successfully produced on a large scale with yield approximately 5 mg/L fermentation broth (King *et al.*, 1992). This is significantly higher than expression using mammalian cell system which is limited to 25 μg/L of condition medium processed (King *et al.*, 1992). Chicken IGF-1 (cIGF-1) has also been cloned and

expressed as fusion proteins in *E. coli* (Upton *et al.*, 1992). Production of this recombinant cIGF-1 has shown to be more efficient than direct extraction from serum.

Both IGF-1 and IGF-2 have been produced as fusion proteins. Therefore additional purification steps are required, for example separation of protein IGFs from the whole protein inclusion bodies (fusion proteins). To date, complete characterisation of IGF has not been achieved, such as the amount of contaminants in the inclusion bodies, the structure of the IGFs, and the physico-chemical properties of the inclusion bodies (eg. particle characteristics, electrophoretic mobility, and isoelectric point). Hence, significant work is required to address these aspects. Wong *et al.* (1997) reported that IGF-2 produced as inclusion bodies has a particle size in the range of 0.35 to 0.40 microns. In general, it can be assumed that the IGF-1 has similar inclusion body particle size as it is expressed using an identical system to the IGF-2. An analog of IGF-1 named LR^3-IGF-1 is employed in this study.

Recombinant IGFs and their analogues are marketed in the US mammalian cell-media markets by GroPep Pty Ltd. It is forecast that the demand for such products will increase as new biopharmaceutical products approach phase III clinical trials. Therefore, it is essential to improve production strategies to achieve a cheaper product and hence, increase competitiveness in the market. This strategy goal can be achieved by improving both the fermentation process and the downstream processing. In fermentation, improvement may be gained by developing and applying an optimal feeding system to produce a high cell-density culture. As described earlier, the downstream processing sequence include the most expensive steps in the whole production process. Therefore, a significant reduction of production cost may be achieved by improving downstream processing strategies and methods.

An alternative separation technique is proposed as a potential replacement for the expensive centrifugation processes commonly applied for inclusion body recovery. In addition to the significant cost penalty for centrifugation, additional difficulty is the similarity in size and density of the inclusion bodies and the cell debris. Other property differences between the inclusion bodies and the cell debris may be exploited to develop alternative separation techniques. Flotation provides a potential method

for this difficult task. This method exploits the physicochemical properties of particulate surfaces, such as hydrophobicity. Despite the wide spread applications of large-scale production of the IGFs and their analogues, their properties, particularly physico-chemical properties, have not been extensively studied. Hence, characterisation of both inclusion bodies is required. Physicochemical properties, such as electrophoretic mobility, particle characteristics and the interaction force between inclusion bodies and an air bubble need to be measured to design flotation recovery systems.

1.3 PHYSICOCHEMICAL PROPERTIES CHARACTERISATION

Physicochemical properties play a key role in various processes, including aggregation, precipitation and flotation recovery. A knowledge of these properties is required for improved and rational design of alternative separation techniques. Flotation is proposed as a potential method for inclusion body recovery. Hence, the physicochemical properties of inclusion bodies including eletrophoretic mobility, the particle characteristics and the interaction forces between inclusion bodies and bubbles must be measured.

Hydrophobicity is normally characterised in terms of contact angle (section 1.5.2.4) and the net surface charge measured as electrophoretic mobility or zeta potential. Electrophoretic mobility (or zeta potential) is measured using various methods, such as electro-osmosis, streaming potential, electrophoresis (micro-electrophoresis) and sedimentation potential (Hunter, 1981). The micro-electrophoresis technique is most commonly used as it can be applied to materials throughout the whole colloid size range (Hunter, 1981) and the equipment for this measurement is readily available (eg. ZetaMaster, Malvern Instruments, Ltd.). The electrophoretic mobility of inclusion bodies as a function of pH and electrolyte concentration in the presence of different cations and anions has been studied and the results are presented in chapter 3.

Particle characteristics such as size, shape, and surface properties are studied using various techniques, including photosedimentation, scanning electron microscopy (SEM) and atomic force microscopy (AFM). These characteristics are important factors in the design of downstream processes, eg. flotation. The particle size of inclusion bodies can be used to predict and/or determine the bubble size required in flotation. Particle shape and surface property also contribute to this. Surface roughness provides a significant contribution to flotation processes, mainly in the bubble formation. For example, particles with rough surface facilitate the formation of bubbles by dissolved gas in water (Ryan and Hemmingsen, 1993). It is suggested that particles with rough surface are capable of trapping gas in their pores or crevices

which may serve as nuclei for the formation of bubbles. Furthermore, Zhou *et al.* (1994) showed that surface roughness of particles together with other factors (such as the surface roughness of container, the high dissolved gas contents, and the presence of solid particles in the liquid) facilitate the initiation of cavities (gas nuclei) and a large number of gas nuclei in the slurry can improve the performance of flotation processes.

In flotation processes, interactions (adhesion) occur between bubble/particle and one particle/other particles. Adhesion forces are important because they control the bubble/particle attachment processes and hence the elementary processes of flotation. A study of adhesion forces between a colloidal particle and a bubble in water was first performed by Butt (1994). This study showed that hydrophilic particles in water experienced repulsive forces when they approached a bubble whereas hydrophobic particles were attached and snapped into the air bubble as soon as they came into contact with the water/air interface. This proved that hydrophobicity plays an important role in the bubble/particle attachment processes. Adhesion forces can be used for studying bubble/particle attachment processes more thoroughly. This may also lead to suggestion for further improvement of bubble/particle attachment processes, for example the improvement of adhesion forces in relation to hydrophobicity. Atomic force microscope (AFM) can be used for studying interaction near and between surfaces due to its capability to measure forces up to 10^{-12} N with high spatial resolution (Hoh *et al.*, 1992). AFM has been used to study various forces involved in the interactions between particles and bubbles (Ducker *et al.*, 1994; Fielden *et al.*, 1996). Hence, atomic force microscopy is proposed in order to examine interaction forces between inclusion bodies and an air bubble. This work is described in chapter 4. It is the first study of protein-bubble interactions.

1.4 ATOMIC FORCE MICROCOPY

Atomic Force Microscopy (AFM) and Scanning Tunnelling Microscopy (STM) are relatively new techniques for microscopic characterisation and analysis, eg. surface characterisation. However, these techniques are very powerful and have been widely applied since their initial development by Binnig *et al.* in 1982 (Lal and John, 1994). These techniques are subset of a larger group of microscopic techniques called Scanning Probe Microscopy (SPM). These include devices such as magnetic force microscope, scanning near-field optical microscope, scanning ion-conductance microscope and scanning electro-chemical microscope (Wickramasinghe, 1989).

Scanning tunnelling microscopy requires conductive samples and is principally employed for analysing metallic and semiconductor surfaces. Recently, a few biological applications of STM have appeared. However, special sample treatments and preparation are required. Atomic force microcopy appears more useful compared to STM for biological applications as non-conducting samples can be examined in a liquid environment. Therefore, analysis of biological samples under physiological conditions is possible at molecular and even atomic scales. A large number of AFM applications to biological research are reported in the literature and these applications are expanding rapidly. Moreover, new applications and methods using the AFM in biological research have been developed. The following sections will discuss the principles and operation of atomic force microscopy and its applications with particular emphasis on biological applications.

1.4.1 Principle of Operation

The Atomic Force Microscope, also known as the Scanning Force Microscope, consists of a sensing probe (tip), optical devices, a scanner for positioning the probe or sample, an electronic control unit, and a computer for controlling the scan parameters as well as generating images. The tip is attached to a cantilever which behaves as a spring. The cantilever is available in a 'V' or 'I' shapes. A photodetector measures

the cantilever deflection as the tip is scanned over the sample (or the sample is scanned under the tip, Figure 1.2). Deflection of the tip is caused by interaction forces between the tip atoms and sample atoms. The signal from the photodetector is then stored in a computer and translated to an image (a map of the surface topography).

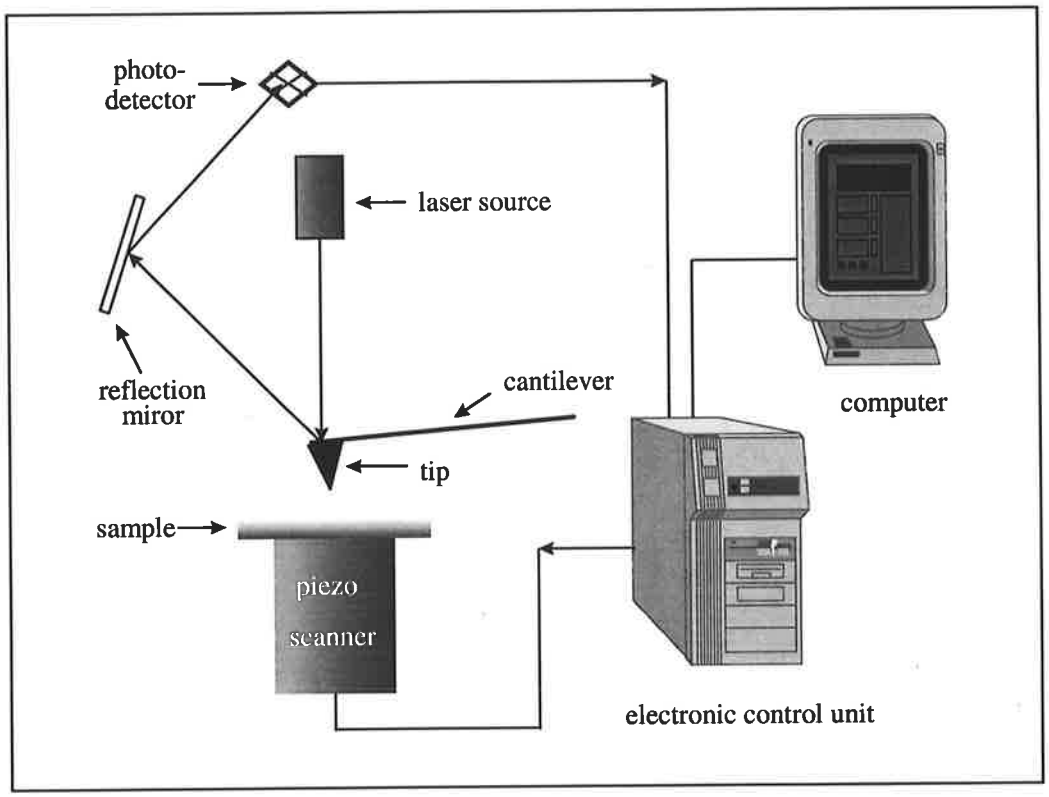

Figure 1.2 Schematic representation of atomic force microscope

A laser light is used to detect the cantilever deflection. It is projected to the reflective top end of the cantilever and this reflection is captured by a multisection photodetector. A photodetector with two or four section is usually employed. Clearly, the amount of reflected laser light captured by the photodetector changes with the cantilever deflection.

The movement of the tip (or the sample) is controlled by a piezoeletric scanner which can control fine movement at high precision. This scanner is composed of piezo ceramics and is able to move in three orthogonal directions (x, y and z). Such

movement is caused by expansion and contraction of piezo ceramics as a consequence of the applied voltage. During AFM imaging, the scanner moves in a raster pattern and the tip deflections are recorded at several points along the raster path. The properties of the piezo ceramics are time dependent. Consequently, scanner nonlinearities are often detected including intrinsic nonlinearity, hysteresis, creep, aging and cross coupling (Howland and Benatar, 1993). These nonlinearities can be corrected by software and hardware corrections. This is usually performed by scanning a standard silicon grid and subsequent corrections are derived from procedures supplied by the AFM's manufacturer. Scanner calibration is recommended to achieve high precision.

1.4.2 Operation Modes

The Atomic force microscope can be operated in two primary scanning modes, contact and non-contact modes. In the contact mode, a tip is brought close to and touches the sample. Whereas in non-contact mode, the tip remains at a finite distance from the samples, usually the distance is slightly more than a few nanometers. The non-contact mode is used for soft samples as it does not perturb the sample. However this mode results reduced resolution compared to the contact mode. Hence, its applications in biological imaging are limited.

Deflection of the tip is caused by the sum of forces (attractive and repulsive). These forces vary according to the mode of operation and the imaging conditions. Tip deflection in the contact mode is mainly caused by the repulsive forces from the overlapping electron orbitals between the tip atoms and the sample atoms. Van der Waals forces are the dominant attractive force. An additional attractive force is present when imaging is performed in air due to the meniscus-surface tension force created by adsorbed layers of water (Lal and John, 1994). Additional attractive forces are also encountered due to electrostatic Coulomb interaction between charges on the specimen and the tip (either occurring naturally or induced because of polarisation),

osmotic pressure due to charge movement and rearrangements, and structural forces: hydration forces, solvation forces, and adhesion forces (Lal and John, 1994).

In contact mode AFM, excessive forces may be experienced by soft samples (eg. biological materials). This may result in sample deformation. This limitation has inspired the birth of a new imaging mode, the intermittent-contact mode. This method has been registered as the tapping mode, a trademark of Digital Instruments, Inc. (Santa Barbara, US). In this mode, the cantilever is vertically vibrated at its resonance frequency and the sample is brought closer so that they come into intermittent contact (tapping). This intermittent contact decreases the amplitude of the cantilever's vibration. Changes in the vibration amplitude are used to generate an image representing surface topography. The tapping mode is preferred for imaging soft samples because it eliminates lateral forces (friction or drag) between the tip and the sample. High resolution images have been obtained using this mode (Hansma *et. al.*,1993). This mode can be employed in air and liquid environments (Hansma *et al.*, 1994).

Other AFM techniques have been developed to meet special purposes including force modulation technique, lateral force microscopy, magnetic force microscopy, phase detection microscopy, scanning capacitance microscopy and thermal scanning microscopy. Detailed discussion of these techniques is available in the literature (Howland and Benatar, 1993; Dinwiddie *et al*, -; Babcock *et al.*, 1995; Magomonov and Whangbo, 1996) and from the manufacturer (eg. http://www.di.com; http://www.topometrix.com).

1.4.3 AFM Applications

AFM has been applied in a wide range of disciplines, particularly in material science, biology, chemistry and physics. Surface topography by AFM is a common procedure for analysing the surface of various materials, such as semiconductor, polymer and biopolymers (eg. proteins). Other important applications of AFM include

measurement of nanomechanical properties (eg. hardness and elasticity) and nanolitography.

Biological applications of AFM have increased dramatically in the past few years. The versatility of AFM in measurements means that it is often the technique of choice for surface imaging. AFM has been employed widely for exploring various biological materials including DNA, proteins, lipid membranes, viruses and cells. Detailed discussion of these applications is available in the literature (Hoh and Hansma, 1992; Hansma *et. al.*, 1993; Lal and John, 1994; Hansma and Hoh, 1994; Ikai, 1996). AFM has also been used to characterise the nanomechanical properties of biological materials, for example viscoelasticity (Radmacher *et al.*, 1994).

The ability of AFM to measure forces at high sensitivity (up to picoNewtons) provides new impetus for studies of micro and molecular interactions. This area is of particular interest in biology as numerous biological processes are governed by interactions at micro and molecular levels. Various techniques for interactions measurements have been developed including chemical force microscopy (Frisbie *et al.*, 1994), colloidal probes (Ducker *et al.*, 1990) and sensor force microscopy (Haselgrubler *et al.*, 1995). A detailed discussion of AFM force measurement is presented in chapter 4.

It is apparent that AFM has significant potential for biological imaging and the exploration of biological processes. Hence, this technique has been adopted to examine the protein inclusion body particles (chapter 3) and the interaction forces between inclusion bodies and an air bubble (chapter5) with potential extension to flotation processes.

1.5 FLOTATION

Flotation is a solid-liquid separation method which exploits the surface properties of particles to enhance attachment of particles onto air bubbles. Particles are attached to air bubbles by hydrophobic interactions. The particles are then transported to the surface of the suspension by rising air bubbles. Consequently, hydrophilic particles cannot be separated using this method without some modifications of their surface chemistry. The surface properties of hydrophilic particles may be modified for complimentary attachment to air bubbles by adding constituents known as collectors. Clearly, understanding the surface properties of particles provides a key factor to achieve a high separation efficiency in flotation recovery.

1.5.1 General Overview

Flotation has been widely exploited for solid-liquid separations in various industrial applications. It has been used in mineral processing since the end of nineteenth century (Kitchener, 1984), for example the treatment of clays and coal. It has also been successfully applied in pulp and paper industries as well as in the application for waste-water and water treatment since about 1960 (Kitcheter, 1984). Examples include recovery of suspended solids, sludge, and a number of heavy metals in waste-water and water treatment. Furthermore, the application of flotation in biotechnology has attracted the interest of a number of researchers. Examples include separation of microbial cells from fermentation broth (Levin *et al.*, 1962; Rubin *et al.*, 1966 & 1968; Miyazu *et al.*, 1974; Hasyim *et al.*, 1995), biodegradable plastic (Cilliers et al., 1994) and soluble protein recovery (Ibuchi *et al.*, 1974 & 1980; Chiang *et al.*, 1980; Miranda *et al.*, 1993; Bremmell *et al.*, 1994).

Several terms have appeared with the flotation development, such as gamma flotation, ion flotation, froth flotation, and column flotation. Gamma flotation is named thus for a flotation process which uses liquid/vapour surface tension control. Yarar and Alvarez (1985) reported that pyrite, chalcocite, and chalcopyrite can be separated

using this method. Ion flotation is a flotation process for separating ions, for example ion flotation of germanium ion. Flotation processes which create foams are called froth flotation. In this method frothers are often added to create foam/froth. Separated solids accumulate in the froth on top of the flotation cell. This method is commonly applied in mineral processing. Recently, flotation has been carried out using a column as a flotation cell. This results in better performance and a reduced space requirement. This method is known as column flotation.

Flotation can be categorised into three main groups according to bubble formation techniques. The methods are dispersed-air, electrolytic, and dissolved-air flotation.

1.5.1.1 *Dispersed-air Flotation*

Dispersed-air flotation is the conventional method of flotation. It is widely used in mineral processing. Air bubbles are created by dispersing air using a sparger at the bottom of a flotation cell. Different types of spargers have been studied and developed for creating smaller and more homogenous bubbles. In this method the air bubble formed is relatively large, typically in the range of 0.5 to 2 mm. This size limits recovery for fine-particle separation. Improved recovery of fine-particle flotation has been reported by applying ultrasound conditioning (Nicol *et al.*, 1986). It is suggested that ultrasound promotes particle aggregation to generate larger particles and the formation of smaller bubbles.

1.5.1.2 *Electrolytic Flotation*

Electroflotation or electrolytic flotation is an unconventional method. The flotation cell consists of two differently charged electrodes carrying out electrolysis of the aqueous part of the suspension. Oxygen and hydrogen are formed during electrolysis and released as bubbles. Since the amount of oxygen and hydrogen created is very small, the bubbles formed are tiny. Flocculation and flotation may also be enhanced

by the presence of the electric field gradient between electrodes without addition of any surfactants (Matis & Zouboulis, 1995c).

This technique has been applied in mineral processing, and in waste-water and water treatment. Electroflotation was proposed for mineral beneficiations in 1946 by Ryvkin *et al.* (Matis & Zouboulis, 1995c). Webster observed the potential use of electrolysis in sewage treatment in 1887 and this method was applied for treatment of London sewage (Matis & Zouboulis, 1995c). Furthermore, this method has been applied for the reduction of suspended solids and chemical oxygen demand (COD), and the removal of phosphates and dissolved toxic metals (eg. Cu, Zn, Ni, and Cd) from plating processes (Matis & Zouboulis, 1995c).

Though electrolytic flotation has potential for use in fine-particle separation, it seems that it is rarely used in commercial processes. This is due to difficulties in scaling up the process and the high cost of operations.

1.5.1.3 *Dissolved-air Flotation*

Air bubbles created in this method are small. Bubbles in the range of 50 to 100 microns can be achieved (Matis & Zouboulis, 1995a). Four main pieces of equipment are required in this process: pressuriser pump, pressuriser tank, pressure-reducing valve and flotation cell. The suspension is pressurised using air in a pressuriser tank up to a pressure of 500 kPa to achieve a high concentration of dissolved air. In the next step, the pressurised suspension is passed through a pressure-reducing valve to the flotation cell. Small air bubbles appear when the pressure is suddenly reduced in the pressure-reducing valve. These bubbles interact with particulate solids in the suspension and carry them to the surface of suspension by buoyancy forces.

Dissolved-air flotation has various applications. The most common application is in waste-water and water treatment since the generated air bubbles are small and this favours the separation of fine-particles (Matis & Zouboulis, 1995a). Fine-particles

(mostly in a sludge form) in waste-water and water treatment as well as heavy metals and salt-like substances are removed using this method. This method is also applied in mineral processing for recovering fine-particle minerals or contaminants.

1.5.1.4 *Biotechnological Applications*

A number of reports on the biotechnological application of flotation have been noted. It has been suggested that flotation is a reliable method for recovering cells from fermentation broth (Levin *et al.*, 1962; Miyazu *et al.*, 1974; Hasyim *et al.*, 1995). Hasyim *et al.* (1995). The hydrophobic nature of constituents (eg. lipopolysacarides, phospolipids, lipoproteins and peptidogycans) forming the cell wall may facilitate their attachment to the bubbles. Some modifications of the conventional flotation technique have been proposed by Hasyim *et al.* (1995). They employed colloidal gas aphron (CGA) dispersion to replace air bubbles for recovering yeast cells. This system may be only suitable for limited cases. Contamination problems may arise from this method if therapeutical products are being processed. The high cost of capital and operation often renders this method less attractive.

Another biotechnological application of flotation is separation of biopolymers, such as proteins, lipids/fats, and polysaccharides. For example, separation of soluble proteins (Ibuchi *et al.*, 1974 & 1980; Chiang *et al.*, 1980), removing fats and proteins in waste treatment (Bremmell *et al.*, 1994). It appears that only limited number of studies have been performed on the application of flotation to protein recovery. Most applications involved waste-water and water treatment of biological/ biotechnological waste where the biopolymers are unwanted items. Miranda *et al.* (1993) were the first to report the application of flotation for recovering proteins. A genetically-engineered enzyme, α-amylase (soluble), was separated from fermentation broth using dispersed-air flotation. They concluded that the flotation of biological materials has similar characteristics to the flotation of minerals. Another significant application of flotation for separation biopolymers was reported by Cilliers et al. (1994). They employed

flotation for the recovery of polyhydroxybutirate (PHB), a biodegradable plastic produced by recombinant *E. coli*.

1.5.2 Principles of Flotation

The elementary process of flotation is bubble/particle attachment and is composed of three steps (Hewit, 1994). First, bubble/particle collision followed by formation of an intervening thin liquid film. This step is controlled by the hydrodynamic conditions. Second, thin film drainage to the point of rupture with the formation of a dynamic three-phase contact. Hydrodynamic and surface forces play an important role in this step. Finally, formation of a stable bubble/particle aggregate is required. The bubble/particle aggregate is stabilised by a balance between the kinetic energy of the bubble-particle aggregate and the force of detachment at the three-phase line of contact.

The efficiency of particle collection is a combination of the three steps as follows (Hewit, 1994):

$$E_{Coll} = E_C \; E_A \; E_S \qquad (1.1)$$

where: E_{Coll} = efficiency of bubble/particle collection

E_C = efficiency of bubble/particle collision

E_A = efficiency of bubble/particle attachment

E_S = efficiency of stability of the bubble/particle aggregate

1.5.2.1 *Bubble/particle collision*

A detailed theory of flotation was presented by Derjaguin and Dukhin (1960/61). They considered three characteristic zones of approach between the bubble and the particle as shown in Fig. 1.3. These zones are distinguished by the type of interaction forces. In zone 1, particle movement is due to hydrodynamic forces. Zone 2 is the

region where there is a charge exchange between the electrical double layers of the bubble and the particle. This results in a diffusiophoretic force, a combination of diffusion rate and electrophoretic force. In zone 3, the particle and the bubble are separated by a very small distance and therefore the interparticle forces are predominant. These forces play an important role in the rupture of the thin liquid film between the bubble and the particle.

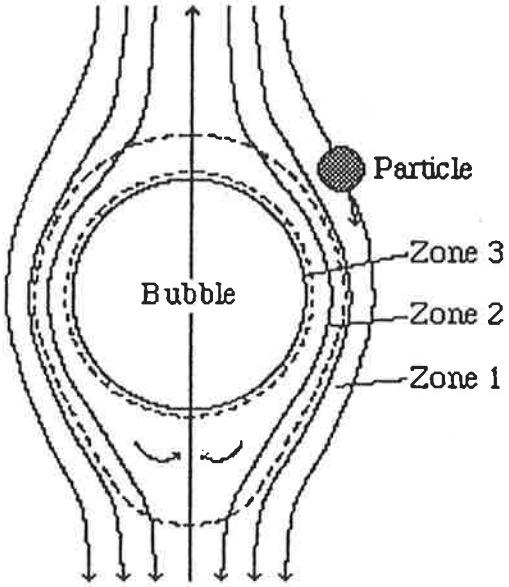

Fig. 1.3 Three zones of bubble/particle approach according to Derjaguin and Dukhin (after Hewit, 1994)

Reay and Ratchliffe (1973) studied the efficiency of collision by considering gravitational forces and ignoring inertial forces. They considered particles with diameters of less than 20 μm and bubbles with diameters of less than 100 μm and found the efficiency of collision, E_C as follows:

$$E_C \ \alpha \ \left(\frac{d_p}{d_b}\right)^n \qquad (1.2)$$

where n is dependent on the relative particle density (ρ_p/ρ_f) and has a value of 2.05 for ρ_p/ρ_f = 2.5, d_p is particle diameter and d_b is bubble diameter.

Schulze (1989) studied the bubble/particle collision efficiency in more detail. The bubble/particle collision efficiency is defined as the ratio of the number of particles encountered a bubble per unit time to the number of particles approaching the bubble at a great distance in a flow tube with a cross sectional area equal to the projection area of the bubble (Schulze, 1989). The ideal collision efficiency or the maximum collision efficiency is given by (Schulze, 1989):

$$E_{id} = \left(1+\frac{d_p}{d_b}\right)^2 \quad ; \; 1 < E_{id} \leq 4 \; for \; d_p \leq d_b \tag{1.3}$$

Schulze (1989) considered three effects on the collision efficiency as the particle trajectories deviate from straight lines for a variety of reasons. First, the interception effect (E_{ic}) is caused by particles following the stream lines of the bubbles without any change in direction. Second, the inertial effect (E_{in}) is due to inertial forces on the particles causing increased collisions. Finally, the gravitational effect (E_G) results from gravitational forces which increase collisions. Therefore, the overall efficiency of collision is given by:

$$E_C = E_{ic} + E_G + \left(1-\frac{E_{ic}}{\left(1+\left(d_p/d_b\right)\right)^2}\right)E_{in} \tag{1.4}$$

A detailed description of the overall efficiency of collision can be found in Schulze (1989).

1.5.2.2 *Bubble/particle attachment*

Two processes, namely collision and sliding, may occur when a particle approaches a bubble at small distances as shown in Fig. 1.4 (Schulze, 1989). Collision (impact) processes take place when a particle collides with a bubble causing a strong deformation of the bubble surface. The particle rebounds unless attachment occurs during the first collision. Sliding processes occur when the collision between particles

and bubbles causes a weak deformation of the bubble surface. In this process, particles slide along the bubble surface.

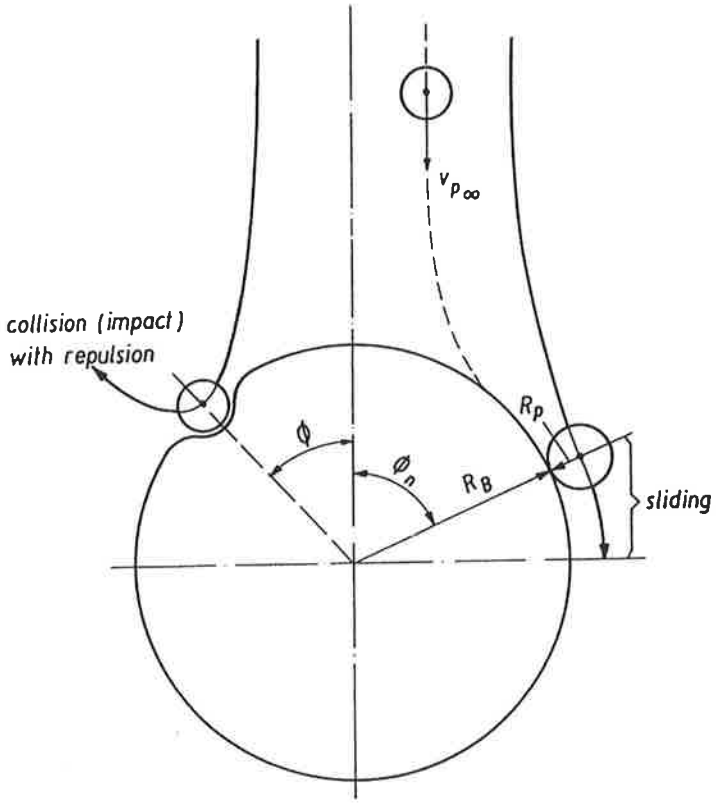

Fig. 1.4 Schematic representation of colliding and sliding processes (after Schulze, 1989)

The contact time, τ_{con} , between the bubble and the particle determines whether attachment can occur or not. Attachment takes place when the thin liquid film drains and ruptures (thin film drainage time, τ_F) followed by formation of a stable three phase line of contact (three phase contact time, τ_{TPC}). The time required for these two events to occur is called the induction time, τ_i . Attachment occurs if contact time is equal or greater than induction time or can be express as follows:

$$\tau_{con} \geq \tau_i = \tau_F + \tau_{TPC} \qquad (1.5)$$

This contact time can be either the collision time, τ_C ,or the sliding time, τ_{sl} . A number of factors determines whether collision processes or sliding processes predominate in flotation. Collision processes occur predominantly with large particles and high relative velocities of particles radially directed to bubble surface (Schulze, 1989). Whereas sliding processes occur predominantly with small particle at small relative velocities. A very high concentration of gas bubbles per unit volume also causes sliding processes (Schulze, 1989). Theoretical and experimental work on the collision time, sliding time, thin film drainage time and the three-phase contact time have been performed by several workers (including Schulze, 1989 and Hewit, 1994, see these references for more detail).

The bubble/particle attachment efficiency (or probability) in relation to induction time was formulated by Yoon and Luttrell (1989). They considered three regions of the flow around the bubble which are characterised by the Reynolds number namely Stokes, intermediate, and potential flow. The attachment efficiencies are as follows:

For Stokes flow:
$$E_A = \sin^2\left(2\arctan e^{\left(\frac{-3v_b\tau_i}{2r_b(r_b/r_p+1)}\right)}\right) \tag{1.6}$$

For intermediate flow:
$$E_A = \sin^2\left(2\arctan e^{\left(\frac{-(45+8\mathrm{Re}_b^{0.72})v_b\tau_i}{30r_b(r_b/r_p+1)}\right)}\right) \tag{1.7}$$

For potential flow:
$$E_A = \sin^2\left(2\arctan e^{\left(\frac{-3v_b\tau_i}{2(r_b+r_p)}\right)}\right) \tag{1.8}$$

Bubble/particle attachment efficiency is also affected by various factors, such as the particle size, the bubble size, the hydrophobicity of particles, the ionic strength of the medium, and the surface roughness of particles.

1.5.2.3 *Stability of bubble/particle attachment*

Attachment of captured particles to a bubble is due to capillary forces along the contact perimeter. Detachment can occur either when the gravitational force on the particle exceed the buoyancy force of the bubble, or when the kinetic energy of bubble/particle aggregate is insufficient for attachment. Therefore, there is a particle size limit for flotation to occur. The maximum particle diameter, d_{max} from a balance of gravitational forces and capillary forces between the particle and the bubble (Scheludko *et al.*, 1976). Another proposed model to estimate the maximum particle diameter considers the range of forces acting on bubble/particle aggregate to determine the energy required to detach the particle from the bubble (Schulze, 1983).

There is a minimum particle diameter for a stable particle/bubble aggregate to be formed. Discussion of the fine particle limit requires consideration of the wetting film which is formed when a particle collides with a bubble (Hewit, 1994). This film is unstable and spontaneously ruptures if the particle is hydrophobic. Scheludko *et al.* (1976) proposed a model for estimating the minimum floatable particle diameter. They considered the role of line tension in the formation of the bubble/ particle aggregate and found that the speed at which the three-phase line of contact spreads across the surface of the solid is most likely the limiting factor. This model was modified by Drelich and Miller (1992) by taking into account the effects of surface imperfections into account in calculating the pseudo-line tension. This pseudo-line tension can be resolved by examining the relationship between hydrophobicity of the particle and bubble size which is characterised by the water contact angle

1.5.2.4 *Contact Angle and Wetting*

Wettability of the particle surface determines whether particles are floatable or not. Wettability is quantified by a contact angle. Large contact angles indicate that particles are poorly wetted or hydrophobic whilst small contact angles designate that particles are hydrophilic. Hysterises of the contact angle (i.e. the difference between

the advancing contact angle and the receding contact angle) is a typical phenomena in contact angle measurement (Hunter, 1989). This phenomena is caused mainly by inhomogeneities on the surfaces. The advancing contact angle (i.e. the contact angle measured after the liquid has advanced part way across the solid surface) is commonly 20°-30° greater than the corresponding receding contact angle (Hunter, 1989). The receding contact angle seems more relevant for flotation studies as the aqueous phase must retreat from the solid, whereas the advancing contact angle appears more applicable for contact angle studies as it is more reproducible (Crawford *et al.*, 1987).

Three-phase contact between a particle, aqueous solution and a gas bubble is described thermodynamically by Young's equation as follows (see Fig. 1.3):

$$\cos\theta = \frac{\gamma_{SG} - \gamma_{SL}}{\gamma_{LG}} \tag{1.9}$$

where: θ is the contact angle and γ_{SG}, γ_{SL} , γ_{LG} are the interfacial tensions of solid/gas, solid/liquid, and liquid/gas respectively.

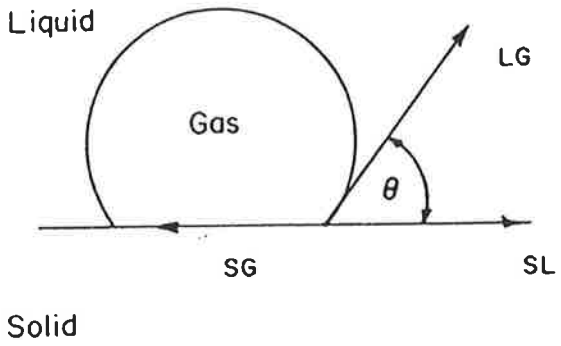

Fig. 1.5. Schematic representation of three-phase contact angle between a particle, aqueous solution, and a gas bubble.

The free energy change of attachment process (i.e. the displacement of the water by the air bubble) per unit area is described by Dupre's equation (Fuestenau *et al.*, 1985):

$$\Delta G = \gamma_{SG} - (\gamma_{SL} + \gamma_{LG}) \quad (1.10)$$

Combining Young's and Dupre's equations, the free energy change can be described in terms of contact angle as follows:

$$\Delta G = \gamma_{SG} (\cos \theta - 1) \quad (1.11)$$

The free energy change can be expressed in terms of work of adhesion of water, W_A , and the work of cohesion of water, W_C (Fuerstenau *et al.*, 1985):

$$\Delta G = W_A - W_C \quad (1.12)$$

Attachment process occur if the work of adhesion of water is lower than the work of cohesion of water ($W_A < W_C$). The work of adhesion consists of three components and is defined as the work required to remove liquid from the solid surface leaving an adsorbed water layer in equilibrium with a saturated gas phase (Fuerstenau *et al.*, 1985). Firstly, Columbic attractive forces at the solid surface provide ionisation energy. Secondly, coordination forces and the dipole interaction of the solvent with the solid surface result in hydrogen bond energy. Finally, dispersion energy arises from solvent interaction with induced dipoles at the solid surface. The work of cohesion for water is the energy to create new surface at the air/water interface or $W_C = 2 \gamma_{LG}$. Therefore, the criteria for flotable particle is $W_A < 2 \gamma_{LG}$.

1.5. 3 Factors Influencing Flotation

Flotation processes are affected by many different factors, including hydrodynamic properties and physico-chemical properties. Hydrodynamic properties include bubble size, bubble coalescence, the terminal velocity of bubbles, and homogeneity. These

will be briefly reviewed in the following sections. Physico-chemical properties, such as electrophoretic mobility (zeta potential) , surface topography, hydrophobicity and adhesion forces, play an important role in the elementary process of flotation. All of these factors interact with each other creating even more complex systems. Therefore, fundamental studies are required to understand the complete flotation process. This study will emphasise characterisation of the physicochemical properties of inclusion body particles. As well, the adhesion (interaction) force between inclusion bodies and an air bubble is examined using an atomic force microscope (AFM).

Bubble size affects the efficiency of bubble/particle collision. Particles cannot collide with too large bubbles due to their small inertial force which is insufficient for collisions to occur. Instead, the particles rather follow the streamline around the bubble. Furthermore, large bubbles have a high terminal velocity and consequently a small residence time hence decreasing the probability of bubble/particle collisions. Bubble size is determined by the method of bubble formation and other factors, such as hydrostatic forces, bubble coalescence, ionic strength and viscosity. In general, bubbles can be formed using three methods which are used as criteria for classifying flotation as described in section 1.5.1. Hydrostatic forces become a significant factor on bubble size when flotation is carried out in a tall flotation column. Bubble size increases as they rise as a result of decreasing hydrostatic forces.

Large bubbles may be formed as a result of bubble coalescence. Bubble coalescence is mainly caused by nonuniformity of bubble size, violent agitation and the presence of a large surface area in contact with the bubble-liquid surface (Matis and Zouboulis, 1995b). Craig *et al.* (1993a & 1993b) reported that bubble coalescence can be reduced/prevented by the addition of salts. The action of salts on bubble coalescence depends on the salt valency and transition concentration (or critical concentration, a concentration where there is no significant changes with an increase in concentration). A higher valency salt is more effective at lower concentration. They found that bases such as KOH have the same effect as salts, but mineral acids HCl and H_2SO_4 have little or no effect on bubble coalescence. Moreover they discovered that sugars (sucrose, glucose, and fructose) also inhibit bubble coalescence. This phenomena occurs as a consequence of the fact that electrolytes can increase surface tension.

Clearly, ionic strength play an important role in reducing bubble coalescence hence increasing flotation efficiency. Viscosity was believed to affect bubble coalescence in such a way that an increase in solution viscosity increases the hydrodynamic barrier and thereby reduces bubble coalescence (Craig *et al.*, 1993a &1993b).

Gas bubbles in water and solutions of inorganic electrolytes are negatively charged (Weyl, 1951; Li and Somasundaran, 1991 & 1992). In the presence of surfactants, bubble charge is determined by the charge of the head group of surfactants (Yoon and Yordan, 1986). These workers discovered that at neutral to alkaline pH, negatively charged bubbles are created in the presence of nonionic and anionic surfactants, and positively charged bubbles are created in the presence of cationic surfactants. In acidic pHs, the opposite charge is obtained. Their work confirmed that a change in pH is more influential than a change in concentration of surfactants.

Bubble charges has been investigated by several workers (Okada *et al.*, 1990; Li and Somasundaran, 1991 & 1992). These charges can be reversed by addition of multivalent salts (Li and Somasundaran, 1991 & 1992). This reversal of charge depends on pH and the concentration of added salts. Clearly, bubble charges may be modified to obtain the desired sign and magnitude of surface charge under any given condition, by adding the required amount of appropriate salts (Li and Somasundaran, 1992).

It is clear that electrolytes greatly influence the flotation processes. This process can be explained by several surface chemical mechanisms proposed by Paulson and Pugh (1996). These workers confirmed that the electrolytes cause disruption of the hydration layers surrounding the particle thereby enhancing bubble-particle capture, reducing the electrostatic interactions, and increasing the charge on the surface of the bubbles to prevent primary bubble coalescence. Cations were discovered to produce stronger effects compared with anions on flotation efficiency (Paulson and Pugh, 1996).

1.6 THESIS STRUCTURE AND STRATEGY

It is apparent that improvements in the production system and downstream processing of protein inclusion bodies (insulin-like growth factor 1 analog, LR^3-IGF-1) are required as the demand of such proteins increase. Several strategies are considered to address this issue. Chapter 1 provides a broad introduction to the properties of inclusion bodies and background information on physicochemical characterisation of such bodies and consider the flotation processes to the fractionation such bodies. The overall thesis structure is presented in Figure 1.6.

In chapter 2, a novel 3-stage feeding strategy is proposed to improve the production yield of inclusion bodies by fed-batch fermentation. This feeding strategy aims at reducing and/or eliminating high level of accumulation of acetate and glucose in the current production method (constant-rate feeding). Other improvements are proposed including amino acid and yeast extract supplementation to increase the size of inclusion bodies and thereby achieve higher productivity.

Flotation is considered as a potential method for the inclusion body recovery. This method exploits differences in surface chemistry between the particles and the cellular debris. As well, interactions between inclusion bodies and air bubbles play a key role in the elementary processes of flotation, particularly the particle-bubble attachment. This work proposes a study of the physicochemical properties of the inclusion bodies and examines the interaction force between inclusion bodies and an air bubble. This work is expected to provide a fundamental basis for a rational design of flotation recovery of inclusion bodies.

Various measurement techniques have been employed to examine the physicochemical properties of the inclusion body including electrophoretic mobility and determination of the particle surface and size characteristics. These are outlined in chapter 3. This work provides essential features required in flotation design. Thereafter, in chapter 4, the interaction force between inclusion bodies and an air bubble is studied using the atomic force microscope. This study is expected to

provide a significant contribution to the fundamentals of the rational flotation process.

Finally, in chapter 5, mathematical models are proposed to describe the inclusion body recovery using dissolved-air flotation technique. As well, a simple, initial design of a dissolved-air flotation system for inclusion body recovery is presented.

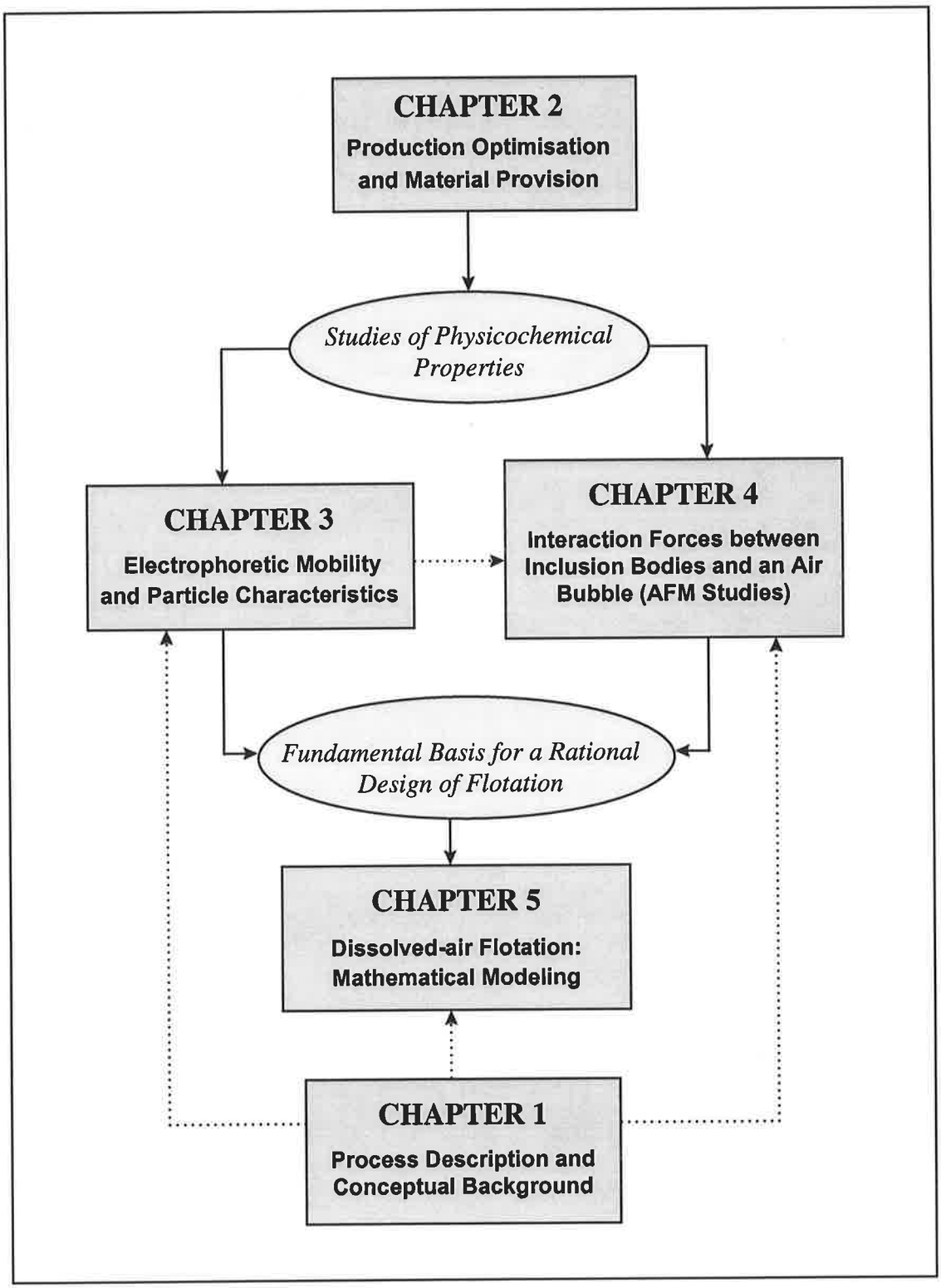

Figure 1.6 Outline of overall thesis structure

Chapter 2

FERMENTATION

LR^3-IGF-1 protein inclusion bodies are produced at large scale by fermentation. Fed-batch operation is normally employed to achieve high cell density culture or high volumetric productivity. The current feeding method utilises constant-rate feeding. A cell concentration of up to 20 g cell dry weight (DCW)/L was achieved. Further productivity improvement (i.e. higher cell density) was not possible as a consequence of the high level of glucose and acetate accumulated in the culture media which inhibit cell growth. This work attempts to address these problems and increase fermentation productivity through improved control and feeding strategies. This work was conducted in collaboration with Yong-Seok Lee, PhD., a postdoctoral fellow in the Department of Chemical Engineering, University of Adelaide.

2.1 INTRODUCTION

2.1.1 Background

An analog of insulin-like growth factor 1, termed Long-R^3-IGF-1 or LR^3-IGF-1 (Francis *et al.*, 1992), is produced as a solid inclusion body (IB) when expressed at high levels in recombinant *E. coli*. This protein is produced in Adelaide by a small biotechnology company, and sold into US markets for use as a mammalian cell-culture supplement. Demand for culture media and consequently this protein is expected to increase as new biopharmaceutical products approach phase III clinical trials. Additionally, the fusion protein can be easily cleaved to give pure IGF-1, which has several clinical uses. There is consequently a need to improve the productivity of the current growth factor production process, preferably through process intensification. A key unit to be optimised for higher yield is the fermenter.

The existing strategy uses a constant-rate fed-batch system and achieves an optical density (600 nm) of approximately 60 or up to 20 g cell dry weight (CDW)/L. Improvement of fermentation process to achieve higher cell density has proved unsuccessful. This failure is attributed to high level of acetate and glucose accumulated in the culture media, and low level of dissolved oxygen concentration. Furthermore, the resulting inclusion body is small, with a typical median diameter of 0.3 μm, making separation of the inclusion bodies from the cellular debris difficult following high-pressure homogenisation.

This work is aimed at improving fermentation productivity and the size of the resulting inclusion body through improved control and feeding strategies. A series of fermentations were conducted in which the feeding strategy was altered. A novel 3-stage feeding strategy was developed. Oxygen transfer was also enhanced with an oxygen-enriched air feed. The following sections outline important aspects of fed-batch fermentation to achieve high cell density culture.

2.1.2 Fed-batch Fermentation

Fermentation has been widely used for the production of speciality chemical and biological materials in small to large quantities. The production of ethanol, citric acids, baker's yeast, acetic acid, and single cell proteins provides examples of large scale fermentation products. High value products, such as insulin, hormones, growth factors, and certain enzymes, are normally produced in small quantity. The cost of fermentation is a key potential element to be minimised in order to achieve market competitiveness.

Three different modes of operation are commonly adopted in biological and chemical processes, namely batch, continuous, and fed-batch (commonly known as semi-batch in chemical processes). In batch fermentation, all nutrients required for one run of fermentation process, except oxygen (for aerobic fermentation), anti-foam agent, and other chemicals for pH adjustment, are initially added to fermenter. The final products are harvested at the end of each batch cycle. By contrast, in continuous fermentation, nutrients are fed to and products are withdrawn from the fermenter continuously at same flow rate and hence constant fermentation volume is maintained. Fed-batch fermentation is a process where one or more nutrients are gradually fed to the fermenter and the products are removed when fermentation is completed. Fed-batch falls between batch and continuous modes in term of microbial environment (Yamane and Shimizu, 1984).

The fed-batch strategy has advantages compared to batch and continuous fermentation, particularly when productivity is affected by changes in nutrient concentrations. Detailed discussion on this topic has been reported by Yamane and Shimizu (1984). Fed-batch fermentation is commonly applied to achieve high cell density. It is effective for handling problems, such as substrate inhibition, glucose effect, catabolite repression, and auxotrophic mutants. As well, the fed-batch mode can extend the operation time (and yield) as nutrients becoming available enabling further cell activity and growth. Moreover, reduction of fermentation broth viscosity and replacement of water lost by evaporation are readily achieved. Fed-batch

fermentation has been extensively used for the production of a plethora of products, such as baker's yeast, single cell protein, antibiotics, amino acids, enzymes, and other metabolites (Yamane and Shimizu, 1984).

The principal objective in a fed-batch fermentation is to control nutrient concentration in culture medium. Hence, based on feeding mode, two classifications are possible, namely without feedback control and with feedback control (Yamane and Shimizu, 1984). Details of the classification are summarised in Table 2.1.

Table 2.1 Classification of fed-batch fermentation

1. Without feedback control
1.1. Intermittent addition
1.2. Constant rate
1.3. Exponential increased rate
1.4. Optimised
1.5. Others
2. With feedback control
2.1. Indirect feedback control
2.2. Direct feedback control
2.3. Constant-value control
2.4. Optimal Control

2.1.3 High Cell-density Fermentation

For proteins that are intracellularly accumulated in recombinant *E. coli*, fermentation productivity is proportional to the final cell-density (volumetric productivity) and the specific productivity (Lee, 1996). Specific productivity is defined as the amount of product formed per unit cell mass per unit time. Volumetric productivity improvement can be achieved in high cell-density fermentation by applying fed-batch operation. This can be done by controlling specific growth rate (μ) and substrate concentration (Yee and Blanch, 1992). High cell density fermentation possesses other

advantages, such as reduced fermentation volume, enhanced downstream processing, reduced waste-water generation, lower production cost, and reduced capital investment in equipment (Lee, 1996).

The supply of nutrients for cell growth is a dominant factor in achieving high cell density cultures. Carbon and nitrogen sources in the media can inhibit cell growth if present at excess concentration. For example , *E. coli* growth is inhibited if nutrients are present in excess of the following limits: glucose (50 g/L), ammonia (3 g/L), iron (1.15 g/L), magnesium (8.7 g/L), phosphorus (10 g/L), and zinc (0.038 g/L) (Riesenberg, 1991a). Such constraints explains the failure to achieve high cell density in batch process by simply increasing the concentration of nutrients (Lee, 1996). Three types of media are commonly used in fermentation, i.e. defined, complex, and semi-defined. High cell density fermentation normally exploits a defined media with concentration known and controlled during fermentation. However, the composition and quality of nutrients in complex media such as yeast extract and peptone can vary. Such variations cause difficulty in fermenter control and significant variations in productivity may result. In some cases, semi-defined or complex media are used to boost product formation (Lee, 1996). Media for high cell density fermentation must provide all the components required for cell growth. Mass composition of dry *E. coli* and the yield coefficients of components in media have been used as a basis for designing a balanced, defined media (Riesenberg *et al.*, 1991b; Paalme *et al.*, 1990; Yang *et al.*, 1992).

Theoretically, the maximum cell density that can be achieved in high cell density fermentation of *E. coli* is 200 g CDW/L (Lee, 1996). The highest cell density reported in literature is lower than 200 g CDW/L, i.e. 174 g CDW/L for E. coli W3110 in dialysis reactor (Markl *et al.*, 1993) and 175.4 g CDW/L for recombinant E. coli producing poly(3-hydroxybutyrate) (Lee and Chang, 1994). The validity of this theoretical maximum cell density is supported by sharp increase in the viscosity of culture broth when the cell density exceeds 200 g CDW/L. The culture becomes almost solid-like above 220 g CDW/L (Mori *et al.*, 1979). Other problems arise as a consequence of high cell density, such as oxygen transfer limitation, poor mixing,

acetate accumulation, and high level of carbon dioxide. These will be discussed thoroughly in relation to this work in section 2.1.4.

Fed-batch fermentation is commonly conducted without any feedback control. Such systems are simpler and cheaper but less effective at achieving high cell concentration. Better control (and higher yield) is achieved by applying feedback control. Yamane and Shimizu (1984) have reviewed this area. Different feeding strategies (eg. constant rate feeding, stepwise increase of feeding rate, and exponential feeding) are commonly used to obtained high cell density. The feeding strategy affects the likely success of high cell density fermentation and productivity. As well, product concentration can be influenced by different feeding strategies (Bech-Jensen and Carlsen, 1990; Yee and Blanch, 1992). Nutrients used as feed contain a growth-limiting substrate, eg. carbon sources. In constant rate feeding, the nutrients are fed to the fermenter at a predetermined rate to increase culture volume. Clearly, the amount of nutrients available relative to the biomass concentration decreases as the cells grow and hence the specific growth rate will decrease. Consequently, the increase of cell concentration slows as fermentation proceeds. In stepwise (or gradual increasing) mode, cell growth is promoted by an increased supply of nutrients at higher cell density. Exponential cell growth can be achieved during the entire fermentation period if the feed rate is increased proportionally to the cell growth. Exponential feeding is designed to maintain a constant specific growth rate and a constant substrate concentration. This method is simple but effective for achieving high cell densities. Another advantage of this method is that acetate production can be minimised by controlling the specific growth rate below the critical level for acetate formation (Lee, 1996). High cell density fermentation of non-recombinant and recombinant *E. coli* has been successfully achieved by applying this feeding strategy and the specific growth rate is generally maintained at between 0.1 and 0.3 h^{-1} to avoid acetate formation (Strandberg and Enfors, 1991; Yee and Blanch, 1992; Helmuth *et al.*, 1994; Korz *et al.*, 1995). Korz *et al.* (1995) has obtained cell concentration of 128 g CDW/L and 148 g CDW/L by applying an exponential feeding mode using glucose and glycerol as carbon sources respectively.

2.1.4 Factors Affecting High Cell Density Fermentation

A variety of factors significantly influences the likelihood of success of high cell density cultivation. These include high levels of acetate, excess glucose concentration, poor oxygen transfer (or an oxygen-limiting condition), poor mixing, high levels of carbon dioxide, and excessive heat generation.

Acetate is produced when *E. coli* is cultivated under anaerobic or oxygen-starved conditions. However during aerobic fermentations, *E. coli* can produce acetate if excess glucose is present in the culture (El-Mansi and Holms, 1989; Luli and Strohl, 1990; Kleman and Strohl, 1994). Acetate concentrations above 5 g/L (pH 7) reduce growth rate, biomass yield, and maximum attainable cell concentrations (Pan *et al.*, 1987; El-Mansi and Holms, 1989; Luli and Strohl, 1990; Bech Jensen and Carlsen, 1990; Han *et al.*, 1992). Moreover, high acetate concentration significantly reduces recombinant protein production (Bech Jensen and Carlsen, 1990; MacDonald and Neway 1990; Shimizu *et al.*, 1992). This detrimental effect is enhanced for recombinant cells compared to non-recombinant cells (Koh *et al.*, 1992). In general, the specific growth rate and the medium used in fermentation affect the formation of acetate (Lee, 1996). A critical specific growth rate exists for acetate formation and this varies with the strains and medium used (Lee, 1996). For example, acetate production commences when the specific growth rate exceeds 0.2 and 0.35 h^{-1} in the presence of complex and defined media respectively (Meyer *et al.*, 1984; El-Mansi and Holms, 1989; Paalme *et al.*, 1990).

Acetate formation can be avoided or suppressed by several approaches. First, the specific growth rate may be controlled below the critical specific growth rate by limiting essential nutrients such as carbon or nitrogen. Second, medium formulation may be altered. For example, acetate is not produced if glycerol provides carbon source (Holms, 1986). Unfortunately, cells grow more slowly using glycerol (Holms, 1986; Korz *et al.*, 1995) and glycerol is more expensive than glucose. Last, metabolic engineering can be used to alter the cell ability to form acetate. For example,

mutation or recombinant DNA technology can be used to create cells that are deficient of enzymes phosphotransacetylase and/or acetate kinase. These enzymes are responsible in formation of acetate from acetyl-CoA (Brown *et al.* 1987). Another strategy is to reduce acetate formation by diverting the flow of catabolic carbon to the production of less toxic metabolites such as ethanol (Ingram *et al.*, 1987) and acetoin (Aristidou *et al.*, 1994).

Glucose is commonly exploited as the carbon source. It is fed to the fermenter to provide sufficient nutrient for cell growth. High level of glucose may accumulate in the culture media when the consumption rate by cells is less than the feeding rate of glucose to the fermenter. High glucose concentration (> 50 g/L) inhibits cell growth (Riesenberg, 1991a) and promotes acetate formation (El-Mansi and Holms, 1989; Luli and Strohl, 1990; Kleman and Strohl, 1994). This problem can be solved for example, by altering feeding strategies to constrain glucose concentration below the critical concentration during fermentation. Exponential feeding strategy appears to be effective as it allows maintenance of a constant low glucose concentration throughout fermentation. Unfortunately, this solution is not a universal panacea and each case must be considered separately.

As the cell concentration becomes high, oxygen often becomes the limiting nutrient. Oxygen transfer can be improved by increased aeration and agitation. However , this only can be done to a certain limit. Another alternative is to employ oxygen-enriched air or pure oxygen. However, pure oxygen is expensive thereby increasing production cost. Furthermore, fermentation can be conducted under pressurise to improve oxygen solubility/transfer (Strandberg and Enfors, 1991). It is also possible to lower the oxygen demand by operating fermentation at low specific growth rate (Lee, 1996). The oxygen limiting problem in high cell density culture is generally solved by a coordination of such strategies.

Mixing often becomes a limiting factor in maintaining fermenter homogeneity as viscosity increases with cell concentration. The distribution of oxygen and nutrients throughout fermenter is strong affected by poor mixing. This may significantly

decrease productivity. Improved design can alleviate this problem, for example using better impeller design and installing baffle in fermenter.

Carbon dioxide (CO_2) is also produced as a result of cell growth. As the cell concentration increases, carbon dioxide released likewise increases. High level of carbon dioxide may result in problems. Partial pressure of CO_2 in excess of 0.3 atm decreases cell growth and promotes acetate formation (Mori *et al.*, 1979; Pan *et al.*, 1987). Fermentation operation under pressurised condition will promote higher carbon dioxide concentration as the solubility of CO_2 increases with pressure.

Significant energy is released during high cell density fermentation. The main sources of energy release are mechanical degradation from agitation (at high rate) and metabolic energy release from cells (Lee, 1996). Heat generation can be reduced by growing cells at a reduced specific growth rate (Lee, 1996). Improved design of cooling system can solve this problem.

2.2 MATERIALS AND METHODS

2.2.1 Strains and Growth

E. coli strain JM101 [SupE thiD (lac$^-$ proAB) F'[traD36 proAB$^+$ lacI^q lacMZ M15]] containing the strictly-regulated plasmid p[Met^1]-pGH(1-11)-Val-Asn-[Arg^3]-IGF-1 (Francis *et al.*, 1992) was grown on a modified C1 media agar plate (containing 100 mg Amp/L) and incubated at 37°C for 24 h.

2.2.2 Shake Flask Culture

An inoculum for the fermenter was prepared in a shake flask containing 20 mL of sterile modified C1 media. The shake flask was inoculated with a single colony from the plate, then incubated at 37°C in a shaker at 200 rpm for 11 hours.

2.2.3 Fed-batch Fermentation

Fermentation was conducted in a 20-L fermenter (Chemap-Fermenter CF2000, Chemap AG, Mannedorf, Switzerland) with an initial volume of 12 L of modified C1 media. A volume of inoculum was added to the fermenter and left overnight to yield 2.4 g CDW/L on the following day. The pH of the culture was maintained constantly at 6.9 using 25% ammonia solution. Temperature was 37°C and dissolved O_2 concentration (DOC) exceeded 60% saturation. Aeration was switched to oxygen-enriched air (mixture of 25% air and 75% oxygen) when the DOC dropped below the 60% limit, at an approximate cell concentration of 3 g CDW/L. Nutrient feeding commenced following glucose exhaustion, at an approximate cell concentration of 13.5 g CDW/L. After 4 h of feeding, the culture was induced with 0.2 mM isopropyl-β-D-thiogalactopyranoside (IPTG) and the fermentation was terminated 5 h later.

Two different feeding strategies were adopted: constant-rate feeding and a novel 3-stage feeding strategy. For constant feeding, nutrient feed was supplied at a rate of 9.7 mL/min or 11.4 mL/min. The 3-stage feeding was PLC-controlled. A schematic graph of this novel 3-stage feeding strategy is summarised in Figure 2.2. The initial stage consisted of exponential feeding for 4 h to provide a constant specific growth rate of $\mu = 0.25\ h^{-1}$ prior to induction. Immediately following induction, a linearly-decreasing feed rate was used for 0.5 h, followed by exponential feeding for 4.5 h at a specific growth rate of $\mu = 0.1\ h^{-1}$.

Optical density (OD_{600}), dry cell weight (DCW), glucose concentration and acetate concentration were monitored throughout the fermentation. Cells were harvested following termination of fermentation process and stored in 2 L bottles then frozen (-20°C) for use in subsequent studies.

2.2.4 Analytical Methods

Glucose concentration was measured using a YSI analyser (2700 SELECT, Yellow Springs Instruments, USA). Acetate concentration was determined using an enzyme assay kit obtained from Boehringer Mannheim (Catalog Number: 148261). Inclusion body size was quantified using a Joyce Loebl Disc Centrifuge (Middelberg *et al.*, 1990). This is detailed in chapter 3 (section 3.2.1.1). Recombinant protein concentration was determined by High Performance Liquid Chromatography (Falconer *et al.*, 1997).

2.2.5 Modified C1 Media

D-Glucose.H_2O, 2.96 g/L (for shake flask) and 40.0 g/L (for fermenter); NH_4Cl, 2.58 g/L; KH_2PO_4, 2.54 g/L; Na_2HPO_4, 4.16 g/L; K_2SO_4, 1.94 g/L; $MgSO_4.7H_2O$, 0.67 g/L; $FeSO_4.7H_2O$, 20 mg/L; $MnSO_4.H_2O$, 5.0 mg/L; $ZnSO_4.7H_2O$, 8.6 mg/L; $CuSO_4.5H_2O$, 0.76 mg/L; trisodium citrate, 88 mg/L; thiamine, 48 mg/L.

2.2.6 Nutrient Feed

D-Glucose.H_2O, 620 g/L; KH_2PO_4, 5.3 g/L; Na_2HPO_4, 79.0 g/L; K_2SO_4, 45.0 g/L; $MgSO_4.7H_2O$, 8.24 g/L. In yeast extract-supplemented nutrient feed, the previous feed was supplemented with 65 g/L yeast extract.

2.3 RESULTS AND DISCUSSION

2.3.1 Constant-rate Feeding

Fermentation profiles for the constant-rate feeding strategy are presented in Figure 2.1. Glucose accumulated to high concentrations (up to 40 g/L) and relatively low cell-densities (21 g CDW/L, OD_{600} = 51) resulted. The highest OD_{600} previously achieved using this standard production method was approximately 80. High acetate accumulation following induction is also typically observed (Figure 2.1). An inclusion body size of 0.32 μm and a fusion-protein concentration of 2.6 g/L, corresponding to an actual IGF-1 concentration of 2.2 g/L, were obtained for the fermentation at a feed rate of 9.7 mL/min.

As expected, a higher cell concentration was achieved at a higher feed rate. An OD_{600} of 73.0 corresponding to 30.8 g CDW/L was obtained when the feed rate increased to 11.4 mL/min. Whereas, an OD_{600} of 50.8 corresponding to 21.6 g CDW/L was achieved at the lower feed rate of 9.7 mL/min. Glucose accumulated to similar high levels (i.e. 40.7 g/L and 35.8 g/L) for feed rates of 9.7 mL/min and 11.4 mL/min, respectively. These values approached the critical concetration (50 g/L). However, acetate accumulation was much higher at increased feed rates, i.e. 126.6 mM at feed rate of 11.4 mL/min compared to 44.8 mM at feed rate of 9.7 mL/min. Acetate accumulation exceeded the critical concentration (5 g/L or 83.3 mM) at the higher feed rate. The high levels of glucose and acetate accumulation limit further improvement in fermentation productivity. An alternative feeding strategy was proposed to reduce glucose and acetate accumulation in the culture and to increase cell concentration.

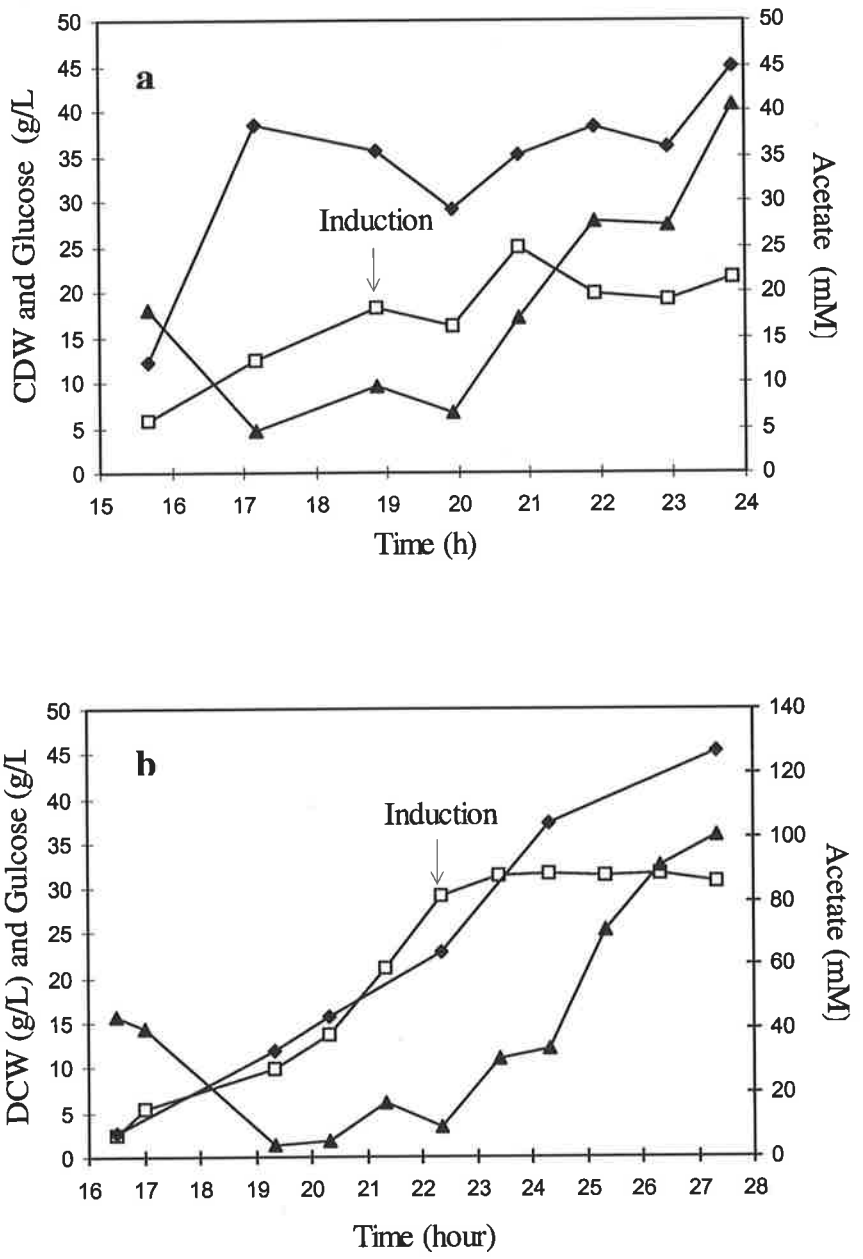

Figure 2.1 Fed-batch fermentation profiles using constant-rate feeding. (□) dry cell weight (DCW), (♦) acetate concentration, (▲) glucose concentration. (**a**) feed rate = 9.7 mL/min; (**b**) feed rate = 11.4 mL/min.

2.3.2 Novel Three-Stage Feeding Strategy

The high acetate and glucose concentrations in Figure 2.1 result from a rapid decrease in specific growth rate following induction (Lee and Ramirez, 1992). A feeding strategy employing three different stages was therefore designed to overcome this problem.

- Stage 1: a high specific growth rate (0.25 h^{-1}) was employed to generate a high cell density before induction and hence a large cell population for the production of recombinant protein.
- Stage 2: a rapidly-decreasing feedrate designed to approximate the rapid drop in metabolic activity following IPTG induction was employed.
- Stage 3: the lower and variable metabolic activity following induction was accounted for with a glucose feed rate designed to support a constant specific growth rate of 0.1 h^{-1}.

The feed profile is summarised in Figure 2.2. Stages 2 and 3 are an approximation to the changes in growth rate observed due to induction shock as described by the shock-recovery model of Lee and Ramirez (1992).

The fermentation profiles for 3-stage feeding are presented in Figure 2.3a. An OD_{600} of 150, corresponding to a dry cell weight of 42 g/L, was achieved. This was nearly double that obtained using constant-rate feeding. Glucose accumulation in fermentation broth was decreased to 6.2 g/L, approximately 15% of the glucose level using constant-rate feeding. Clearly, this method overcomes glucose accumulation problems. Following induction, acetate gradually accumulated and reached a level of 44 mM at the end of fermentation. This acetate concentration remained excessive. However, it could be reduced by further optimisation of the feed profile. For example, the drop in metabolic activity post induction could be better approximated using three stages: a linearly decreasing stage; a stage with $\mu = 0.1\ h^{-1}$; and a stage with some constant $\mu < 0.1\ h^{-1}$.

A recombinant protein concentration of 4.3 g/L corresponding to an actual IGF-1 concentration of 3.6 g/L was achieved, with an inclusion body size of 0.33 μm. The

recombinant protein concentration was much higher than that obtained using constant-rate feeding. Unfortunately, no improvement in inclusion body size was observed. This suggests the increase in total product is solely due to the increased biomass concentration. There are several possible reasons why we did not see an increase in the specific ratio of product to biomass. Further optimisation of the feed profile to restrict acetate below the inhibitory concentration may be necessary. Optimisation of other key parameters (e.g., IPTG concentration) may also be necessary, although previous tests suggest relative insensitivity (data not shown). Translational limitation for this strong promoter have previously observed (Jorgensen *et al.*, 1997), so this is a likely limit to further productivity increases. To test this, a 3-stage fed-batch fermentation with yeast-extract-supplemented nutrient feed after induction was conducted.

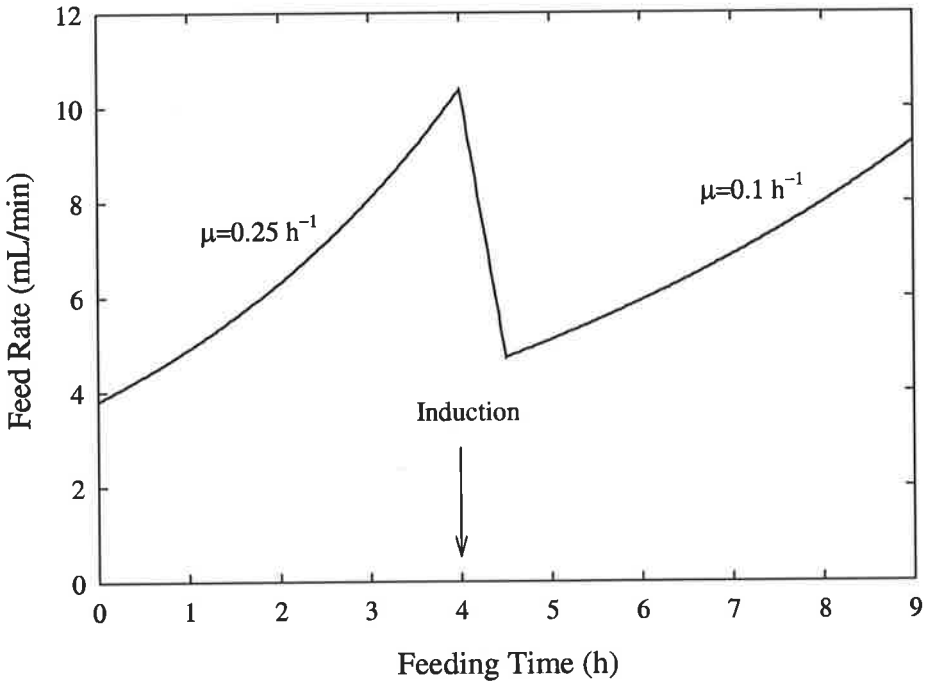

Figure 2.2 The novel 3-stage feeding strategy.

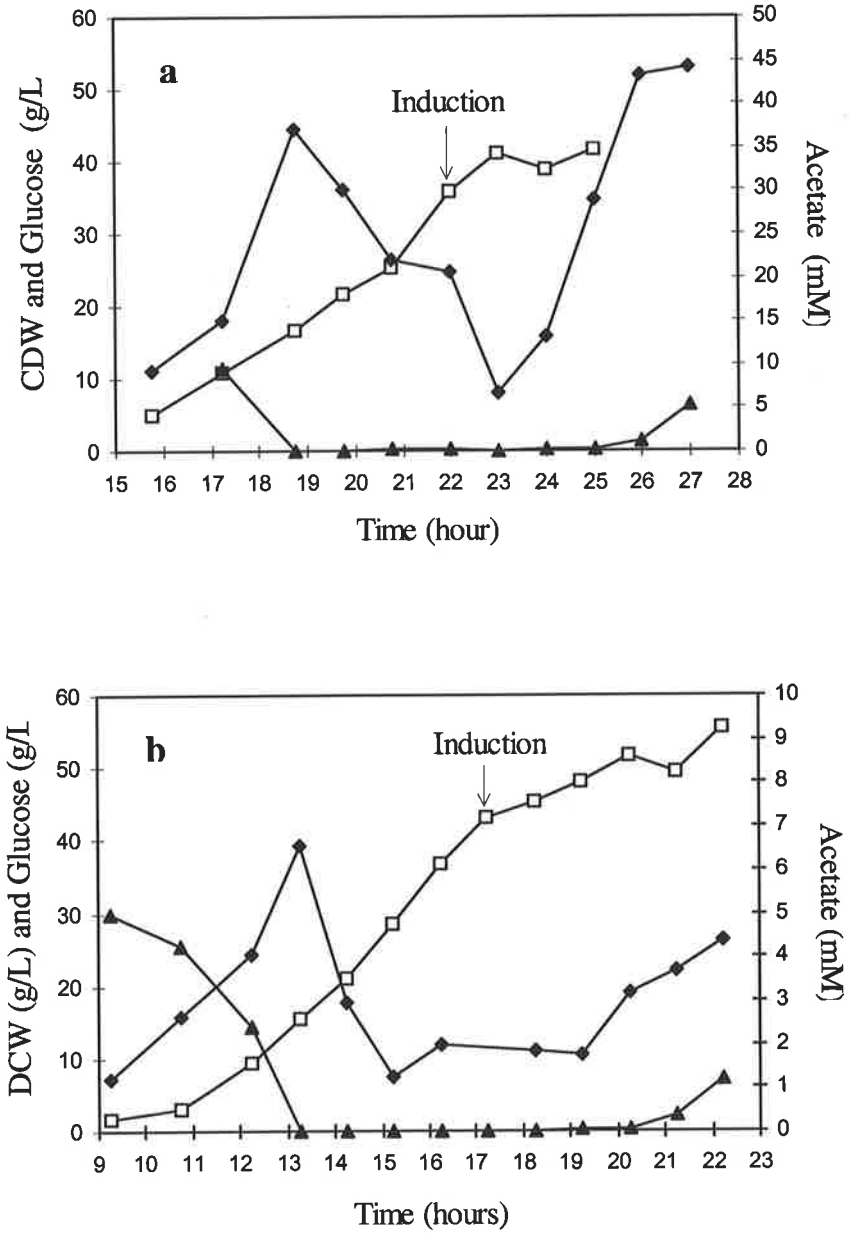

Figure 2.3 Fed-batch fermentation profiles using exponential feeding. (□) dry cell weight (DCW), (♦) acetate concentration, (▲) glucose concentration. (**a**) without yeast-extract supplementation; (**b**) with yeast-extract supplementation.

Fermentation profiles for exponential feeding with yeast-extract-supplemented nutrient are presented in Figure 2.3b. An OD_{600} of 163, corresponding to a dry cell weight of 56 g/L, was achieved. This was higher than that obtained using exponential feeding without yeast extract supplementation. Glucose accumulation was reduced to a level of 7.3 g/L. After induction, acetate gradually accumulated and reached a level of 4.4 mM at the end of fermentation. This is much lower than for the previous fermentations. A recombinant protein concentration of 3.7 g/L, corresponding to an IGF-1 concentration of 3.0 g/L, and an inclusion body size of 0.32 μm were achieved. Yeast extract supplementation did not improve inclusion body size. A lower recombinant protein level was also obtained. The presence of yeast extract may enhance the growth of cells and thus reduce the rate of protein expression, or may simply alter the amino acid balance. This will influence the metabolic flux through amino acid pathways and may reduce overall protein expression.

Table 2.2 Summary of fermentation results

Parameters	Feeding Strategies			
	Constant rate		3-stage	3-stage, YE*
	A	B		
Optical Density (OD_{600})	50.8	73.0	150.0	163.0
Cell Dry Weight (g CDW/L)	21.6	30.8	41.8	55.6
Glucose concentration (g/L)	40.7	35.8	6.2	7.3
Acetate concetration (mM)	44.8	126.6	44.3	4.4
Fusion-protein concentration (g/L)	2.6	-	4.3	3.7
Actual IGF-1 concetration (g/L)	2.2	-	3.6	3.0

** with yeast extract supplement*
A: feed rate = 9.7 mL/min
B: feed rate = 11.4 mL/min

2.4 CONCLUSION AND RECOMMENDATION

A summary of the fermentation results is presented in Table 2.2. This work details the novel 3-stage feeding procedure improved the productivity of IGF-1 fusion protein using recombinant *E coli* JM101. Glucose and, consequently, acetate accumulation were greatly decreased. Recombinant fusion protein concentration was increased from 2.6 g/L to 4.3 g/L, corresponding to an actual IGF-1 concentration of 3.5 g/L. However, inclusion body size was not altered by the novel feeding strategy nor by the supplementation of yeast extract. Further investigation of factors altering inclusion body size and protein expression level, and further optimisation of the feeding strategy, has the potential to further increase the already-high IGF-1 concentration achieved in this study.

Chapter 3

ELECTROPHORETIC MOBILITY AND PARTICLE CHARACTERISTICS

Physicochemical properties play an important role in the bioprocessing, particularly in the downstream processing. These properties can be manipulated to improve existing techniques or to design new technologies for downstream processing. Unfortunately, only scant information on the physicochemical properties of inclusion bodies is available in the literature. This study aims to fill this gap. Electrophoretic mobility and particle characteristics of inclusion bodies are studied using various methods, including micro-electrophoresis, sodium dodecyl sulphate polyacrylamide gel electrophoresis (SDS-PAGE), scanning electron microscopy (SEM) and atomic force microscopy (AFM).

3.1 ELECTROPHORETIC MOBILITY

3.1.1 Background

The electrokinetic potential of fine particles is normally characterised as a zeta potential (ζ, mV) derived from electrophoretic mobility (u_E , $m^2/V.s$) measurements using the classical Helmholtz-Smoluchowsky relationship as follows:

$$u_E = \frac{\varepsilon}{\eta}\zeta \tag{3.1}$$

where $\varepsilon = \varepsilon_r\varepsilon_0$, in which ε_r and ε_0 are the relative dielectric constant of the electrolyte solution and the dielectric constant of vacuum respectively, and η is the viscosity of the solution. The following assumptions are necessary to derive this correlation: the radius of curvature of the particle surface is large compared to the Debye-screening length (κ^{-1}), the particle surface is nonconducting, the applied electric field strength and the field of the double layer are additive, the charge is homogeneously distributed over the particle surface and the viscosity, dielectric constant, and ion conductivities in the double layer, outside the plane shear, are equal to their bulk values (van der Wal, 1997). However, in complex colloidal systems such as protein inclusion bodies and cell debris, these underlying assumptions are easily violated. Hence, electrophoretic mobility provides a better descriptor of surface properties in these systems. A detailed discussion of this topic is beyond the scope of this work but it is readily available in the literature (Hunter, 1981 & 1986; Lyklema, 1995).

Electrokinetic or zeta potential is the average electrostatic potential of a solid surface which is measured at the surface of the shear layer (an imaginary surface which is considered to lie close to the solid surface and within which the fluid is stationary). It is usually denoted by the Greek symbol, zeta (ζ) (Hunter, 1981). Zeta potential can be measured from four different electrokinetic effects: electrophoresis, electro-osmosis, streaming potential, and sedimentation potential (for details, see Hunter, 1981). Zeta potential is very important in flotation processes because it is a quantitative measure

of the ability of the particle to be floated. Flotation is strongly affected by the surface charge (or ζ) of both the particles and the bubbles (Collins and Jameson, 1977; Okada *et al.*, 1990). The zeta potential of bubbles has been described in section 1.3.3 therefore this section will focus on protein inclusion body and cell debris particles.

The surface charge of solids is controlled by ionic species. Ionic species that exert a fundamental control on the surface charge and the dispersed phase are known as potential determining ions (p.d.i.). In other words, these ions are the ions that generate the surface charge. In general, the surface properties of oxides and proteins are primarily influenced by pH and by the salt concentration to a lesser extent (Hunter, 1993). Therefore, the simple H^+ and OH^- ions are the p.d.i. for oxides and proteins. Ionic species that do not specifically interact with the surface are called indifferent ions. These ions do not govern the surface charge but they may be involved in the extension of the double layer out into the solution (Hunter, 1981). Other ionic species enter the inner part of the double layer and undergo a specific interaction with the surface. These are referred to as specifically adsorbed ions. The adsorption of these ions at the surface is affected by forces (chemical and physical) other than simply by the electrical potential (Hunter, 1981).

At a certain bulk concentration of p.d.i., the net surface charge is zero. This is referred to as the point of zero charge (p.z.c.). This point is determined by a direct measurement of the surface charge as a function of p.d.i. concentrations. Another important point called the isoelectric point (i.e.p.) is obtained by adjusting the p.d.i concentration until the zeta potential equals zero. These points may or may not be coincident. Fig.3.1 illustrates that changes in indifferent electrolyte concentrations do not affect the i.e.p. but they alter the zeta potential at other p.d.i. concentration (Hunter, 1981).

The difference between specifically adsorbed ions and indifferent ions is that specifically adsorbed ions can reverse the sign of the zeta potential and may cause a shift in the p.z.c. as the ion concentration is increased, whereas indifferent ions can only reduce the zeta potential asymptotically to zero (Hunter, 1981; 1993). The

forces involved in specific adsorption may be either chemical or physical. Physically adsorbed ions do not influence the p.z.c. or i.e.p. however they can reverse the sign of zeta potential. Chemically adsorbed ions can shift the p.z.c. and can remain adsorbed even when the underlying surface has the same sign. These phenomena can be seen in Figure. 3.2. An increase in concentration of the specifically adsorbed ions produces an increase in positive charge at a fixed concentration of p.d.i. This causes a shift in the p.z.c. to lower concentrations of the positive potential determining ions, for example to high pH for oxides and proteins (Hunter, 1981). Similarly, specifically adsorption of anions produces a shift with opposite direction which tends to make zeta potential more negative. The point at which zeta potential changes its sign is called zeta potential reversal (p.z.r.) when it is caused by a specific adsorption process (Hunter, 1981).

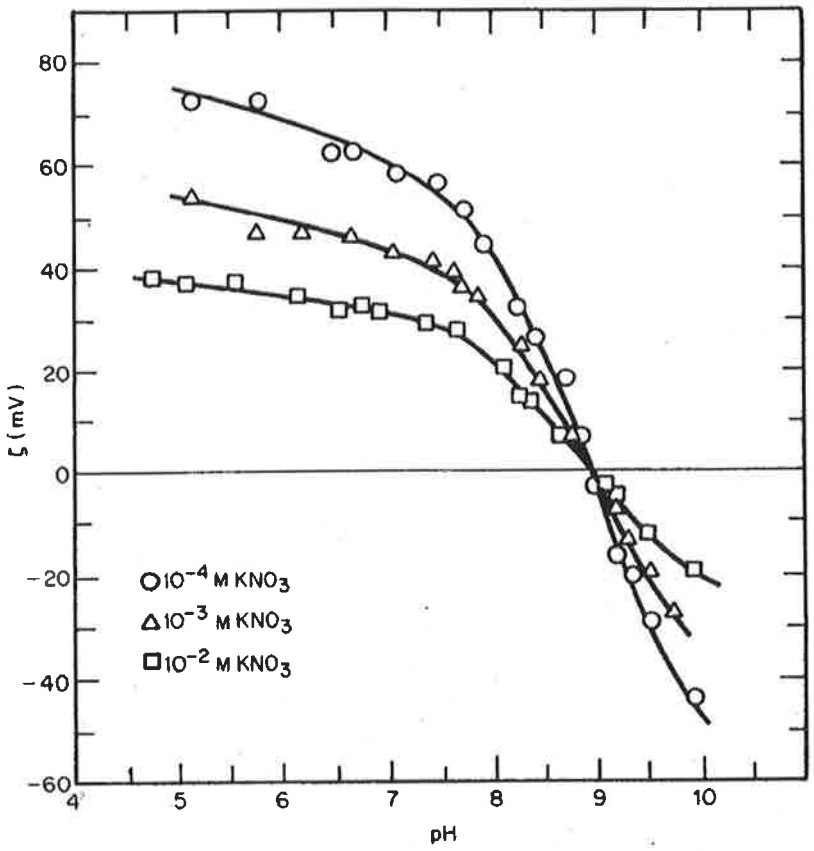

Fig. 3.1 The variation of zeta potential of 0.05 g/L TiO_2 colloid as a function of pH in aqueous solutions of KNO_3 (indifferent electrolyte) at 25°C (after Wiese and Healy,1975, taken from Hunter, 1981)

Bubble/particle attachment is facilitated by hydrophobic interactions. Therefore, an understanding of the hydrophobicity of particles is an important factor in the design of flotation processes. The hydrophobicity of particles can be measured in term of contact angle, as described in section 1.3.2.4, and electrophoretic mobility. The smaller the magnitude of electric mobility of particles the more hydrophobic the particles as there are less electrostatic interactions that can be made with water. Hence, maximum hydrophobicity is achieved when electrophoretic mobility equals zero.

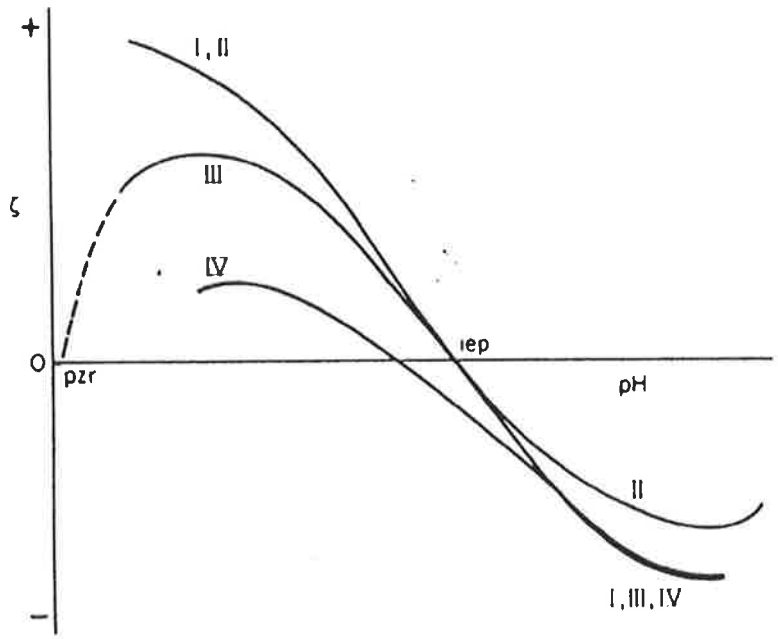

Fig. 3.2 Zeta potential of an oxide at various pH values in the presence of different types of electrolyte: I: indifferent electrolytes; II: physically adsorbed cation; III: physically adsorbed anion; IV: chemically adsorbed anion (after Fuerstenau, taken from Hunter, 1981)

Flotation processes are better operated with the electrophoretic mobility of particles equivalent to zero. This hypothesis is supported by the results of a study conducted by Collins and Jameson (1977). They found that the maximum flotation rate was achieved when the zeta potential of the particles equalled zero. They argued that coalescence between bubbles and the particles is inhibited by double layer repulsion as the charge on the particles and the bubble increases. Moreover, coagulation of

particles can occur prior to flotation when the zeta potential is zero (Collins and Jameson, 1977). This is beneficial for flotation of colloidal particle as larger particles are formed as a result of coagulation. However, this is undesirable when selective separation between two different colloidal particles is the goal (Collins and Jameson, 1977). It is essential to ensure that the particles have a sufficient charge to prevent coagulation but not large enough to inhibit collision through double layer repulsion. A charge of around 20 mV is considered optimal (Collins and Jameson, 1977).

It is clear that electrophoretic mobility is an important factor for successful flotation processes. Therefore a map of electrophoretic mobility as a function of pH and ionic strength has been undertaken. This information deduced from this work may be used to characterise flotation behaviour and suggest avenues for possible improvement.

3.1.2 Materials and Methods

3.1.2.1 *Inclusion Body Purification*

Two litres (2 L) of stored, frozen fermentation broth were thawed. Cells were harvested by centrifugation (Beckman Centrifuge Model J2-21M) at 11,000 *g* for 10 min, followed by resuspension in 2 L buffer solution containing 20 mmol/L Tris(hydroxymethyl)aminomethane Base (Tris Base) and 50 mmol/L NaCl at pH 8.5 (HCl was added to adjust pH). Next, the suspension was homogenised (7 passes in a 15MR APV Gaulin high-pressure homogenizer (CD valve) at 55.2 MPa). Homogenate was centrifuged at 11,000 *g* for 15 min and resuspended in 2 L buffer (20 mmol/L Tris Base and 5 mmol/L EDTA, pH 8.0) to give a suspension for further purification by three different strategies:

- ***Procedure A:*** Urea granules were added to the suspension to a final concentration of 2 M. The suspension was then centrifuged at 11,000 *g* for 10 min. The pellet was washed twice with buffer solution (20 mmol/L Tris Base, pH 7.5).
- ***Procedure B:*** A pellet produced according to procedure A was suspended in buffer solution (20 mmol/L Tris Base, pH 7.5). Triton X-100 was added to a final

concentration of 2% (v/v). The suspension was centrifuged at 11,000 *g* for 10 min then washed twice with buffer solution (20 mmol/L Tris Base, pH 7.5).

- ***Procedure C:*** This (standard) procedure commenced by incubating the suspension for 3 h at 20°C following addition of lysozyme to a final concentration of 0.02% (w/v). The inclusion bodies were collected by centrifugation (11,000 *g* for 15 min) and suspended in a buffer solution (20 mmol/L Tris Base, pH 7.5) followed by addition of Triton X-100 to a final concentration of 2% (v/v). Treated inclusion bodies were washed twice with buffer solution (20 mmol/L Tris Base, pH 7.5).

Some of the final inclusion bodies pastes from each procedure were frozen for other analysis (SDS-PAGE and AFM) and the rest was resuspended in 250 mL Milli-Q water adjusted to pH 7.5 using KOH solution followed by dialysis against 2 L Milli-Q water at pH 7.5 (5 h, 4 times, pH adjusted by KOH addition) for electrophoretic mobility measurements.

3.1.2.2 *Cell Debris Purification*

A similar procedure using a fed-batch fermentation was performed in the absence of an induction process to produce inclusion body-free cells. An optical density (at 600 nm) of 160 was achieved. The fermentation broth was stored in two litres bottles at - 20°C which was then used for cell debris samples.

Two litres (2 L) of frozen inclusion body-free fermentation broth were thawed. Cells were harvested by centrifugation at 11,000 *g* for 10 min followed by resuspension in 2 L buffer solution (20 mmol/L Tris Base and 5 mmol/L EDTA, pH 8.0). The suspension was then homogenized at 55.2 MPa using 7 passes. Cell debris was collected by centrifugation and washed twice using Milli-Q water at pH 7.5 followed by dialysis against 2 L Milli-Q water at pH 7.5 (5h, 4 times). KOH solution was added to adjust pH of Milli-Q water.

3.1.2.3 *Sample Preparation and Electrophoresis*

Electrophoretic mobility was measured at different pH, in the presence of different electrolytes (KNO_3, $Mg(NO_3)_2$, K_2SO_4, and $Mg(SO_4)$) at different salt concentrations (0.001 N, 0.01 N, 0.05 N, and 0.1 N). In each case, 400 µL of dialysed inclusion body or cell-debris suspension was added to 1 L of electrolyte solution. KOH or HNO_3 solutions were added to adjust pH. Then the sample was left for 1.5 h to equilibrate with room temperature (20°C). Electrophoretic mobility was measured using a ZetaMaster (Malvern Instruments Ltd., Worcestershire, UK). Ten measurements were taken for each sample and an average was calculated.

3.1.2.4 *Sodium Dodecyl Sulfate Polyacrylamide Gel Electrophoresis (SDS-PAGE)*

The purity of protein inclusion body paste was analysed by Sodium Dodecyl Sulfate-Polyacrylamide Gel Electrophoresis (SDS-PAGE) according to the Laemmli method (Laemmli, 1970). Briefly, 0.2 g of sedimented wet protein inclusion body paste was resuspended in 1 mL Milli-Q water and mixed thoroughly. 100 µL of this suspension was diluted with 400 µL of sample buffer (62.5 mmol/L Tris-HCl pH 6.8, 20% (v/v) glycerol, 2% SDS, 5% β-mercaptoethanol, 0.025% bromophenol blue) and boiled for 4 min prior loading into the gel wells. Electrophoresis was conducted using a PROTEAN® IIxi vertical electrophoresis cell with a 15% acrylamide separating gel and a 4% stacking gel according to the standard operating procedure supplied by Bio-Rad Laboratories (Sydney, Australia). All consumables and instruments were obtained from Bio-Rad Laboratories (Sydney, Australia).

3.1.3 Results and Discussion

3.1.3.1 *Electrophoretic Mobility*

The electrophoretic mobility of protein inclusion bodies and cell debris in different electrolyte solution as a function of pH and electrolyte concentration is summarised in Figures 3.3 and 3.4. As expected, increasing the electrolyte concentration decreases the magnitude of electrophoretic mobility for both protein inclusion bodies and cell debris due to electrical double-layer compression (Hunter, 1981). Only the effects of monovalent and divalent ions (K^+, Mg^{2+}, NO_3^- and SO_4^{2-}) on electrophoretic mobility were measured. Trivalent cations were not investigated as they induced precipitation in the pH range studied. Electrophoretic mobility measurement of protein inclusion bodies in the presence of $Cr(NO_3)_3$ was unstable due to precipitation (Figure 3.5).

The sub-plots in Figure 3.3 demonstrate that divalent cations and anions compress the electrical double layer more than monovalent ions at the same concentration. The magnitude of electrophoretic mobility is lowered in the presence of divalent ions. For example, inclusion body electrophoretic mobility is reduced more by the divalent cation Mg^{2+} than by the monovalent cation K^+ (Figure 3.3, KNO_3 and $Mg(NO_3)_2$). Furthermore, the divalent cation produced a more significant effect in the region where the net surface charge is negative (pH > 6). Likewise, the presence of divalent anion SO_4^{2-} reduced the inclusion body electrophoretic mobility magnitude more than a monovalent one (NO_3^-), and a stronger effect occurred in the region where the net surface charge is positive (Figures 3.3, K_2SO_4 and $MgSO_4$). The lowest eletrophoretic mobility was observed in the presence of both a divalent cation Mg^{2+} and a divalent anion SO_4^{2-} (Figure 3.3, $MgSO_4$).

Specific adsorption of anions and cations occurred as illustrated by the shift in the common intersection point (c.i.p.) of the curves (Lyklema, 1995). Adsorption of an anion shifts the c.i.p. towards the region of increased negative charge (Figures 3.3, KNO_3 and K_2SO_4). Likewise, specific adsorption of a cation shifts the c.i.p. towards the region of positive charge (Figures 3.3, $Mg(NO_3)_2$ and $MgSO_4$). Specific divalent

cation adsorption counterbalances the effect of specific anion adsorption and returns the c.i.p. to zero charge (Figures 3.3, $Mg(NO_3)_2$ and $MgSO_4$), whereas the c.i.p. shifts towards negative charge in the presence of monovalent cation (Figures 3.3, KNO_3 and K_2SO_4). This evidence demonstrates that anion specific adsorption effects are more dominant than monovalent cation specific adsorption effects and divalent cation specific adsorption effects are as strong as anion specific adsorption effects. Also, a divalent cation produced more pronounced effects on electrophoretic mobility than a monovalent cation.

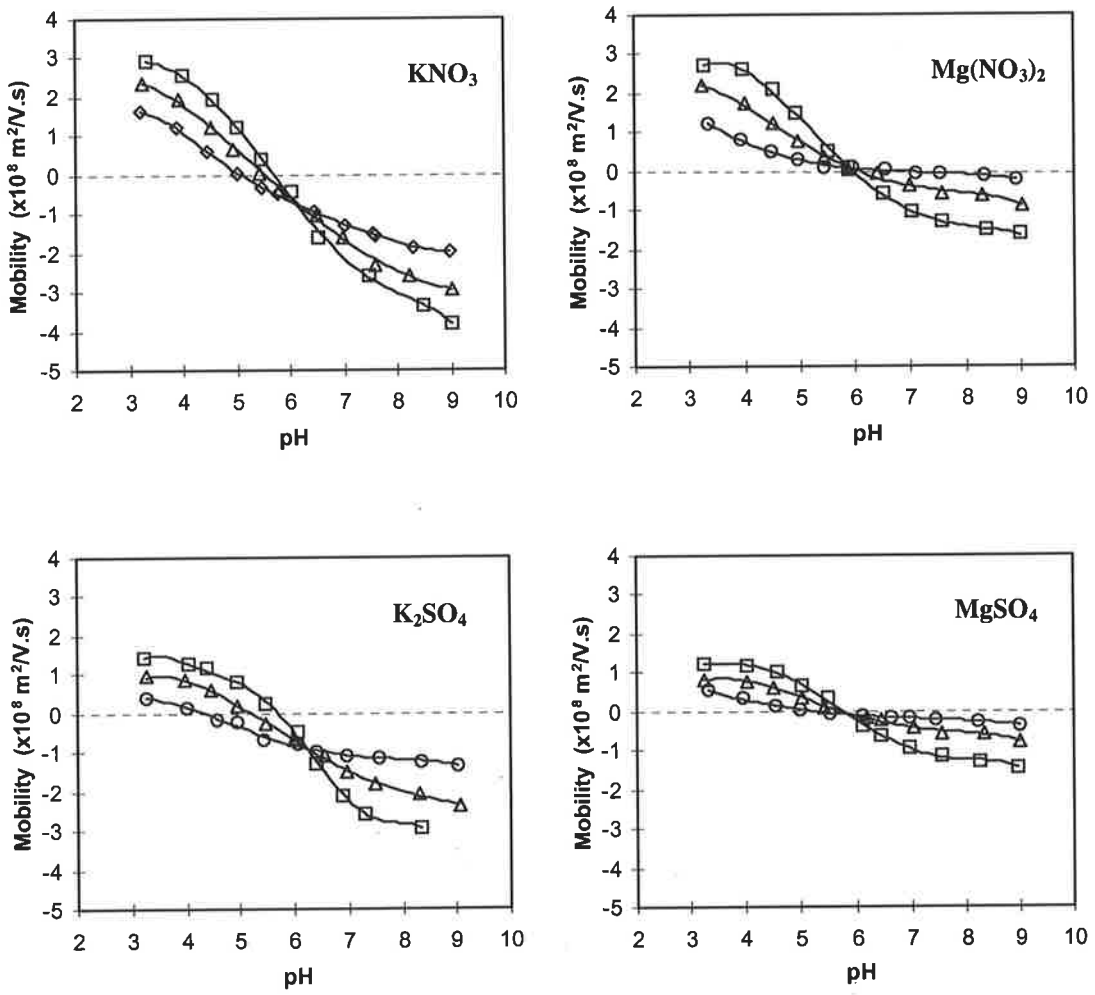

Figure 3.3 Electrophoretic mobility of protein inclusion bodies as a function of pH measured in different electrolytes and various electrolyte concentrations: (□) 0.001 N, (Δ) 0.01 N, (◊) 0.05 N, (○) 0.1 N.

The cation and the anion both affect the electrophoretic mobility of the cell debris. However, the effect of anions on the cell debris was not as great as for protein inclusion bodies (Figure 3.4). This may be a consequence of the cell debris possessing a strong negative charge. Again, the presence of the divalent cation produces a stronger effect than that for the monovalent cation as confirmed by a comparison of Figures 3.4, KNO_3 and K_2SO_4 to Figures 3.4, $Mg(NO_3)_2$ and $MgSO_4$ respectively. Specific adsorption of cations and anions was detected and similar trends to those occurring in protein inclusion bodies were observed.

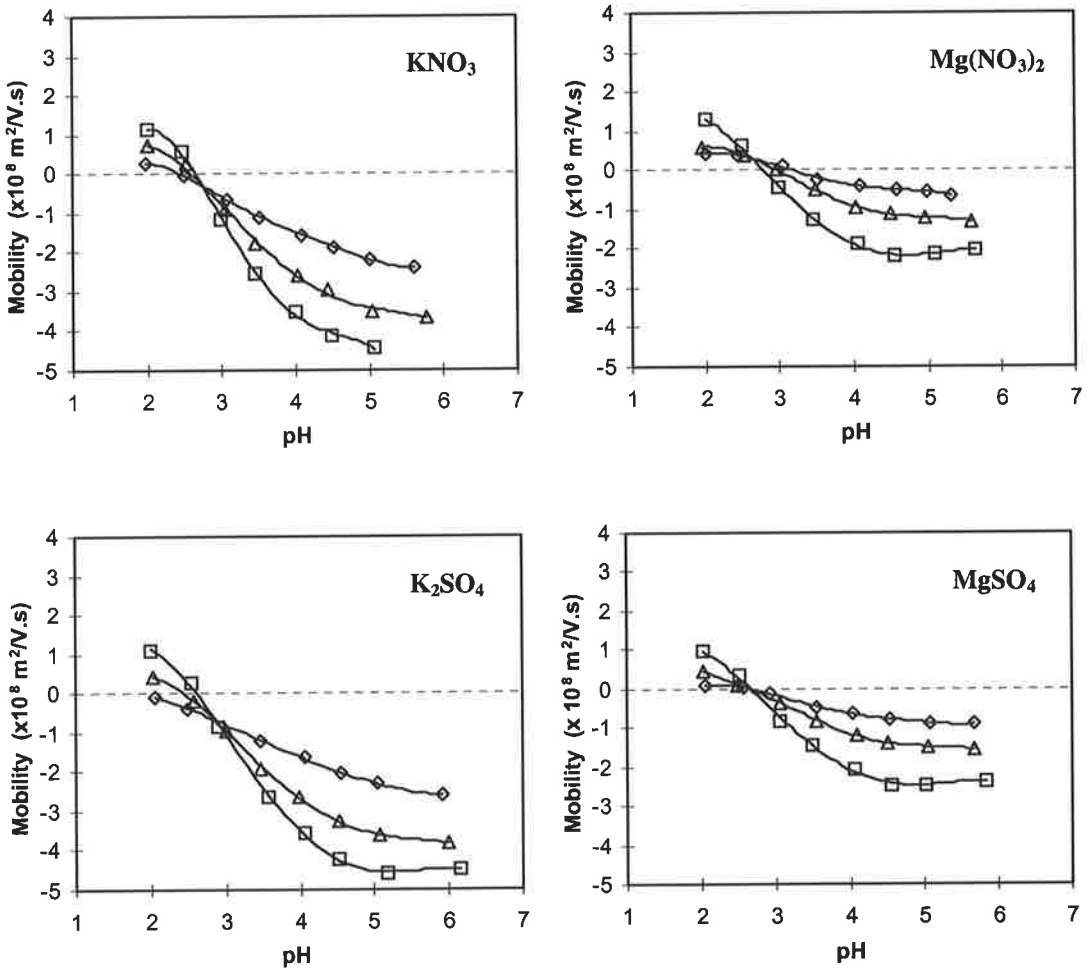

Figure 3.4 Electrophoretic mobility of cell debris as a function of pH measured in different electrolytes and various electrolyte concentrations: (□) 0.001 N, (Δ) 0.01 N, (◊) 0.05 N

The measured isoelectric points of protein inclusion bodies and cell debris in different electrolytes at various electrolyte concentrations are summarised in Table 3.1. Cell debris possess a much lower isoelectric point (eg. 2.7 in 0.001 M KNO_3) than protein inclusion bodies (eg. 5.7 in 0.001 M KNO_3). The difference (ΔpI) is approximately 3 units. It suggests that cell debris is strongly negatively charged when compared to the protein inclusion bodies. This difference is significant and may be exploited to enable fractionation of protein inclusion bodies from cell debris using, for example, a flotation cell.

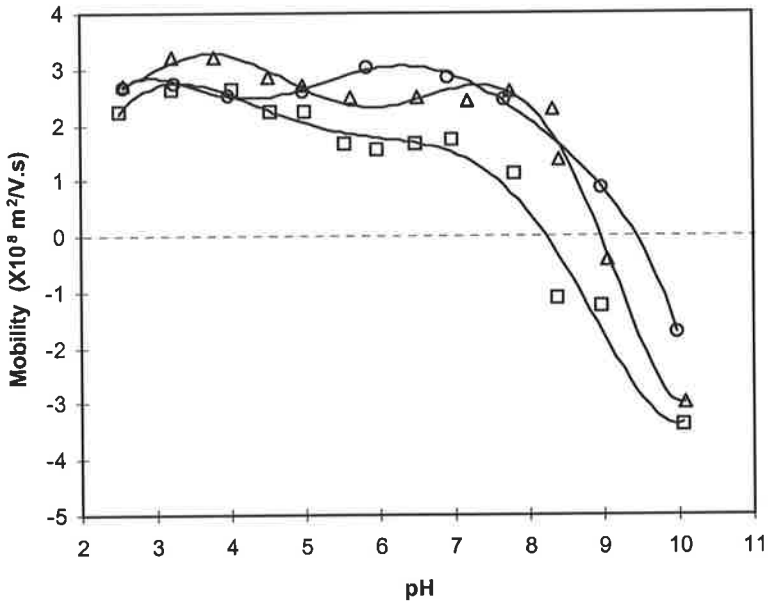

Figure 3.5 Electrophoretic mobility of protein inclusion bodies as a function of pH measured in various $Cr(NO_3)_3$ concentrations: (□) 0.001 N, (Δ) 0.01 N, (◊) 0.05 N

The isoelectric point (i.e.p.) of pure protein inclusion bodies (insulin-like growth factor analog LR^3-IGF-1) calculated using ANGIS program is approximately 9 (Milner, 1999). This value is much higher than isoelectric point obtained from the current micro-electrophoresis measurements (i.e.p. below 6). It is also possible that a direct comparison between the i.e.p. of purified inclusion bodies and pure protein is not possible due to surface orientation of charged amino acid groups. It is, however, more likely that the presence of contaminants including membrane proteins, plasmid

encoded proteins, phospolipids, polysaccharides, and nucleic acids (Kane and Hartley, 1991) are responsible for the observed lowering of isoelectric points. This postulate was confirmed from the results of SDS-PAGE analysis which demonstrated that the protein inclusion bodies used in electrophoretic mobility measurements contain some residual contaminants (Figure 3.7, lane 5). It is likely that such contaminants are bound tightly to the surface of protein inclusion bodies (Kane and Hartley, 1991) and hence they are retained on the surface despite the cleaning processes. Another possibility is that the contaminants are entrapped when inclusion bodies are formed (Paul *et al.*, 1983). Different cleaning strategies were undertaken and the properties of the resulting inclusion bodies were measured. The results presented in Table 3.2 demonstrate that differences in isoelectric points do occur, and consequently the i.e.p. is very sensitive to the extent of inclusion body cleanliness. Hence, we examined the feasibility of using sensitive i.e.p. measures to assess inclusion body purity.

Table 3.1 Isoelectric points of protein inclusion bodies and cell debris in different electrolyte and electrolyte concentrations.

Substances	Electrolyte Concentration ($\times 10^{-3}$ N)	Iso electric points (i.e.p.)			
		KNO_3	$Mg(NO_3)_2$	K_2SO_4	$MgSO_4$
protein inclusion bodies	1	5.7	5.9	5.7	5.8
	10	5.5	5.9	5.3	5.8
	100	5.1*	5.9	4.4	5.8
cell debris	1	2.7	2.8	2.6	2.7
	10	2.6	3.0	2.4	2.7
	100	2.5	3.1	< 2	2.7

*electrolyte concentration: 50 x 10^{-3} N

3.1.3.2 *Inclusion Body Purity*

The purity of the protein inclusion bodies cleaned with different strategies was analysed by SDS-PAGE and the results are presented in Figure 3.7. Protein inclusion bodies (insulin-like growth factor LR^3-IGF-1 analog) are shown by the last band on the SDS-PAGE gel. They possess a molecular weight of 9.1 kDa. The homogenate

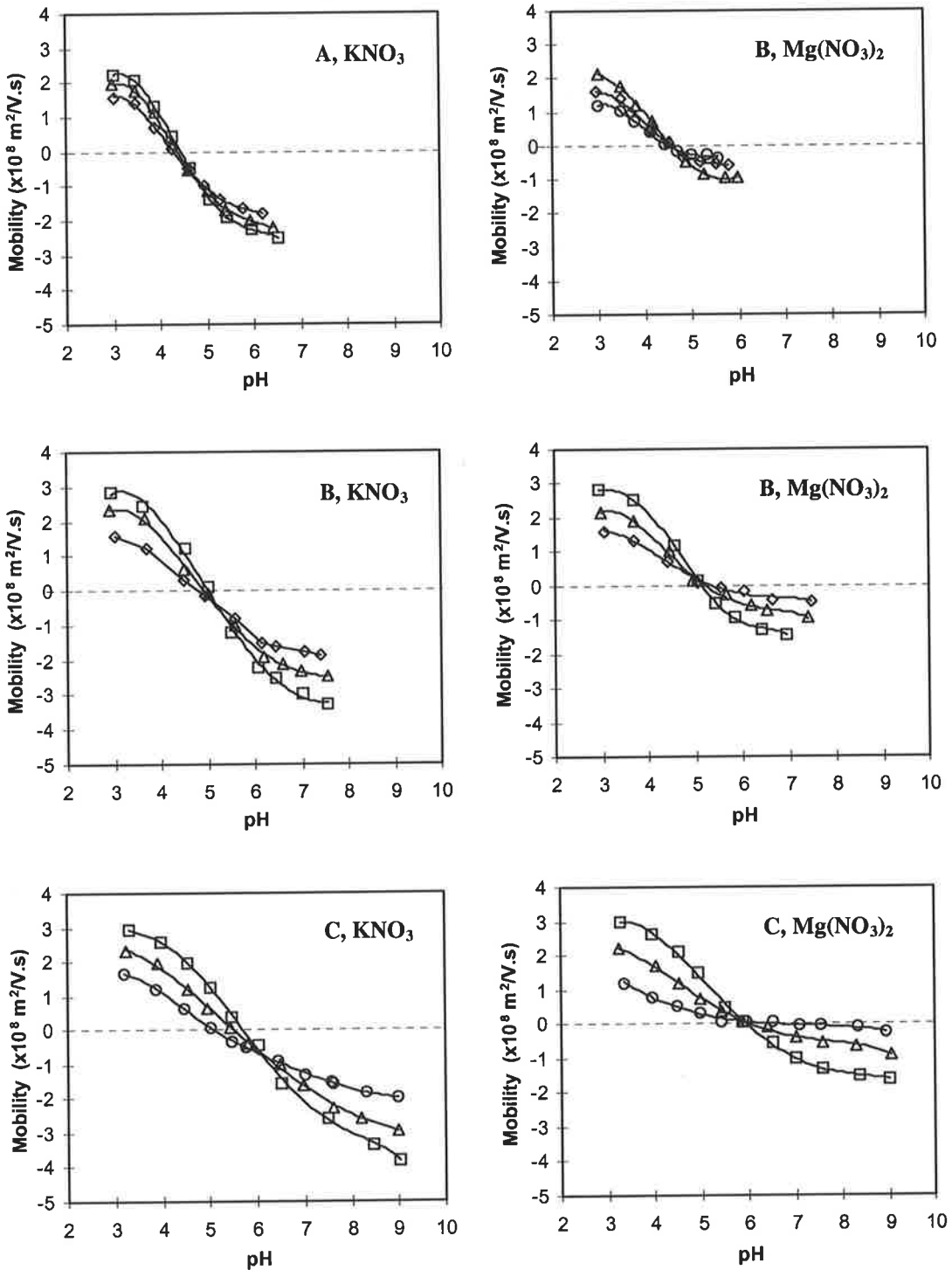

Figure 3.6. Electrophoretic mobility of protein inclusion bodies purified with different procedures (A,B, and C) measured in the presence of different electrolytes and various electrolyte concentration: (□) 0.001 N, (△) 0.01 N, (◊) 0.05 N, (○) 0.1 N.

contains numerous contaminants as shown by the bands on lane 2 (Figure 3.7). Three different cleaning strategies were devised and applied to reduce the level of contaminants as described in Materials and Methods. These procedures were effective, but not perfect as evidenced by the decrease in the number and intensity of bands (Figure 3.7, lanes 3 to 5) but not their elimination. Furthermore, the last band (corresponding to protein inclusion bodies) became denser and larger, indicating that the relative concentration of protein inclusion bodies increased as a result of contaminant removal during the cleaning sequence. The purity of protein inclusion bodies obtained from procedure C exceeded that from procedures B and A, respectively.

Figure 3.6 shows the electrophoretic mobility of protein inclusion bodies purified by the different procedures. In the presence of a monovalent cation (K^+), the electrophoretic mobility curves shifts towards higher pH. As a consequence the isoelectric point increases, for example in 0.001 M KNO_3 from 4.5 to 5.7. A similar pattern was observed in the presence of the divalent cation (Mg^{2+}). The isoelectric point of protein inclusion bodies obtained by using procedure C was higher than those from procedures B and A, respectively (Table 3.2). The purity of the inclusion bodies followed the same trend as the isoelectric points. Hence, the isoelectric point of the inclusion bodies provides a qualitative measure of their purity. A higher isoelectric point corresponds to cleaner inclusion bodies.

Table 3.2 Isoelectric points of protein inclusion bodies purified with different procedures (A, B, and C) in the presence of KNO_3 and $Mg(NO_3)_2$.

Electrolyte	Electrolyte Concentration (x 10^{-3} N)	Isoelectric points (i.e.p.)		
		Procedure A	**Procedure B**	**Procedure C**
KNO_3	1	4.5	5.0	5.7
	10	4.4	5.0	5.5
	100	4.3*	4.9	5.1*
$Mg(NO_3)_2$	1	4.8	5.3	5.9
	10	4.7	5.2	5.9
	100	4.6*	5.1	5.9

*electrolyte concentration: 50 x 10^{-3} N

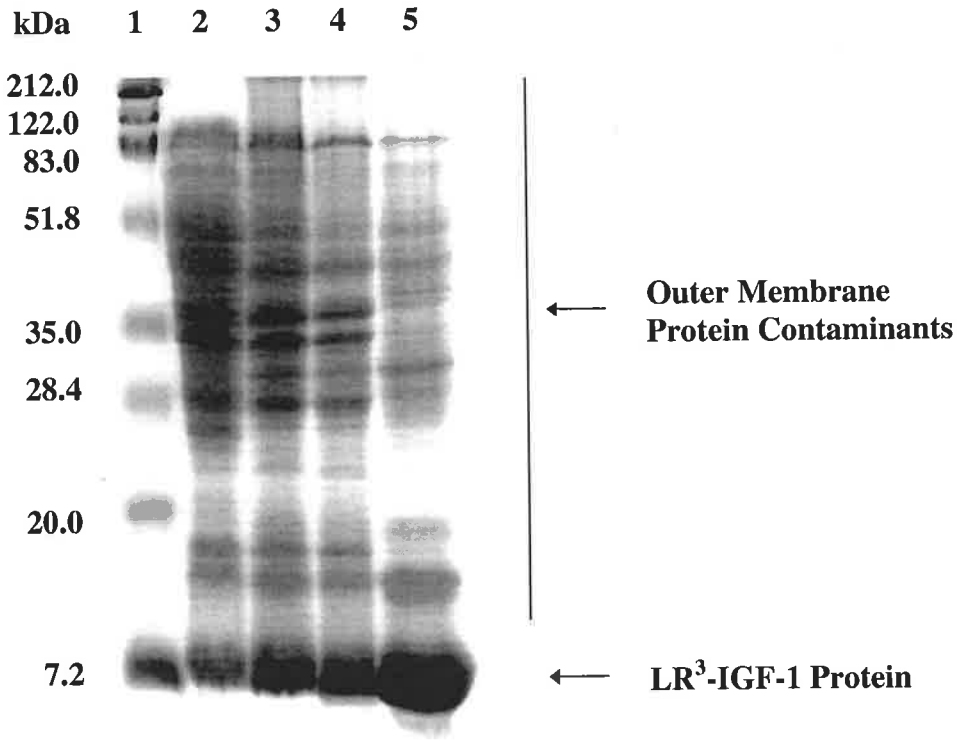

Figure 3.7. SDS-PAGE Gel. Lane 1: Prestained standard containing Myosin (212 kDa), β-galactosidase (122 kDa), Bovine serum albumin (83 kDa), Ovalbumin (51.8 kDa), Carbonic anhydrase (35 kDa), Soybean trypsin inhibitor (28.4 kDa), Lysozyme (20 kDa), and Aprotinin (7.2 kDa). Lane 2: Homogenate (7 passes at 55 mPa). Lane 3-5: Protein inclusion body samples purified with Procedures A, B, and C respectively.

3.2 PARTICLE CHARACTERISTICS

3.2.1 Background

Particle characteristics, such as size (diameter), shape and surface properties, are important features to be considered in bioprocesses. These characteristics provide basic physical features which can be exploited to improve the performance of bioprocesses and/or to design new fractionation techniques for bioprocessing. Therefore, these characteristics were examined. First, the particle size of protein inclusion bodies were measured using photosedimentation technique (Middelberg *et al.*, 1990). Next, scanning electron microscopy and atomic force microscopy techniques were employed to examine the shape and surface properties of the protein inclusion bodies.

3.2.1.1 *Joyce-Loebl Disk Centrifuge*

There are numerous techniques available for particle size determination. Dynamic light scattering technique (or photon correlation spectroscopy) is commonly employed to determine the size of fine particles due to its simplicity, rapid results and ease of reporting. However, this technique has limitations, eg. its low resolution and sensitivity to interference by large particles and dust present in the sample. This technique has been applied to measure particle size of inclusion bodies (Jin, 1992) and cell debris (Olbrich, 1989; Angerkvist and Enfors, 1990; Jin *et al.*, 1994). Pretreatment using DNase and RNase was required for cell debris measurement due to interference from dissolved polymeric materials (nucleic acids) on scattered light. Hence, this technique may not be reliable for measurement of heterogenous sample such as inclusion bodies in the suspension of homogenate. Middelberg *et al.* (1990) explored photosedimentation technique for sizing biological samples such as *E. coli* cells, inclusion bodies and cell debris. This technique is reliable for sizing biological samples and has been previously used by Taylor *et al.* (1986) for measuring inclusion

body particle size. Hence, this technique was adopted in this study for measurement of inclusion body size.

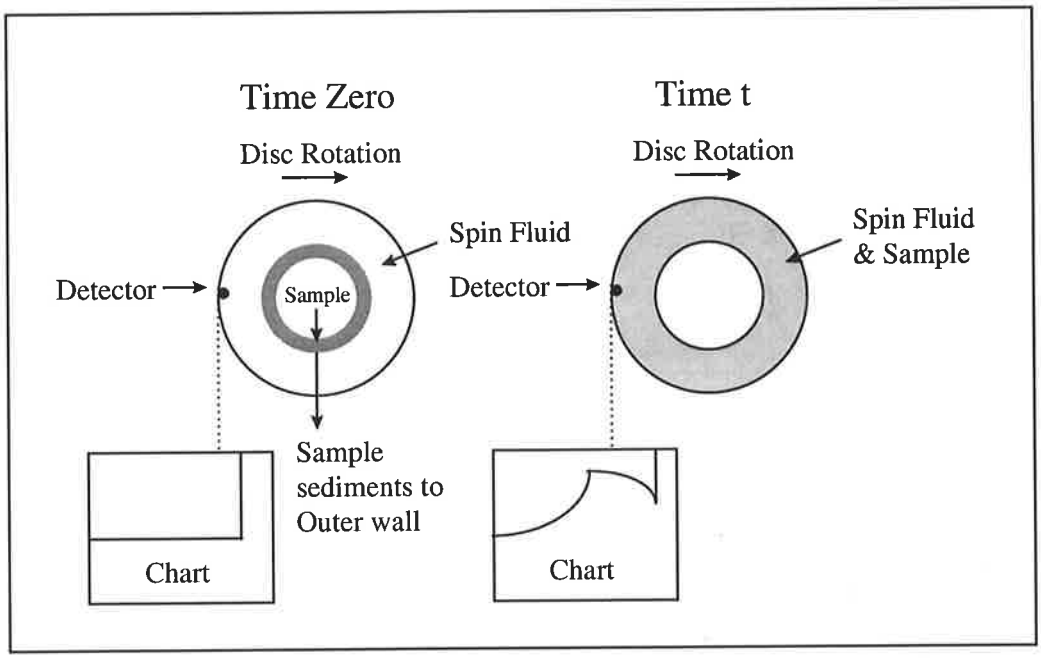

Figure 3.8 Schematic diagram of Joyce-Loebl Disc Centrifuge (after Middelberg *et al.*, 1990).

The stokes diameter is determined from photosedimentation technique using Joyce-Loebl DCF4 disc centrifuge (Joyce-Loebl Ltd., Gateshead, UK). This technique exploits the principle of sedimentation under increase gravity. A schematic diagram of this disc centrifuge is presented in Figure 3.8. The centre of the analyser is a hollow rotating disc. Spin fluid is injected to the centre of the rotating disc followed by buffer-liquid injection. The buffer layer diffuses into the spin fluid forming a shallow density gradient in the spin fluid due to the acceleration and deceleration of the disc. The sample is then injected and forms a layer at the inner radius of the spin/buffer liquid annulus. Hence, all particles in the sample start at nearly identical radii and experience a net centrifugal force (Middelberg *et al.*, 1990). This centrifugal field causes particle movement (settling) towards the outer annulus where the particles pass through the detector. The intensity of the light captured by detector decreases due to scattering and absorption of the light by particles. The absorbance of the spin

fluid at the detection radius are recorded as a function of time. The size of the particle (Stokes diameter) can be obtained by applying Equation (3.2) (Taylor *et al.*, 1986).

$$D = \sqrt{\frac{18\eta \ln\left(\frac{r_d}{r_o}\right)}{\tau_s \Delta\rho\omega^2}} \qquad (3.2)$$

where: D is the particle size, η is the fluid viscosity, r_o is the particle start radius ($\tau_s = 0$), r_d is the detector radius, τ_s is the time for particles sedimentation from r_o to r_d, ω is the angular velocity and $\Delta\rho$ is the density difference between the particles and the fluid.

3.2.1.2 *Scanning Electron Microscopy (SEM)*

The birth and development of electron microscopes have been intimately associated with biological research. However, the electron microscope has also been extensively used in other areas, such as polymer and material science. Three major types of electron microscopes exist, i.e. transmission electron microscope (TEM), scanning electron microscope (SEM) and scanning transmission electron microscope (STEM). The TEM projects electrons through a very thin slice of specimen (eg. tissue) to produce two dimensional image. Whereas the SEM produces an image that gives the impression of three dimensions. The STEM which features of both the transmission and scanning electron microscopes is less widely applied than the first two modes. In this work, SEM is employed to explore the particles of protein inclusion bodies.

In SEM, images are derived from scanning a fine beam of electrons with energies up to 30 or 40 keV across the sample surface in a raster or pattern of parallel lines (Watt, 1985). A number of phenomena occur when a beam of electrons impinges on an object in a vacuum and the most important phenomena for SEM are the emission of secondary electrons (low energy) and reflection of high-energy back-scattered electrons from primary beam (Watt, 1985). The intensity of both the secondary and

back-scattered electrons is very sensitive to the topography of the sample. This electron current is collected and amplified then the variation is translated to form images. Currently, SEM could resolve 3.5 nm with magnification up to 200,000× (Bozzola and Russell, 1992).

SEM is operated under vacuum and requires special preparation of samples. Sample preparations for biological materials is normally complicated and differs from sample to sample. Standard sample preparations for biological materials include cleaning, fixation, dehydration, drying, specimen mounting and coating (for non-conducting samples). Detailed discussion of SEM principles and other aspects including operating procedure and sample preparation is readily available in the literatures (Kay, 1965; Hearly *et al.*, 1972; Watt, 1985; Bozzola and Russell, 1992).

SEM has been used for qualitative analysis of inclusion bodies (Marston, 1986; Bowden *et al.*, 1991) and cell disintegrates (Quirk and Woodrow, 1984; Harrison *et al.*, 1991). SEM can also be used for quantitative measurements, eg. particle size measurement and particle size distribution. However this application is limited by the effects of sample preparation. For example, particles may shrink or deform following a series of conventional treatment steps in sample preparation. This limitation has been previously noted by Bailey *et al.* (1995) who employed electron microscopy for measuring cell debris from *E. coli* following homogenisation with chemical treatment. Furthermore, this method is limited statistically due to the small sample population measured.

3.2.1.3 *Atomic Force Microscopy (AFM)*

Atomic force microscopy (AFM) is powerful technique for surface analysis. AFM has been used extensively for surface analysis tool in biological research due to its ability to image non-conducting samples in liquid environment (physiological conditions). The principles and operations of AFM are outlined in section 1.5. This section discusses aspects of surface analysis by contact mode atomic force microscopy.

In the contact mode (also known as the repulsive mode or DC mode), a constant small force (usually 1-10 nN) is applied at the surface of the sample (Ikai, 1996) and the tip makes direct physical contact with the sample. This small force is maintained constant by the feedback circuit. As the tip scans across the sample surface, the cantilever is deflected (up and down) following the pattern of the surface. This deflection is measured optically using laser light that is reflected by the back (upper side) of the cantilever to a four-section photodiode detector. The photodiode detector generates a current signal proportional to the light intensity received by the upper and lower sections of the photodiode detector to the feedback circuit. The feedback system maintains the current difference between the upper and lower diodes at a fixed preset value resulting constant loading force on to the sample surface. The amount of deflection of the cantilever can be calculated from the change in the light intensity received by the photodiode detector. The resulting change in the detector current signal is used in forming the AFM image.

Contact mode is the commonly explored mode for topographical imaging due to its simplicity and ease of operation. The topographical image can be obtained relatively quickly. However, the contact mode may cause problems to soft samples, eg. biological samples. Despite the small force applied to the sample surface, some biological (soft) materials may experience unacceptably large deformation.

Samples for topographical imaging are usually adsorbed onto atomically flat surfaces (substrate), such as freshly cleaved mica, glass, HOPG (highly oriented pyrolitic graphite), silicon wafer and gold-coated mica (Ikai, 1996). The correct substrate can be chosen from a knowledge of their features, for example, HOPG surface is hydrophobic uncharged and mica surface is hydrophilic negatively charged (Lal and John, 1994). Special treatment (eg. chemical treatment) of the substrate surface is common to obtain surface properties that facilitate sample attachment. Examples include gold treatments with a variety of agents for DNA imaging (Lal and John, 1994).

Various type of AFM tips are available. The prefabricated silicon nitride cantilevers with an integrated tip are the most commonly used. Numerous shapes, lengths and

thickness of cantilevers are fabricated and their elastic spring constants vary in the 0.01-50 N/m range (Magonov and Whangbo, 1996). The shape of the tip apex and the elastic spring constant (k) of the cantilever are important factors. A tip with a relatively dull apex is not suitable for imaging highly corrugated surfaces as the real topography may be hidden by the convolution of the tip geometry and the sharp surface features (Magomonov and Whangbo, 1996). Cantilevers with small spring constants are suitable for imaging soft samples whereas rigid cantilevers are required for measuring nanomechanical properties of sample surfaces and for dynamic mode AFM (Magomonov and Whangbo, 1996).

Contact mode AFM has been successfully used for imaging various samples. Images of crystals (eg. AgBr, gold film, HOPG, mica and Si wafer), structures (eg. carbon coating, compact disc and superlattice), polymer and biomaterials have been reported (Sarid, 1994). Biological applications of contact mode AFM include imaging of red blood cells, bacterial cells (*E. coli, bacillus, bacteriorhodopsin*), bacteriophages, DNA, and proteins.

3.2.2 Materials and Methods

3.2.2.1 *Particle Size Analysis*

Particle size analysis was performed using a DCF4 (Joyce Loebl) disc centrifuge (Applied Imaging Ltd, Gateshead, U.K.) using a standard water spin fluid scheme (Middelberg *et al.*, 1990). The density difference between inclusion body and buffer was taken as 260 kg/m^3 to convert sedimentation velocities to size data solely for data presentation. Details of standard conditions applied in this measurement are summarised in Table 3.3. Fresh homogenate (7 passes) was used for preparation of the samples.

3.2.2.2 *Scanning Electron Microscopy Analysis*

A drop of the dialysed inclusion body suspension (procedure C) or homogenate (7 passes) was laid on a sample holder and dried. The dried sample was then coated with standard carbon and gold coating using a Denton Vacuum Coater (Denton Vacuum Inc., Cherry Hill, New Jersey, USA) prior to imaging. Images were obtained using Phillip XL30 Field Emission Scanning Electron Microscope .

3.2.2.3 *Atomic Force Microscopy Analysis*

Frozen inclusion bodies (procedure C) were thawed and suspended in Milli-Q water to a final concentration of 1 g/L. This suspension was then sonicated for 5 x 1 minute with a 1 minute break for rupturing aggregates formed during freezing. A freshly cleaved mica surface (1 cm^2) was treated with 1 M $ZnCl_2$ solution and incubated for 30 minutes to obtain a positively charged surface. A drop (5μL) of the sonicated suspension was laid on the treated mica surface and incubated for 30 minutes followed by two water rinses and vacuum drying for 2 hours. This sample was then attached

(using clear double side sticky tape) to a round metal plate which finally mounted on the magnetic base of the AFM sample holder. This sample was probed using an AFM (NanoScope III Multiprobes AFM, Digital Instruments, Inc., Santa Barbara, USA) by employing contact mode as described in the AFM users' manual (Digital Instruments, Inc., Santa Barbara, USA). Standard silicon nitride (Si_3N_4) tips with spring constant of 0.06 N/m (Nanoprobes, Digital Instruments, Inc., Santa Barbara, USA) were used. Following application, the tips were cleaned by organic wash (chloroform and ethanol) then water rinsed and finally vacuum dried for 15 minutes. An image of size of 100 μm × 100 μm was initially taken followed by subsequent magnification of specific areas of interest.

Table 3.3 Standard conditions of Joyce Loebl Disc Centrifuge Analysis

Spin Fluid (SF)	20 mL Water
Buffer Fluid (BF)	1.5 mL 20% Ethanol-Water
Sample Volume and Suspension	0.5 mL 20% Ethanol-Phosphate Buffer
Disc Speed (rpm)	8000
Machine Gain	6.0
r_o (cm), equation 3.2	4.01
r_d (cm), equation 3.2	4.82
η (cP), equation 3.2	1.14
$\Delta\rho$ (kg m^{-3}), equation 3.2	260
Time = 0 s	Inject SF
Time = 60 s	Inject BF
Time = 90 s	Boost 70
Time = 150 s	Boost 70
Time = 210 s	Boost 20
Time = 300 s	Inject Sample

3.2.3 Results and Discussion

3.2.3.1 *Particle Size Analysis*

The mean size of protein inclusion bodies is approximately constant (very narrow variation) between fermentations in the range of 0.30 to 0.33 μm (discussed previously in chapter 1). Errors in particle size measurements or data interpretations may contribute to this variation. Therefore, in general the mean particle size of protein inclusion bodies is 0.3 μm. A summary of the results of particle size analysis of protein inclusion bodies following various fermentation strategies is presented in Table 3.4. The particle size of protein inclusion bodies from numerous fermentations with constant rate feeding (not listed in Table 3.3) showed similar values and was within the typical range.

Inclusion body size is an important parameter in the recovery or purification processes. The particle size of the inclusion bodies is a key factor for determining the *g* force required for effective separation in centrifugation processes. Particle size is also an important determinant for choosing the correct flotation techniques. Tiny bubbles are required to float fine particles (eg. inclusion bodies). Dissolved-air flotation (DAF) appears as a potential technnology for the recovery of inclusion bodies due to its ability to form very small bubbles.

Table 3.4 Summary of the mean particle size of protein inclusion bodies from various fermentations.

Fermentation Feeding Strategies	Mean particle size (μm)
Contant rate feeding	0.32[a]
	0.30[b]
Novel 3-stage feeding	0.33
Novel 3-stage feeding, YE[c]	0.32

a. feed rate = 9.7 mL/min
b. feed rate = 11.4 mL/min
c. with yeast extract supplement

3.2.3.2 *SEM Analysis*

SEM analyses of homogenate (7 passes at 55 MPa) and inclusion bodies are presented in Figures 3.9 and 3.10. As shown in the SEM images, protein inclusion bodies (LR^3-IGF-1) posses an irregular shape and rough surfaces. Similar irregularity in shape has been observed for the inclusion body particles of human growth hormone (hGH) and the β-subunit of human chorionic gonadotropin (βhCG) (Mukhopadhyay, 1997). By contrast, a highly regular and cylindrical shape was observed for β-lactamase inclusion body (Bowden *et al.*, 1991). This suggests that the shape of inclusion body particles can vary over a wide range as well as their particle size (Mukhopadhyay, 1997)

The nature of the inclusion body particles may facilitate contamination attachment and hinder its subsequent removal during cleaning processes. By contrast, this surface roughness of protein inclusion bodies can be advantageous for dissolved-air flotation recovery as particles with rough surfaces enhance bubble formation by dissolved gas in water (Ryan and Hemingsen, 1993). In addition, particle surface roughness together with other factors, including the surface roughness of the container, high dissolved gas content, and the presence of solid particles in liquid, facilitate the initiation of gas nuclei/cavities (Zhou *et al.*,1994). It is also likely that the shape irregularity of the inclusion body particles may facilitate the bubble-particle attachment processes in flotation.

Figure 3.9 shows homogenate with cell debris surrounding inclusion bodies. Cell debris agglomerates and forms a compact structure where individual elements cannot be identified. Qualitative analysis of homogenate by SEM is not reliable due to this problems. Special sample preparation procedures of cell debris are required for SEM qualitative analysis as previously reported (Quirk and Woodrow, 1984; Harrison *et al.*, 1991).

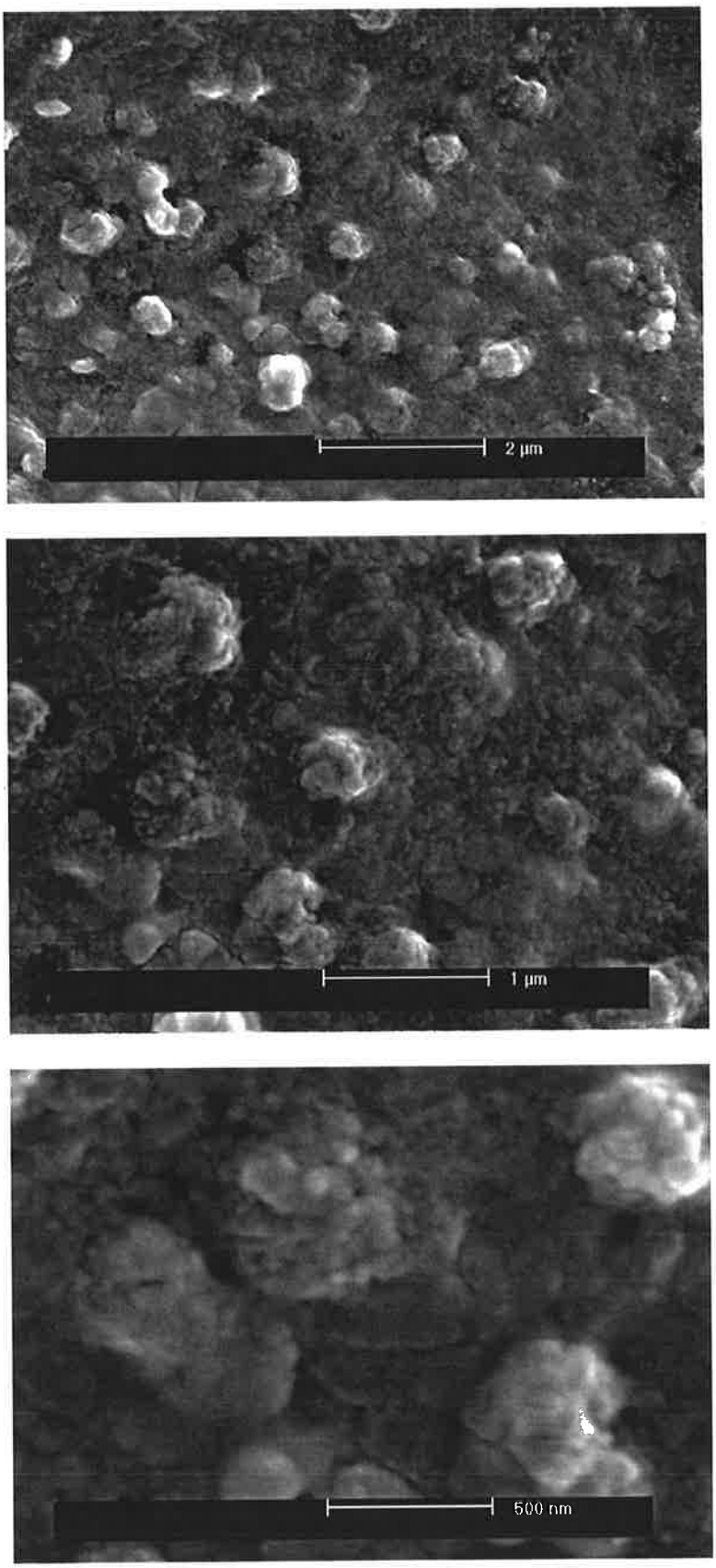

Figure 3.9 Scanning electron microscopy images of homogenate (7 passes at 55 MPa) in various magnifications

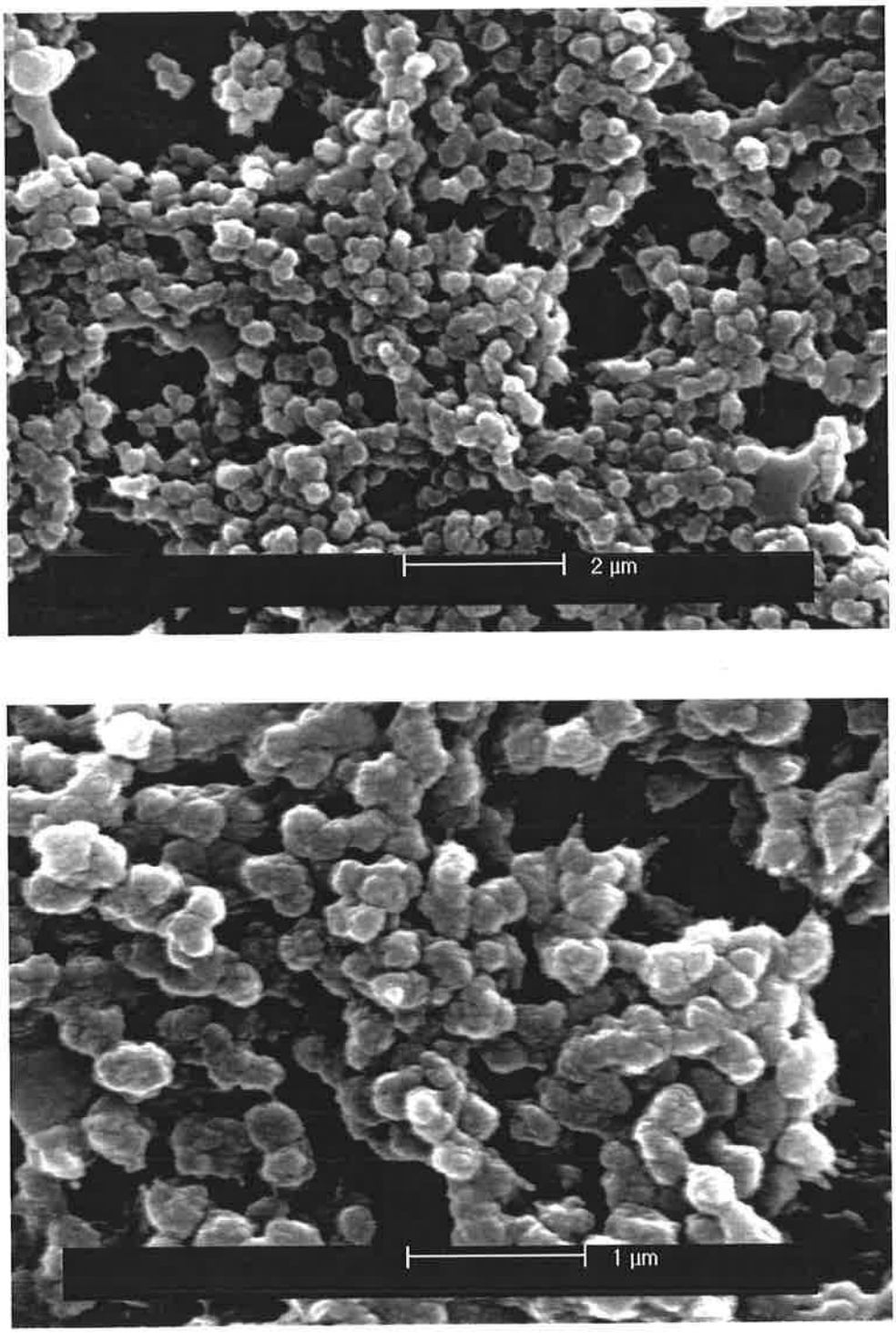

Figure 3.10a Scanning electron microscopy images of protein inclusion bodies (purified using procedure C) in various magnifications

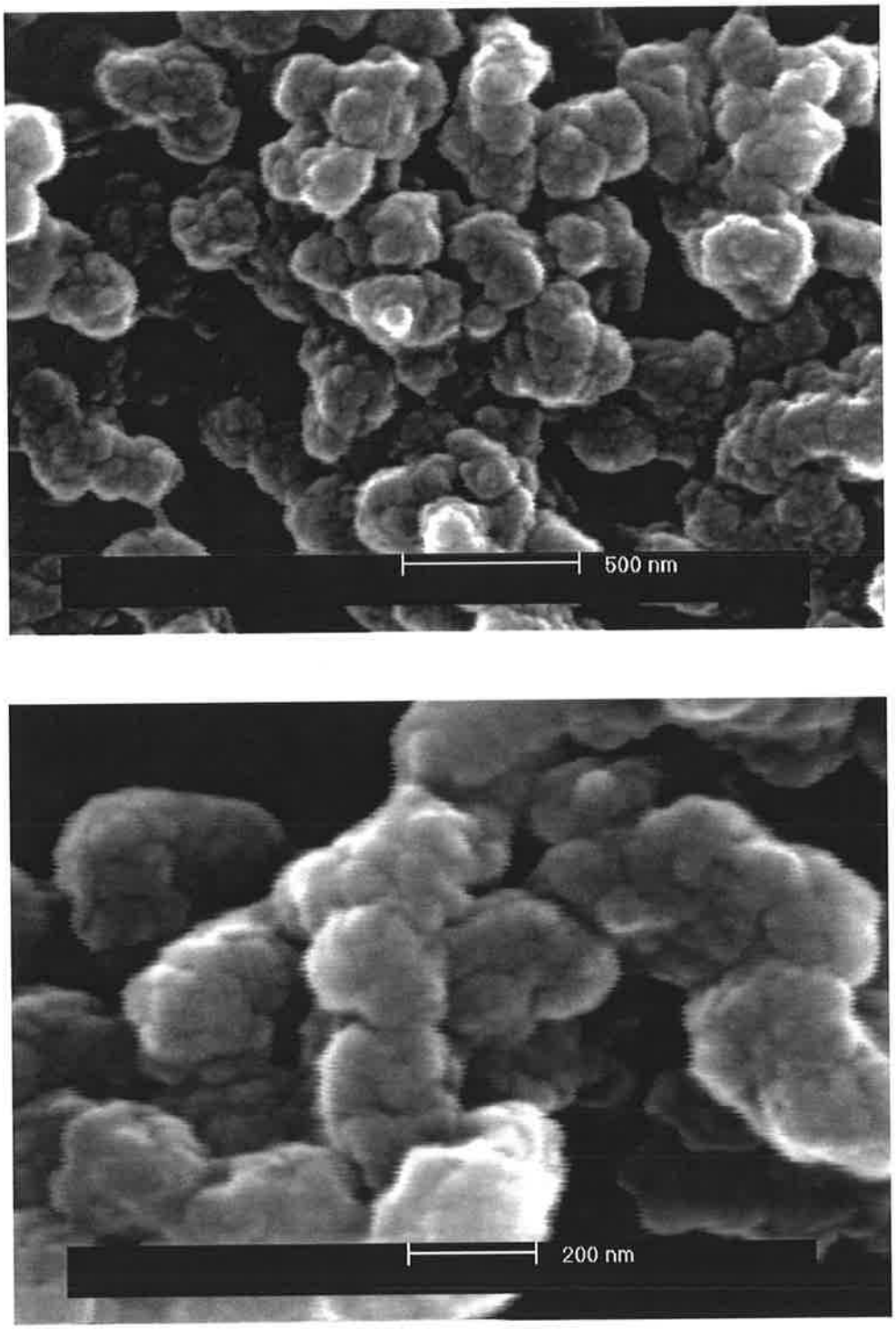

Figure 3.10b Scanning electron microscopy images of protein inclusion bodies (purified using procedure C) in various magnifications

3.2.3.3 *AFM Analysis*

A freshly cleaved mica was used as substrate because it is inexpensive and relatively simple to use. Contact mode AFM analysis of a freshly cleaved mica was conducted to examine its surface topography. Images were taken from several parts of the mica surface (1×1 cm^2) at different magnification. The AFM analysis concluded that the mica surface was extremely flat as shown in the following 10×10 nm^2 image (Figure 3.11). This proves that mica is reliable for use as a sample substrate.

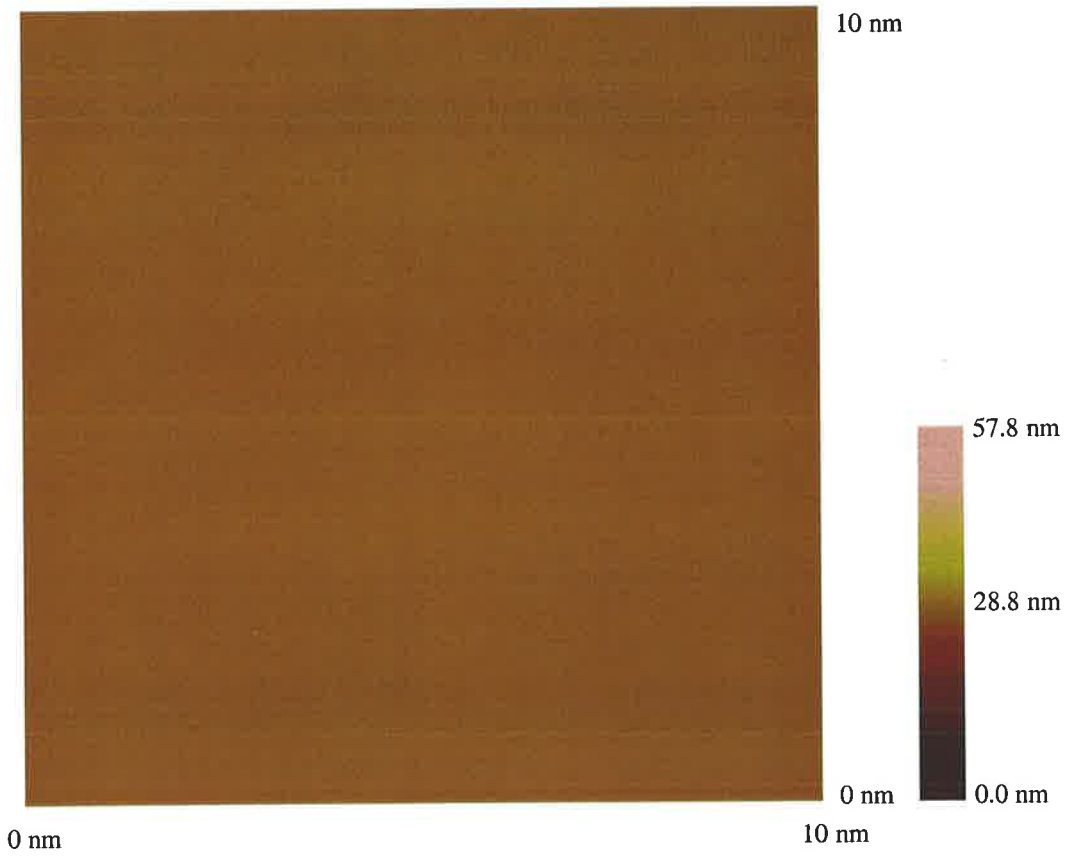

Figure 3.11 Freshly cleaved mica surface imaged by contact mode AFM (10×10 nm^2) shows its flat surface.

Both mica surface and protein inclusion bodies possess a negative charges. Hence, electrostatic attachment of these inclusion body particles onto the mica surface cannot

be carried out due to the electrostatic repulsion of similar charges. This lack of inclusion body particles adherence onto the mica surface was confirmed (Figure 3.12). Hence, the mica surface was treated with a strong cationic solution ($ZnCl_2$) to obtain a positively charged surface. This treatment was successful as many particles then attached to the mica surface (Figure 3.13).

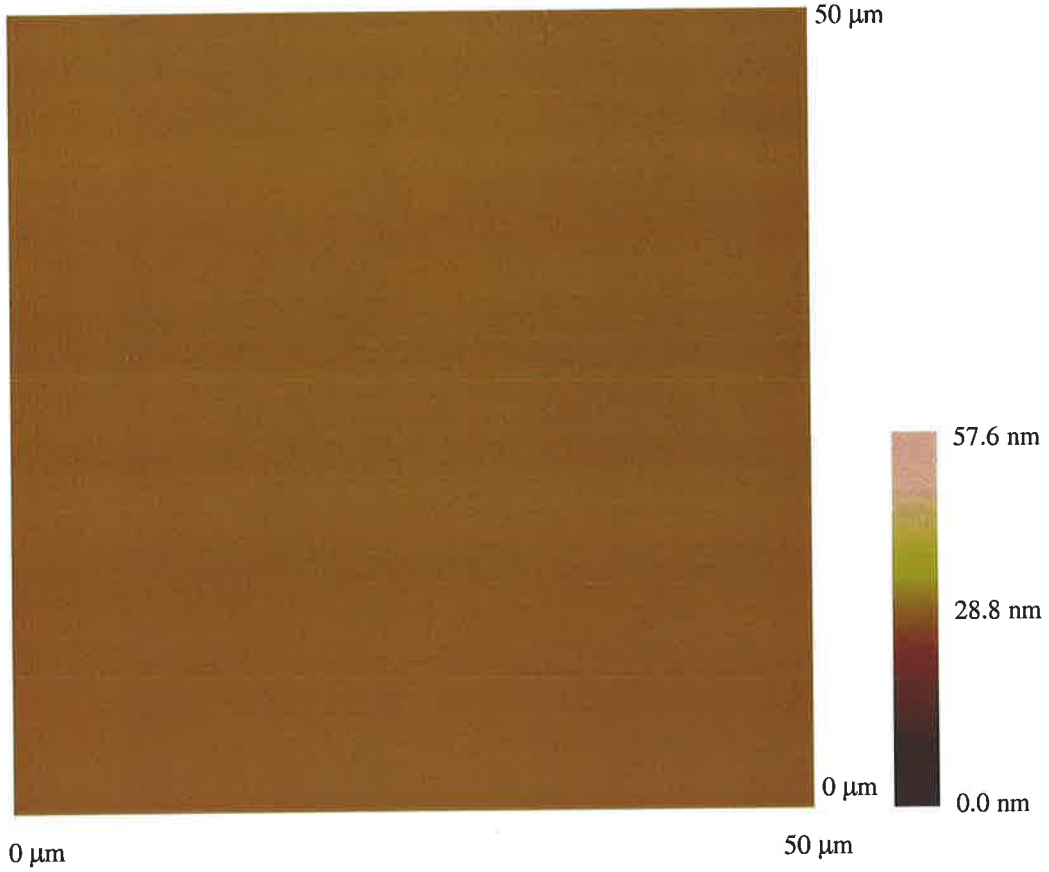

Figure 3.12 AFM image (50×50 μm^2) of protein inclusion bodies laid on a freshly cleaved mica surface which shows that there are no inclusion body particles attached securely on the mica surface

AFM images of protein inclusion bodies at different magnifications are presented in Figures 3.13 to 3.17. Two types of data were collected during AFM scanning to form images, i.e. deflection and height data. Deflection data was recorded from the current signal of the photodiode detector. Height data was obtained from the piezo movement in the Z direction as a result of feed-back circuit in maintaining constant loading force throughout scanning. The AFM images obtained are relatively comparable to SEM

images (Figure 3.10). These results confirm that inclusion bodies posses an irregular shape and rough surfaces. Aggregates were present in the sample (Figures 3.13 to 3.17). These aggregates are formed during sample preparation or they were already present in the sample suspension prior application to the substrate (mica). However, single particle of inclusion bodies can still be identified easily from these AFM images, particularly from images generated from the height data (Figures 3.14 to 3.16). Surface roughness of inclusion bodies is easily seen from images at high magnification, particularly images generated from the deflection data (Figure 3.17).

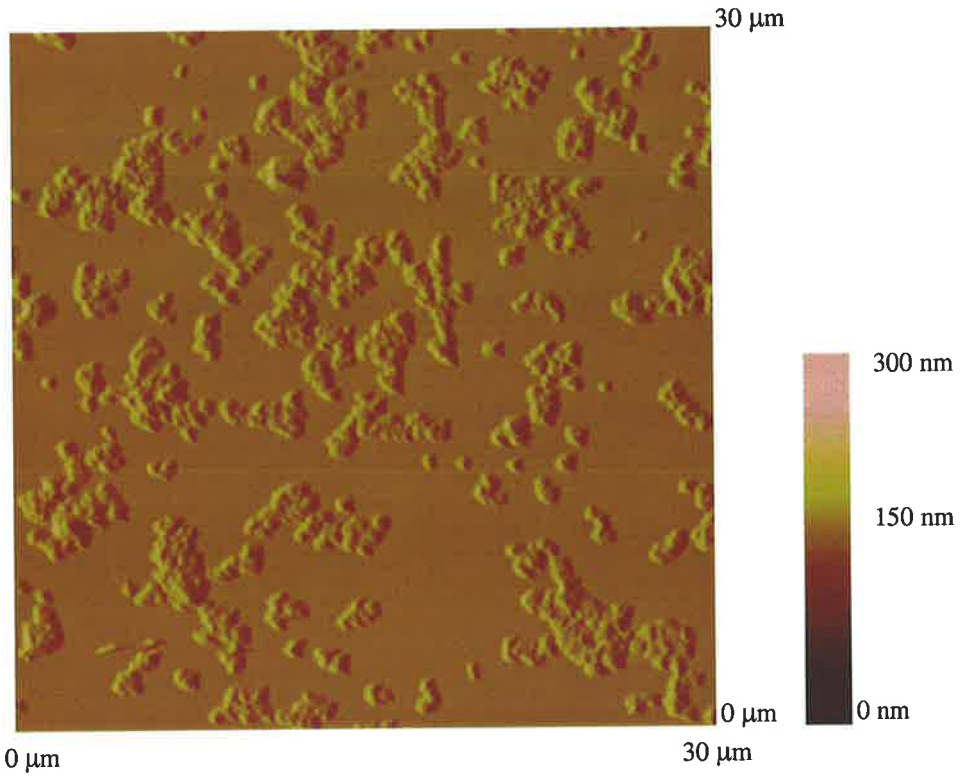

Figure 3.13 Protein inclusion bodies imaged by contact mode AFM. Large aggregates are present in the sample.

The resolution of AFM images is not as good as SEM resolution. Various factors, such as larger than optimal sample size and tip properties, contribute to this reduced resolution. Inclusion body particles are relatively large and hence on the flat mica substrate they form a 'hilly' texture and the presence of aggregates exaggerates this 'hilly' texture. The silicon nitride tips have a height of several microns therefore they

can be used to examine samples with surface corrugations below 1 μm (Magomonov and Whangbo, 1996). A single inclusion body particle has surface corrugations less than 1 μm and so the tips should be able to perform measurements. However, the aggregates can be as high as 2 μm and hence the tip performance is lowered. Defective images were observed (as shown by arrows in Figure 3.17) due to the tip-sample convolution effects. Triangular shapes detected in the imaged particles (shown by arrows in Figure 3.17) reflect the tip shape. The uniform pattern of these images (also known as tip artefacts) show that they do not represent real structure but a defective structure formed as a result of tip-sample convolution effects. This phenomena has previously been noted and reported in details by Schwarz *et al.* (1994). Detailed study of the comparison of SEM and AFM techniques used for surface topography characterisation has been reported by Castle and Zhdan (1997). They claimed that AFM (at similar magnification) can reveal much more detail of surface topography compared to SEM. Also, AFM can disclose three-dimensional information not available in SEM. However, they also experienced similar problems (i.e. tip artefacts) shown by the tip-shape in the AFM image.

Sharper tips are likely to improve resolution. The current tips used were silicon nitride tips which have a pyramidal shape with an opening angle at the apex of about 70° (Figure 4.4). Such tips are not very sharp. Sharper tips are commercially available and are known as super tips or ultra tips and are usually conical in shape. The disadvantage of sharper tips is that they are less robust compared with standard pyramidal tips. Improved sample preparation procedures can also enrich the resolution, particularly avoiding large aggregates in the sample. Sample treatment by sonication for different time period has been performed. Treatment by sonication for 5 x 1 minutes with one minutes break each cycle appears reliable. The concentration of inclusion bodies also contributes to the aggregation process. The lower the suspension concentration the less the aggregation as fewer particles are present. Sample concentration of 0.1, 0.5, 1, 2 and 4 g/L were examined. The 1 g/L sample concentration provided the best results where enough number of particles are present in the suspension. Fresh inclusion bodies produced better samples as aggregates are not initially present in the suspension. Aggregates are normally formed when

inclusion bodies are frozen. Unfortunately, frozen inclusion bodies were used instead of fresh inclusion bodies due to geographical constraints and ease of handling need.

A strong hysteresis is generally observed in the AFM measurements in air (ambient-condition) due to the capillary force associated with the surface contamination layer (Magomonov and Whangbo, 1996). This contamination layer is formed when the sample surface is in contact with water vapour in air. This contact promotes hydration of water vapour on to the sample surface. This hysteresis can be avoided by conducting AFM measurements under liquid. The hysteresis effect may also contribute to the low resolution obtained in this experiment. AFM measurement under liquid may increase the resolution. However, the strength of the sample attachment on to the substrate surface in liquid environment has to be considered carefully. Buffer solutions are commonly used in the measurements and these may affect the electrostatic interaction used for sample attachment. If the samples are not securely attached onto the substrate surface, they may be dragged by the tip movement. Attachment of sample on to the substrate surface by chemical bonds is stronger and this technique appears to be more reliable as long as sample structure is not affected. Silicon wafer substrate is suitable for use in this method as it can stand with 'harsh' chemical treatment. Mica may also be used but its multi-layer structure can create problems. This method is used to attached protein inclusion body particles on to the tip and discussed in chapter 4.

In addition, the contact mode AFM can cause sample deformation because the tip is physically in contact with the sample surface and a certain constant force is applied to the sample surface. Soft samples are particularly affected, such as protein and other biological materials. Two other operating modes have been developed to solve this problems, i.e. non-contact mode (Luthi *et al.*, 1994; Wong and Descouts, 1995) and tapping mode in air (Zhong *et al.*, 1993), in gas (Hansma *et al.*, 1994) and in liquid (Hansma *et al.*, 1995). Unfortunately, these modes of operation are far more complicated than the contact mode. The non-contact mode is unpopular due to its poor resolution. However, tapping mode is becoming popular for biological applications due to its high resolution without any effects from sample deformation by the tip. In the tapping mode, the cantilever (and the tip) is vertically oscillated at high

frequency as it scans the sample. The tip and the sample come into intermittent contact (tapping) when the sample surface approaches the vibrating tip, causing a reduced oscillation amplitude. The changes of oscillation amplitude generates the signals for creating the image. A much shorter tip-sample contact time and reduced tip-sample lateral forces can be maintained, hence sample deformation is avoided. Hansma *et al.* (1993) obtained high resolution results by tapping mode. The tapping mode incurs a significant disadvantage when operated under liquid as the oscillations are significantly damped.

In summary, Contact mode AFM appears to be reliable method for imaging protein inclusion bodies. The images obtained are comparable to SEM images although the resolution was poorer than that from the SEM. Special sample preparation are required for this measurement, particularly preventing aggregation and/or eliminating aggregates. Chemical bond attachment of samples onto the substrate surface may be applied to obtained securely attached samples. Also, a tapping mode AFM has the potential to provide improved image resolution.

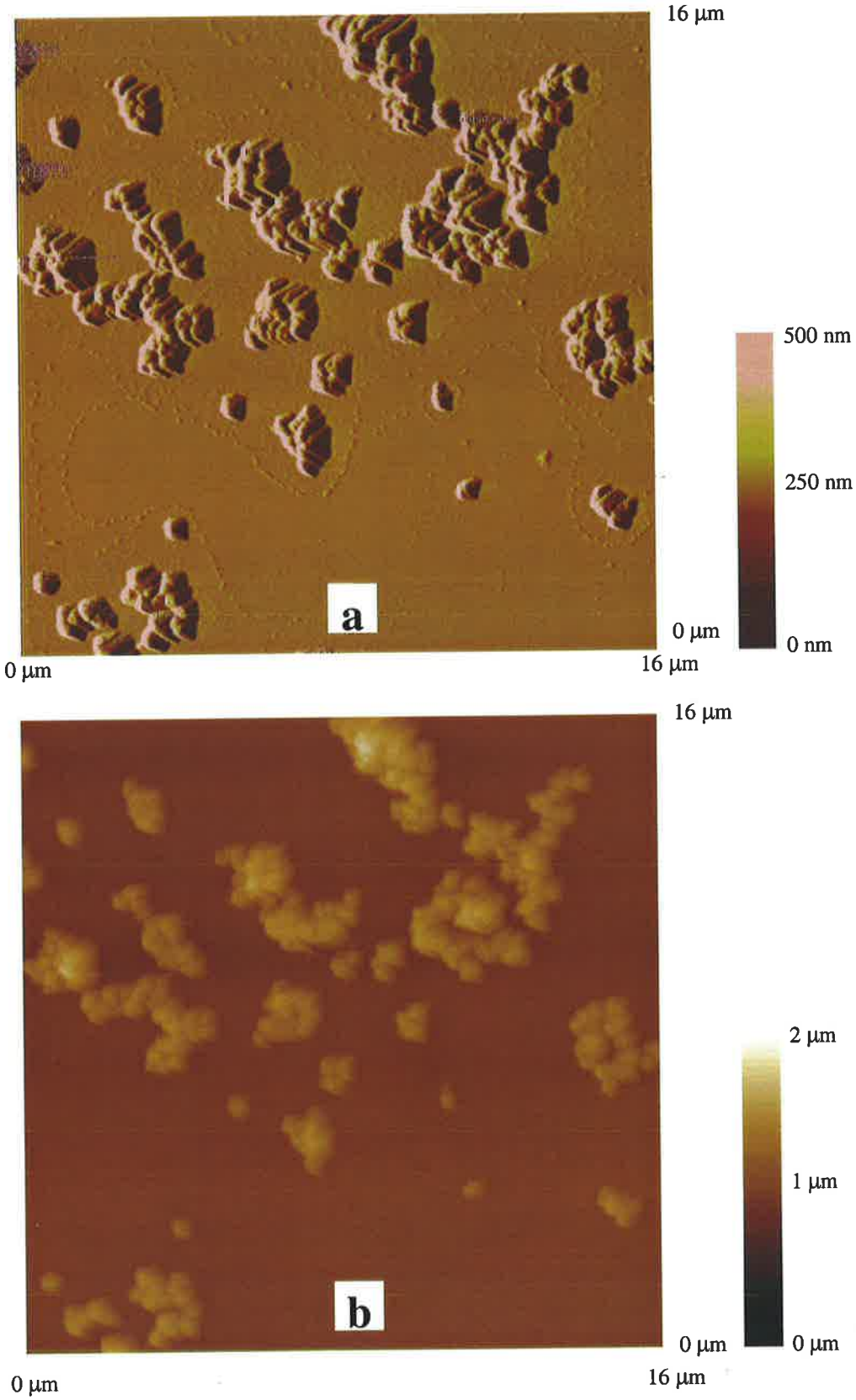

Figure 3.14 AFM images of protein inclusion bodies derived from deflection data (a) and height data (b). Single particle of inclusion bodies can be identified easily, particularly from height data (b).

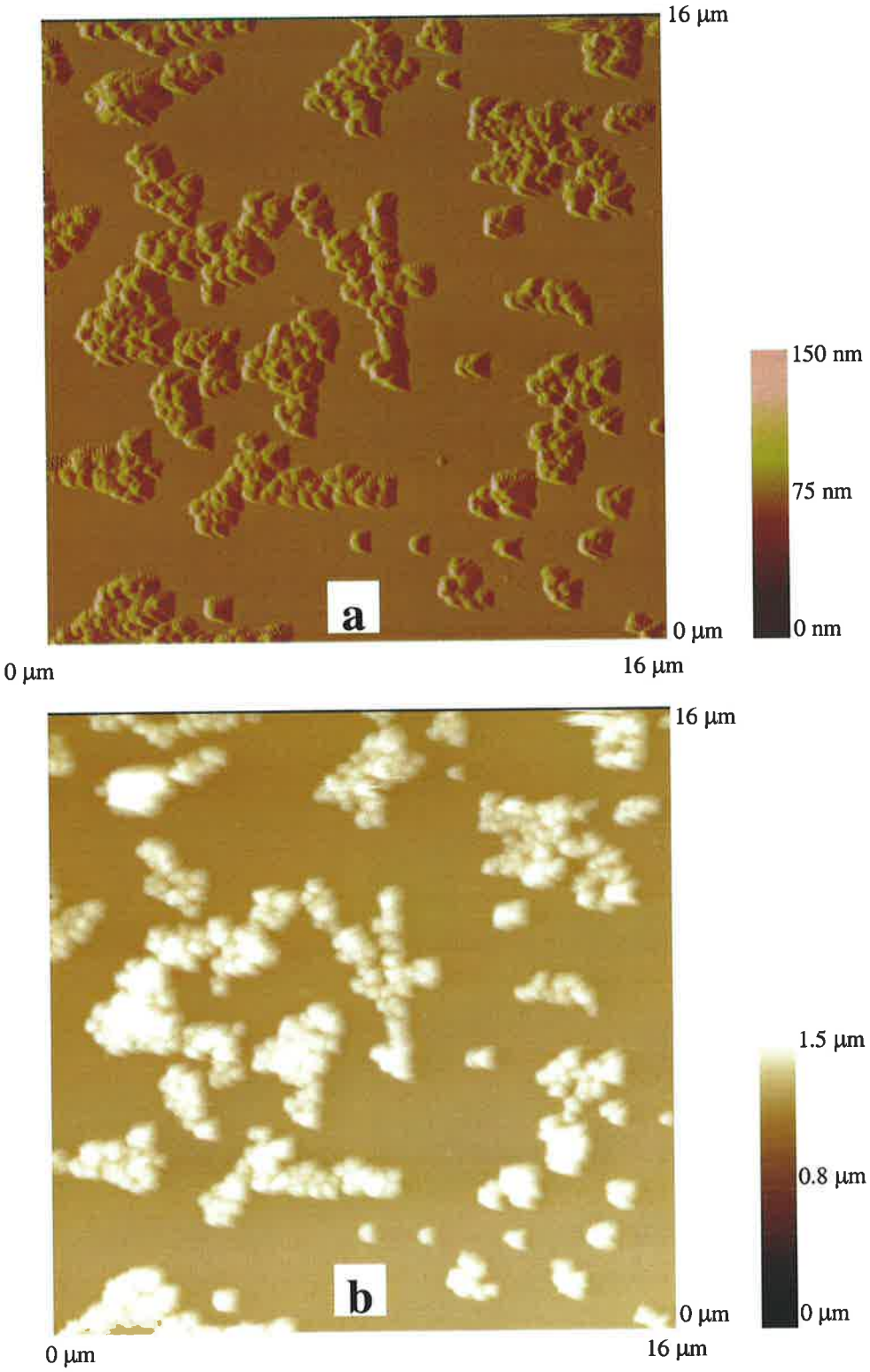

Figure 3.15 AFM images of protein inclusion bodies formed from (a) deflection data and (b) height data, a magnification of a certain area in previous image (figure 3.13). Aggregates can be seen clearly as well as single particle of inclusion bodies.

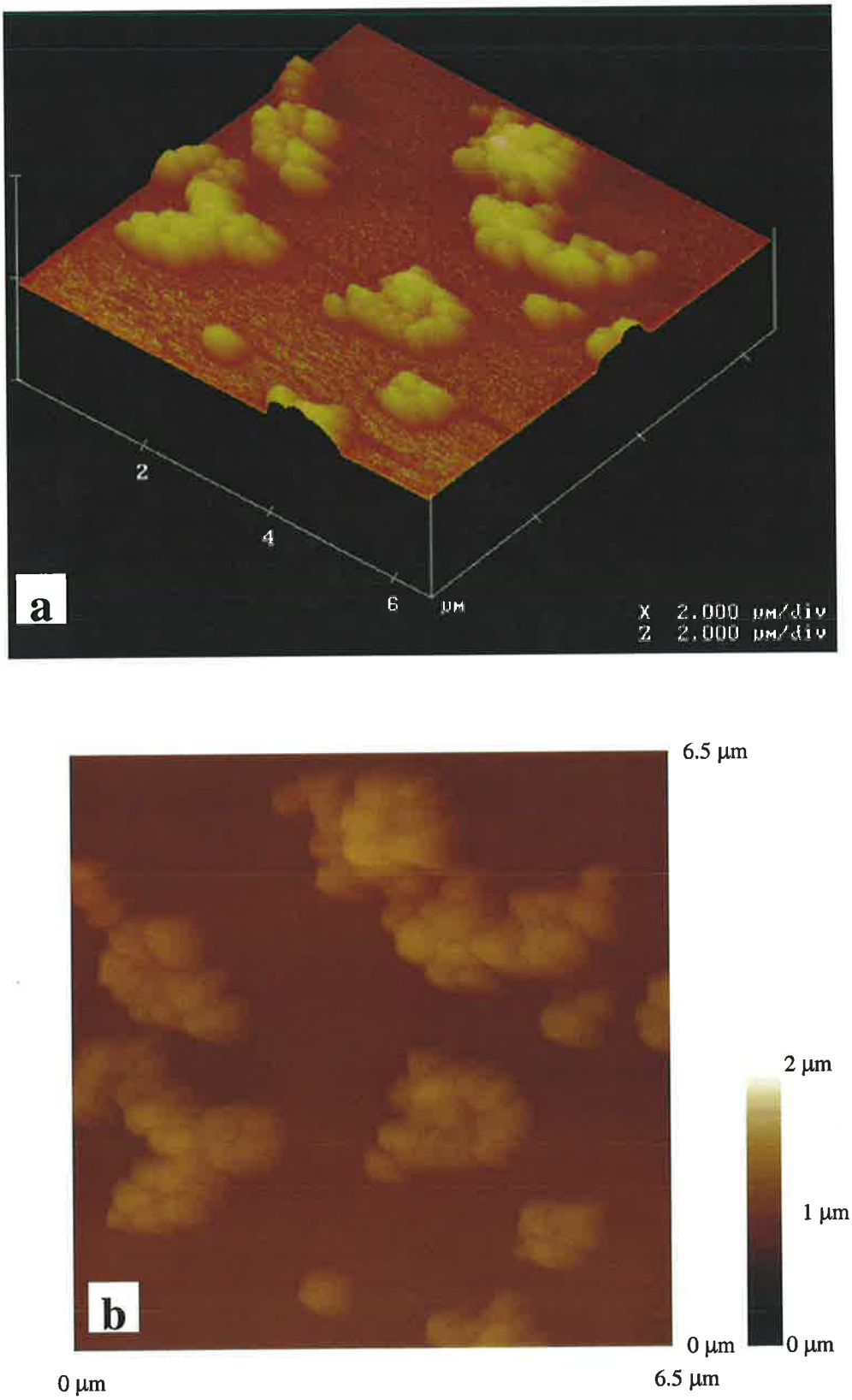

Figure 3.16 AFM images of inclusion bodies presented in three dimension (a) and two dimension (b). Both images are derived from height data.

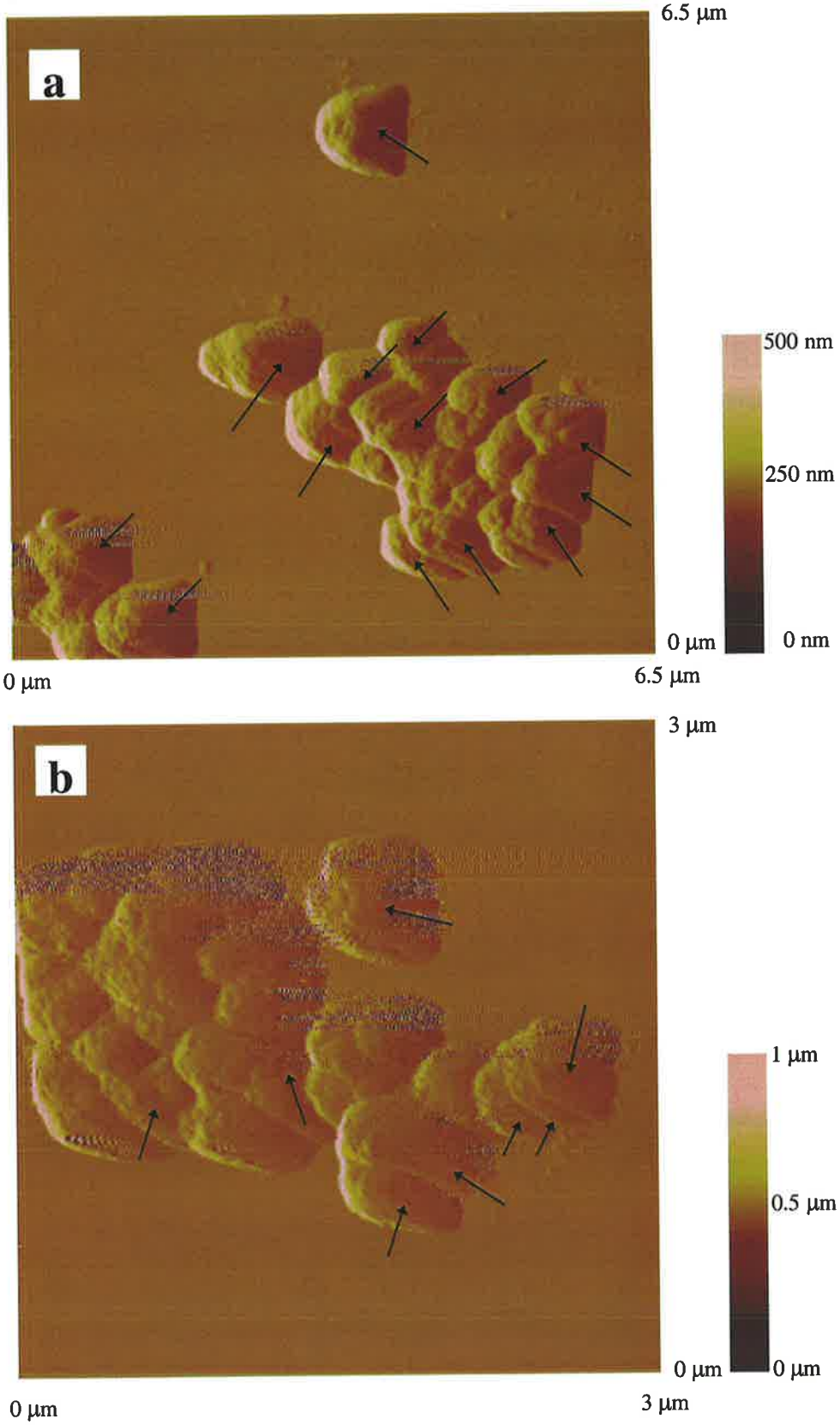

Figure 3.17 (a) AFM image of inclusion bodies obtained from magnification of a certain area in the previous image (figure 3.15) and (b) is obtained from re-scanning a certain area of (a). Arrows show the defective shapes (triangular-like shapes) appear in the image which reflect the tip-like shape. This uniform pattern of defective shapes are due to the tip-sample convolution effects.

3.3 CONCLUSION AND RECOMMEDATION

Electrophoretic mobility and the particle characteristics of an insulin-like growth factor analog LR^3-IGF-1 protein inclusion bodies have been studied. Cations and anions affect the electrophoretic mobility of protein inclusion bodies as well as cell debris. Divalent ions produce stronger effects than monovalent ions. The effects of electrolyte concentration on electrophoretic mobility follow a general trend, ie. the higher the electrolyte concentration the lower the magnitude of the electrophoretic mobility due to compression of the electrical double layer. The isoelectric point of cell debris is much lower than that for protein inclusion bodies. This suggests that they may be potentially separated using flotation. Experimental work in the electrophoretic mobility study indicates that the isoelectric point (electrophoretic mobility) provides a qualitative measure of inclusion body purity, as the isoelectric point increased for cleaner inclusion bodies.

Protein inclusion bodies (LR^3-IGF-1) have a mean particle diameter of 0.3 μm. The particle size of inclusion bodies for various fermentation strategies varied in the range of 0.30 to 0.33 μm. Surface analysis by SEM and AFM demonstrates that these inclusion bodies posses an irregular shape and a rough surface. The AFM images are comparable to the SEM images although the resolution is poorer. AFM appears to be a potential method for surface analysis of inclusion bodies due to its ability to do measurement under liquid environment coupled with spatial resolution up to the sub-nanometer scale. Higher resolution can be achieved by improvement of sample preparation and using sharper tips (eg. super tips or ultra tips). Careful sample preparation is essential to obtain a high resolution image. Aggregation is a major problem in the sample preparation of inclusion bodies. In addition, the tapping mode of the AFM is a promising operation mode to be applied as it can avoid sample deformation, particularly for soft biological materials, such as protein inclusion bodies.

Chapter 4

INTERACTION FORCES BETWEEN PROTEIN INCLUSION BODIES AND AN AIR BUBBLE: *An AFM Study*

Flotation has a great potential for protein inclusion body recovery. The bubble-particle attachment process (i.e. the interactions between particles and bubbles), is a key element in flotation processes and a careful study such interactions is essential to the rational design of flotation processes.

Atomic force microscopy (AFM) is a relatively new but powerful technique. It is capable of measuring forces up to picoNewtons consequently it has been applied to a variety of biological/ biotechnological processes. Moreover, the ability to conduct force measurement in a liquid environment provides additional benefits. Hence, this technique has been applied to study the interaction forces between protein inclusion bodies (LR^3-IGF-1) and an air bubble as a function of pH and ionic strength. This work should provide fundamental data and insight for the rational design of protein inclusion body recovery using flotation.

4.1 BACKGROUND

Atomic force microscope has been an increasingly important tool in biological/ biotechnological research. In addition to its basic ability in surface imaging (discussed in chapter 3), new applications and techniques have been developed. These applications include the use of AFM in probing and measuring nanomechanical properties and other fundamental interactions between surfaces (eg. adhesion forces). These areas of interests are of great consequence in physics, chemistry, material science, biology and other disciplines. Adhesion forces up to picoNewtons (pN = 10^{-12} N) may be measured using AFM. Adhesion between surfaces is important in a variety of biological processes, such as DNA replication, the action of drug in the human body and molecular interactions within the cells. Given the AFM's ability to examine microscopic forces, an obvious application is to measure the interaction forces between inclusion bodies and an air bubble. The following sections will discuss such force measurement and all associated aspects.

4.1.1 Tip-Sample Interactions

Tip-sample interactions play a key role in AFM measurements particularly in contact mode AFM and imaging of soft samples (eg. biological materials). Hysteresis may be observed as a result of tip-sample interactions after the tip first touches the sample surface and is then retracted. Additional energy is required to detach the tip from the sample surface. This is shown by an additional extension of cantilever deflection. The microscopic forces (long range forces) responsible for this include surface capillary forces and van der Waals forces, and/or macroscopic forces, such as adhesion forces between the tip and the sample surface. This phenomena has been applied to examine a variety of fundamental interactions in biological processes, eg. ligand-receptor, antibody-antigen, enzyme-substrate, etc. The technique is rapidly becoming a major tool for examining interactions in biological processes. This is a particular consequence of the AFM's ability to undertake both qualitative and quantitative measurements. The high level of spatial resolution also adds benefits in

biological applications, particularly in biological imaging and measurements of interactions in high proximity.

Force measurement is initially aimed at improving the AFM's image resolution by monitoring and minimising the attractive forces between the tip and sample (Prater *et al.*, -). Large adhesion forces may damage the sample and probe, reduce image resolution and create unwanted artifacts. Adhesion forces between silicon nitride tips and a mica surface have been measured in air. It was to be in the order of 100 nanoNewtons (nN), however this force is drastically reduced (to ~1 nN) when the measurements are conducted in water (Weisenhorn *et al.*, 1989). Surface capillary force is believed responsible for such a large adhesion force in the ambient environment. Surface capillary forces appear when a thin contamination layer is formed from condensed water vapour and/or other contaminants in air. Lower adhesion forces measured under vacuum (Grigg *et al.*, 1992) and in reduced humidity environments (Thundat *et al.*, 1993a) have confirmed the role of surface capillary forces on the observed adhesion force. Hence, a liquid or vacuum environment is favoured for AFM measurements. A liquid environment is particularly beneficial for biological applications as most of biological processes occur in a liquid (or physiological) environment.

Van der Waals forces in a certain extent are generally much smaller than the surface capillary forces. Very tiny (even non-detectable) van der Waals forces are commonly observed. A theoretical calculation of van der Waals forces suggests that such forces may be substantially reduced in the presence of particular solvents, especially ethanol (Hartman, 1990). This hypothesis has been confirmed by force measurements in ethanol and other solvents. The result is a dramatic reduction of adhesion forces (Weisenhorn *et al.*, 1992; Hutter and Bechhoefer, 1993b; Hutter and Bechhoefer, 1994). Even an addition of a small amount of ethanol in water reduces the forces by a factor of 100 compared to those for pure water. Ethanol's ability in removing organic contaminants from the sample surface may contribute to this effect. Ozone or ultraviolet radiation have been reported as effective methods for removing organic contaminants from AFM tips (Thundat *et al.*, 1993a & 1993b). The resulting adhesion force is reduced when tips cleaned in this manner are used for force

measurements. The combination of tip cleaning, careful attention to the environment of measurement and other improvement may reduce tip-sample forces below 0.1 nN (Prater *et al.*, -) and consequently higher AFM resolution results.

4.1.2 AFM Force Measurements

Figure 4.1 illustrates a typical force curve obtained from AFM force measurement. This curve includes a description of the adhesion force observed from the tip attachment and detachment processes clearly. The tip commences in position (A) with no contact between the tip and the sample surface. As the tip moves (down) towards the surface, it may jump into contact (B) with the sample surface if a sufficient attractive force exists from the sample surface. Once contact is made with the sample surface, cantilever deflection increases as the tip is further extended towards the sample. At this point, the tip may indent into the sample if the cantilever is sufficiently stiff (high spring constant). This phenomena is used to measure the nanomechanical properties of a material of interest. The elasticity of the sample surface can be derived from the slope or shape of the contact region (C). Next, the tip is retracted from the sample surface when a certain loading force is reached. As the tip is withdrawn from the sample surface, the tip adheres to the sample surface as shown resulting in an additional tip deflection (D) which passes the initial contact point on the approach region (B). This change is a consequence of adhesion (or interactions) formed during the tip-sample contact. Tip adhesion ruptures as the tip is retracted further and contact ceases (E), the tip then returns to its initial position. This additional tip deflection represents the force required to break the tip-sample adhesion or in other words it represents the adhesion force between the tip and the sample.

Figure 4.1 is derived from the scanner position and signal (voltage) sensed by a position sensitive detector (PSD) . The scanner position represent the Z-position (the tip position from the sample) and the PSD signal represents the deflection of the cantilever (due to forces exerted on the cantilever). Cantilever deflection can be calculated by dividing the PSD signal (V) by the sensitivity (V/nm). As the cantilever

behaves like a spring, the adhesion (interaction) force is proportional to the cantilever deflection as described by Hooke's law (equation 4.1).

$$F_{ad} = k.x \tag{4.1}$$

where F_{ad} is the force exerted on the spring (N) that causes x unit of extension/compression of the spring (m) and k is the spring constant (N/m).

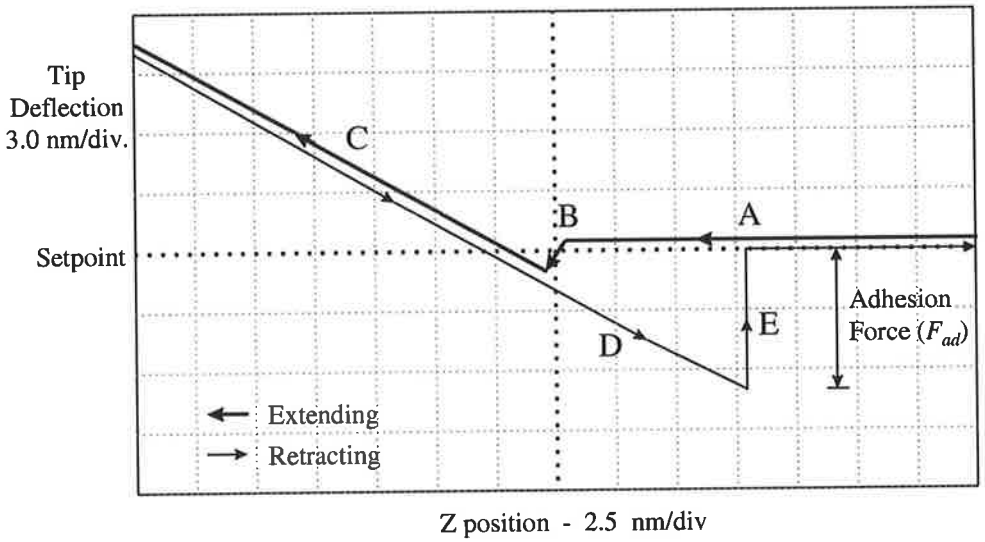

Figure 4.1 A typical force curve of AFM force measurement (as shown on the NanoScope III SPM system) plots the deflection of cantilever as the tip is extended towards the sample and retracted from the sample. The excess deflection observed when the tip is retracted from the sample surfaces (D) is known as adhesion (interaction) force between the tip and the sample surface.

Derivation of the adhesion force requires knowledge of the sensitivity and spring constant. Hence, high accuracy is paramount in the instrument's sensitivity and spring constant determination/measurement. The sensitivity is set automatically by the software. The AFM must be calibrated and adjusted prior to force measurements as described in the Reference Manual (Olympus Co. Ltd., Tokyo, Japan). The spring constant of cantilevers can be determined directly or indirectly. Various methods of spring constant determination have been developed (Cleveland *et al.*, 1993; Hutter and

Bechhoefer, 1993a; Senden and Ducker, 1994; Smith and Howard, 1994; Sader *et al.*, 1995; Torii *et al.*, 1996; Gibson *et al.*, 1996; Sader *et al.*, 1999). Spring constant determination is now regarded as routine procedure in AFM force measurements. Thus, practical considerations (eg. simplicity and ease of use) and accuracy have become the criteria for choosing the spring constant calibration method. Unfortunately, some calibration procedures are overly lengthy and complicated, and may require special preparation and tools.

A simple indirect method of spring constant calibration has been proposed by Ikai and Arakawa at the Tokyo Institute of Technology, Japan. They have adopted a similar principle to the method of spring constant calibration using thermal vibration analysis proposed by Hutter and Boechhoefer (1993a). In this case, a standard cantilever with a predetermined spring constant value provides a reference standard to determine other cantilever spring constants. The method is based on the phenomena that a difference in tip deflection between extension and retraction processes is observed when the tip is touched against a hard surface. This tip deflection difference (Δ) changes proportionally with scan rates as illustrated below (Figure 4.2). The scan rate *vs* Δ plot for different cantilevers yields different slopes proportional to their spring constants (Figure 4.2, b). Hence, the unknown spring constant may be determined by comparing the slope to that of the standard cantilever (known or predetermined spring constant). This method is relatively simple, easy to perform and provides reproducible/accurate results in a short time. Therefore, this method is adopted for this study. A cantilever spring constant calibration can be performed at the end of each experiment (force measurements).

Another important factor contributing to AFM accuracy is the precision with which the AFM scanner moves the tip over the sample (or the sample under the tip). The AFM scanner is made of piezoceramic actuators which alter their dimensions under an applied voltage. A hollow tube scanner is the most commonly used. It can moves the tip (or the sample) in all three mutually perpendicular directions, namely x, y and z (Binnig and Smith, 1986). The maximum scan size that can be achieved depends on the scanner characteristics, including the dimension (length, diameter, and wall thickness) of scanner tube and the strain coefficients of the particular piezoeletric

ceramic from which it is fabricated (Howland and Benatar, 1993). A typical AFM scanner can scan laterally (x and y) from tens of angstroms to over 100 microns and distinguish height (z) variations from sub-angstroms to about 10 microns (Howland and Benatar, 1993). Longer scanner tubes allow greater movement (or larger scan size) but as a consequence their accuracy in fine movement is significantly reduced. On the other hands, short scanner tubes provide improved accuracy in fine movement and may be more precisely controlled and stabilised. Therefore, imaging with high magnification is usually conducted using short scanner tubes.

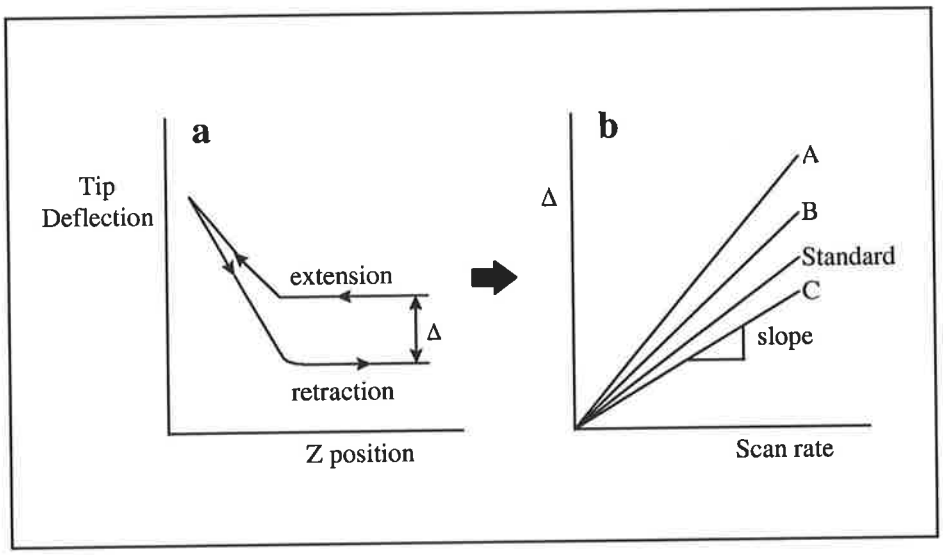

Figure 4.2 Cantilever calibration curves. (a) A typical AFM force curve obtained at high scan rate, a difference in tip position (Δ) after extension and retraction is commonly observed. (b) A plot of scan rates versus tip position differences shows linear correlation and the slope of this plot is proportional to the cantilever spring constant. Different cantilevers (A, B, C and Standard) has different slopes which represent different cantilever spring constants.

High spatial resolution, compact structure and high response speed are typical features for the piezoelectric scanner. However, scanner nonlinearities are also commonly found in practice, such as intrinsic nonlinearity, hysteresis, creep, aging and cross coupling (Howland and Benatar, 1993). Such effects are commonly minimised or eliminated by software and hardware corrections. Software corrections include sophisticated algorithms containing equations that model the scanner tube's nonlinear

response to applied voltage. The parameters of the algorithms are determined from scanner calibration procedure (Howland and Benatar, 1993). Hardware corrections may be achieved by a variety of techniques including optical, capacitive and strain-gauge techniques. More detailed discussion of this topic is available in the literature (Griffith *et al.*, 1990; Barret and Quate, 1991; Howland and Benatar, 1993). As a consequence of such factors, regular scanner calibration should be performed using a standard calibration grid. A standard procedure for scanner calibration is normally supplied by the AFM manufacturer in their Users' Manual.

4.1.3 Applications of AFM Force Measurement

As mentioned earlier, the high sensitivity/resolution and experimental versatility of the AFM has seen it widely applied in different disciplines including physics, chemistry, material science and biology. It can sense micro-forces up to picoNewtons (pN = 10^{-12} N) and is easily operated in diverse environments, including vacuum, air and liquid.

Aspects of fundamental interaction forces, such as van der Waals and electrostatic forces have been studied (Ducker *et al.*, 1990; Butt, 1991a & 1991b; Weisenhorn *et al.*, 1992). The measurements of electrostatic forces in liquid suggests that electrostatic tip-sample interactions depend strongly on pH and salt concentrations (Butt, 1991a & 1991b; Kekicheff *et al.*, 1993). It has been suggested that adjustment of pH and salt concentration to modify the repulsive electrostatic force may negate attractive van der Waals force (Butt, 1991a & 199b).

The AFM's high sensitivity for force measurements has been exploited to sense chemical interactions between different functional groups. AFM force measurement has been used by Burnham *et al.* (1990) to distinguish two similar samples, one with a surface terminated with CH_3 and the other with CF_3. Tips may be chemically modified (functionalised) to attach functional groups and then used as chemical sensors to detect the attractive/repulsive forces between the molecules on the tip and

target molecules on the sample surface. This technique, also known as chemical force microscopy, was proposed by Lieber and his team at Harvard University. They studied adhesion and friction between combinations of acid (-COOH) and methyl ($-CH_3$) functional groups using functionalised gold-coated tips and sample (Frisbie *et al.*, 1994; Noy *et al.*, 1995). They determined that forces between functional groups were distinctive. Forces between COOH and COOH functional groups being the strongest followed by CH_3- CH_3 and COOH- CH_3 respectively. Further studies of chemical force microscopy involving other functional groups, such as CH_3, OH, NH_2, COOH, $CONH_2$ (van der Vegte and Hadziioannou, 1997) and CH_3, NH_2, SO_3H (Tsukruk and Bliznyuk, 1998) have been reported. Chemical force microscopy introduced the possibility of chemical surface mapping if a library of force data between all possible combinations of functional groups is available. Another strategy of tip modifications has been proposed with glass beads functionalised and attached to the tip/cantilever. This approach has been used to study the nature of hydrophobic interactions (Ducker, 1992; Rabinovich and Yoon, 1994).

Colloid force measurement is another important application of AFM force measurement. Colloidal force measurement was initially reported by Ducker *et al.* (1990 and 1991) and Li *et al.* (1993). Attachment of colloidal particle, such as silica and polystyrene beads, onto the tip/cantilever is routinely performed to provide a colloidal probe. Colloidal probes have been used in studies of interactions between similar surfaces, including interactions between silica (Ducker *et al.*, 1990), gold (Biggs and Mulvaney, 1994), titanium dioxide (Larson *et al.*, 1993 & 1995) and zirconia (Biggs and Healey, 1994) as well as dissimilar surfaces, such as interactions between silicon oxide and titanium dioxide (Larson *et al.*, 1995), silica and α-alumina (Veermasuneni *et al.*, 1996), iron oxide and silica (Toikka *et al.*, 1996) mica and silica (Toikka and Hayes, 1997). Moreover, AFM can be used for studying colloid forces involving interfaces, such as interactions between a colloidal glass particle and an air bubble or water drop (Butt, 1994), interactions between a colloidal particle and oil droplet (Mulvaney *et al.*, 1996) and particle-drop interactions (Snyder *et al.*, 1997). This technique has a great potential for use in flotation studies where a fine particle is captured and transported by air or gas bubbles to the surface of solution. This possibility will be discussed further in the following section.

Biological applications or AFM force measurement have expanded rapidly as most biological processes (such as DNA replication, protein synthesis, drug interactions, etc) are governed by intermolecular interactions. In addition, the use of AFM force measurement to quantify the nanomechanical properties of biological materials (such as friction and elasticity) is routine. Examples include examination of the microelastic properties of biological materials, such as bone (Tao *et al.*, 1992), cartilage and living cells (Weisenhorn et al., 1993) and lysozyme (Radmacher *et al.*, 1994). A similar technique to the colloidal probe has been devised by Bowen *et al.* (1998). A single yeast cell is glued to the tipless cantilever. This cantilever is then used to measure the adhesion force between the cell and a freshly cleaved mica surface. Such measurement will aid in understanding biological and medical processes where adhesion is important.

Tip modification techniques have been extended to measure interactions forces at molecular levels. A study of binding strength between cell adhesion proteoglycans (molecules containing a mixture of sugars and proteins) has suggested this adhesion may be responsible for the structural integrity in the marine sponge (Dammer *et al.*, 1995). Frank and Belfort (1997) evaluated the intermolecular forces between extracellular polysaccharides by adsorbing the polysaccharides molecules on the sample and a colloidal probe (a silica sphere attached onto an AFM tip/cantilever). Ligand-receptor interactions are common in living system. The strength and specificity (affinity) of these interactions are the major interests in biological research. AFM measurements of binding forces between individual ligand and receptor pairs (biotin-avidin) have been reported (Florin *et al.*, 1994; Moy *et al.*, 1994a & 1994b). In these measurements, the tip is modified so that the tip outer surface is coated with avidin as shown in Figure 4.3. The sample is prepared by coating agarose beads with various forms of biotin, a ligand that binds to avidin. Individual ligand-receptor binding forces can be determined by analysing the variation in the adhesive forces and blocking free biotin on agarose beads with avidin molecules to minimise the free biotin available for binding with avidin on the tip. The binding force for biotin-avidin is measured as 160 pN whilst that for iminobiotin-avidin is 85 pN. Using similar methods, the binding forces between complementary single stranded DNA has been

measured by Lee *et al.* (1994). This work has been extended by Boland and Ratner (1995). They created self-assembled monolayers of DNA bases on a gold-coated sample surface and an gold-coated AFM tip. The binding force, which represents hydrogen bonds between complimentary bases, was detected when complimentary base pairs were present on the tip and sample, eg. adenine (A) on the tip and thymine (T) on the sample. This work may lead to the development of AFM-based DNA sequencing technique.

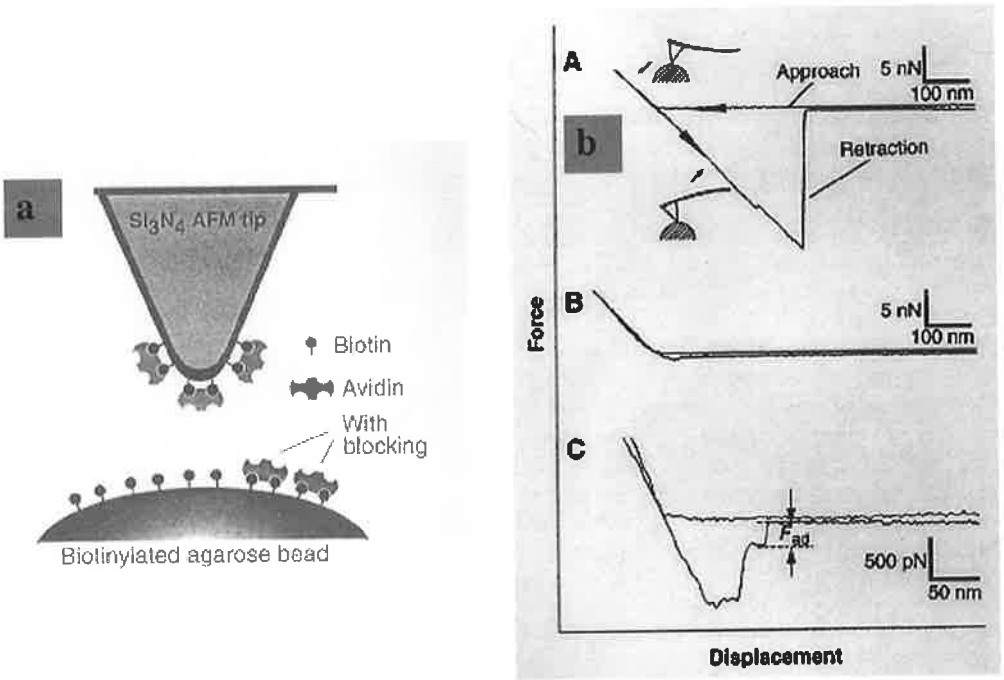

Figure 4.3 AFM force measurement of ligand-receptor binding force: (a) schematic diagram of the avidin-functionalised AFM tip and the biotinylated agarose bead, shown here partially block with avidin; (b) Cantilever deflection curves on approach and retraction of an avidin tip on a biotinylated agarose bead (A) before and (B) after blockage with an excess of free avidin (200 μg/mL), (C) Magnification of a force scan on a biotinylated agarose bead approximately 95% blocked with free avidin, Fad is the measured unbinding force plotted (after Florin *et al.*, 1994).

Further improvement of tip modification has lead the development of sensor force microscopy as proposed by Schindler and co-workers (Haselgrubler *et al.*, 1995). In this technique, a single biological molecule is attached to the AFM tip on the end of a

molecular tether (an elastic linker molecule, also called spacer) which is a few nanometers long based on polyethylene glycol (PEG) molecules. This spacer allows the biological molecule attached to it to orient such that proper binding can be formed with the target molecule in the sample surface. This technique has been employed to measure the binding force between human serum albumin (HSA) and its associated antibody (Ab_{HSA}). The resulting force was 470 pN. This provide a significant improvement for biological force measurements as most biological interactions are stereo-specific, for example enzyme-substrate interactions. Moreover, this technique facilitates the measurement of binding forces between a limited number of molecules pairs or even single molecules pair. The influence of other interactions on the specific interactions being measured may also be reduced. Such a technique has been adopted by Ikai's research group at the Tokyo Institute of Technology to study protein folding/refolding. AFM force measurement has also been applied to study the affinity or specificity of biological interactions (bindings), such as examination of specific antigen-antibody binding (Browning-Kelley *et al.*, 1996) and antibody recognition (Raab *et al.*, 1999).

It is clear that AFM has significantly contributed to the progress of biological research. There has been rapid progress in AFM techniques and development since the early 1990s. I believe that AFM will play a more significant role in future biological research leading us to a realisation of the Molecular or Nano World.

4.1.4 Experimental Design and Strategies

In this work, AFM is employed to study interactions between protein inclusion bodies and an air bubble. This attachment process play a key role if protein inclusion bodies are recovered from cell debris by flotation. To conduct this study, an experimental design and various experimental strategies have been developed. Measurements were performed using an AFM suitable for biological applications (Olympus NV2500aqac Scanning Probe Microscope manufactured by Olympus Co. Ltd., Tokyo, Japan). This AFM has incorporated an inverted microscope which adds an additional benefit, i.e.

visual observation of sample and processes during measurements. In this system the piezo scanner moves the tip over the sample. This is opposite to the Digital Instrument system used for imaging inclusion bodies (chapter 3) where the piezo scanner moved the sample under the tip. Details of the standard operation and experimental procedures are outlined in section 4.2.6. and in the Users' Manual supplied by the manufacturer. The interaction forces between protein inclusion bodies and an air bubble were measured via the tip-sample interactions. Therefore, protein inclusion bodies must be attached to the tip and a small and stable air bubble must be formed as discussed in the following sections.

Tip Modifications

Standard silicon nitride (Si_3N_4) tips for contact mode AFM (Digital Instruments, Inc., Santa Barbara, USA) were used in this study as they have low nominal spring constants. Details of these tips are summarised in Figure 4.4.

Chemical linkage with a cross linker or spacer is adopted to attach the inclusion body particles on to the tip. The cross linker is added to extend the 'bridge' between inclusion body particle and the tip. The aim is to minimise the influence of the tip-sample interactions (long range forces) on the interaction force between inclusion body and bubble measured. Silanisation is the most commonly employed method for chemical modification of the tip. The method proposed by Brzoska *et al.* (1992) was adopted with some modification. Thiols or amines terminal functional groups can be attached to the tip surface through silanisation. SPDP (*N*-succinimidyl 3-[2-pyridyldithio] propionate) is used as a cross linker. SPDP is a heterobifunctional cross linker containing one *N*-hydroxysuccinimide (NHS) residue and one pyridyl disulfide residue which are reactive to primary amines ($-NH_2$) and sulfhydrils (-SH) respectively.

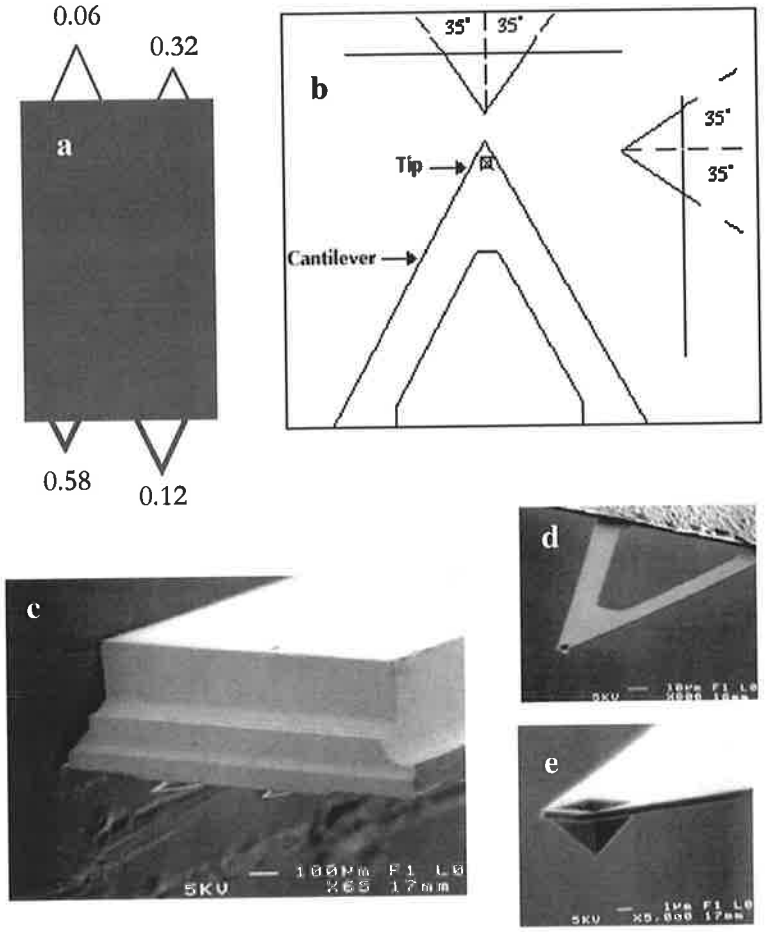

Figure 4.4 Details of standard silicon nitride (Si_3N_4) tips. (a) Schematic diagram of 4 cantilevers (V shape) with two different length (100 and 200 μm) and thickness attached on a single substrate, showing approximate spring constants. (b) Schematic diagram of the tip sidewall angles, the tip shape is square pyramidal with tip half angle of 35° and nominal tip radius of curvature of 26-60 nm. SEM image of (c) two cantilevers on substrate, (d) a single cantilever and (e) a Si_3N_4 tip. (*after Digital Instruments, Inc. Santa Barbara, CA, USA, http://www.di.com*).

Some amino acids, including lysine, arginine, asparagine and glutamine, carry primary amine functional group in their side chains and only cystein possesses sulfhydril functional group in its side chain. LR^3-IGF-1 protein consists of 83 amino acids, including those which possesses the primary amine and sulfhydril functional groups. The percentage of primary amines (17%) is more than double that of sulfhydrils percentage (7%) in this protein and when the protein is in its native form, these free sulfhydrils react to each other and form 3 disulfide bond. Therefore, it was

considered more reliable to attach this protein to the tip through its free primary amine groups. As a consequence the tip is silanised using MTS (3'-mercaptopropyl-trimethoxy-silane) providing free SH groups on the tip surface which then react with pyridyl disulfide residue of the cross linker during cross linking reaction. The free NHS residue of the cross linker reacts with free primary amines present in the protein inclusion bodies. The schematic diagram of inclusion body attachment to the AFM tip is summarised in Figure 4.6.

The attachment of protein inclusion bodies to the tip may be assessed by a fluorescent technique. Protein inclusion bodies are labelled using fluorescein isothiocyanate (FITC) so that they may be detected by fluorescent microscope following tip modifications. FITC is chosen for labelling because it binds to an amine group of lysine present in the protein inclusion bodies (Figure 4.5). A scanning confocal microscope optical (SCOM) was employed to examine the FITC-labelled protein inclusion bodies attached to the tip.

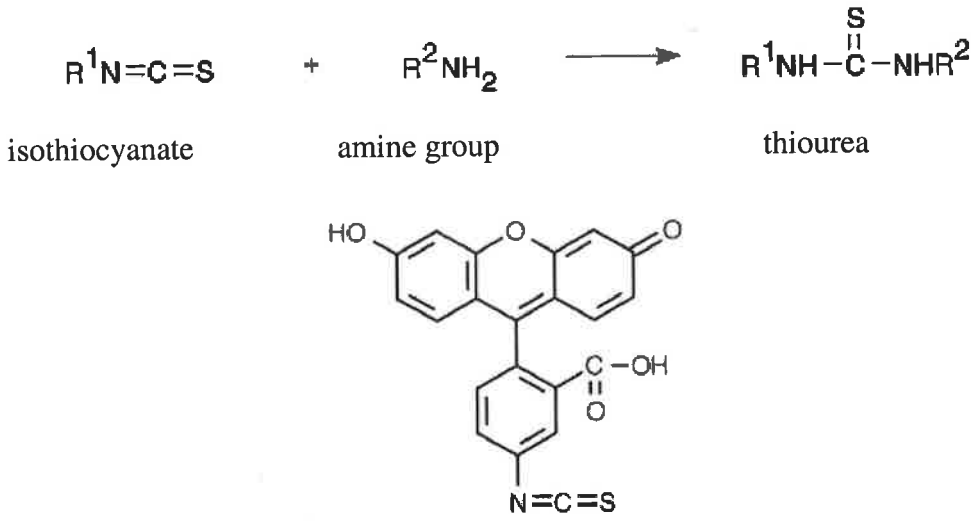

Fluorescein Isothiocyanate (FITC)

Figure 4.5 Structure of FITC (F-148, MW = 389.38) and its reaction with protein, isothiocyanate reacts with amine group (of lysine) forming thiourea which binds fluorescein to the protein inclusion bodies.

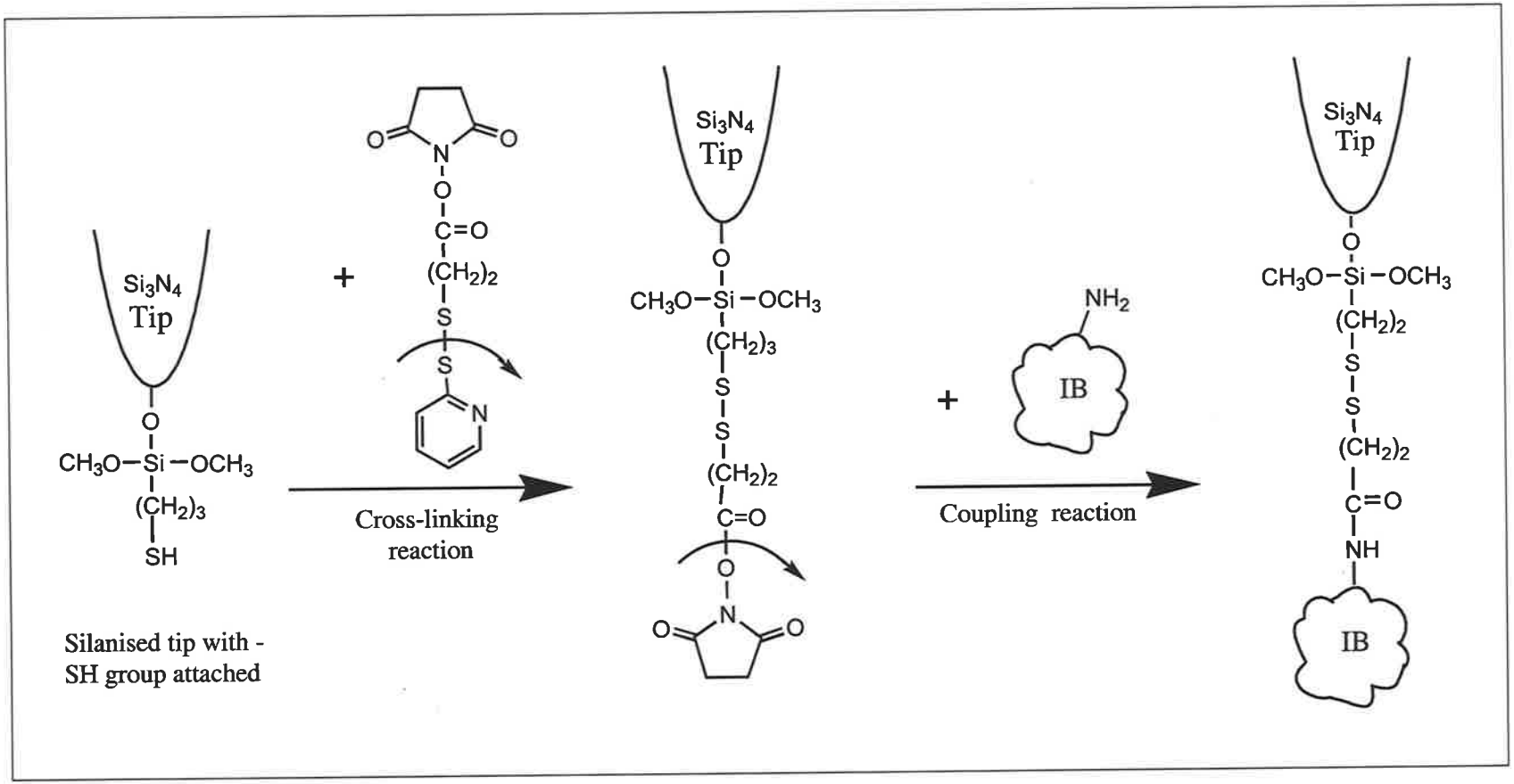

Figure 4.6 Schematic diagram of chemical reaction involved in tip modifications where protein inclusion body particles are attached to the AFM tip through a cross linker (SPDP) linked to -SH functional group on the silanised tip.

Bubble Formation

Small bubbles are required in flotation of fine particles, such as inclusion body particles (discussed in chapter 1). An aim of this work is to conduct the experiment with bubbles of similar size to those employed in practice. Bubble diameters in the range of 10 to 120 μm are typically obtained in dissolved-air flotation system (Takahashi *et al.*, 1979; Zabel, 1984; De Rijk *et al.*, 1994; Fukushi *et al.*, 1998). Such bubbles are generated by dissolving air under pressure (typically 350-550 kPa) and then lowering the pressure by release to atmospheric pressure through nozzles or pressure reducing valves (eg. needle valves) in the flotation tank. This technique is hard to perform where a single bubble must be generated and then attached to the bottom surface of the liquid cell. Also, fine bubbles are hard to handle and observe visually. As an alternative, an air bubble with diameter of approximately 1 mm was formed using a gas chromatography syringe with a fine needle. This bubble is then attached to the scratched surface at the bottom of the liquid cell. The surface was scratched using a sharp needle to ease bubble attachment as it provided a higher surface contact area.

Liquid Cell and Experiment Setting

A plastic petridisc (35 mm in diameter) was employed as for the liquid cell. This shape matches the base of the sample holder of the inverted microscope. The disc is chosen as it is inexpensive, easy to obtain, and transparent thereby allowing visualisation by microscope from the bottom. The petridisc is filled with an appropriate buffer solution prior bubble formation. A schematic of the setting for interaction force measurement is presented in Figure 4.7.

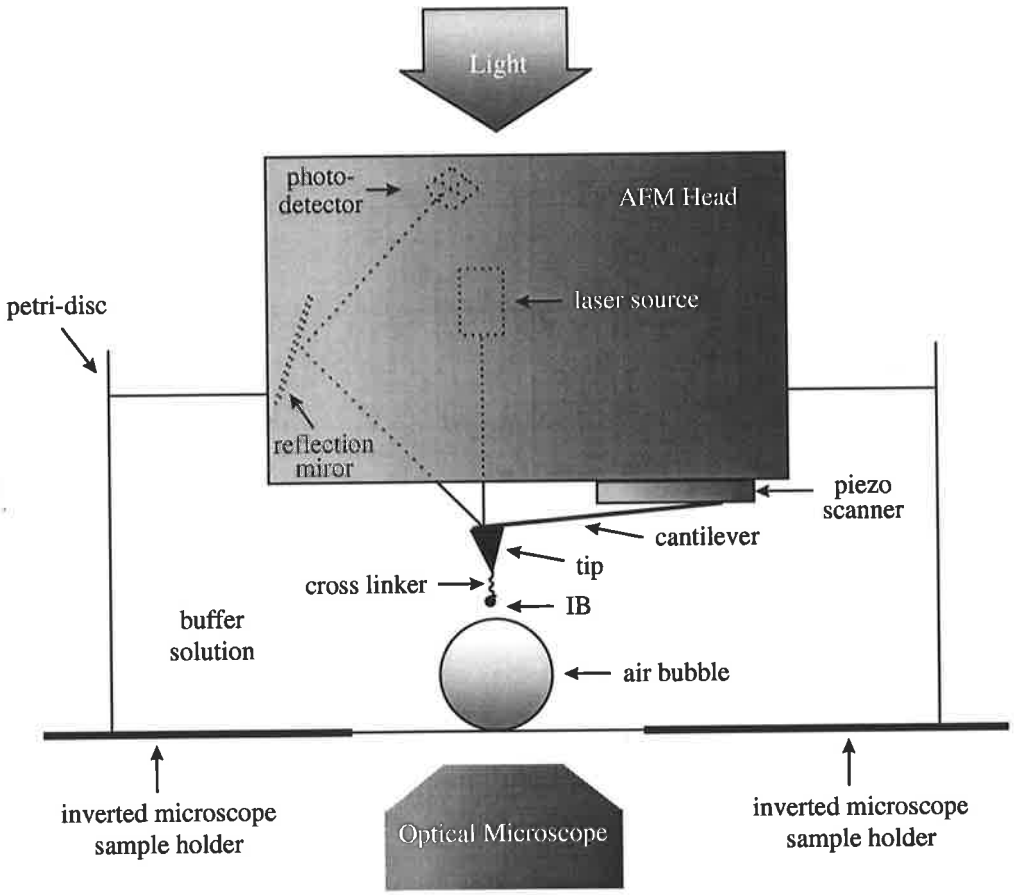

Figure 4.7 Schematic diagram of AFM force measurement setting.

4.2 MATERIALS AND METHODS

4.2.1 Sample Preparation

Frozen inclusion bodies (procedure C, chapter 3) were thawed and suspended in 5 mL phosphate buffer (0.05 M, pH 8) to a final concentration of 1 g/L. This suspension was then sonicated (Silent Sonicator) for 5x1 minutes with 1 minute interval break to rupture aggregates formed during freezing and storing. Sample (fluorescent) labelling is then carried out.

4.2.2 Sample (Fluorescent) Labelling

Fluorescein isothiocyanate (FITC) F-143 used for labelling protein inclusion bodies was purchased from Molecular Probe, Inc. (Eugene, OR, USA). FITC is reactive to the amine groups in inclusion bodies. This labelling permits confirmation of attachment of the inclusion bodies on to AFM tips (tip modifications). FITC is added to the inclusion body suspension (1 g/L) at protein to FITC molar ratio of 1 : 4. LR^3-IGF-1 protein and FITC have molecular weights of 9110.6 Da and 389.38 Da respectively, hence 0.16 mg of FITC was added to the 5 mL inclusion body suspension, then stirred and incubated at 4°C for 20 hours . The sample bottle is wrapped with aluminium foils to avoid exposure to light. Unbound FITC was removed using an adsorption column (Sephadex G-25, Pharmacia, Sweden). Prior to sample injection, this column was cleaned and equilibrated using a phosphate buffer saline (PBS) solution (0.05 M, pH 7) for approximately 15 minutes. The remaining PBS solution on top of the column is removed following 2 mL sample injection. The column was next eluted using PBS solution (0.05 M, pH 7). The eluent then passed through a UV spectrometer (SJ-1541 Eluent Absorbance, Ichibashi Co. Ltd., Japan) to measure absorbance at 280 nm. The eluent is collected once the first peak appears in the absorbance chromatograph. The yield of the FITC labelling can be assessed by measuring the absorbance of eluent at two different wavelength (280 nm and 490 nm)

using U-3210 Spectrophotometer (Hitachi Co., Ltd., Japan). The molar ratio of reacted FITC to protein can be calculated from Equation 4.2. The molar ratio obtained is normally in the range of 2-4. Another assessment (visual) is also conducted using a scanning confocal optical microscope (SCOM).

$$MolarRatio(FITC : protein) = 2.87 \frac{A_{490}}{(A_{280} - 0.35A_{490})} \quad (4.2)$$

4.2.3 Tip Modification

Standard silicon nitride (Si_3N_4) probes were used in force measurements. These were obtained from Digital Instruments, Inc. (Santa Barbara, CA, USA). The probes consist of a V-shape cantilever integrated with a sharp square pyramidal tip at the end (for details see figure 4.4). The long (200 μm) and thin cantilever with a nominal spring constant of 0.06 N/m was employed in force measurement as it possesses the smallest spring constant and hence the highest sensitivity.

Protein inclusion bodies were attached to the tip by covalent bonds through a spacer (crosslinker). The tip modifications procedure consists of a number of steps adopted and modified from Brzoska *et al.* (1992). First, the tip surface was cleaned by rinsing with chloroform, ethanol and Milli-Q water then vacuum dried. The clean tips were then oxidised in order to permit silanisation. The oxidised tips were silanised using 3'-mercaptopropyl-methoxysilane (Aldrich Chem. Com., US) to yield a free reactive thiol group (-SH). The silanised tips were cross-linked with *N*-succinimidyl3-(2-pyridyldithio)propionate (SPDP) obtained from Pierce (Rockford, IL, US). SPDP is a heterobifunctional crosslinker, containing one *N*-hydroxysuccimide (NHS) residue and one pyridyl disulfide residue. The pyridyl disulfide residue reacts with the free -SH group of the silanised tip, leaving its NHS residue free which then reacts with amino ($-NH_2$) group of the protein inclusion bodies (protein linking). The tip modification procedure is summarised in Table 4.1 and the chemical reactions

involved in tip modification processes are summarised in Figure 4.5. Evaluation of tip modifications was performed using scanning confocal optical microscope (SCOM).

Table 4.1 Sequential steps in the tip modifications procedure

1. SURFACE CLEANING :
   - rinse twice with chloroform
   - rinse twice with ethanol
   - rinse twice with Milli-Q water
   - vacuum dry for 10-15 min.
2. OXIDATION :
   - incubate in H_2SO_4 / H_2O_2 mixture (7:3) for 15 min.
   - rinse twice with Milli-Q water
   - vacuum dry for 10-15 min.
3. SILANISATION (THIOLATION):
   - incubate in toluene / MTS[a] mixture(100:2) for 1 hour
   - rinse twice with toluene
   - rinse twice with ethanol
   - rinse twice with PBS[b] solution (0.05 M, pH 7)
   - vacuum dry for 10-12 hours
4. CROSS-LINKING :
   - dissolve SPDP[c] (1.25 mg) in DMSO[d] (200 µL) and dilute with ethanol (1.8 mL)
   - incubate the silanised tips in the SPDP solution for 1 hour
   - rinse twice with Milli-Q water
5. PROTEIN LINKING :
   - incubate the treated tips in the inclusion body suspension for 1 hour
   - rinse the modified tips twice with Milli-Q water or buffer solution

a. MTS = 3-mercaptopropyl-trimethoxysilane
b. PBS = phosphate buffer saline
c. SPDP = N'-succinimidyl 3-(2-pyridyldithio)propionate
d. DMSO = dimethyl sulfoxide (Aldrich Chem.Co., US)

4.2.4 Scanning Confocal Optical Microscopy

A MCR-600 Scanning Confocal Optical Microscope (Bio-Rad Laboratory, California, USA) was employed to evaluate the sample labelling and tip modifications results. Sample preparation for FITC-labelling evaluation is as follows: a drop (50 μL) of FITC-labelled inclusion body suspension was laid on a microscope objective glass and covered with a thin glass cover, it was then placed on the sample holder of the SCOM for imaging. The inclusion body-modified tip was placed on the microscope objective glass and located in the sample holder of SCOM for examination. A laser light was focused by an objective lens onto the object and the reflected fluorescent light is focused back onto a photodetector via a beam splinter. In SCOM, a confocal aperture (or pinhole) is placed in front of the photomultiplier tube detector to prevent detection of unfocussed light. Images are formed by scanning the focussed spot relative to the object which was then stored in a computer-imaging system. For a more complete description, the reader should consult the available literature (Sheppard, 1993). Light contrast and lens focus were adjusted where necessary to obtain optimal image.

4.2.5 Bubble Formation

Small air bubbles were created by a 5 μL Hamilton 700 Series Microliter™ Syringe (Alltech Associates, Pty. Ltd., NSW, Australia) using a fine removable needle. A petridisc of diameter 3.5 cm was employed as a liquid cell. A small area with a roughened surfaces was created in the centre of the petridisc's bottom by scratching the surface with a sharp needle. The roughened surface holds the air bubble due to increased contact area. The petridisc was next filled with a buffer solution and a small air bubble was formed in this solution. To ensure uniform bubble size throughout the experiment, the air volume used for creating the bubble was controlled at a fixed value. To achieve this goal, the syringe's shaft was adjusted to ensure that the needle was filled with air. Then, 0.5 μL of air was pumped out and a tiny bubble formed at the end of the needle. This bubble was laid on the rough surface of the petridisc very carefully until it attached to the surface. Force measurement may then be performed.

4.2.6 Force Measurement

Force measurement was undertaken using an Olympus NV2500aqac Scanning Probe Microscope (Olympus Co., Ltd., Tokyo, Japan). The modified tip was located in the cantilever holder and mounted to the AFM head. The AFM head was then configured as shown in Figure 4.7. Next, the laser light was activated and adjusted to obtain optimal reflection as described in the AFM users' manual.

The optical microscope was used to position the tip at the centre of the bubble. The step motor is then activated to move the tip down towards the bubble. The tip's approach is observed by optical microscope and motion was stopped when the tip is in close proximity to the bubble's surface. Finer steps (approximately100 to 200 nm) are then carefully performed until the tip touches the bubble surface. This is indicated by an internal signal jump in the monitor oscilloscope or by direct visual observation on a monitor linked to the optical microscope. Next, the tip is lifted approximately 1-2 μm until the tip and the bubble are no longer in contact. False engagement is performed by inputting the set point lower than the set signal, eg. inputting setpoint of -1 V (it should be, for example, 0 V in normal engagement) when the set signal was -1 V. This false engagement activates the feed-back system without having the tip touching the bubble surface. Active feedback system is required to conduct any measurements. Automatic feed-back system is engaged by clicking the automatic tip approach button. Force versus distance measurement is then conducted using force calibration mode. Final tip-bubble separation distance is adjusted by fine steps of tip approach until the force curve appears in the monitor. Stable force curve is obtained by adjusting the tip-bubble separation and other parameters, including z scan start (position the graph horizontally on the force curve), graph range (scales the vertical axis of the graph to show more or less of the force curve) and setpoint (positions the graph vertically on the force curve by setting the horizontal centre line at the setpoint value indicated). After stable force curve is obtained, the sensitivity is calibrated and the force curve is recorded.

The interaction force between the inclusion bodies and an air bubble was measured at various pH (3, 4, 5, 6, 7, 8, 9, 10) and electrolyte concentrations (0.05 M, 0.1 M and 0.2 M). Due to a wide range of pH range used, two different buffers were employed, i.e. citric acid buffer (pH 3 to 6) and tris buffer (7-10). NaCl is added to the buffer to maintain a constant ionic strength throughout the working pH range. At each condition, approximately one hundred force curves were recorded with the experiment repeated 3 times from a false engagement. The aim was to ensure measurement consistency. Control experiments were performed to distinguish if the measured force was the interaction force between inclusion body and the bubble (or not). Such test were performed by measuring the interactions force between the air bubble and a bare-tip, a silanised tip and an SPDP-modified tip.

4.2.7 Spring Constant Calibration

The cantilever spring constant was calibrated using a method developed by Ikai and co-workers at the Tokyo Institute of Technology (Japan). The method is based on the principle that a difference in cantilever deflection occurs between extension and retraction when the tip is subjected to hard surfaces. This difference changes proportionally with the scan rate (Figure 4.2). If the scan rate is plotted against the difference between retraction-extension deflections (Δ), then the spring constant can be estimated from the slope of the plot. The value of the spring constant of a cantilever (tip) may be determined by comparing the slope of the Δ *vs* scan rate plot to the slope of a standard cantilever with a known/predetermined spring constant value. Tip calibration was performed in aqueous environment, similar to the environment for force measurements at six different scan rates (0.543, 5.01, 9.3, 16.3, 21.7, 32.6 Hz). A silicon nitride tip with a pre-determined spring constant (0.0740 N/m) was used as a standard.

4.3 RESULTS AND DISCUSION

4.3.1 Sample Labelling and Tip Modifications

Figure 4.8 shows images of the FITC-labelled protein inclusion bodies scanned with an SCOM. As expected, FITC appears to be suitable for labelling protein inclusion bodies as it binds to $-NH_2$ functional group (of lysine) present in inclusion bodies. The absorbances of labelled inclusion bodies at 280 and 490 nm were 0.0515 and 0.0338 respectively which correspond to a molar ratio of FITC bound to the inclusion bodies of 2.45 (Equation 4.2). This value lies within the range commonly used for labelling (2 to 4). Inclusion body aggregates are clearly apparent as shown by large spots in Figure 4.8.a. These aggregates were probably formed when the sample was frozen for storing & transporting and/or during sample preparation. This problem has been previously encountered when topographical images of the inclusion bodies were performed using AFM (chapter 3). Therefore, the sample suspension was sonicated to break up aggregates such as smaller form and more uniform particles. A series of experiment of different duration sanction were conducted. Soncation for 5 intervals of 1 minute with a 1 minute pause appears adequate to obtain relatively uniform particle size as shown by Figure 4.8.b. A control experiment was performed by imaging an unlabelled sample and a blank image is typically obtained as shown in Figure 4.8.c.

SCOM images of inclusion bodies-modified tip may be used to determine if a modified tip's performance is acceptable for AFM force measurements. A typical modified tip as illustrated in Figure 4.9.a was employed in AFM force measurement. FITC-labelled protein inclusion bodies were detected at the end of cantilever where the tip is located (shown by an arrow). However, tip modifications may also result in a modified cantilever with an unmodified tip (Figure 4.9.b), i.e. no inclusion bodies are attached to the tip. Incorporation of inclusion bodies onto the chemically modified tip is the critical step in the modification processes. Clearly, process improvement of this step is essential.

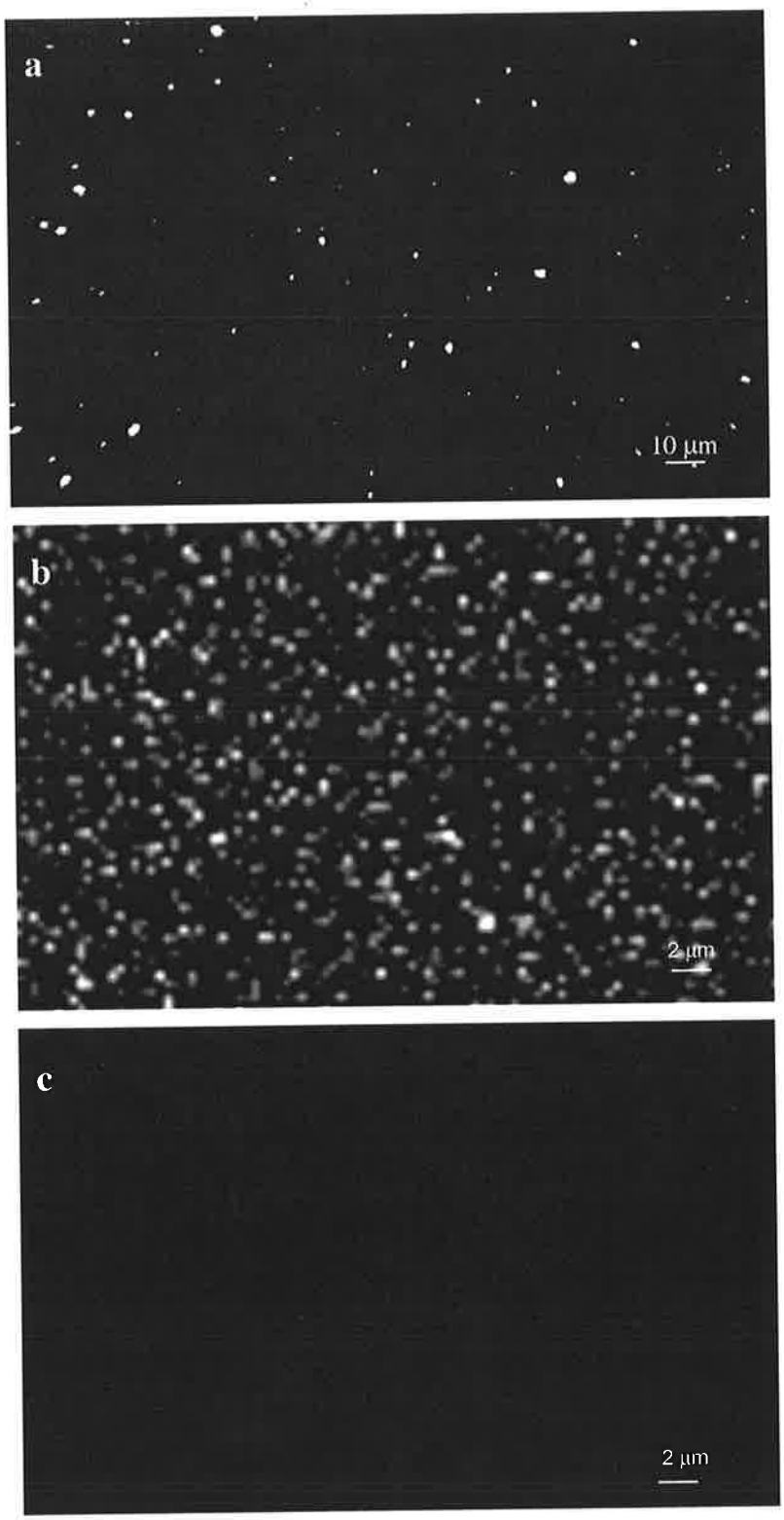

Figure 4.8 FITC-labelled protein inclusion bodies imaged by an SCOM. (a) Inclusion body sample suspension was not subjected to sonication, showing aggregates of inclusion bodies. (b) Inclusion body sample suspension was sonicated (5 x 1 minutes) showing relatively more uniform particle size. (c) A typical control image of unlabelled inclusion body sample .

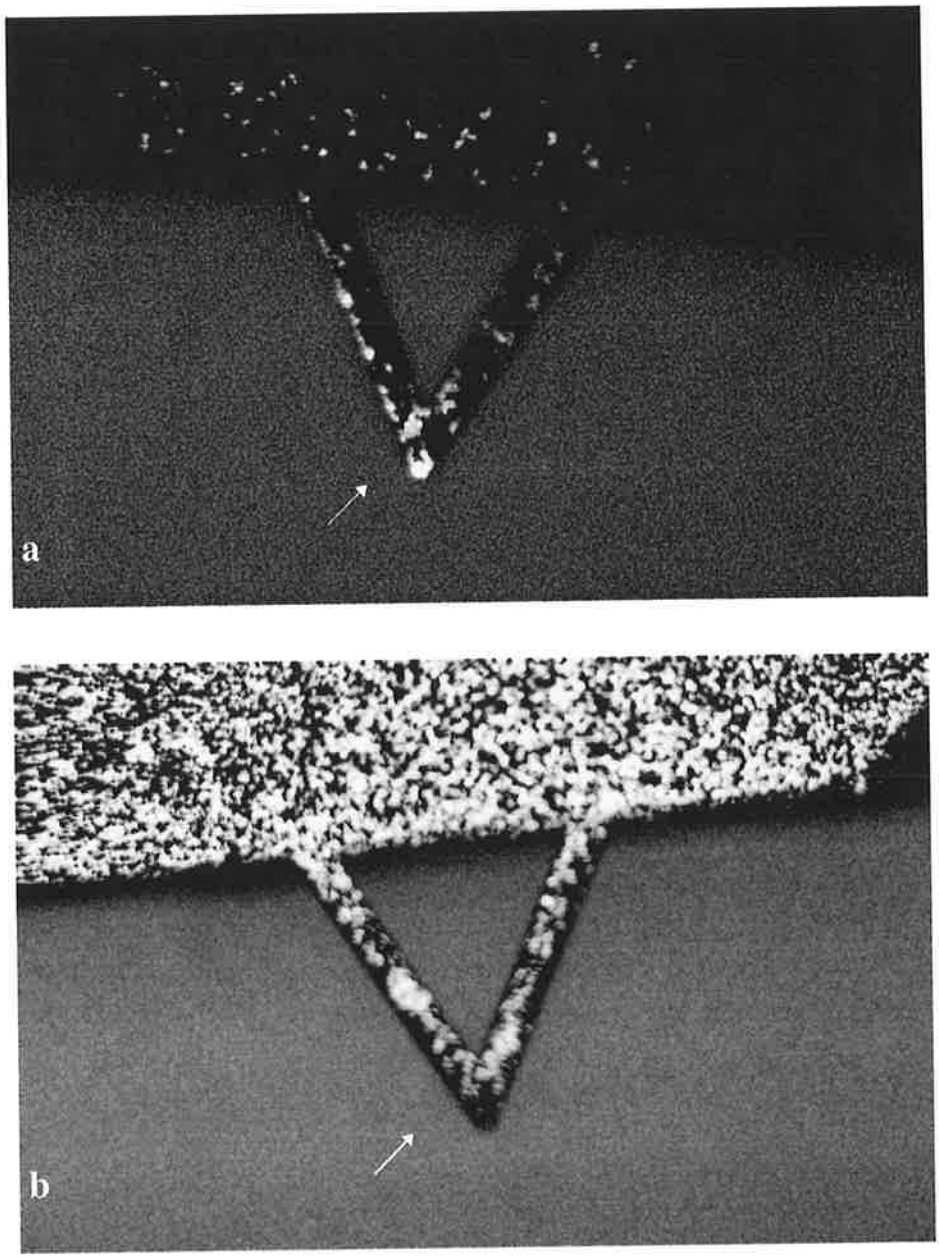

Figure 4.9 A modified cantilever/tip imaged by an SCM shows (a) FITC-labelled protein inclusion bodies (10 mg/L) attached to the tip (arrow) and (b) none of the inclusion bodies attached to the tip (arrow)

It is possible to modify the tip without modifying the cantilever. For example, only the tip may be incubated with inclusion body suspension or else all cantilever surfaces except the tip may be blocked to prevent inclusion body attachment. Attachment of inclusion bodies to the cantilever may be prevented by chemical or physical means. Chemical blocking agents modify the cantilever surface such that attachment onto the surface is not possible. Physical blockage is normally performed by covering the

cantilever surface with an inert material to which the inclusion bodies do not adhere. The physical methods are complex and difficult to use. The initial solution, ie the chemical modification of the tip only, is simpler and easier to perform. Hence, modification of the tip only or minimisation of the modified area was attempted. During the tip modification processes (from silanisation to incubation with inclusion bodies) the cantilever/tip is held by the AFM. The tip may then be moved towards the solution and then submerged in the solutions. In this manner, contact of the cantilever with the solution can be avoided. Unfortunately, this process is not easily performed due to the small size of the cantilever and tip. Once the cantilever touches the solution, it often snaps into the solution due to surface tension effects. Vaporisation of the solution poses another problem in this method. After some time had elapsed, it was observed that the tip was no longer submerged in the solution (again a consequence of vaporisation/evaporation of the solution). The silanisation and cross linking reactions were carried out in an organic solvent environment the solvent's volatility meant that vaporisation is unavoidable. Hence, the coating strategy could only be applied to the last step, i.e. protein inclusion bodies incorporation onto the tip. The tips location must be monitored and altered from time to time to compensate for solution volume reduction due to evaporation. However, the limited movement allowed in the AFM system severely constrains the positioning of the cantilever/tip and the tendency of cantilever to snap into the solution cannot be avoided. Improvement are possible, for example by using a micro-manipulator where movement can be controlled very easily and precisely with the help of appropriate optical microscopes. Evaporation of sample solution remains a problem. This could be reduced by incubating the tip in a closed system (eg. a small contained room/space) where evaporation would substantially lower.

Another problem is that tip modifications are affected by the concentration of inclusion body sample. Theoretically, the possibility of inclusion bodies attachment to the tip can be increased by using higher sample concentrations. Unfortunately using a highly concentrated sample results in an excessive number of particles attaching to the cantilever and tip surface. This is undesirable as shown in Figure 4.10. Different concentration of inclusion body sample were examined and a sample concentration of 10 mg/L appeared optimal.

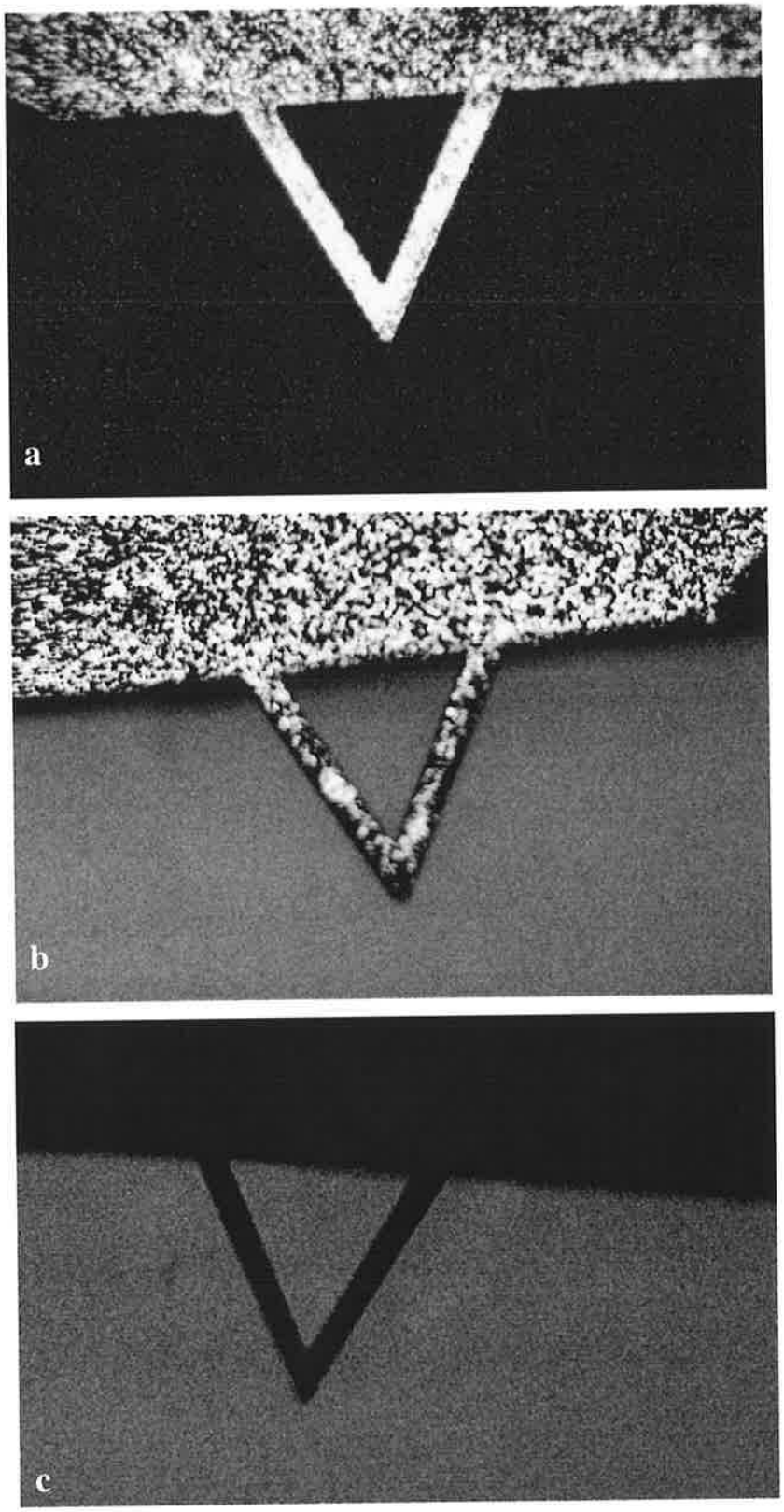

Figure 4.10 SCM images of cantilevers/tips modified at different concentrations of FITC-labelled protein inclusion bodies, (a) 1 g/L and (b) 0.2 g/L, show variation in degree of protein attachment. A typical non-modified cantilever/tip SCM image (c) was taken for each imaging as a control.

Extra care is required during tip modification processes as the tip and cantilever are very delicate and extremely sensitive to any small forces. Deformed or broken cantilevers/tips were often observed following the modification processes. Hence, careful checking of the state of cantilevers/tips with an optical microscope prior each step of modification processes is recommended. Large cantilever deflection due to surface tension effects were observed (under optical microscope) when the cantilever was inserted perpendicularly into solutions. Such treatment may deform or break the cantilever and/or affect the cantilever/tip physical properties. Excessive deflection can be avoided by inserting the cantilever into solutions on its side. Figure 4.11 shows a deformed cantilever following tip modifications. Clearly, SCOM analysis is vital so that one may evaluate the results of tip modifications and ensure the reliability of the tip for use in AFM force measurements.

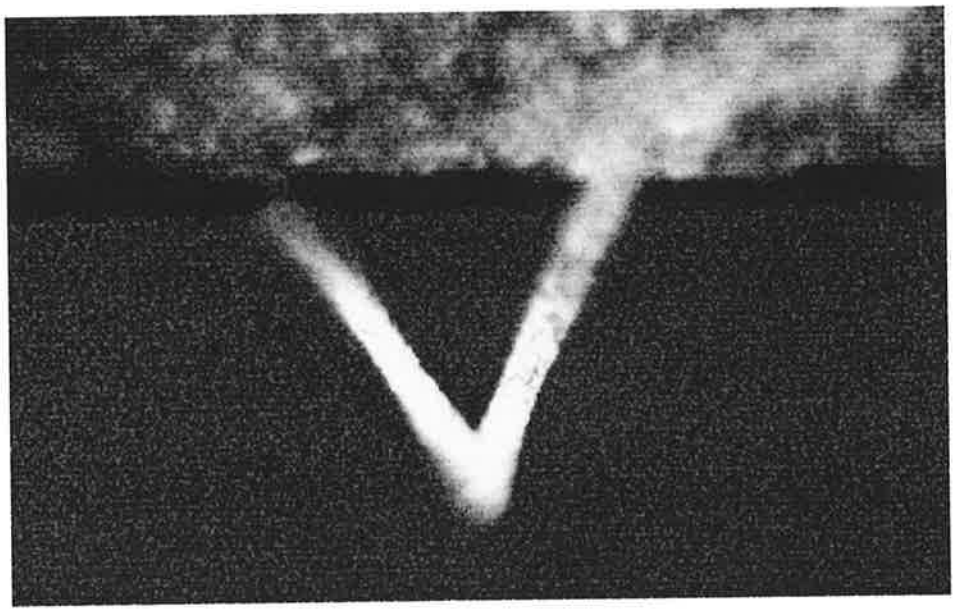

Figure 4.11 SCOM image of modified tip with FITC-labelled inclusion bodies showed that the modified cantilever was bent by tip modification treatment.

4.3.2 Tip Calibration

The results of the spring constant calibration are plotted in Figure 4.12 and the slope of these plots is proportional to the spring constant. The spring constant of the standard cantilever is known and hence a comparison of slopes of standard with the other cantilevers permit spring constant calculation (Table 4.2) Linear plots are obtained with a high degree of significance (indicated by R^2 values in excess of 0.97 for all cantilevers (Table 4.2)). Clearly, the spring constant calibration is reliable and accurate. Materials are added/attached to the cantilever during tip modifications and these may explain the reduction in cantilever spring constants (i.e. the spring constant decreases in order of silanised tip, SPDP-modified tip and IB-modified tip, respectively). The nominal spring constant value may vary depending on the thickness of cantilever which could vary during the production process. This may explain the larger spring constant for silanised cantilever compared to bare cantilever. According to the manufacturer (Digital Instruments, Inc., Santa Barbara, USA), the Si_3N_4 cantilever's thickness may vary in the range of 0.4 μm to 0.7 μm. The nominal spring constant supplied by the manufacturer which is 0.06 N/m assuming a cantilever thickness of 0.6 μm.

Table 4.2 Cantilever spring constants obtained from calibration

Cantilever/tip	slope	R^2	k (N/m)
Standard	1.4714	0.9878	0.0740
Bare	1.3372	0.9751	0.0673
Silanised	1.4827	0.9905	0.0746
SPDP-modified	1.0228	0.9802	0.0514
IB-modified	0.9437	0.9814	0.0475

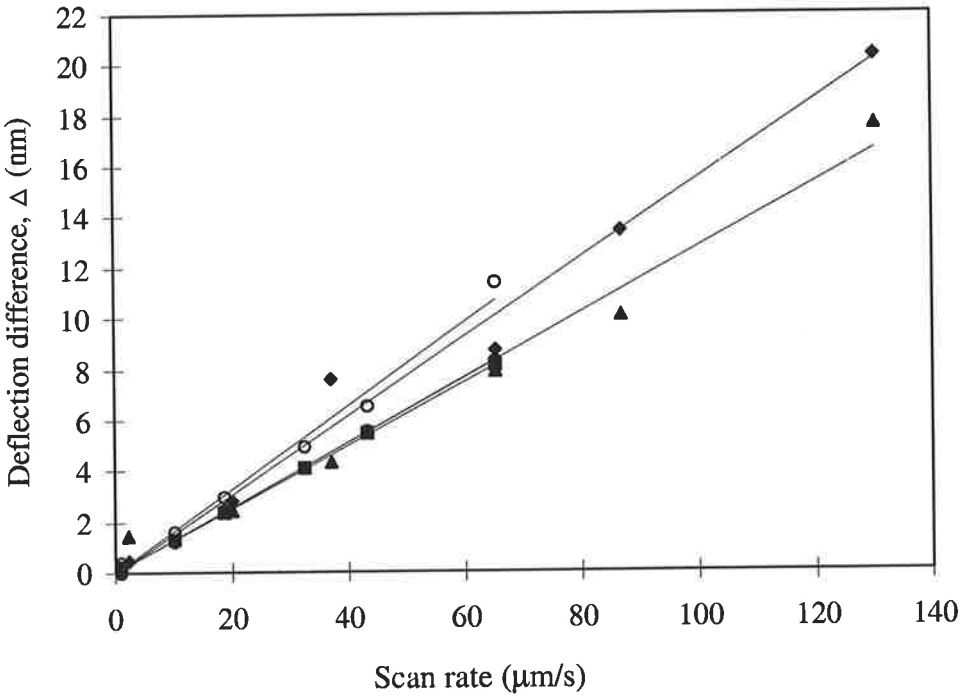

Figure 4.12 Spring constant calibration curve plots of scan rate versus deflection difference between extension- retraction (Δ) for various cantilevers/tips: o standard, ■ bare, ◆ silanised (-SH terminal group), ● SPDP-modified and ▲ IB-modified .

4.3.3 Bubble Formation and Experimental Setting

Stable air bubbles with diameter of less than 1 mm were produced and attached securely to the bottom of liquid cell. The attachment was facilitated by the scratched surface (Figure 4.13). Such bubbles were stable for several hours and in some cases for up to few days, with a slight reduction in the bubble size observed. By contrast, bubble detachment was often observed if air bubbles were attached to smooth surfaces of liquid cell.

The inverted microscope improves observation of the tips and experimental set-up. Different magnifications of microscope may be used and these are then manipulated to obtain the best view. A typical microscope view of two different cantilevers mounted on their substrate is presented as Figure 4.14. A longer cantilever (200 μm) was employed for force measurement as it possessed a lower spring constant

(manufacturer value: 0.06 N/m) and improve sensitivity. The laser beam position is adjusted so that it falls on the top end reflective area of the cantilever. This cantilever is positioned such that the tip is located at the centre of the air bubble (Figure 4.15). During this process, the laser beam is switched off as it hinders precise observations due to its high intensity coupled with reflection from the air bubble (Figure 4.15.c).

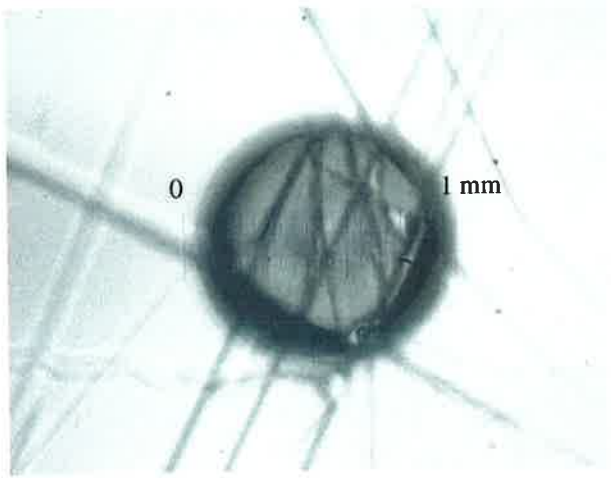

Figure 4.13 A typical air bubble formed using GC syringe has diameter of less than 1 mm, as shown by a 1 mm scale microscope ruler placed under the liquid cell.

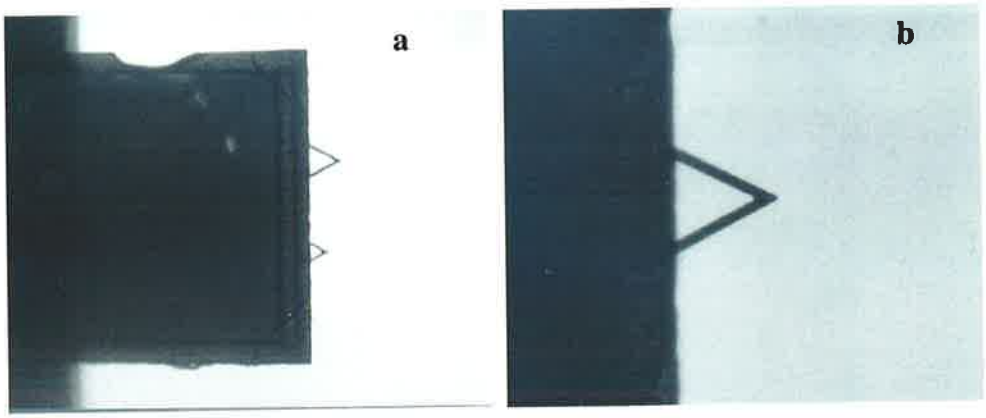

Figure 4.14 A typical microscope view of two different Si_3N_4 cantilevers mounted on the substrate (a) and longer cantilever (200 μm) is employed for measurement (b).

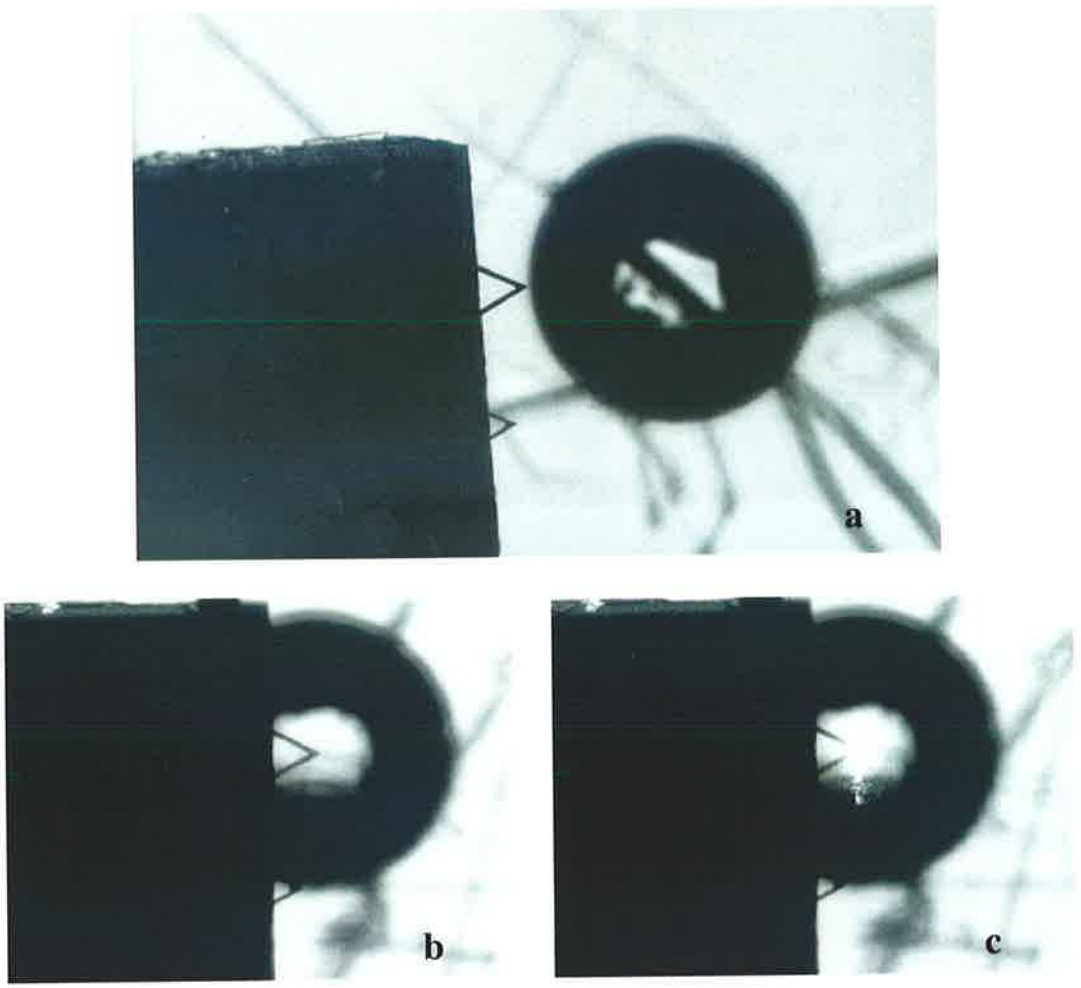

Figure 4.15 Microscope's views of tip positioning to the centre of the air bubble: the cantilever is positioned on the centre line of the air bubble(a) and the cantilever/tip is positioned in the centre of the air bubble (b) with laser beam falls on its end reflective area (c).

Next, the tip approaches the air bubble in a series of fine steps controlled by piezo motor. The point at which the tip touches the air bubble surface detected by the oscilloscope screen (indicates the cantilever deflection) and by direct visual observation on the microscope's screen. When the tip was few microns above the air bubble, false engagement was then performed to activate the AFM feedback system. A final carefully controlled tip approach is conducted to reduce the tip-bubble distance to approximately 500 nm to 1 μm. This is done manually until the tip touches the bubble. It is retracted to detach the tip from the bubble. The distance of tip approach and tip retraction can be used to estimate the tip-bubble distance. This is used to

control the final fine tip approach again with the tip-bubble distance in the range of 500 nm to 1 μm. Finally, force measurement is performed and force curve is recorded.

4.3.4 Interaction Forces

Force measurement and reliability

Interaction forces were calculated using Hooke's Law (Equation 4.1) where the tip deflections (x) are obtained by converting signal output (tip deflections) recorded from AFM measurements with the spring constant value obtained from calibrations (section 4.3.2). For each combination of buffer concentration and pH, 3 sets of approximately 100 force measurements per set were performed to ensure sufficient data were collected to satisfy statistical requirements. A complete set of data detailing interactions forces and the resulting force curves in various buffer concentrations at various pHs are summarised in Appendix A.

Typical force curves obtained from AFM measurements of the interactions forces between an inclusion body and an air bubble (in 0.1 M buffer concentration at various pH values) are presented in Figure 4.16. As expected, the interaction force varies with pHs. This will be further discussed in the following sections. In most cases, the resulting force curves followed a normal distribution as illustrated in Figure 4.17 with a standard deviation in the range of 4 to 11% (or 0.6 nN to 1.3 nN). As well, the three independent sets produced more or less similar mean values (Figure 4.18). This confirms that the experimental results were reproducible. The means of the three sets interaction force data represents the overall measured interaction force. This value is considered as the interaction force at a given buffer concentration and pH.

Air bubbles are deformable and consequently when a particle approaches an air bubble, bubble deformation may occur. When the net interaction forces between the particle and the bubble are repulsive, the particle pushes the bubble surface from its

equilibrium position. In addition, the net attraction forces causes bubble deformation in which the bubble surface moves towards the particle forming ellipsoidal shape-like. This phenomena has been considered in the measurement of particle-bubble interactions (Ducker *et al.*, 1994; Fielden *et al.*, 1996). Stiffness of the bubble (K_b) represents the tendency for bubble deformation (Ducker *et al.*, 1996). This bubble stiffness can be calculated from the slope of the measured extending force curve to the left after it passes the point of the tip-sample interactions (blue circle) in Figure 4.19. A typical bubble stiffness in pure water (approximated from Equation 4.4) is K_b = 0.065 ± 0.005 N m^{-1}(Ducker *et al.*, 1994).

Assuming that the bubble and the AFM cantilever act as two springs in series, the measured stiffness (K_m) is given by (Ducker *et al.*, 1994):

$$\frac{1}{K_m} = \frac{1}{K_s} + \frac{1}{K_b} \tag{4.3}$$

where K_s is the cantilever stiffness (cantilever spring constant), the bubble stiffness can be measured experimentally by measuring the cantilever deflection per unit sample translation when pushed against a hard surface (C_h) and the cantilever deflection per unit sample translation when pushed against the bubble (C_b). The stiffness of the bubble is calculated as follows:

$$K_b = \frac{K_s}{\left(\frac{K_s}{K_m} - 1\right)} = \frac{K_s}{\left(\frac{C_h}{C_b} - 1\right)} \tag{4.4}$$

Bubble deformation is neglected in our force measurements for the following reasons. First, a small bubble possesses a high surface tension which preserves its surface configuration from deformation, in other words, small bubbles are relatively stiff. The size of the air bubble employed in our experiments is less than 1000 μm. Second, the inclusion body particle size (0.3 μm) is much smaller than the air bubble size and thus the viscous force opposing film drainage is very small (Ducker et al., 1994). Hence, bubble deformation is very small in the inclusion body-bubble interactions. Ducker *et*

al. (1994) has concluded that the bubble deformation is negligible in their measurement although they employed much bigger particle size (a silicon particle with diameter 6-10 μm).

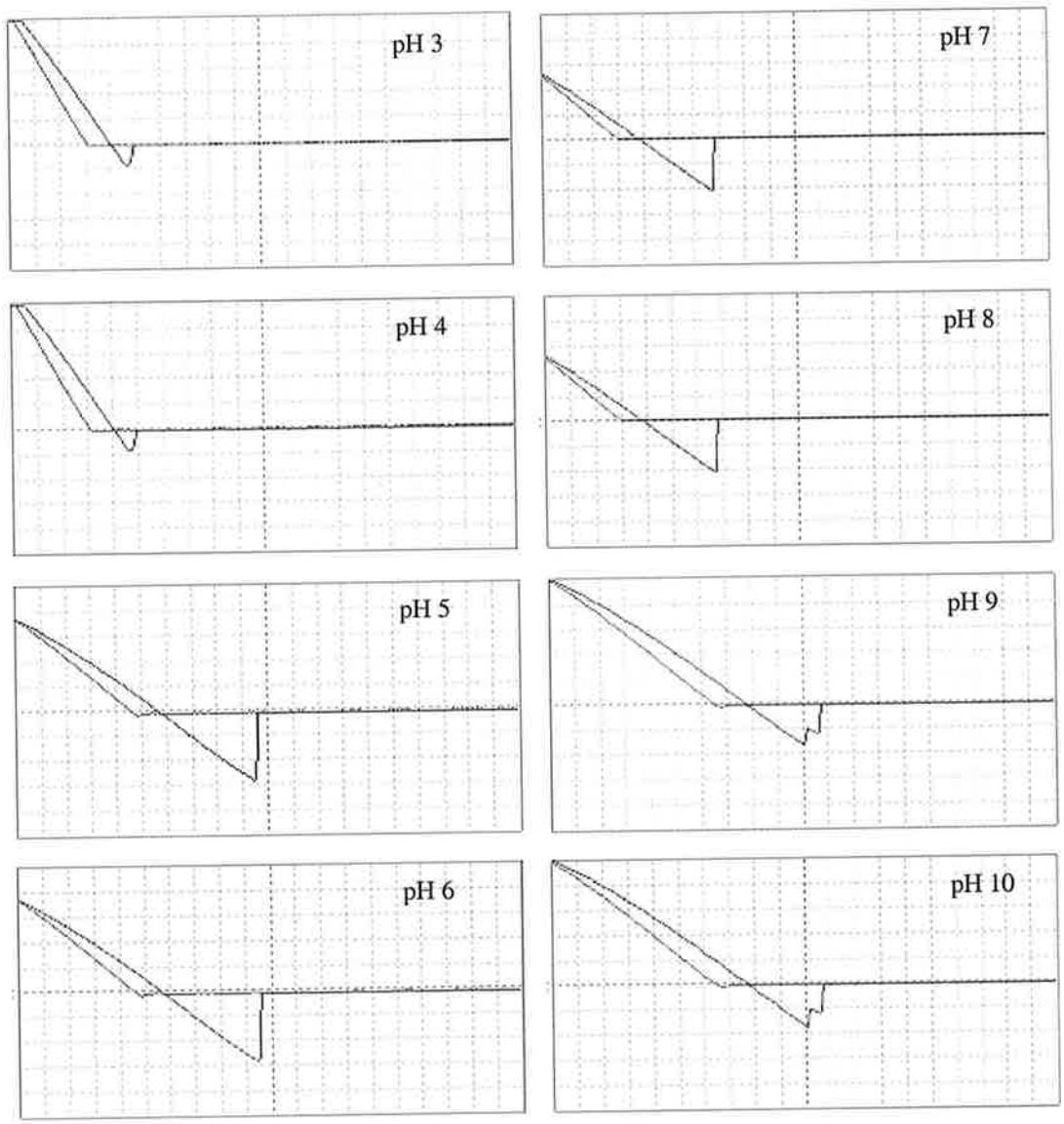

Figure 4.16 AFM force curve of interactions between inclusion body and an air bubble as plots of z position versus tip deflection. The measurements were conducted in 0.1 M buffer solution at various pH values. The unit of z position (x axis) is 0.15 μm/division. The unit of tip deflection (y axis) is 0.1 μm/division for pH 3 to 4 and 0.2 μm/division for pH 5 to 10. For all pH values, the z range and scan rate are 2 μm (except pH = 3 and 4, 1μm) and 0.5 Hz, respectively.

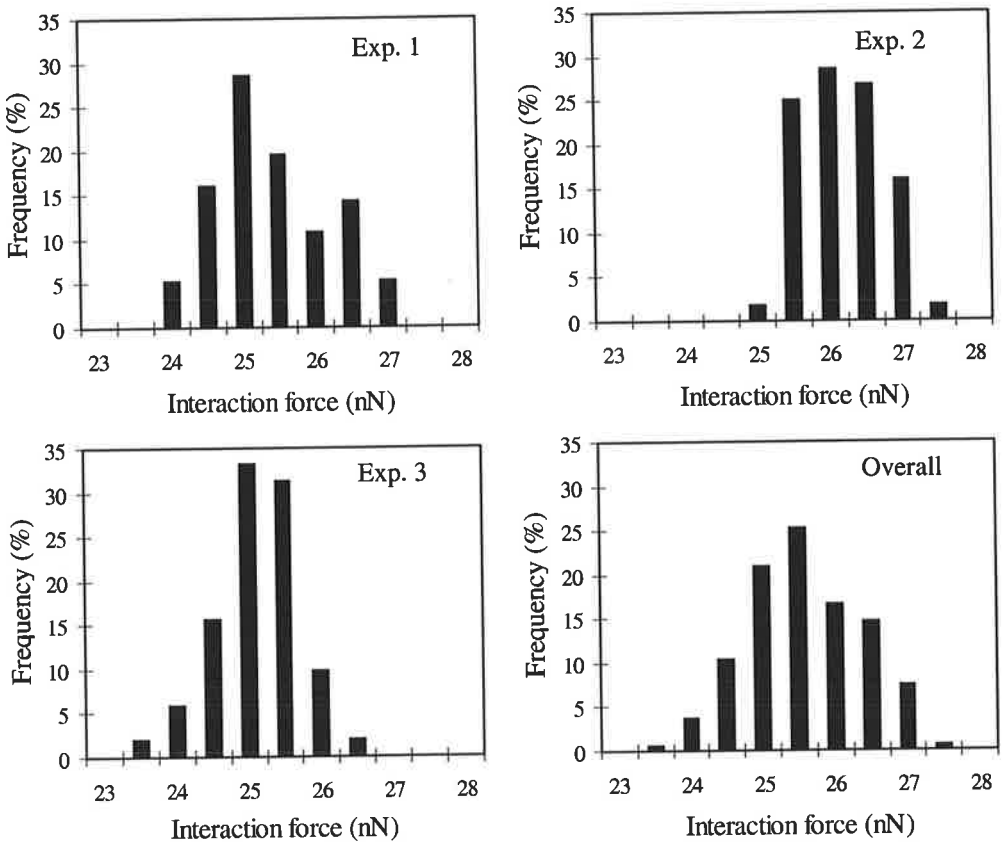

Figure 4.17 Interaction forces between inclusion body and an air bubble in 0.1 M buffer solution at pH 5 follow a normal distribution. Three sets of approximately 100 AFM force measurements for each set were performed.

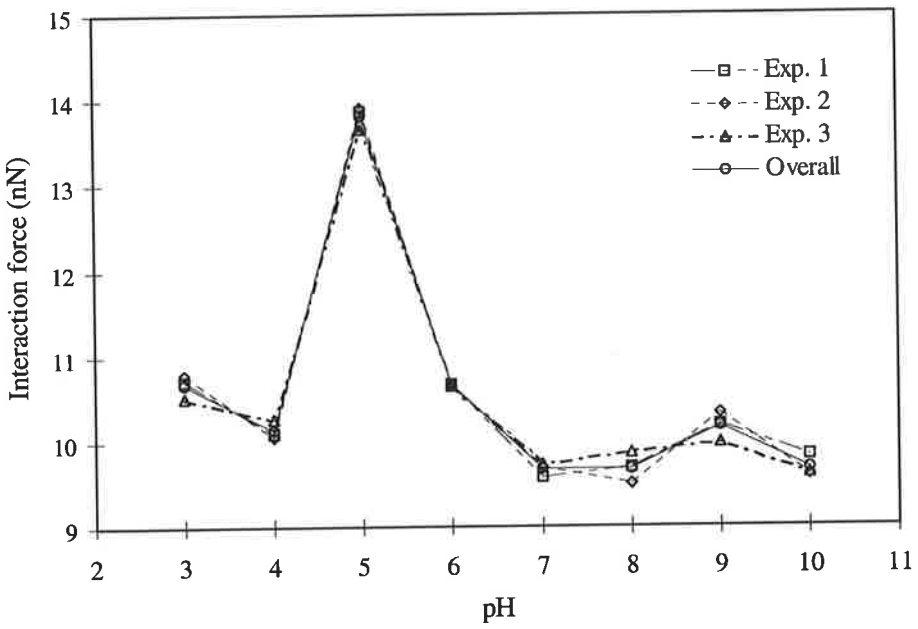

Figure 4.18 Interaction forces between inclusion body and an air bubble (in 0.1 M buffer solution) obtained from the three sets of AFM force measurements yield similar mean values.

Force Analysis

Several forces may contribute to the interactions between a particle and a bubble. These include equilibrium forces, such as the van der Waals, electrostatic double layer, hydration and hydrophobic forces, and nonequilibrium forces, such as viscous forces (Ducker *et al.*, 1994). Gravitational forces can be ignored due to small size of particles. Additionally, surface and capillary forces (due to air nuclei trapped on particle surfaces) have been suggested as a possible contributor to this interactions (Fielden *et al.*, 1996). These forces are applicable to the interactions between an inclusion body and an air bubble system. Viscous forces may be neglected as the measured forces are independent of velocity (Ducker *et al.*, 1994). The van der Waals forces for dissimilar bodies (in this instance the inclusion body and the air bubble) can be attractive or repulsive (Israelachvili, 1992). The electrostatic double layer forces are expected to be repulsive for pH values above 5 as air bubbles in water or inorganic (eg. NaCl) solution are negatively charged at all pH values (Weyl, 1951; Li and Somasundaran, 1991 & 1992) and the inclusion bodies are negatively charged at a pH of approximately above 5 units (section 3.1.3).

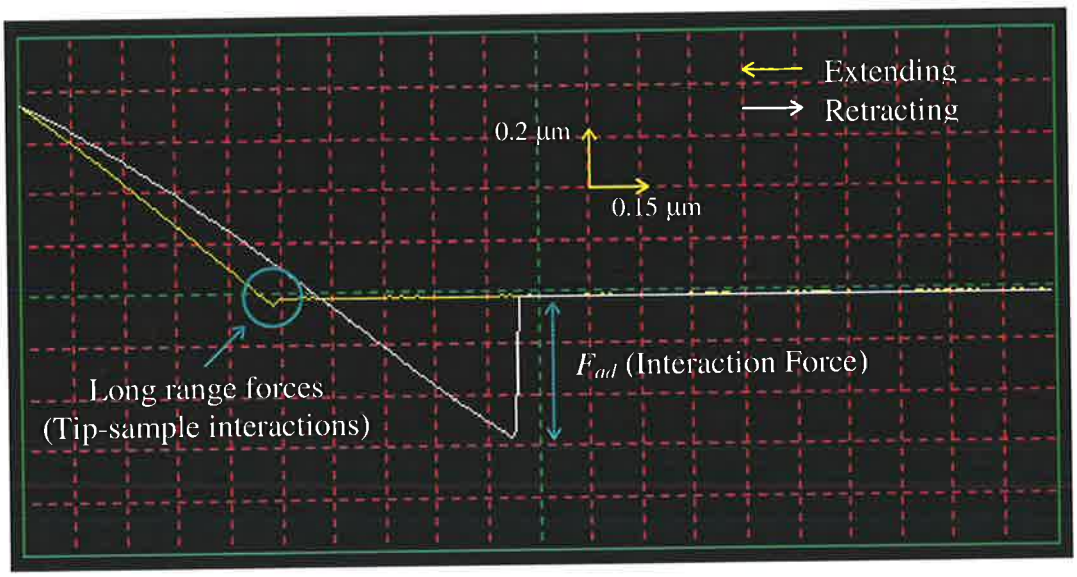

Figure 4.19 A typical force curve obtained from AFM measurement of adhesion force between inclusion body and air bubble (in 0.1 M Buffer, pH 6), showing tip-sample interactions due to long-range forces and adhesion force (F_{ad}) referred as interaction force in this study.

An analysis of the forces mentioned previously could be performed by observation of the AFM force curve as the tip approaches the bubble (extending curve) as illustrated in Figure 4.19. It appears that net attractive forces result from the tip-sample interactions (in this instance inclusion body-bubble interactions) due to long range forces as shown by the curve marked with the blue circle in Figure 4.19. These long range forces were not the prime focus of this work. Detailed discussion of this topic is readily available in the literature (Butt, 1991; Weisenhorn *et al.*, 1992; Ducker *et al.*, 1994; Senden and Drummond, 1995). Our main interest lay with the adhesion force, which is detected as the tip is pulled from the bubble (retracting curve, refer to Figure 4.19). As indicated, various forces such as van der Waals, electrostatic double layer, hydrophobic, and surface and capillary forces may contribute to this adhesion force. Such forces are then referred to as interaction forces. The adhesion force quantifies the strength of the interactions between an inclusion body and an air bubble. This is a significant fundamental parameter in flotation design. Consequently, discussion of the experimental results will focus principally on this issue.

Inclusion Body-Bubble Interaction Forces

As expected, the interaction forces between the inclusion body and an air bubble varies with buffer concentration and pH (Figure 4.20 and Table 4.3). The strongest interactions are observed at 0.1 M buffer concentrations whilst interactions at buffer concentration of 0.2 M appears to be stronger than that at 0.05 M. This does not follow the general rule. It was expected that the interaction forces would increase with increasing concentration due to the reduction of Debye length (κ^{-1}) which diminishes the electrostatic repulsion (Butt, 1991). However, the experimental results did not follow this pattern. This behaviour is a consequence of the variety of forces responsible for the overall interactions measured as an adhesion force. A similar discrepancy has also been noted by Ducker *et al.* (1994) and Fielden *et al.* (1996) where they observed attractive forces for silica particle and bubble interactions which should be repulsive according to the Derjarguin-Landau-Verwey-Overbeek (DLVO) theory. The experimental results confirms the significant contribution of other forces

(hydrophobic forces in particular) to the interaction force. The stronger forces measured in 0.1 M buffer compared to 0.2 M, suggest that the hydrophobic forces are affected by ionic strength. It is possible that there is a certain point beyond which hydrophobic forces are affected by ionic strength. The highly compressed double layer at high ionic strength may limit (to some extent) the hydrophobic interactions between bubble and inclusion body. Unfortunately, the fundamental basis of hydrophobic forces (interactions) remains unclear and hence, quantitative analysis of these forces is not possible.

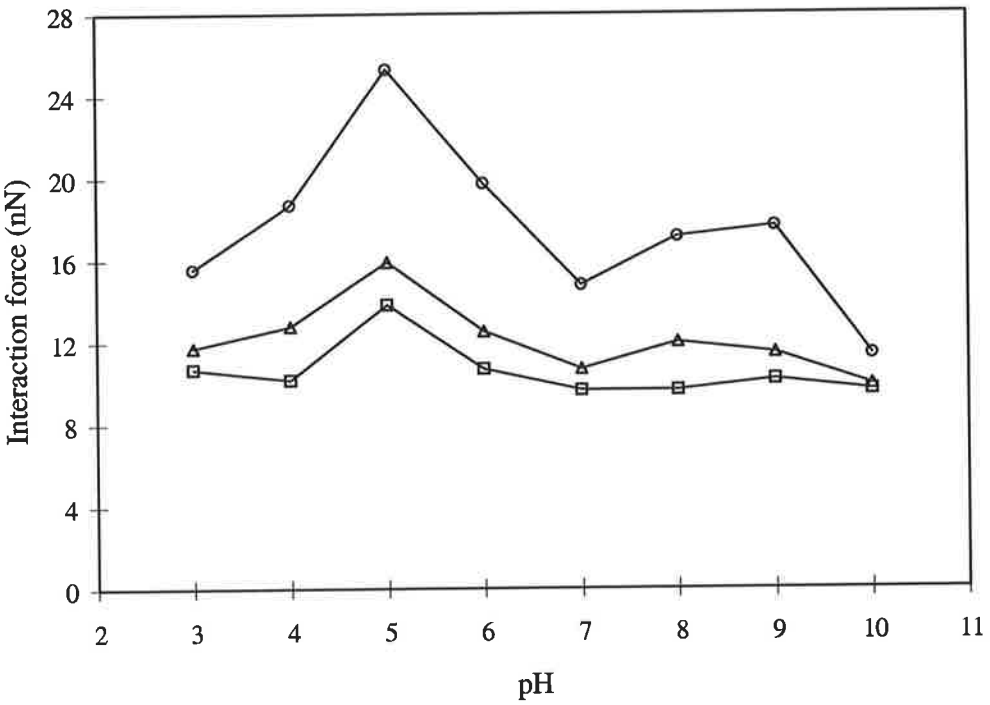

Figure 4.20 Interaction forces between inclusion body and an air bubble in various pH and buffer concentrations: (□) 0.05 M, (○) 0.1 M and (△) 0.2 M.

Non-monotonic variation of the interaction force with pH shows the effect of electrostatic forces. This can be explained by considering the surface charge on the inclusion body and the bubble. The largest interaction force occurred at pH = 5 for all buffer concentrations. This is in agreement with the results of electrophoretic mobility study of the inclusion bodies (chapter 3). The surface charge magnitude of

inclusion body is minimum at the approximately pH 5 to 6 depending on the ionic strength. In this pH range, hydrophobic properties are expected to be dominant due to minimisation of electrostatic effects. The magnitude of air bubble surface charge decreases with ionic strength and increases with pH (Li and Somasundaran, 1992). Despite their negative charge in inorganic salt (eg. NaCl) solutions at all pH value (Weyl, 1951; Li and Somasundaran, 1992), air bubbles are hydrophobic in nature (Ducker *et al.*, 1994). This may cause less significant effects of ionic strength on air bubbles. As well, since the air bubbles are negatively charged throughout the pH range, the effects of pH on the inclusion body are more pronounced than those on the air bubbles. This is confirmed by the strongest interaction forces being measured at pH 5 rather than at lower pHs.

Table 4.3 Interaction forces between inclusion body and an air bubble measured by AFM in various buffer concentrations and pH.

	Interactions forces (F_{ad}, nN)		
pH	0.05 M	0.1 M	0.2 M
3	10.67 ± 1.15	15.60 ± 0.82	11.76 ± 0.95
4	10.14 ± 0.63	18.70 ± 1.30	12.77 ± 1.12
5	13.82 ± 0.80	25.33 ± 0.65	15.92 ± 0.79
6	10.66 ± 0.51	19.75 ± 0.69	12.52 ± 0.90
7	9.67 ± 0.43	14.80 ± 0.85	10.72 ± 0.99
8	9.68 ± 0.61	17.11 ± 0.71	12.02 ± 0.98
9	10.16 ± 1.03	17.69 ± 1.13	11.47 ± 0.81
10	9.68 ± 0.78	11.36 ± 0.84	9.90 ± 0.89

Interaction Force between Various Tips and an Air Bubble

All inclusion body-modified tips used for measurements have been examined using the SCOM technique. However, it remains a possibility that the measured interactions are not the interactions between inclusion body and an air bubble but those of bare tip or modified tip (silanised or SPDP-modified) with an air bubble . Therefore, control

experiments were performed for three different tips, i.e. bare, silanised and SPDP-modified tips, to determine if a difference exists for various tips and bubble interactions. Typical force curves and interaction force data are presented in Appendix A (Figures A.3 and A.4; table A.2 to A.4). The interaction force between silanised tip and an air bubble appears the strongest (range: 27.6 to 82.24 nN) whilst that for a bare tip was the weakest (1.3 to 11.4 nN). The interaction force between an air bubble and SPDP-modified tip (14.2 to 33.3 nN) or IB-modified tip (9.6 to 25.3 nN) are intermediate with the interaction force for SPDP-modified tip stronger than that for IB-modified tip. A force spectrum has been constructed from the interaction forces between various tips and an air bubble measured in various buffer concentrations and pH (Figure 4.21). This force spectrum demonstrates clearly that the interaction force between an air bubble and various tips differs from one tip to another. Hence, it is reasonable to conclude that the reported interaction forces represent the interactions between the inclusion body and the bubble.

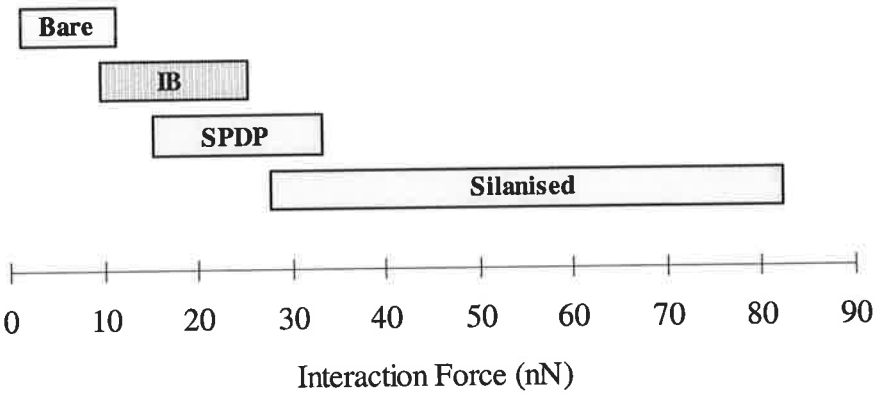

Figure 4.21 The force spectrum of interaction forces between various tips and an air bubble measured by AFM in various buffer concentration and pH.

Figure 4.22 illustrates the interaction forces between an air bubble and various tips (including bare, silanised and SPDP-modified tips) in a variety of buffer concentrations and pHs. Relatively similar pattern of ionic strength effects on the interaction forces were observed for these tips, i.e. the strongest interactions forces are detected for 0.1 M buffer concentrations. However, no general pattern of the effect of

pH on the interaction forces emerged. This evidence supports the previous suggestion that pH has a stronger effect on the inclusion body compared to the air bubbles. A discontinuity was observed for several of the curves in Figure 4.22, for example the bare tip-bubble interactions at 0.1 M buffer and the silanised tip-bubble interactions at 0.2 M buffer. This discontinuity may be caused by the change in buffer solution for the two different pH ranges, i.e. acetic acid buffer (saline) for pH 3-6 and tris buffer (saline) for pH 7-10.

The bare tip used in this study was carefully washed with organic solvents (chloroform and ethanol) and treated with UV light. This treatment causes the tip surface to become hydrophilic and explains why the lowest interaction forces measured were for the bare tip. The strongest interaction forces occurred for silanised tip and suggests that the tip surface became hydrophobic due to silanisation (SH termination) whilst the SPDP-modified tip is less hydrophobic compared to silanised tip. A similar observation was reported by Tsukruk and Bliznyuk (1998). They found that the adhesion force between a silanised tip (NH_2 terminated) and a silanised (NH_2 terminated) silicon wafer was significantly stronger than the adhesion forces between a Si_3N_4 tip and a Si_3N_4 surface.

Final Remarks

The attachment of inclusion body particle to the tip may result in successful attachment of one or more particles. Consequently, the measured interaction forces may be contributed by a single or multiple inclusion body particles. This constraint has been anticipated. A cross linker (SPDP) a few nanometer long was introduced as a *bridge* connecting the inclusion body particle and the tip. As the tip is pyramidal in shape, it is expected that the sharp end of the pyramid provides a very small area which limits the number of SPDP molecules incorporated and hence reduces the possible number of attached inclusion body particles. The length of the cross linker provides an extension from the tip surface and hence reduces the possibility of the tip surface influencing the measured interaction forces. In addition, the inclusion body

particles are *hung on* the tip surface at various height due to the geometry of the tip. This reduces the possibility of interaction force measurement between a bubble and many inclusion body particles.

The SCOM examination did not permit any evaluation of the number of inclusion bodies attached to the tip due to limited resolution of the optical microscope. A possible method to examine the tip and attached bodies is by scanning electron microscopy. However, this technique requires a special sample treatment/preparation, such as gold-coating. It must also be performed in vacuum. These constraints prohibit accurate examination of the attached inclusion bodies due to the possibility of changes (deformation) during sample preparation processes. Consequently, evaluation of the tip by the SEM was not undertaken in this study. However, tip examination by SEM should be considered.

The advances in micro- and nano-technology should result in improvement of the possibility of single particle attachment to the tip. Several recommendations have been proposed earlier (section 4.3.1) to improve tip modification techniques. In addition, the micromanipulator and high resolution optical microscope may be employed to pick a single inclusion body particle and position it in such a way to ensure single particle attachment to the tip surface. This approach may also be possible applied using AFM or both AFM and micromanipulator can be employed concurrently.

A more significant reduction in the possibility of the tip surface influence on the interaction force measurement may be achieved by applying longer cross linkers. For example, polyethylene glycol (PEG) - base cross linkers have longer chains which will provide *a longer bridge* for the tip and the inclusion body particles. The length of this cross linker depends on the PEG polymerisation. The advanced methods in polymer synthesis may produced significantly long chain of PEG with required physical property, eg. the chain's strain strength.

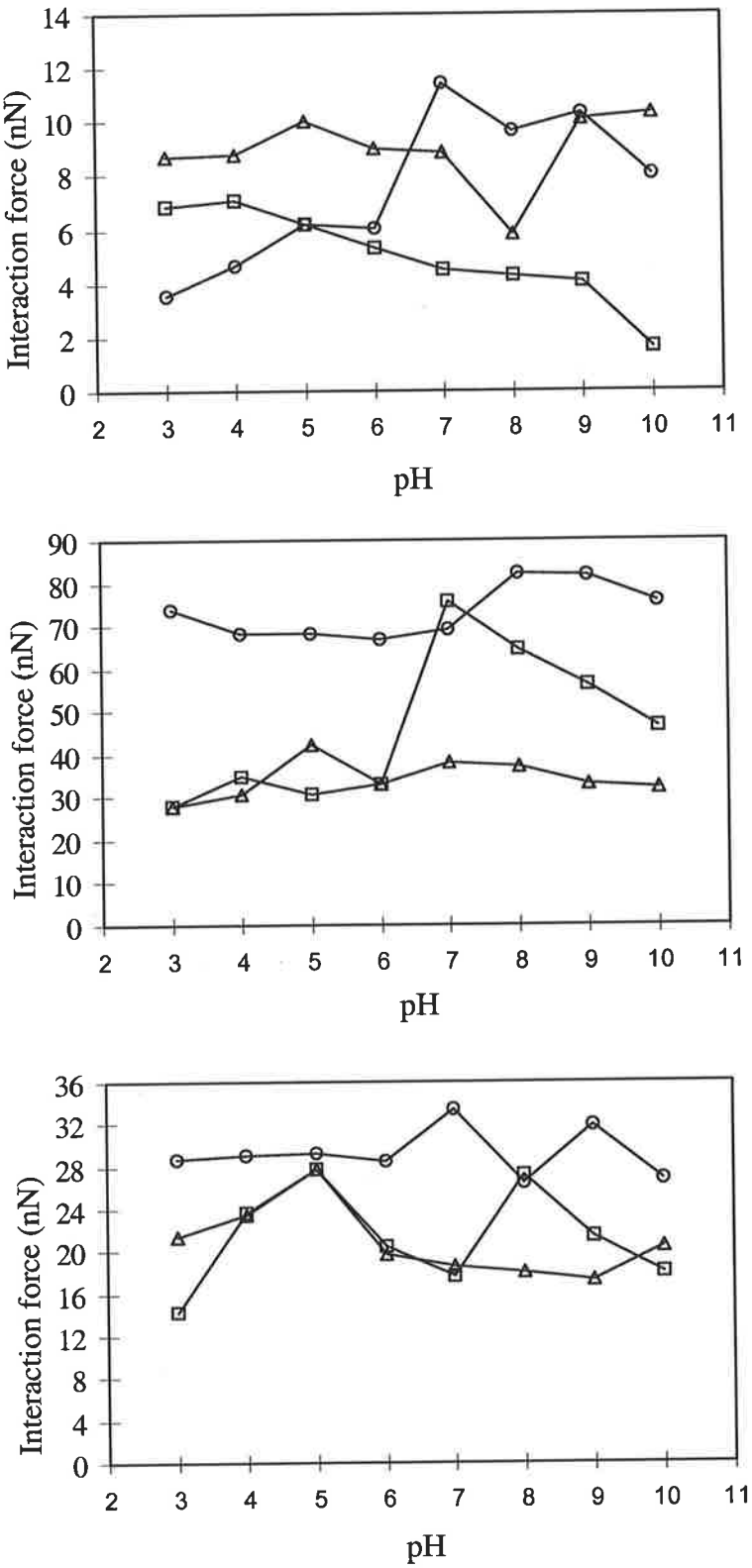

Figure 4.22 Interaction forces between an air bubble and bare tip (a), silanised tip (b) and SPDP-modified tip (c) measured in various pH and buffer concentration: (□) 0.05 M, (○) 0.1 M and (△) 0.2 M.

4.4 CONCLUSION AND RECOMMENDATION

AFM appears to be reliable and a powerful technique for measuring interaction forces between an inclusion body and an air bubble. The interaction forces measured in various buffer concentration and pH lie in the range of 9.7 to 25.3 nN and are reproducible with standard deviation of 4-11 %. Control experiments have confirmed that the possible influence from other interactions (i.e. bare tip/bubble, silanised tip/bubble and SPDP-modified tip/bubble) is negligible as shown by distinctive force spectrum (Figure 4.21) for each case. The highest interaction forces were measured in 0.1 M buffer and at a pH of 5 for all buffer concentration. Hydrophobic forces provide a stronger contribution to overall interaction force than electrostatic double layer forces. It also appears that the ionic strength affects the hydrophobic forces. The effects of pH are significantly stronger to the inclusion body compared to the air bubble. The surface and capillary forces may also contribute to the interaction forces. The rough surface of inclusion body particles may facilitate entrapment of air nuclei on their surface.

The chemical modification technique used for attaching inclusion body to the AFM tip has been demonstrated as reliable. The attachment results may be examined by the SCOM technique. As well, the FITC labelling technique is suitable for inclusion body detection. Tip modification should be performed with extreme care as the cantilever/tip combination is very small and delicate. Examination of the cantilever/tip prior AFM measurement is recommended.

Recommendations are included to improve tip modification and particle attachment. This study confirms the potential of AFM for further exploration of other applications which will bring the *Nano World* era into reality.

Chapter 5

DISSOLVED-AIR FLOTATION :

Mathematical Modeling

Dissolved-air flotation (DAF) has been used widely in wastewater and water treatment for decades. This method has a great potential for inclusion body recovery. The population balance model developed by Tambo *et al.* is adopted and modified. A model is proposed for the recovery of inclusion bodies by DAF. The model has also been extended to the case when aggregation is introduced to promote bigger particles. The key parameters of DAF design and operation are resulted from this model which represent equilibrium and kinetics requirements for the performance of DAF.

5.1 PRINCIPLES OF DISSOLVED-AIR FLOTATION

Dissolved-air flotation (DAF) has been exploited primarily for waste-water and water treatment because it can produce very small bubbles (less than 100 μm (Edzwald, 1995)). The bubbles are formed by the pressure reduction of air-saturated water/solution. This sudden reduction decreases the solubility of the air in water/solution. As a consequence fine bubbles are released. DAF is normally categorised into three different types: vacuum flotation, micro-flotation and pressure flotation (Zabel, 1992). In vacuum flotation, water is saturated with air at atmospheric pressure. Small bubbles appear in the water when vacuum is applied to the flotation cell. This method is seldom applied because of a limit to the dissolved air, operation is confined to the batch mode and the high cost of vacuum system (Zabel, 1992). Micro-flotation is also less popular as a consequence of limited dissolved air and the requirement for tall columns. In this method, water is saturated with air at atmospheric pressure at the bottom of a tall column. Bubbles are formed as this air-saturated water flows upward as a consequence of the reduced hydrostatic pressure. Pressure flotation is the most commonly employed method.

Pressure flotation, generally known as DAF, can be grouped into 3 categories: full-flow, split-flow and recycle-flow DAF. In the full-flow DAF, the inlet stream is pressurised with air whereas only a portion of inlet stream is pressurised with air in the split-flow mode. In the recycle-flow setup, a fraction of clarified effluent is recycled to the flotation cell following saturation with air to supply air bubbles. Each mode has advantages and disadvantages depending on the application. For example, full-flow and split-flow may be unsuitable for handling fragile flocs as they may be destroyed by the applied pressure. In this case, recycle-flow DAF may be more appropriate.

In general, the elementary processes of flotation as outlined in chapter 1 (section 1.5.2) apply to DAF. However, there are some notable features unique to DAF. For

example, the bubble size is very small and in some cases may be smaller than particles (eg. floc separation in water treatment).

5.1.1 Bubbles

Bubble Formation and Size

Bubble formation in DAF consists of two steps, i.e. nucleation and growth (Edzwald, 1995). Bubble nuclei are formed when an air-supersaturated water flows across nozzle (pressure reducing valve) creating a sudden pressure reduction. This phenomena follows the thermodynamic principle of minimising the free energy change. If air is assumed as an ideal gas, the critical diameter of bubble nucleus (d_{cb}) for homogenous nucleation is given as:

$$d_{cb} = \frac{4\sigma}{\Delta P} \tag{5.1}$$

where σ is the surface tension and ΔP is the pressure difference (reduction) across the nozzle. Figure 5.1 shows the critical diameter of the bubble nucleus as a function of pressure change (reduction). Smaller nuclei are formed at higher pressure changes, i.e. higher saturation pressure produces finer bubbles. The formation of bubble nuclei is easier in a heterogenous system, particularly in the presence of particles or other surfaces containing scratches and crevices (Ryan and Hemmingsen, 1993; Zhou *et al.*, 1995). As well, impurities present in the water (eg. detergent) may increase the rate of generation of bubble nuclei (Jackson, 1994). Such nuclei grow into bubbles in the second step.

A typical bubble size in the range of 10 to 120 μm is commonly obtained (Takahashi *et al.*, 1979; Zabel, 1984; De Rijk *et al.*, 1994; Fukushi *et al.*, 1998) with a mean bubble size of 40 μm (Edzwald, 1995) to 60 μm (Fukushi et al., 1998). The bubble size created in DAF depends on the saturator pressure and the injection flow rate

(Takahasi *et al.*, 1979). Bubble size decreases with the saturator pressure. However, an increase in pressure above 500 kPa has a small effect on the bubble size (Heinanen *et al.*, 1992; De Rijk *et al.*, 1994). To obtain small bubbles, saturator pressure of 400 to 600 kPa is recommended (Edzwald, 1995). Increased bubble growth due to coalescence and reduced hydrostatic pressure is negligible in DAF systems (Takahasi *et al.*, 1979). The type of the nozzle or pressure reducing valve also affects the bubble size (Zabel, 1984; Fukushi *et al.*, 1998). This is a consequence of the differences in pressure drop for various nozzles or pressure reducing valves. A typical experimental measurement of bubble size is presented in Figure 5.2.

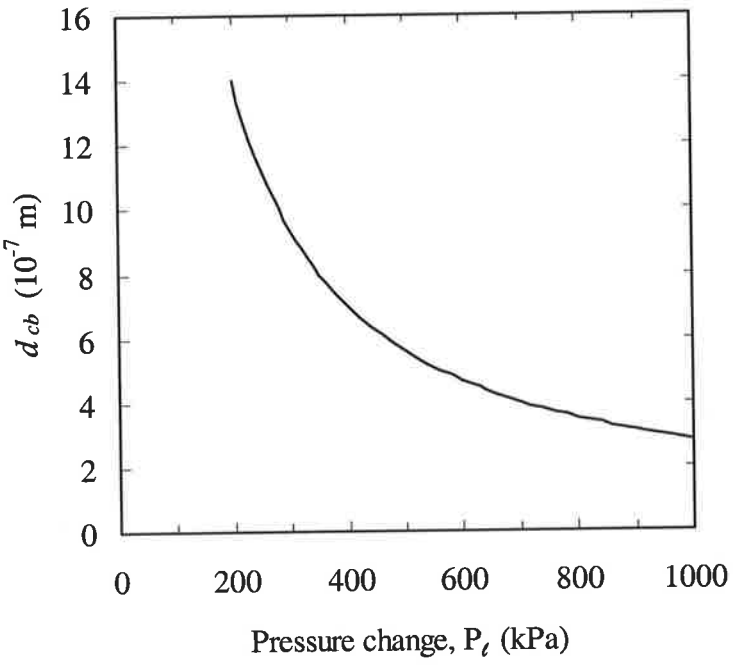

Figure 5.1 Critical diameter of bubble nucleus for homogeneous nucleation of air in water at 20°C as a function of the pressure change (after Edzwald, 1995).

Rise Velocity of a Bubble

The rise velocity (also known as terminal velocity) of a bubble varies with the diameter of the bubble. The rise velocity of small bubbles increase linearly with the

bubble size. However, this linear correlation is no longer valid for medium and large bubbles. Hence, Clift *et al.* (1978) proposed three regimes according to the shape of the rise bubbles, i.e. spherical, ellipsoidal and spherical-cap regimes. Bubbles produced in DAF are confined to the spherical regime. Since the air bubbles formed in DAF are very small, they rise under laminar flow conditions. For bubble size less than 130 μm, the bubble rise velocity can be calculated using Stokes' Law as follows (Zabel, 1992):

$$v_b = \frac{g(\rho_w - \rho_a)d_b^{\,2}}{18\mu} \tag{5.2}$$

where: v_b is the rising velocity of the bubble, g the gravity constant, ρ_w and ρ_a the density of water and air, respectively, d_b the bubble diameter and μ the dynamic viscosity of water.

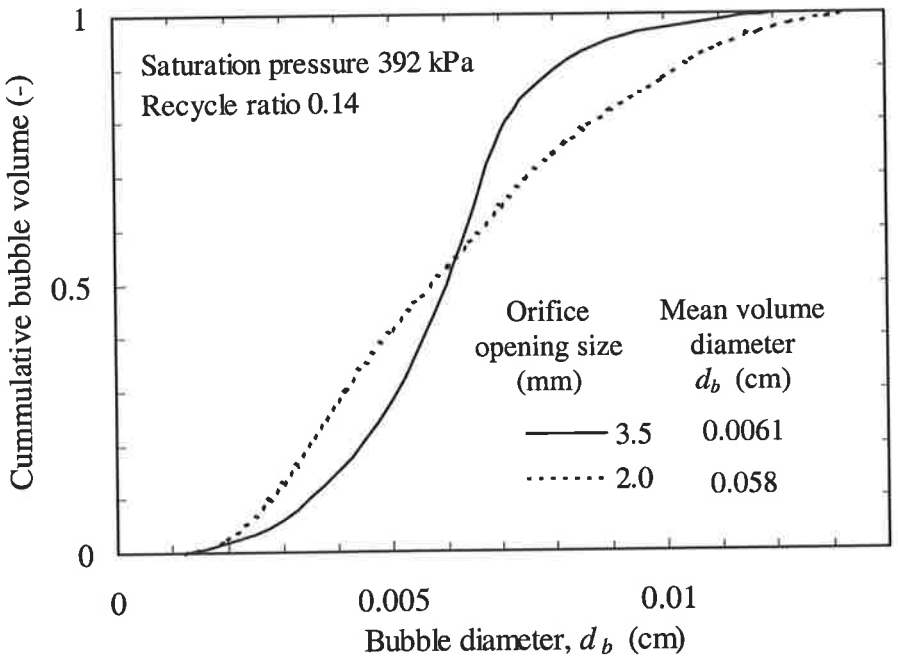

Figure 5.2 Size distribution of bubbles for continuous flow experiment (after Fukushi *et al.*, 1998)

Stokes' Law assumes that the bubble motion is equivalent to the motion of a solid sphere under laminar flow condition. However, the rise velocity of a very small bubble in liquid is altered by the non-rigid surface of the bubble. Hence, the rise velocity of bubble follows the Rybczynski-Hadamard correlation (Levich, 1962):

$$v_b = \frac{g(\rho_w - \rho_a)d_b^{\,2}}{6\mu}\frac{\mu+\mu_a}{2\mu+3\mu_a} \tag{5.3}$$

Since the viscosity of water is much larger than that of air $(\mu \gg \mu_a)$, the rising velocity of the bubble can be simplified into equations (5.4) as follows:

$$v_b = \frac{g(\rho_w - \rho_a)d_b^{\,2}}{12\mu} \tag{5.4}$$

5.1.2 Bubble-Particle Interactions

Several mechanisms has been proposed for agglomeration between bubble and floc (Kitchener and Gochin, 1981). These mechanisms include entrapment of bubbles within a condensing network of flocs, growth of bubbles from nuclei within flocs and attachment of bubble to flocs during collision. These mechanism are proposed mainly for the removal of floc in waste-water and water treatment where flocculation and/or coagulation may be performed concurrently. The second mechanism is likely to occur in most cases, particularly in wastewater and water treatment. This is because bubble nucleation is enhanced in heterogeneous system as previously discussed. However, in general, the third mechanism is considered dominant. In general, particle-bubble interaction analysis is based on this mechanism as outlined in chapter 1 (section 1.5.2).

Hydrophobicity has also been acknowledged as an important factor in DAF. Despite their hydrophobic nature, the small air bubbles generated in DAF are highly negatively charged (Okada and Akagi, 1987; Fukushi *et al*, 1998). As a consequence,

electrostatic repulsion is expected as the particles are normally negatively charged. Hence, charge alteration (reduction, neutralisation or reversal) is recommended to minimise this electrostatic repulsion.

It has been suggested that charge neutralisation of the particle and production of hydrophobic particles provides favourable conditions for DAF (Edzwald, 1995). This suggestion is in agreement with the experimental results. In wastewater and water treatment, this is usually performed by addition of flocculant and/or coagulant. For example, addition of a coagulant (polyaluminium chloride, PACl) decreased the negative charge of green algae (*Chlorella vulgaris*) and the DAF process was improved significantly (Edzwald, 1995). In this case, the addition of flocculant and/or coagulantp rovide larger particles which are then readily removed by DAF. Charge neutralisation may alter the hydrophobicity of the particle. It has been suggested that for many particles, hydrophobicity may be increased by simply reducing the particle charge (Edzwald, 1995). A detailed discussion of hydrophobicity has been presented in chapter 4.

5.1.3 Bubble Requirement for DAF

Several factors affect the performance of DAF processes, such as bubble size and bubble concentration (and particle concentration). A knowledge of these variable is essential to design an appropriate DAF unit, for example a saturator and a flotation tank. Bubble concentration has been a major concern in DAF design because of its direct effect on recovery efficiency.

The air (bubbles) requirement for DAF may be expressed by three different measures: air bubble mass concentration (C_r), air bubble volume concentration (ϕ_b) and air bubble number concentration (N_b). Assuming air is an ideal gas, the amount of air dissolved in water can be calculated by Henry's Law as follows:

$$P = Hx \tag{5.5}$$

where: P is the partial pressure of the gas in the gas phase, x mole fraction of the gas in the liquid phase and H the Henry's Law constant. Assuming that the air is a single component gas and incorporating efficiency factor of the saturator into Henry's Law, the mass concentration of air in the saturator (Edzwald, 1995) is:

$$C_{sat} = f\frac{P_t}{H_a} \tag{5.6}$$

where: C_{sat} is the mass concentration of air in water, f efficiency factor of the saturator, P_t the total pressure of the saturator and H_a Henry's Law constant for air (4.18 kPa/mg/L at 20°C).

Air is primarily composed of nitrogen (~79%) and oxygen (~21%). Oxygen solubility exceeds that for nitrogen, consequently the percentage of nitrogen in the air increases in a closed saturator system. At steady state, the saturator air is approximately 88% nitrogen and 12% oxygen causing a reduction of approximately 9% in the dissolution of air compared to saturation with atmospheric air (Edzwald, 1995). The efficiency factor, f, is introduced to compensate for this effect and to allow for mass transfer efficiency differences in various saturators. Saturator efficiency (f) for unpacked and packed saturators is typically 60-70 % and 90%, respectively (Edzwald, 1995).

The amount of air bubbles supplied to the flotation tank can be varied by altering saturator pressure and the recycle ratio in a DAF system with recycle system. Table 5.1 presents the variation of bubble concentrations with recycle ratio. For DAF with recycle, the mass concentration or air per unit volume (C_r) can be calculated from a mass balance in the flotation tank (Edzwald, 1995):

$$C_r = \frac{(C_{sat} - C_a)R_r - K_{if}}{1 + R_r} \tag{5.7}$$

The air bubble volume concentration can also calculated from equations (5.8) and (5.9).

$$\phi_b = \frac{C_r}{\rho_{sat}} \tag{5.8}$$

$$N_b = \frac{6\phi_b}{\pi d_b^{\,3}} \tag{5.9}$$

where: C_{sat} is the air bubble mass concentration in the recycle stream, equation (5.6), C_a the dissolved air concentration remaining in the solution at atmospheric pressure, K_{if} the influent flow saturation factor given by (C_a - C_0) where C_0 is the mass air concentration of the influent flow and ρ_{sat} the density of air saturated with water vapour (1.19 mg/cm^3 at 20°C)

Table 5.1 Air bubble mass, volume and number concentrations as a function of recycle ratio for a constant saturator pressure 483 kPa*.

R_r (%)	C_r (mg/L)	ϕ_b (ppm)	N_b (#/mL)
5	3.50	2900	8.75×10^4
8	5.45	4600	1.20×10^5
10	6.68	5600	1.70×10^5
15	9.59	8000	2.40×10^5

** Overall efficiency of 70% for dissolving air and for the saturator, 20 °C.*

Normally, the bubble requirement for DAF is varied depending on the application and the solid concentration. For example, for the thickening of activated sludge, the volume or air required is usually proportional to the solid content, in contrast to the water treatment where the volume air required mainly depends on the volume of water to be processed (Zabel, 1992). Typical values of air/solids ratios in commercial practice for sludge thickening are 15 to 30 mL air/g solids whilst for water treatment

approximately 380 mL air/g solids corresponding to 8-10 g air/m^3 raw water (for a solid concentration in the raw water of 20 mg.L) (Zabel, 1992). A typical clarification result (measured as turbidity of processed water) as a function of air supplied to flotation tank in water treatment is presented in Figure 5.3. Excess air bubbles are normally required to ensure adequate collisions between particles and bubbles (Zabel, 1992).

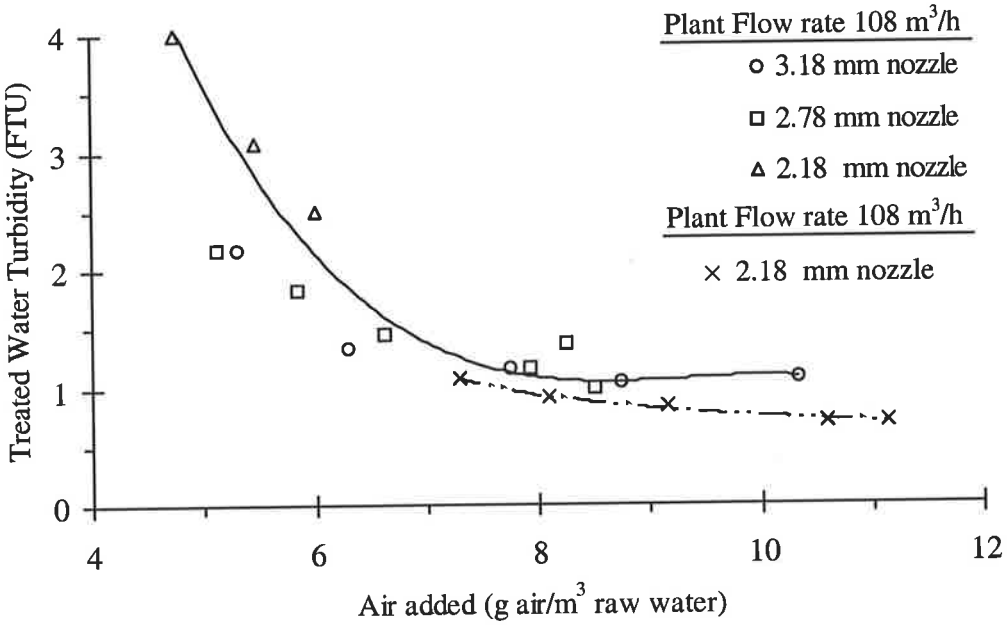

Figure 5.3 Effect of air added to the performance of flotation (after Rees *et al.*, 1979).

5.2 DAF KINETICS MODELS

Two major models have been proposed for DAF modelling, i.e. the single collector collision(SCC) model by Edzwald and co-workers (Edzwald *et al.*, 1990; Malley and Edzwald, 1991; Edzwald, 1995) and the population balance (PBT) model by Tambo and co-workers (Tambo *et al.*, 1986; Fukushi *et al.*, 1995). These models have been developed and tested in the application of DAF in water treatment. A comparison of these models is presented in Table 5.2.

Table 5.2 Comparison of SCC (Edzwald *et al.*) and PBT (Tambo *et al.*) models: typical values of parameters and concepts (after Fukushi *et al.*, 1995).

	PBT model	**SCC model**
Generated Air Bubble		
Size range, d_a (μm)	10-120 (Ave: 60)	10-100 (Ave: 40)
Rise velocity, v_b (cm/sec)	$v_b = g\, d_b^2/12\mu$	$v_b = g\, d_b^2/18\mu$
Zeta potential (mV)	-150 (at pH 7)	not measured
Pressure, P (kPa)	392	345-585
Recycle ratio, R_r	0.1	0.08
Concentration, N_b (cm^{-3})	10^4 - 10^5	10^4 - 10^5
Produced Flocs		
Size range, d_p (μm)	10^0 - 10^3	10^0 - 10^2 (best: 10-30)
Density, ρ_p (g/cm^3)	floc density function	1.01 (assumed)
Suitable mobility (μm/secVcm)	0 to +1 (clay floc) -1 to +1 (colour floc)	0.5 or less
Bubble-Floc Collision		
Collision model	Population balance	Single collector collision
Flow regime	Turbulent flow	Lamina flow
Mechanism	Locally isotropic turbulence, viscous subrange diffusion	Brownian diffusion, interception, gravity
Attachment mechanism	Electrical-charge interactions (coverage of precipitated coagulant on a floc surface)	Electrical-charge interactions, water layer at floc surface
Rise velocity of agglomerate, v_{bp} (cm/sec)	According to Eq. 5.19 0.1-2.6 (observed)	Nearly equal to v_b about 0.3

5.2.1 Single Collector Collision (SCC) Model

Edzwald *et al.* developed the SCC model based on the single collector collision theory. This model has been widely employed in a variety of applications, including froth flotation (Flint and Howard, 1971), dispersed air flotation (Reay and Ratchclift, 1973), air filtration (Friedlander, 1977) and water filtration (Yao *et al.*, 1971; O'Melia, 1980 & 1985; Tien, 1989). The collision mechanisms includes Brownian diffusion (η_D), interception (η_I) and gravity settling (η_G). The single collector collision efficiency defines the ratio of particle-bubble collision rate to particle-bubble approach rate. The total collision efficiency is

$$\eta_T = \eta_D + \eta_I + \eta_G \tag{5.10}$$

The individual collision efficiency can be derived from particle trajectory analysis (and substituting v_b in Equation (5.2)) expressed as follows:

$$\eta_D = 6.18\left(\frac{kT}{g\rho_w}\right)^{\frac{2}{3}}\left(\frac{1}{d_p}\right)^{\frac{2}{3}}\left(\frac{1}{d_b}\right)^{\frac{2}{3}} \tag{5.11}$$

$$\eta_I = \frac{3}{2}\left(\frac{d_p}{d_b}\right)^2 \tag{5.12}$$

$$\eta_G = \left(\frac{\rho_p - \rho_w}{\rho_w}\right)\left(\frac{d_p}{d_b}\right)^2 \tag{5.13}$$

where: k is Boltzman's constant, T absolute temperature, d_p particle diameter, d_b bubble diameter, ρ_p particle density, ρ_w water density, μ water viscosity, v_b bubble rise velocity and g gravitational force acceleration.

The removal efficiency of particles by a single bubble (R) is expressed as

$$R = \alpha_{pb}\eta_T (100\%) \tag{5.14}$$

where α_{pb} is the attachment efficiency (fraction of successful collision). The rate of particle removal can be obtained by extending the particle removal by a single bubble to a system containing a bubble concentration of N_b.

$$\frac{dN_p}{dt} = -(\alpha_{pb}\eta_T)(A_b v_b N_b)N_p \tag{5.15}$$

where N_p is particle number concentration and A_b projected area of the bubble. This equation is often simplified similar to first-order chemical kinetics as follows:

$$\frac{dN_p}{dt} = -kN_p \tag{5.16}$$

where $k = (\alpha_{pb}\eta_T)(A_b v_b N_b)$

The rate of particle removal can be expressed in terms of the bubble volume concentration (N_b) and bubble diameter (d_b), setting $A_b = \pi/4\, d_b^{\,2}$.

$$\frac{dN_p}{dt} = -\frac{3}{2}(\alpha_{pb}\eta_T)\frac{(\phi_b v_b N_p)}{d_b} \tag{5.17}$$

It can also be expressed as the particle removal rate per flotation tank depth (dh) as follows

$$\frac{dN_p}{dh} = -\frac{3}{2}(\alpha_{pb}\eta_T)\frac{(\phi_b N_p)}{d_b} \tag{5.18}$$

The right hand side of Equation (5.18) is identified as the key parameters for design and operation of DAF. $(\alpha_{pb}N_p)$ represents pre-treatment parameters prior flotation

and $\eta_T(\phi_b/d_b)$ represents flotation reaction zone parameters. Detailed description of these parameters is summarised in Table 5.3.

Table 5.3 Summary of SCC model parameters and effects on design and operation

Parameter	Dependence	Comments
	PRE-TREATMENT PARAMETERS	
α_{pb} (particle-bubble attachment efficiency)	1. Particle-bubble charge interactions 2. Hydrophilic nature of particles	1. Favourable flotation: requires reduction in particle charge and hydrophobic particle 2. Increase α_{pb} to 1: optimum coagulation and pH conditions
N_p (particle number concetration)	1. Raw water quality 2. Coagulant type and conditions 3. Flocculation time	1. Concentration and size of particles 2. Coagulant may add particles 3. Flocculation may reduce N_p and increase d_p
	REACTION ZONE - FLOTATION TANK	
η_T (total single collector efficiency)	1. Particle-bubble collisions from diffusion and interception 2. Minimum η_T for $d_p \approx 1$ μm	1. Increase η_T : produce floc size of 10's of microns 2. Short flocculation times
d_p (bubble diameter)	Controlled by pressure difference across nozzle and injection flow	1. Desire microbubbles: range 10-100 μm, median 40 μm 2. $\eta_T \propto d_p^{-2}$; rate of collection of particles $\propto d_p^{-1}$ 3. Smaller bubbles: better performance
ϕ_b (bubble volume concentration)	1. Saturator pressure 2. Recycle ratio	1. Increasing ϕ_b increases N_b: more bubbles for collection of particles 2. Increase ϕ_b: more bubble volume for reducing floc density

5.2.2 Population Balance (PBT) Model

Tambo *et al.* developed their PBT model based on the population balance model of bubbles, particles, bubble-particle agglomerates and the rate of bubble-particle collision and attachment. DAF is considered to consist of four steps: 1) coagulation and flocculation prior the flotation (pre-treatment); 2) bubble generation; 3) bubble-particle collision and attachment in a mixing zone; 4) rise of the bubble-particle agglomerates in a flotation tank. This model represents parameters in steps 3 and 4.

The PBT model describes the process of bubble-particle collision and attachment as well as the rising velocity of the bubble-particle agglomerate. The model is formulated by counting the number of particles (flocs) with attached *i* bubbles ($n_{f,i}$, cm^{-3}) within an elapsed time of mixing (t, sec.). Several assumptions were adopted to derive the model (Fukushi *et al.*, 1995), such as the bubble size does not vary throughout the time, particle detachment is negligible, a maximum attachable number of bubbles on a certain size particle (floc) exists and the agitation intensity in a mixing zone can be expressed by the mean effective energy dissipation rate (following the theory of local isotropic turbulence).

The rising velocity of bubble-particle(floc) agglomerate was derived by incorporating the buoyancy of attached bubbles and the change of particle (floc) density with the size into Stoke's correlation. The floc density function was developed previously (Tambo and Watanabe, 1979). The correlations for calculating the rising velocity of bubble-particle agglomerate (v_{bp}) are as follows:

$$v_{bp} = \frac{4g}{3\mu K_{Fd}} \frac{i(\rho_w - \rho_a) - a(d_p/1)^{-K_P}(d_p/d_b)^3}{i + (d_p/d_b)^3} d_{bp} \qquad (5.19)$$

$$d_{bp} = (d_p + id_b)^{\frac{1}{3}} \qquad (5.20)$$

$$K_{Fd} = \frac{16id_b^2 + 45d_p^2}{id_b^2 + d_p^2} = \frac{16i + 45(d_p/d_b)^2}{i + (d_p/d_b)^2} \qquad (5.21)$$

where K_{Fd} is the constant of drag force (16 for bubbles and 45 for flocs), K_P the constant of the floc density function, d_{bp} the diameter of the bubble-particle(floc) agglomerate.

Generally, the PBT model is more applicable to DAF practice compared to the SCC model. In the SCC model, the flow regime is laminar and collision occurs due to Brownian diffusion, interception and gravity settling. Given the bubble and particle size, the Brownian diffusion and gravity settling contribution in the collision process will be minor. Edzwald and co-workers (1990, 1991) have pointed out that the gravity settling was negligible in their model. Hence, interception is in dominant mode in the collision process. However, in practical DAF system, the bubble-particle mixing zone is in turbulent flow. Hence, the SCC model may be more suitable for dispersed air flotation or froth flotation (Fukushi *et al.*, 1995). Another limitation of the SCC model is that is best applied to the batch mode.

By contrast, The PBT model satisfy the normal requirements of practical DAF systems, i.e. a turbulent flow regime in the mixing zone where the collision and attachment of bubble and particles occurs. As well, this model has been further developed (Matsui *et al.*, 1998) to extend its coverage. The initial model was developed for the case where the particle (floc) was larger than the bubble ($d_p < d_b$). In the improved model, both cases (i.e. $d_p > d_b$ and $d_p < d_b$) are considered. This model is applicable to the removal of inclusion bodies by DAF. In this case, the particle (d_p = 0.3 μm) is smaller than the bubble ($d_b \approx$ 10- 120 μm). A detailed discussion of the model is presented in the following section.

5.3 DAF MODELING FOR INCLUSION BODY RECOVERY

5.3.1 Model Development

The PBT model developed by Tambo and co-workers (Matsui *et al.*, 1998) is adopted with modifications. This model was initially developed for applications in wastewater and water treatment to remove flocs from water. Flocs were formed by flocculation and/or coagulation processes prior flotation. As a consequence, the model incorporates the effect of these processes into the population balance model, eg. by introducing a particle porosity (ϕ). In our model, we have not initially considered pre-treatment to form bigger inclusion body aggregates (this could be possible). The mean diameter of inclusion bodies is approximately 0.3 μm (chapter 3) and typical bubble size generated in DAF is in the range of 10 to 120 μm with mean diameter of 60 μm (Fukushi *et al.*, 1998). Hence, the model is developed for bubble diameter larger than particle diameter ($d_b > d_p$).

Rise velocity of bubble-particle agglomerate

Consider j particles attached on a single bubble forming an agglomerate, then the rising velocity of bubble-particle agglomerate can be derived by equating forces upon this agglomerate as follows:

$$\frac{\pi}{6}(\rho_w - \rho_a) g d_b^{\,3} - \frac{\pi}{6} j(\rho_p - \rho_w) g d_p^{\,3} = F_D \qquad (5.22)$$

The bubble-particle agglomerate can rise if the buoyancy force of this agglomerate is larger than the gravitational force and the drag force. In this case, the gravitational force is much smaller than the buoyancy force given that the particle is much smaller than the bubble, hence it is reasonable to assume that:

$$\frac{\pi}{6}(\rho_w - \rho_a)gd_b^{\ 3} \cong \frac{\pi}{6}\rho_w gd_b^{\ 3} \gg \frac{\pi}{6}j(\rho_p - \rho_w)gd_p^{\ 3} \tag{5.23}$$

Then Equation (5.22) can be rewritten as

$$\frac{\pi}{6}\rho_w gd_b^{\ 3} = F_D \tag{5.24}$$

For the bubble-particle agglomerate, the particles attached to the bubble may retard motion on its surface (Levich, 1962). This is similar to the case for a rigid particle moving in liquid. Hence, by taking the sphericity (φ) of the agglomerate into account, the drag force (F_D) may be expressed as

$$F_D = 3\pi\mu d_{pb}v\varphi^{-\frac{1}{2}} \tag{5.25}$$

When the particle is smaller than the bubble and the number of particles (j) attached on the bubble is large, the diameter of the agglomerate (d_{pb}) can be approximated by:

$$d_{pb} = (d_b^{\ 3} + jd_p)^{\frac{1}{3}} \tag{5.26}$$

Substitution of Equations (5.25) and (5.26) into Equation (5.24) results the rising velocity of bubble-particle agglomerate:

$$v_{pb} = \frac{g\rho_w d_b^{\ 3}}{18\mu(d_b^{\ 3} + jd_p^{\ 3})^{\frac{1}{3}}}\varphi^{\frac{1}{2}} \tag{5.27}$$

Kinetics of bubble-particle agglomeration

The collisions and attachments between bubbles and particles in flotation tank/column is assumed to be a heterogeneous agglomeration process. The model of bubble-

particle agglomeration involves of the rate of collision and attachment between bubbles and particles and a population balance between bubbles, particles and bubble-particle agglomerates. The collision frequency between bubbles and particles is assume to follow a second order kinetics (Suffman and Turner, 1956; Levich, 1962; Fukushi *et al*, 1995) expressed as:

$$N = kn_a n_d \tag{5.28}$$

where N is the collision frequency between bubbles and particles ($m^{-3}s^{-1}$), k the collision rate coefficient ($m^{-3}s^{-1}$), n_a the number concentration of remaining bubble (m^{-3}) and n_d the number of concentration of particles with diameter of d (m^{-3}).

The collision between bubbles and particles is facilitated by motion in the fluid due to turbulence and by the relative motion between particles and bubbles as a consequence of gravity and turbulence. However the relative motion due to turbulence is negligible as turbulent acceleration is much smaller compared to gravitational acceleration in the fluid flow of DAF (Suffman and Turner, 1956). Hence, the rate of collision constant is derived by taking into account the effect of collisions due to motion within turbulent fluid and gravitational relative motion (Suffman and Turner, 1956) simultaneously as follows

$$k = \sqrt{k_T^{\,2} + k_G^{\,2}} \tag{5.29}$$

where, k_T is a collision rate coefficient contributed by the turbulent fluid motion and expressed as (Suffman and Turner, 1956, Levich, 1962):

$$k_T = aG(d_b + d_p)^3 = a\sqrt{\frac{\varepsilon}{\mu_w}}(d_b + d_p)^3 \tag{5.30}$$

where, a is a constant (0.209 according to Suffman and Turner (1956) and 0.385 according to Tambo *et al.* (1981)) and ε the rate of energy dissipation per unit volume

of fluid (Wm^{-3}). k_G is a collision coefficient which relates to the relative gravitational motion and given by (Levich, 1962):

$$k_G = \frac{1}{36}\sqrt{\frac{2\pi}{3}}(d_p + d_b)^2[(\rho_p - \rho_w)d_p{}^2 - (\rho_b - \rho_w)d_b{}^2]\frac{g}{\mu} \tag{5.31}$$

Since the gravitational force is much smaller than the buoyancy force (Equation 5.23), then k_G can be rewritten into:

$$k_G = \frac{1}{6}\sqrt{\frac{2}{3\pi}}\rho_w(d_p + d_b)^2\frac{g}{\mu}\frac{\phi_b}{d_b}\frac{1}{n_a} \tag{5.32}$$

If the flotation condition is homogenous (well mixed), the collisions is predominantly caused by particle transport by turbulent flow motion, hence:

$$k \cong k_T \tag{5.33}$$

Assuming a uniform particle and bubble size, the decrease of particle number by collision-attachment to bubble is

$$\frac{dn}{dt} = -\alpha k n_{a,0} n \tag{5.34}$$

where n is the number concentration of remaining particles (m^{-3}), α the attachment efficiency of bubble-particle collision (dimensionless), k the collision rate constant (m^3s^{-1}) and $n_{a,0}$ the initial number concentration of bubbles (m^{-3}).

The attachment efficiency represents the ratio of successful collisions to all collisions. As a number of particles attached to the bubble increases, the likelihood of successful attachment in the consecutive collisions decreases. Hence, the attachment efficiency is proportional to the number of attachment sites on the bubble. Consider j particles with an initial attachment efficiency of α_0 and a maximum number of particle attachable to the bubble equals to m_a, the attachment efficiency can be written as:

$$\alpha = \alpha_0 \left(1 - \frac{j}{m_a} \right) \tag{5.35}$$

The particle is attached to the bubble surface, hence the maximum number of particle attachable to the bubble surface is in proportion to the bubble surface area ($\approx d_b^2$) and in opposite proportion to the area occupied by a single particle attached to the bubble surface ($\approx d_p^2$). Hence, the maximum number of particle attachable to the bubble is

$$m_a = \alpha_0 \left(\frac{d_b}{d_p} \right)^2 \tag{5.36}$$

Population Balance Model

Several assumptions have been made to derive the population balance of bubbles, particles and bubble-particle agglomerates in the contact zone of flotation tank/column. These include:

1. Bubbles and particles are uniform in size, i.e. their size distribution is neglected.
2. Bubble coalescence is negligible.
3. Many particles may attach to a single bubble but a single particle may not attach to more than one bubble.
4. Detachment of particle from bubble is negligible.

Consider j particles attached to bubbles with initial bubble number concentration of $n_{a,0}$ (m^{-3}), the population balance equation for the number of particles is:

$$n_0 - n = j n_{a,0} \tag{5.37}$$

where n_0 is the initial number concentration of particles (m^{-3}) and n is the number concentrations of remaining particles (m^{-3}). The number concentration of remaining particles (unattached to bubbles) as a function of time can be derived by integration of Equation (5.34) following substitutions of Equations (5.35) and (5.37) as follows:

$$\frac{n}{n_0}\frac{1}{1-\frac{n_0}{m_a n_{a,0}}+\frac{n}{m_a n_{a,0}}}=\exp\left[-K\left(1-\frac{n_0}{m_a n_{a,0}}\right)t\right] \tag{5.38}$$

where $K=\alpha_0 k n_{a,0}$, is the rate constant (s^{-1}).

The number concentration of unattached particles in the separation zone can be obtained by introducing the hydraulic detention time of a contact zone (contact zone residence time or contact time) into t in Equation (5.38). A certain condition exists where there is not sufficient bubbles for attachment with given number of particles. This condition occurs when the initial particle concentration is greater than the maximum available bubbles for bubble-particle attachment, i.e. $n_0 > m_a n_{a,0}$. This condition is undesirable in DAF. A new parameter is introduced as a measure of this condition, i.e. a ratio of supplied over consumed bubbles, A_{SC}. DAF is favoured if A_{SC} is greater than unity.

$$A_{SC} \equiv \frac{m_a n_{a,0}}{n_0} \tag{5.39}$$

When bubbles are in excess ($A_{SC} \gg 1$), then Equation (5.38) can be simplified into

$$\frac{n}{n_0} \cong \exp(-Kt) \tag{5.40}$$

Bubble Concentration Requirement

The air-solid ratio and air supply-consumption ratio have been employed widely as important parameters in the design and operation of DAF. The air-solid ratio is particularly important in DAF recovery of high concentration suspension (Zabel, 1992). For DAF with partial recycle-flow pressure, the air solid ratio (A_s) is defined as:

$$A_S = \frac{\Delta P a_m R_r}{S_s} \tag{5.41}$$

where, ΔP is the pressure difference (Pa), a_m the quantity of air released per volume of water per unit of pressure difference ($kg.m^{-3}.Pa^{-1}$), R_r the recycle ratio and S_s the suspended solid concentration of influent ($kg.m^{-3}$).

The air-solid ratio can also be stated as a function of the suspended solid concentration in the contact zone (S_{sr}) and the bubble volume concentration (ϕ_b) or the bubble number concentration ($n_{a,0}$) as follows:

$$A_s = \frac{\rho_b \phi_b}{S_{sr}} = \frac{\pi \rho_b n_{a,0} d_a^{\ 2}}{6 S_{sr}} \tag{5.42}$$

The relationship between the air-solid ratio and the ratio of supplied over consumed air bubbles (also known as the air supply-consumption ratio) can be obtained by combining Equations (5.39) and (5.42).

$$A_{SC} = \frac{m_a S_{sr}}{\frac{\pi}{6} \rho_a d_a^{\ 3} n_0} A_S \tag{5.43}$$

and the mass concentration of suspended solid in contact zone is written as:

$$S_{sr} = \frac{\pi}{6} \rho_p d_p^{\ 3} n_0 \tag{5.44}$$

Substituting Equation (5.44) into (5.43), the ratio of supplied over consumed air bubbles (in number) can be represented as:

$$A_{SC} = \alpha_a \left(\frac{\rho_p d_p}{\rho_a d_b} \right) A_S \tag{5.45}$$

5.3.2 Summary of Key Parameters

Performance of DAF is usually assessed by two different parameters, namely equilibrium and kinetics requirements. In the proposed model, the equilibrium requirement is represented by the air-solid ratio (A_S) or the air supply-consumption ratio (A_{SC}). The kinetic requirement is represented by the rate constant, K. The correlations of these key parameters are summarised as follows:

Equilibrium requirement:

$$A_{SC} \equiv \frac{m_a n_{a,0}}{n_0} \tag{5.39}$$

$$A_s = \frac{\rho_b \phi_b}{S_{sr}} = \frac{\pi \rho_b n_{a,0} d_a^{\,2}}{6 S_{sr}} \tag{5.42}$$

$$A_{SC} = \alpha_a \left(\frac{\rho_p d_p}{\rho_a d_b} \right) A_S \tag{5.45}$$

Kinetics requirements:

$$\frac{n}{n_0} \frac{1}{1 - \frac{n_0}{m_a n_{a,0}} + \frac{n}{m_a n_{a,0}}} = \exp\left[-K \left(1 - \frac{n_0}{m_a n_{a,0}} \right) t \right] \tag{5.38}$$

where $K = \alpha_0 k n_{a,0}$, is the rate constant (s^{-1})

The rising velocity of the bubble-particle agglomerate has also been introduce as follows:

$$v_{pb} = \frac{g \rho_w d_b^{\,3}}{18 \mu (d_b^{\,3} + j d_p^{\,3})^{\frac{1}{3}}} \varphi^{\frac{1}{2}} \tag{5.27}$$

5.3.3 Results and Discussion

Equation (5.45) implies that the air supply-consumption ratio is proportional to the air-solid ratio by a factor of $\alpha_a(\rho_p d_p / \rho_a d_b)$. The requirement of the air-solid ratio may be interpreted as the necessary quantity of air supplied in excess of that consumed by bubble-particle collision-attachment. The diameter of the air bubble depends on the saturator pressure and the type of nozzle or pressure reducing valves, but is usually around 50 μm (Edzwald and Wingler, 1990; Fukushi *et al.*, 1998). By considering the steric configuration of the attachment of particles to a bubble, Mitsui *et al.* (1998) assumed the value of α_a approximately 1. Since, the diameter of air bubble is roughly constant and the density of the particle and the air are fixed, then the size of the particle dictates the correlation between A_{SC} and A_S. Given a value of A_{SC} (eg. 1, a minimum air requirement), the air solid ratio (A_S) increases with the particle size (d_p). This is simply because the maximum number of particle attached to a bubble (m_a) is less for larger particles (given a fixed bubble size). As well, an increased buoyancy force (due to air bubbles) is necessary to compensate for the larger gravitational force.

For clay-aluminium flocs, Matsui *et al.* (1998) suggested that $A_{SC} \cong 0.01\ A_S$. Hence, the air supply-consumption ratio of 1 or larger indicates the air-solid ratio of 0.01 or larger ($A_S \geq 1$ when $A_{SC} \geq 1$). The air-solid ratio is suggested to be the parameter that balances the gravity forces due to suspended solids with the buoyancy force due to air bubbles (Matsui *et al.*, 1998). Typical values of the air-solid ratio in wastewater and water treatment practice are 0.018 to 0.036 (Melbourne and Zabel, 1977).

The density of inclusion bodies is assumed 1260 $kg.m^{-3}$ (Middelberg, 1996). The density of air at standard condition is approximately 1.29 $kg.m^{-3}$ (Perry's Chemical Engineers Handbook). The mean diameter of inclusion bodies is known to be 0.3 μm. Assuming α_a equals to 1 and the diameter of bubble is approximately 50 μm, the proportional factor between the air supply-consumption ratio and the air-solid ratio is 5.86. This factor is much larger than the normal value proposed by Tambo *et al.* (0.01). Consequently, an extremely high value of the air-solid ratio results. This effect is a consequence of the density of the inclusion bodies. In the case of flocs, the density is relatively small, very similar to that of water or slightly lower. Such a large

air-solid ratio would clearly be uneconomic and it is obvious that aggregation of the inclusion bodies is necessary if a practical process is to be devised.

For the system, the kinetics requirement can be analysed in term of the number of particles not yet attached to the bubbles (Equation (5.38)). The rate constant, $K = \alpha_0 k n_{a,0}$, represents the rate of the particle attachment. Clearly, this rate constant is a function of the initial bubble concentration ($n_{a,0}$) and the collision rate coefficient (k) which primarily depends on the particle size (d_p) and to a smaller extend the bubble concentration (ϕ_b). Clearly, the bubble concentration and the particle size will affect the kinetics of particle removal by bubbles. The design of DAF must satisfy both equilibrium and kinetics requirements. As the particle size of inclusion bodies is fixed, then the bubble concentration is the key parameter in DAF design and operation for inclusion body recovery.

Clearly, if we desire a practical and economic process, inclusion body aggregation must be introduced prior the DAF step. In general, particles tend to aggregate when the net surface charge (known as electrophoretic mobility or zeta potential) equals or nearly zero. The electrophoretic mobility study has indicated that the isoelectric points of inclusion bodies lies in the range of 5 to 6 depending on the ionic strength (chapter 3). This result has also been supported by the measurements of inclusion body-bubble interaction forces (chapter 4). The largest interaction force observed was at pH 5. These imply that inclusion bodies are likely to aggregate at pH approximately 5 to 6. Our initial experience in the laboratory indicates that inclusion bodies are easily aggregated to form larger particles. Treated particles were observed to sediment a short time after pH treatment. Hence, such a step needs to be introduced to enhance the recovery by DAF and provide an economic process. Time constraints did not permit for the experimentation on this step, but the key operation conditions have been identified.

A number of considerations should be taken into account as a consequence of introduction of an aggregation step. The proposed model does not consider particles as aggregates. The aggregation process for inclusion bodies is similar to that for

flocculation and/or coagulation in the wastewater and water treatment. The model derivation suggested by Tambo *et al.* for wastewater and water treatment applications can be employed. Hence, a number of adjustments must be performed to incorporate the aggregation process into the proposed DAF model.

Modeling for the recovery of inclusion body aggregates

As a consequence of the aggregation process, pores are present in the aggregate and hence a particle porosity (ϕ) must be introduced. Thus, the mass concentration of suspended solid in contact zone (S_{sr}) can be rewritten:

$$S_{sr} = \frac{\pi}{6}\rho_p(1-\phi)d_p{}^3 n_0 \tag{5.46}$$

A mass balance of on aggregated particles suggests that:

$$(1-\phi)\rho_{ib} + \phi\rho_w = \rho_{pb} + \rho_w \tag{5.47}$$

ρ_{ib} is the density of inclusion bodies (identical to ρ_p in the case of zero aggregation) and consequently in this case ρ_p in all Equations must be replaced by to the density of the aggregates. The buoyant density of the aggregate particle, ρ_{pb} may be expressed in the following correlation (Tambo and Watanabe, 1979):

$$\rho_{pb} = \rho_{pbo} d_p{}^{-e} \tag{5.48}$$

where ρ_{pbo} is a coefficient related to the size-density relationship of the aggregate particle ($kg.m^{-3}.m^e$) and e is a constant related to the size-density relationship of the aggregate particle (dimensionless). In the case of water treatment flocs, the value of e is approximately 1 (Tambo and Watanabe, 1979; Tambo *et al.*, 1981). If it is assumed that this also applies to inclusion body aggregates, then substitution of Equations

(5.36), (5.46), (5.47) and (5.48) into Equation (5.43) provides the air supply-consumption ratio as:

$$A_{SC} = \frac{\alpha_a \rho_{ib} \rho_{pbo}}{(\rho_{ib} - \rho_w)\rho_b d_b} A_S \tag{5.49}$$

As was the case without an aggregation process, A_{SC} is proportional to A_S but a complex proportional factor has been introduced.

Any aggregation process will affect both the equilibrium and kinetics requirements. Larger sized aggregates have a higher probability of collisions and the DAF performance will improve by icreasing bubble-particle collision rate. However, an increase in air supply is necessary for larger particles. This is a complex trade off that is worthy of detailed experimental study and theoretical study (including model validation). As stated earlier, a study of this was initiated by time constraints have limited process to very preliminary and rudimentary studies (simply confirming that promotion of aggregation is possible). Such studies will provide a challenge for future workers.

5.4 CONCLUSION AND RECOMMENDATION

A DAF model has been derived based on population balance theory. The model is based on previous work in the water treatment area. It is proposed as a potential tool for the design of DAF systems for the recovery of inclusion bodies. The performance of DAF is described in terms of equilibrium and kinetics requirements. As expected, the model implies that the air-solid ratio or the air supply-consumption ratio are the key parameter for equilibrium requirement and the particle size and the bubble concentration are the key parameter representing kinetics requirement. Unfortunately, the air-solid ratio required for inclusion body recovery is much larger than to those for floc removal in the wastewater and water treatment and suggested exceeds 5.86. This is not likely to provide an economical process.

Consequently, aggregation of inclusion bodies will be necessary to enhance their recovery by DAF. A modified model is proposed to incorporate aggregation aspects in the DAF model. The model produces similar broad conclusions to those obtained from the model without aggregation. However, the proportional factor relating the air supply-consumption ratio and the air-solid ratio is expressed by more complex correlation. Aggregation will provide an increased bubble-aggregate collision rate. This will be offset to some extent by increased settling forces to be overcome. A detailed trade off is required. It is recommended that a detailed experimental program be undertaken to validate the model and determine unknown constants. The model should then provide a valuable design tool to consider flotation as an alternative to centrifugation or filtration for inclusion body recovery.

Chapter 6

OVERALL DISCUSSION AND CONCLUSION

This study has demonstrated the importance of the physicochemical characterisation in downstream processing of recombinant proteins, in particular for separation process based on differences in surface chemistry such as flotation. The physicochemical properties of an insulin-like growth factor 1 analog, LR^3-IGF-1, have been characterised. These include electrophoretic mobility, particle characteristics and interaction forces between inclusion bodies and an air bubble. Various methods have been employed including micro-electrophoresis, SDS-PAGE, scanning electron microcopy and atomic force microscopy. In addition, optimisation of the production of the inclusion bodies was performed by fed-batch fermentation with improved feeding strategy. Finally, mathematical models have been proposed to design inclusion body recovery using dissolved-air flotation technique by taking into account the physicochemical properties previously studied.

The demand of a variety of proteins and other biological materials have increased dramatically in the past few decades as a result of the exploration of their potential clinical applications. This has forced biotechnological industry to improve the production system and subsequent downstream processing for achieving competitiveness in the market place.

Insulin-like growth factor 1 analog LR^3-IGF-1 is produced in recombinant *E. coli* as insoluble aggregates known as inclusion bodies. This protein is marketed as a media supplement for mammalian cell cultures. The demand for this protein is expected to increase as new biopharmaceutical products approach phase III clinical trials which demand in increased supply of tissue and cell cultures' media. The protein is currently produced by fed-batch fermentation using a constant-rate feeding strategy. High level of glucose and acetate accumulation resulted. This inhibits cell growth and introduces a significant limitation on productivity improvement. Hence, an optimised feeding strategy, called a novel 3-stage feeding profile, has been proposed to decrease or eliminate these problems (chapter 2).

The application of this new feeding profile has reduced glucose accumulation significantly and as a result higher cell concentration has been achieved. Protein concentration has increased approximately two fold. Fusion protein concentration of 4.3 g/L corresponding to an actual IGF-1 concentration of 3.6 g/L has been achieved. Several attempts were made to increase the size of the inclusion bodies, such as the application of yeast extract supplemented nutrient feed. Unfortunately, improvement in inclusion body size was not achieved. This has consequences for subsequent downstream processing.

The existing method for inclusion recovery is centrifugation following homogenisation to release the IB from the cell. This method incurs a high capital and operating cost. As well, the size similarity between inclusion bodies and cell debris limits separation performance. Hence, it is obvious that an alternative fractionation technique is necessary. Dissolved-air flotation (DAF) is considered as a potential method for inclusion body recovery. This technique has been widely applied in

wastewater and water treatment for decades. However, fundamental understanding of DAF processes remains poor.

The exploration and synthesis of downstream processing sequence is normally performed by a traditional engineering (empirical) approach which does not provide fundamental understanding of the process. Recent advances in various scientific and technological disciplines have allowed fundamental study of processes from micro to molecular levels, for example using the Atomic Force Microscopy technique. Studies of DAF are normally performed with this engineering approach, possibly due to practical reasons. This may contribute to the relatively poor understanding of the fundamental basis of DAF. Clearly, fundamental understanding will improve design and lead to an efficient DAF system.

Physicochemical characteristics of particles and the interactions between the particle and the bubble dictate the elementary processes of flotation. Unfortunately, these have not been extensively researched. Hence, this work aims to rectify this deficiency. A fundamental approach is applied replacing the tradition empirical engineering approach. This study is expected to provide fundamental basis for a rational design of flotation recovery.

The electrophoretic mobility measurements provide a net surface charge map of the inclusion bodies and cell debris as a function of electrolyte type, ionic strength and pH. This map may be exploited and employed for the improvement of chemical and physical processes, such as aggregation, precipitation and flotation. Several significant outcomes have been identified from the measurement of the electrophoretic mobility:

- The net surface charge of inclusion bodies is a minimum at approximately pH 5 to 6 depending on the ionic strength and the type of electrolytes present in the solution. The net surface charge reduces with ionic strength and the valency of the electrolytes.
- Cell debris are highly negatively charged at normal pH and their isoelectric points (i.e.p. ≈ 2-3) are significantly lower than inclusion bodies (i.e.p. ≈ 5-6). Clearly,

there exists the possibility for separating inclusion bodies from the debris based on this isoelectric point difference.

- The electrophoretic mobility or the isoelectric point of inclusion bodies can be employed as a qualitative measure of the purity of inclusion bodies.

The first result will be useful in several processes, such as aggregation and flotation, and analysis of surface chemistry including electrostatic and hydrophobic properties. Particle aggregation is normally promoted when the net surface charge of the particles is minimum, i.e. approximately at or close to its isoelectric point. This phenomena was observed in our laboratory and confirmed by the presence of particles in the short time. In addition, such a condition is generally favourable to flotation separation since the possible electrostatic repulsion between particles and bubbles is minimal. An electrophoretic mobility map of inclusion bodies can be employed to predict their surface chemistry which provides valuable insight for several processes, for example flotation. It is expected that the surface of the inclusion bodies will become more hydrophobic approximately at or close to the isoelectric point as a consequence of the minimal surface charge. This prediction has been confirmed by the results of the AFM measurement of the interaction forces between inclusion bodies and an air bubble.

The difference in isoelectric point of inclusion bodies and cell debris may be exploited to design the optimal conditions for their separation, eg. using flotation. For example, at pH5-6, inclusion bodies posses minimum surface charge whilst cell debris is highly negatively charged. At this condition, inclusion body-bubble attachment should be favoured compared to cell debris-bubble attachment. At pHs less than 5, aggregation between the inclusion bodies and cell debris may be promoted by the attractive electrostatic interactions. This aggregation is clearly undesirable.

It appears the majority of impurities incorporated with inclusion bodies are negatively charged. Larger isoelectric points were observed in inclusion bodies subjected to more extensive purification. This difference provides practical and qualitative measure of protein purity. Electrophoretic mobility measurement is easily performed in a short time. By contrast, standard purity tests may be complex, expensive and

time consuming, for example using high performance liquid chromatography (HPLC). This initial finding may lead to a simple quantitative tool for analysis of inclusion bodies purity. However, various aspects need refinement and extensive validation of the method is required.

Particle characteristics including particle size and the surface nature of the inclusion bodies has been examined using various techniques. The mean particle size of the inclusion bodies is approximately 0.3 μm. The scanning electron microscopy has shown that inclusion bodies posses an irregular shape and rough surface. This was confirmed by the AFM imaging results. Particle characteristics may be employed to design and/or improve fractionation techniques. The potential of AFM for surface imaging was noted with some recommendation proposed to improve image resolution. The shape irregularity and surface roughness may be beneficial for flotation processes This will be discussed in later sections.

Clearly, mapping of electrophoretic mobility and particle characteristics are essential as they have direct and indirect implications to physico-chemical processes and the fundamental surface chemistry of the particles (inclusion bodies).

Atomic force microscope (AFM) is a new tool, with significant potential for surface imaging and force measurement. It can resolve at the nanometer scale and measure forces to picoNewtons. This powerful tool has become increasingly important in numerous studies at the micro to molecular levels. It is particularly beneficial for biological applications as it can perform measurements in liquids in which most biological processes occur. In this study, AFM has been employed to measure the interaction forces between inclusion bodies and an air bubble. Such interaction forces contribute to the bubble-particle attachment, an important component of the elementary processes in flotation. Measurement of interaction forces between an inorganic particle and an air bubble have been performed by several workers (Butt, 1994; Ducker *et al.*, 1994; Fielden *et al*, 1996). They employed a standard silica sphere and attached it to the AFM tip. The interaction (adhesion) force between a silica particle and an air bubble was then measured. This measurement has permitted

an analysis of the forces involved in the bubble-particle interaction. This is a niche for gaining a fundamental understanding of flotation processes.

To date, the measurement of interaction forces between an air bubble and a designated particle in a commercial flotation process has not been performed. All measurements used a standard particle. This may be due to some practical reasons. Measurement of the interaction force between the designated particle and the bubble will provide the designer of flotation system with useful information to optimise process conditions. Hence, the interaction forces between inclusion bodies and an air bubble were quantified using AFM (chapter 4). Inclusion body particles were attached to the AFM tip by chemical modification. The tip is silanised to functionalise its surface with a SH group. A cross linker was introduced as a *bridge* between the functionalised tip surface and inclusion body particle. One end of the cross linker is reactive to SH group and forms a strong covalent bond by coupling reaction. The other end of the cross linker is reactive to an amine (NH_2) group which is readily available in the inclusion bodies.

The introduction of a cross linker between inclusion bodies and the tip surface provide several benefits including a reduction in the number of attached particles to the tip surface and a reduction of the possibility of influence from the tip surface on the interaction force. The tip modification strategy appears reliable for inclusion body attachment although some modifications and improvement may be required to achieve improved and controllable inclusion body attachment.

Interaction forces between inclusion bodies were measured by AFM in various buffer concentration and at a variety of pH. Three sets of 100 measurements per set were performed for each combination of buffer concentration and pH. In most cases, the force measured followed a normal distribution and the mean values of the three sets were similar. This indicates highly reproducible measurements and thus, it can be concluded that AFM is reliable for this force measurement.

The measured interaction forces lie in the range of 9.7 to 25.3 nN with standard deviations of 4 to 11%. The interaction force between various tips and bubbles

depends upon the type of tip. This confirms that the measured force indicates the strength of the inclusion body-bubble interaction. As expected, this force varies with buffer concentration (ionic strength) and pH. The largest interaction forces measured was at pH 5 for all buffer concentrations. The electrophoretic mobility measurements also indicated that inclusion bodies posses minimal net surface charge at pH 5-6. This suggests that contribution of other forces to the overall interaction force measured is significant. Hydrophobic forces provided more pronounced effects compared to the electrical double layer forces. It also appears that the ionic strength affects the hydrophobic forces. The effects of pH are significantly stronger for the inclusion bodies compared to the air bubble. Clearly, interdependency among various physicochemical properties exists. Consequently, a comprehensive examination of physicochemical properties will provide useful fundamental understanding in numerous applications.

Dissolved-air flotation has been proposed as a potential technique for inclusion body recovery. Mathematical models have been developed based on a population balance model identifying several key parameters for the design of a DAF system. Both equilibrium and kinetics requirement influence the performance of the DAF system. The air supply-consumption ratio and the air-solid ratio are the key parameters for equilibrium requirement whilst the particle diameter and bubble concentrations are central to the kinetics requirement. Physicochemical properties derived in this work have been incorporated to the analysis of the mathematical model and the design of the DAF system. As noted previously, inclusion body aggregation may be promoted at pH = 5-6. This factor has been considered in the mathematical models, some modifications have been introduced to accommodate aggregation process. This has demonstrated the importance of physicochemical properties.

Major achievement and contributions:

- Measurement of interaction forces between inclusion bodies and an air bubble using AFM, including tip modifications to attach the inclusion bodies to the AFM tip. This is the first measurement performed on a designated particle instead of the

standard particle normally employed (eg. silica particle). This work has also demonstrated the potential application of the AFM fundamental studies and imaging, particularly in the biotechnology field.

- Characterisation of the physicochemical properties of inclusion bodies (and cell debris to a certain extent) including electrophoretic mobility and various particle characteristics (size, surface nature). Such properties are not readily available in the literature.

- Development of DAF mathematical models for the inclusion body recovery. This should provide an impetus for the exploitation of DAF in biotechnology.

- Optimisation of the fed-batch fermentation through improved feeding strategy (novel 3-stage feeding profile). This has significantly improved the production yield.

In summary, this work has demonstrated the importance of physicochemical properties of inclusion bodies for their separation processes, in particular flotation. A map of physicochemical characteristics, in particular electrophoretic mobility and inclusion body-bubble interaction forces, provides a fundamental basis for a rational design of DAF system. These results have been implemented in the mathematical modeling of DAF system for inclusion body recovery. Physicochemical studies have suggested that aggregation process should be promoted to enhance the performance of DAF. This has also been incorporated into the mathematical model. Additionally, the production of inclusion bodies using fed-batch fermentation has been improved by applying an optimised feeding strategy resulting a significant increase in the production yield.

NOMENCLATURE

a	constant (0.209 according to Suffman and Turner (1956), and 0.385 according to Tambo *et al.* (1981))
a_m	the amount of air released per volume of water per unit of pressure difference ($kg.m^{-3}.Pa^{-1}$)
A_b	projected area of the bubble ($= \pi/4 d_b^2$, m^2)
A_S	air solid ratio
A_{SC}	ratio of supplied over consumed bubbles or air supply-consumption ratio
A_{280}	absorbance at wavelength 280 nm
A_{490}	absorbance at wavelength 490 nm
C_a	dissolved air concentration remaining in the solution at atmospheric pressure (mgL^{-1})
C_o	mass air concentration of the influent flow (mgL^{-1})
C_{sat}	mass concentration of air in water (mgL^{-1})
C_r	mass concentration of air per unit volume (mgL^{-1})
d_{cb}	critical diameter of bubble nucleus (m)
d_b	bubble diameter (m)
d_p	particle diameter (m)
d_{bp}	diameter of the bubble-particle(floc) agglomerate (m)
d_{pb}	diameter of the agglomerate (m)
d_{max}	maximum particle diameter (m)
D	particle size (m)
e	constant related to the size-density relationship of the aggregate particle
E_C	efficiency of bubble/particle collision
E_A	efficiency of bubble/particle attachment
E_{Coll}	efficiency of bubble/particle collection
E_G	gravitational effect
E_{ic}	interception effect
E_{id}	ideal collision efficiency or maximum collision efficiency

E_{in}	inertial effect
E_S	efficiency of stability of the bubble/particle aggregate
f	saturator efficiency factor
F_{ad}	adhesion force (or interaction force, nN)
F_D	drag force (N)
g	gravitational constant (ms^{-2})
h	height of flotation tank/column (m)
H	Henry's Law constant
H_a	Henry's Law constant for air (4.18kPa/mg/L at 20°C)
j	number of particle
k	Boltzman's constant
k	collision rate constant in collision frequency correlations ($m^{-3}s^{-1}$) or spring constant in Hooke's Law (Nm^{-1})
k_G	collision coefficient which relates to the relative gravitational motion
k_T	collision rate coefficient contributed by the turbulent fluid motion
K	rate constant of particle-bubble attachment ($= \alpha_o k n_{a,o}$, s^{-1})
K_{if}	influent flow saturation factor
K_{Fd}	constant of drag force (16 for bubbles and 45 for flocs)
K_p	constant of the floc density function
m_a	maximum number of particle attachable
n	number concentration of remaining particles (m^{-3})
n_a	number of concentration of remaining bubble(m^{-3})
$n_{a,0}$	initial number concentration of bubbles (m^{-3})
n_d	number of concentration of particles with diameter of d (m^{-3})
n_0	initial number concentration of particles (m^{-3})
N	collision frequency between bubbles and particles ($m^{-3}s^{-1}$)
N_b	bubble volume concentration (m^{-3})
N_p	particle number concentration (m^{-3})
P	partial pressure of the gas in the gas phase (Pa)
P_t	saturator total pressure (Pa)
r_b	radius of bubble (m)
r_d	detector radius (m)

r_p	radius of particle (m)
r_0	particle start radius (m)
R	removal efficiency of particles by a single bubble
R_r	recycle ratio
S_S	suspended solid concentration of influent ($kg.m^{-3}$)
S_{sr}	suspended solid concentration in the contact zone ($kg.m^{-3}$)
t	time (s)
T	absolute temperature (K)
u_E	electrophoretic mobility ($m^2V^{-1}s^{-1}$)
v_b	rise velocity of the bubble (ms^{-1})
v_{bp}	rise velocity of bubble-particle agglomerate (ms^{-1})
W_A	work of adhesion of water (N.m)
W_C	work of cohesion of water (N.m)
x	mole fraction of the gas in the liquid phase (in Henry's Law) or cantilever deflection in Hooke's Law (m)

Greek Symbols

α	attachment efficiency of bubble-particle collision
α_{pb}	*particle-bubble* attachment efficiency (fraction of successful collision)
α_0	efficiency of initial attachment
ΔG	free energy change of attachment process (N.m)
ΔP	pressure difference across nozzle or pressure reducing valve (Pa)
$\Delta\rho$	density difference between particle and fluid (kgm^{-3})
ε	rate of energy dissipation per unit volume of fluid (Wm^{-3}), or relative dielectric constant (= $\varepsilon_r\varepsilon_0$) in the Helmholtz-Smoluchowsky relationship
ε_r	dielectric constant of electrolyte solution
ε_0	dielectric constant of vacuum
ϕ_b	bubble volume concentration

γ_{SG}	interfacial tensions of solid/gas (N/m)
γ_{SL}	interfacial tensions of solid/liquid (N/m)
γ_{LG}	interfacial tensions of liquid/gas (N/m)
η	viscosity (m.Pa.s or cP)
η_T	total single collector efficiency
η_D	collision mechanisms include Brownian diffusion
η_I	interception
η_G	gravity setting
φ	sphericity (of particle)
κ^{-1}	Debye-screening length or double layer thickness (m)
μ	specific growth rate in fermentation (h^{-1}) or viscosity of water (m.Pa.s or cP)
μ_a	viscosity of air (m.Pa.s or cP)
θ	contact angle
ρ_w	density of water (kgm^{-3})
ρ_a	density of air (kgm^{-3})
ρ_p	density of particle (kgm^{-3})
ρ_f	density of fluid (kgm^{-3})
ρ_{pbo}	coefficient related to the size-density relationship of the aggregate particle ($kgm^{-3}m^e$)
ρ_{ib}	density of inclusion bodies (kgm^{-3})
ρ_{sat}	density of air saturated with water vapour (kgm^{-3}; 1.19 mg/cm^3 at 20°C)
σ	surface tension (Nm^{-1})
τ_C	collision time (s)
τ_{con}	contact time between the bubble and the particle (s)
τ_F	thin film drainage time (s)
τ_i	induction time (s)
τ_s	time for particle sedimentation from r_0 to r_d (s)
τ_{sl}	the sliding time (s)

τ_{TPC}	three phase contact time (s)
ω	angular velocity
ζ	zeta potential (mV)

REFERENCES

Angervist, I. and Enfors, S.O. 1990. Characterisation of *E. coli cell* disintegrates from a bead mill and high pressure homogeniser. *Biotechnol Bioeng.* **36**: 1083-1089.

Aristidou, A.A., San, K-Y., and Bennet, G.N. 1994. Modification of central metabolic pathway in *Escherichia coli* to reduce acetate accumulation by heterologous expression of the *Bacillus subtilis* acetolactate synthase gene. *Biotechnol. Bioeng.* **44**: 944-951.

Babcock, K., Dugas, M., Manalis, S. and Elings, V. 1995. Magnetic force microscopy: Recent advances and applications. *Mat Res Soc Symp Proc.* **vol. 355**: 311-322.

Bailey, S.M., Blum, P.H. and Meagher, M.M. 1995. Improved homogenisation of recombinant *E. coli* following pretreatment with guanidine hydrochloride. *Biotechnol Prog.* **11**: 533-539.

Barret, R.C. and Quate, C.F. 1991. Optical scan-correction system applied to atomic force microscopy. *Rev Sci Instrum.* **62**(6); 1393-1399.

Bech-Jensen, B. and Carlsen, S. 1990. Production of recombinant human growth hormone in *Escherichia coli*: Expression of different precursors and physiological effects of glucose, acetate, and salts. *Biotechnol. Bioeng.* **36**: 1-11.

Biggs, S., and Mulvaney, P. 1994. Measurements od the forces between gold surfaces in water by atomic force microscopy. *J Chem Phys.* **100**(11): 8501-8505.

Biggs, S. and Healey, T.W. 1994 Electrosteric stabilisation of colloidal zirconia with low molecular weight polyacrylic acid. *J Chem Faraday Trans.* **90**(22): 3415-3421.

Binnig, G., Rohrer, H., Gerber, Ch., and Weibel, E. 1982. Surface studies by scanning tunneling microscopy *Phys Rev Lett.* 1982. **49**: 57-61.

Binnig, G, Quate, C. F., and Gerber, Ch. 1986. Atomic force microscope. *Phys Rev Lett.* **56**(9): 930-933.

Binnig, G. and Smith, D.P.E. 1986. Single-tube three-dimensional scanner for scanning tunneling microscopy *Rev. Sci. Instrum.* **57**: 1688-1689.

Boland, T., and Ratner, B.D. 1995. Direct measurement of hydrogen bonding in DNA nucleotide bases by atomic force microscopy. *Proc Natl Acad Sci USA.* **92**: 5297-5301.

Bowden, G. A., Paredes, A. M., and Georgiou, G. 1991. Structure and morphology of protein inclusion bodies in *Escherichia coli*. *Bio/Technol.* **9**: 725-729.

Bowen, W.R., Hilal, N. Lovitt, R.W. and Wright, C.J. 1998. Direct measurement of interactions between adsorbed protein layers using an atomic force microscope. *J Colloid Interface Sci.* **197**: 348-352.

Bozzola, J.J. and Russell, L.D. 1992. *Electron microscopy: Principles and techniques for Biologists*. Jones and Bartlett Publisher. Boston.

Bremmell, K.E., Jameson, G.J., and Farrugia, T.R. 1994. Agglomeration and flotation of fats and proteins. *Chem Eng Australia* **19**(3): 23-26.

Brown, T.D.K., Jones-Mortimer, M.M., and Konberg, H.L. 1987. The enzymatic interconversion of acetate and acetyl coenzyme A in *Escherichia coli*. *J. Gen. Microbiol.*. **102**: 327-336.

Browning-Kelley, M. E., Wadu-Mesthrige, K., Hari, V., and Liu, G. Y. 1997. Atomic force microscopic study of specific antigen/antibody binding. *Langmuir*. **13**: 343-350.

Brzoska, J.B., Shahidzadeh, N., and Rondelez, F. 1992. Evidence of a transition temperature for the optimum deposition of grafted monolayer coatings. *Nature.* **360**(24): 719-721.

Burnham, N.A., Dominguez, D.D., Mowery, R.L., and Colton R.J. 1990. Probing the Surfaces of Monolayer Films with an Atomic-Force Microscope. *Phys Rev Lett.* **64**(16): 1931-1934.

Butt, H.J. 1991a. Electrostatic interaction in atomic force microscopy. *Biophys J.* **60**: 777-785.

Butt, H.J. 1991b. Measuring electroatatic, van derWaals, and hydration forces in electrolyte solutions with an atomic force microscope. *Biophys J.* **60**: 1438-1444.

Butt, H. J. 1994. A technique for measuring the force between a colloidal particle in water and bubble. *J Colloid Interface Sci.* **166**: 109-117.

Castle, J.E. and Zhdan, P.A. 1997. Charactersation of surface topography by SEM and SFM: problems and solutions. *J Phys D: Appl Phys.* **30**: 722-740.

Chiang, W. C., Iibuchi, S., and Yano, T. 1980. Single and multicomponent equilibria in bubble separation of organic materials. *Agri Biol Chem.* **44**(8): 1803-1809.

Cilliers, J.J., Johnson, L.S., and Harrison, S.T.L. 1994. Solid-Liquid Separation of PHB by froth flotation. *Separations Biotechnology* **3** (Pyle, D.L., ed.). SCI. Cambridge.

Cleveland, J.P., Manne, S., Bocek, D., and Hansma, P.K. 1993. A nondestructive method for determinig the spring constant of cantilevers for scanning force microscopy. *Rev Sci Instrum.* **64**(2): 403-405.

Clift, R., Grace, J.R. and Weber, M.E. 1978. *Bubbles, drops, and particles.* Academic Press. New York.

Collins, G. L. and Jameson, G. J. 1977. Double-layer effects in the flotation of fine particles. *Chem Eng Sci.* **32**: 239-246.

Craig, V. S. J., Ninham, B. W., and Pashley, R. M. 1993a. The effect of electrolytes on bubble coalescence in water. *J Phys Chem.* **97**: 10192-10197.

Craig, V. S. J., Ninham, B. W., and Pashley, R. M. 1993b. Effect of electrolytes on bubble coalescence. *Nature.* **364**(July): 317-319.

Crawford, R., Koopal, K., and Ralston, J. 1987. Contact angle on particles and plates. *Colloids Surf.* **27**: 57.

Dammer, U., Popescu, O., Wagner, P., Anselmetti, D., Guntherodt, H-J., and Misevic, G.N. 1995. Binding Strength Between Cell Adhension Proteoglycans Measured by Atomic Force Microscopy. *Science.* **267**: 1173-1175.

Dejarguin, B.V. and Dukhin, S.S. 1960/61. Theory of flotation of small and medium-size particles. *Trans Inst Mineral Metallurgy.* **70**: 221.

De Rijk, S.E., van der Graaf, J.H.J.M and Den Blanken, J.G. 1994. Bubble size in flotation thickening. *Wat Res.* **28**: 465-473.

Dinwiddie, R. B., Pylkki, R. J., and West, P. E. -. Thermal conductivity contrast imaging with a scanning thermal microscope. *Thermal Conductivity.* **22**: 668-677.

Drelich, J., Miller, J. D., and Good, R. J. 1992. The effect of surface heterogeneity on pseudo-line tension and the flotation limit of fine particles. *Colloid Surf.* **69**: 35-43.

Drelich, J., Miller, J. D., and Good, R. J. 1996. The effect of drop (bubble) size on advancing and receding contact angles for heterogeneous and rough surfaces as observed with sessile-drop and captive-bubble technique. *J Colloid Interface Sci.* **179**: 37-50.

Ducker, W. A., Cook, R. F., and Clarke, D. R. 1990. Force measurement using an AC atomic force microscope. *J Appl Phys.* **67**(9): 4045-4052.

Ducker, W. A., Senden, T. J., and Pashley, R. M. 1991. Direct measurement of colloidal force using an atomic force microscope. *Nature.* **353**: 239-241.

Ducker, W.A., Senden, T.J., and Pashley, R.M. 1992. Measurement of Force in Liquids Using a Force Microscope. *Langmuir.* **8**(7): 1831-1836.

Ducker, W.A., Xu, Z. and Israelachvili, J.N. 1994. Measurements of hydrophobic and DLVO forces in bubble-surface interactions in aqueous solutions. *Langmuir* **10**: 3279-3289.

Edzwald, J.K. and Wingler, B.J. 1990. Chemical and physical aspects of dissolved-air flotation for the removal of algae. *Aqua.* **39**: 24-35.

Edzwald, J.K., Malley, J.P. and Yu, C. 1991. A conceptual model for dissolved-air flotation in water treatment. *Wat Supply.* **9**: 141-150.

Edzwald, J.K. 1995. Principles and applications of dissolved air flotation. *Wat Sci Technol.* **31**(3-4): 1-23.

El-Mansi, E. M. T. and Holms, W. H. 1989. Control of carbon flux to acetate excretion during growth of Escherichia coli in batch and continuous cultures. *J. Gen. Microbiol..* **135**: 2875-2883.

Falconer, R.J. 1997. *Chemical Extraction of Recombinant Protein from the Cytoplasm of Escherichia coli.* PhD thesis, University of Adelaide.

Falconer, R.J., O'Neill, B.K., Middelberg, A.P.J. 1996. Chemical permeabilisation of *Escherichia coli*: an alternative to mechanical disruption. In Proceedings of the 1996 world congress of chemical engineering (San Diego, USA). American Institute of Chemical Engineers. **vol. 2**: 639-643.

Fielden, M.L., Hayes, R.A. and Ralston, J. 1996. Surface and capillary forces affecting air bubble-particle interactions in aqueous electrolyte. *Langmuir.* **12**: 3721-3727.

Flint, L. R. and Howarth, W. J. 1971. The collision efficiency of small particles with spherical air bubbles. *Chem Eng Sci.* **26**: 1155-1168.

Florin, E-L., Moy, V. T., and Gaub, H. E. 1994. Adhesion forces between individual ligand-receptor pairs. *Science.* **264**: 415-417.

Francis, G.L., Ross, M., Ballard, F.J., Milner, S.J., Senn, C., McNeil, K.A., Wallace, J.C., King, R. and Wells, J.R.E.. 1992. Novel recombinant fusion protein analogues of insulin-like growth factor (IGF)-1 indicate the relative importance of IGF-binding protein and receptor binding for enhanced biological potency. *J Molec Endo.* **8**: 213-223.

Frank, B.P and Belfort, G. 1997. Intermolecular forces between extracellular polysaccharides measured using the atomic force microscope. *Langmuir.* **13**: 6234-6240.

Friedlander, S.K. 1977. *Smoke, Dust and Haze.* John Wiley and Sons. New York.

Frisbie, C. D., Rozsnyai, L. F., Noy, A., Wrighton, M. S., and Lieber, C. M. 1994. Functional group imaging by chemical force microscopy. *Science.* **265**: 2071-2074.

Fuerstenau, M. C., Miller, J. D., and Kuhn, M. C. 1985. *Chemistry of Flotation.* Society of Mining Engineers. New York.

Fukushi, K., Tambo, N. and Matsui, Y. 1995. A kinetic model for dissolved air flotation in water and wastewater treatment. *Wat Sci Technol.* **31**(3-4): 37-47.

Fukushi, K., Matsui, Y. and Tambo, N. 1998. Dissolved air flotation: experiments and kinetic analysis. *J Water SRT - Aqua.* **47**(2): 76-86.

Gibson, C.T., Watson, G.S., and Myhra, S. 1996. Determination of the spring constants of probes for force microscopy / spectroscopy. *Nanotechnol.* **7**: 259-262.

Griffith, J.E., Miller, G.L. and Green, C.A. 1990. A scanning tunneling microscope with a capacitance-based position monitor. *J Vac Sci Technol B.* **8**(6): 2023-2027.

Grigg, D.A., Russell, P.E., and Griffith, J.E. 1992. Tip-sample forces in scanning probe microscopy in air and vacuum. *J Vac Sci Technol A.* **10**(4): 680-683.

Gupta, M. N. and Mattiasson, B. 1994. Novel technologies in downstream processing. *Chem Industry.* (17): 673-675.

Han, K., Lim, H.C., Hong, J. 1992. Acetic acid formation in *Escherichia coli* fermentation. *Biotechnol. Bioeng.* **39**: 663-671.

Hansma, H. G., Gould, S. A. C., Hansma, P. K., Gaub, H. E., Longo, M. L., and Zasadzinski, J. A. N. 1991. Imaging nanometer scale defects in langmuir-blodgett films with the atomic force microscope. *Langmuir.*7: 1051-1054.

Hansma, H.G., Sinsheimer, R.L., Groppe, J., Bruce, T.C., Elings, V., Gurley, G., Bezanilla, M., Mastrangelo, I.A., Hough, P.V.C., and Hansma, P.K. 1993. Recent advances in atomic force microscopy of DNA. *Scanning.* **15**: 296-299.

Hansma, P.K., Cleveland, J.P., Radmacher, M., Walters, D.A., Hilner, P.E., Bezanilla, M., Prater, C.B., Massie, J., Fukunaga, L., Gurley, J., and Elings, V. 1994. Tapping mode atomic force microscopy in liquids. *Appl Phys Lett.* **64**(13):1738-1740.

Harrison, S.T.L., Chase, H.A. and Dennis, J.S. 1991. The disruption of *Alcaligenes entrophus* by high pressure homogeniser: Key factors involved in the process. *Bioseparation.* **2**: 155-166.

Hart, R.A., Lester, P.M., Reifsnyder, D.H., Ogez, J.R., and Builder, S.E. 1994. Large scale *in situ* isolation of periplasmic IGF-1 from *E. coli. Bio/Technol.* **12**: 1113-1117.

Hartman, U. 1990. van der Waals interactions in force microscopy. *Adv Mater.* **2**(12): 594-597.

Hartman, U. 1991. van der Waals interactions between sharp probes and flat sample surfaces. *Phys Rev B.* **43**(3): 2404-2407.

Haselgruebler, T., Amerstorfer, A., Schindler, H. and Gruber, H.J. 1995. Synthesis and applications of a new poly(ethylene glycol) derivative for the crosslinking of amines with thiols. *Bioconjugate Chem.* **6**(3): 242-248.

Hasyim, M. A., SenGupta, B., and Subramaniam, M. B. 1995. Investigations on the flotation of yeast cells by colloidal gas aphron (CGA). *Bioseparation.* **5**: 167-173.

Hearly, J.W.S., Sparrow, J.T. and Cross, P.M. 1972. *The use of scanning electron microscope.* Pergamon Press. Oxford.

Heinanen, J., Jokela, P. and Peltokangas, J. 1992. Experimental studies on the kinetics of flotation. In *Chemical Water and Wastewater Treatment II.* (Klute and Hahn, eds.). Springer-Verlag. New York.. pp. 247-262.

Helmuth, K., Korz, D.J., Sanders, E.A. and Deckwer, W-D. 1994. Effect of growth rate on stability and gene expression of recombinant plasmids during continuous and high cell density cultivation of *Escherichia coli* TG1. *J Biotechnol.* **32**: 289-298.

Hewit, D. 1994. *Thin film drainage and bubble/particle attachment in froth flotation.* PhD thesis. the University of South Australia. Adelaide, Australia.

Hewit, D., Fornasiero, D., and Ralston, J. 1994. Bubble particle attachment efficiency. *Mineral Eng.* **7**(5/6): 657-665.

Hoh, J. H., Cleveland, J. P., Prater, C. B., Revel, J. P., and Hansma, P. K. 1992. Quantisized adhesion detected with the atomic force microscope. *J Am Chem Soc.* **114**: 4917-4918.

Hoh, J. H. and Hansma, P. K. 1992. Atomic force microscopy for high resolution imaging in cell biology. *Trends Cell Biol.* **2**: 208-213.

Holms, W.H. 1986. The central metabolic pathways of *Escherichia coli*: relationship between flux and control at a branch point, efficiency of conversion to biomass, and excretion of acetate. *Curr. Top Cell Regul.* **28**: 69-105.

Howland, R. and Benatar, L. 1993. *A practical guide to scanning probe microscopy.* Park Scientific Instruments. California. USA.

Humbel, R E. 1990. Insulin-like growth factors I and II. *Euro J Biochem.* **190**: 445-462.

Hunter, R. J. 1981. Zeta Potential in Colloid Science: *Principles and Applications.* Academic Press. London.

Hunter, R. J. 1989. *Foundation Colloid Science.* Vol. 1. Oxford Science Publication. Oxford.

Hunter, R. J. 1993. *Introduction Modern Colloid Science.* Oxford Science Publication. Oxford.

Hutter, J.L., and Bechhoefer, J. 1993a. Calibration of atomic-force microscope tips. *Rev Sci Instrum.* **64**(7): 1868-1873.

Hutter, J.L., and Bechhoefer, J. 1993b. Manipulation of van der Waals forces to improve image resolution in atomic-force microscopy. *J Appl Phys.* 73(9): 4123-4129.

Hutter, J.L., and Bechhoefer, J. 1994. Measurement and manipulation of van der Waals forces in atomic-force microscopy. *J Vac Sci Technol B.* **12**(3): 2251-2253.

Iibuchi, S., Yano, T., and Torikata, Y. 1974. Adsorption of hemoglobin and casein onto air bubbles. *Agri Biol Chem.* **38**(2): 395-400.

Iibuchi, S., Chiang, W. C., and Yano, T. 1980. Optimum particle size and air flow rate in bubble separation of isoelectric casein coagula. *Agri Biol Chem.* **44**(8): 1811-1816.

Ikai, A. 1996. STM and AFM of bio/organic molecules and structures. *Surf Sci Reports.* **26**: 261-332.

Ingram, L.O., Conway, T., Clark, D.P., Swell, G.W., and Preston, J.F. 1987. Genetic engineering of ethanol production in *Escherichia coli. App Enviro. Microbiol.* **53**: 2420-2425.

Israelachvili, J.N. 1992. *Intermolecular and Surface Forces.* 2nd edition. Academic Press, San Diego.

Jackson, M.L. 1994. Energy effects in bubble nucleation. *Ind Eng Chem Res.* **33**: 929-933.

Jin, K. 1992. Studies of scale-up of production and recovery of recombinant protein formed as inclusion bodies. PhD thesis. the University of London. London, UK.

Jin, H., Uddin, M. S., Huang, Y. L, and Teo, W. K. 1994. Purification and renaturation of recombinant human lymphotoxin (tumour necrosis factor beta) expressed in *Escherichia coli* as inclusion bodies. *J Chem Technol Biotechnol* **59**: 67-72.

Jorgensen, L., Thomas, C.J., O'Neill, B.K. and Middelberg, A.P.J. 1997. Investigation if the relationship between protein, message and inducer concentrations in recombinant *E. coli* cells. *J Micobiol Biotechnol.* **7**: 21-24.

Kane, J F and Hartley, D N. 1991. Properties of recombinant protein-containing inclusion bodies in *Escherichia coli.* In *Purification and Analysis of Recombinant Proteins* (R. Seetharam and S.K. Sharma, eds.). Marcell Dekker, New York. pp. 121-145.

Kay, D.H. (ed.) 1965. Techniques for electron microscopy, 2nd edition. Blackwell Scientific Publications. Oxford.

Kekicheff, P., Marcelja, S., Senden, T.J., and Shubin, V.E. 1993. Charge reversal seen in electrical double layer interaction of surfaces immersed in 2:1 calcium electrolyte. *J Chem Phys.* **99**(8): 6098-6113.

King, R, Wells, J R E, Krieg, P, Snoswell, M, Brazier, J, Bagley, C J, Wallace, J C, Ballard, F J, Ross, M, and Francis, G L. 1992. Production and characterization of recombinant insulin-like growth factor-I (IGF-I) and potent analogues of IGF-I, with Gly or Arg substituted for Glu3, following their expresion in *Escherichia coli* as fusion protein. *J Mole Endocrinol.* **8**:29-41.

Kitchener, J.A. 1984. The froth flotation process: Past, present and future - in brief. In *the Scientific Basis of Flotation.* (Ives, K.J., ed.) NATO ASI Series. Martinus Nijhoff Publisher. Boston. pp. 3-51.

Kitchener, J.A. and Gochin, R.J. 1981. The mechanism of dissolved air flotation for potable water: basis analysis and a proposal. *Wat Res.* **15**: 585-590.

Kleman, G. L. and Strohl, W. R. 1994. Acetate metabolism by *Escherichia coli* in high-cell-density fermentation.. *App. Environ. Microbiol.* **60**: 3952-3958.

Koh, B.T., Nakashimada, U., Pfeiffer, M., and Yap, M.G.S. 1992. Comparison of acetate inhibition on growth of host and recombinant *Escherichia coli* K12 strains. *Biotechnol. Lett.* **14**: 1115-1118.

Korz, D.J., Rinas, U., Helmuth, K., Sanders, E.A. and Deckwer, W-D. 1995. Simple fed-batch technique for high cell density cultivation of *Escherichia coli. J. Biotechnol.* **39**: 59-65.

Laemmli, U.K. 1970. Cleavage of structural proteins during the assembly of the head bacteriophage T4. *Nature.* **227**: 680-685.

Lal, R and John, S. A. 1994. Biological applications if atomic force microscopy. *Am J Phys.* **266**: C1-C21.

Larson, I., Drummond, C.J., Chan, D.Y.C., and Grieser, F. 1993. Direct Force Measurements between TiO_2 Surfaces. *J Am Chem Soc.* **115**: 11885-11890.

Larson, I., Drummond, C.J., Chan, D.Y.C., and Grieser, F.1995. Direct Force Measurements between Dissimilar Metal Oxides. *J Phys Chem.* **99**(7): 2114-2118.

Lee, G.U., Chrisey, L.A., and Colton, R.J. 1994. Direct Measurement of the Forces Between Complementary Strands of DNA. *Science.* **266**: 771-773.

Lee, J. and Ramirez, W.F. 1992. Mathematical modelling of induced foreign protein production by recombinant bacteria. *Biotechnol Bioeng.* **39**: 635-646.

Lee, S.Y. and Chang, H.N. 1994. Effect of complex nitrogen source on the synthesis and accumulation of poly(3-hydroxybutyric acid) by recombinant Escherichia coli in flask and fed-batch cultures. *J. Environ. Polymer Degrad..* **2**: 169-176.

Lee, S.Y. 1996. High cell density culture of *Escherichia coli*. *Trends Biotechnol.* **14**: 98-105.

Leung, O. M. and Goh, C. 1992. Orientational ordering of polymers by atomic force microscope tip-surface interaction. *Science*. **255**: 64-66.

Levich, V.G. 1962. *Physicochemical Hydrodynamics*. Prentice Hall Inc. Englewood Cliffs, New Jersey.

Levin, G.V., Clendenning, J.R., Gibor, A., and Bogar, F.D. 1962. Harvesting of algae by froth flotation. *Appl Microbiol.* **10**: 169.

Li, C. and Somasundaran, P. 1991. Reversal of bubble charge in multivalent inorganic salt solutions - effect of magnesium. *J Colloid Interface Sci.* **146**(1): 215-218.

Li, C. and Somasundaran, P. 1992. Reversal of bubble charge in multivalent inorganic salt solutions - effect of aluminium. *J Colloid Interface Sci.* **148**(2): 587-591.

Li, Y. Q., Tao, N. J., Garcia, A. A., and Lindsay, S. M. 1993. Direct measurement of interaction force between colloidal particles using the scanning force microscope. *Langmuir*. **9**: 637-641.

Luli, G. W. and Strohl, W. R. 1990. Comparison of growth, acetate production, and acetate inhibition of *Escherichia coli* strains in batch and fed-batch fermentation. *App. Environ. Microbiol.* **56**: 1004-1011.

Luthi, R., Meyer, E., Howald, E., Haefke, H., Anselmetthi, D., Dreyer, M., Ruetschi, M., Bonner, T., Overney, R., Frommer, J. and Guntherodt. 1994. Progress in noncontact dynamic force microscopy. *J Vac Sci Technol B* **12**(3): 1673-1676.

Lyklema, J. 1995. *Fundamentals of Interface and Colloid Science*. Academic Press. London. **vol. 2**. pp. 3.1-3.232.

MacDonald, H.L. and Neway, J.O. 1990. Effects of medium quality on the expression of human interleukin-2 at high cell density in fermenter cultures of *Escherichia coli* K12. *Appl. Environ. Microbiol.* **56**: 640-645.

Magonov, S. N. and Whangbo, M-H. 1996. *Surface Analysis with STM and AFM: experimental and theoretical aspects of image analysis*. VCH. Weinheim.

Malley, J.P. and Edzwald, J.K. 1991. Concepts for dissolved air flotation treatment of drinking water. *Aqua*. **40**: 7-17.

Markl, H., Zenneck, C., Dubach, A., and Ogbonna, J.C. 1993. Cultivation of *Escherichia coli* to high cell densities in a dialysis reactor. *Appl. Microbiol. Biotechnol.* **39**: 48-52.

Marston, F. A. O. 1986. The purification of eukaryotic polypentides synthesized in *Escherichia coli. Biochem J.* **240**: 1-12.

Matis, K.A. and Zouboulis, A.I. 1995a. An Overview of the process. In *Flotation Science and Engineering*. Marcell Dekker, Inc. New York.

Matis, K.A. and Zouboulis, A.I. 1995b. The role of bubble/particle size. In *Flotation Science and Engineering*. Marcell Dekker, Inc. New York.

Matis, K.A. and Zouboulis, A.I. 1995c. Electrolytic flotation: an unconventional flotation. In *Flotation Science and Engineering*. Marcell Dekker, Inc. New York.

Matsui, Y., Fukushi, K. and Tambo, N. 1998. Modeling, simulation and operational parameters of dissolved air flotation. *Aqua*. **47**(1): 9-20.

Meagher, M. M., Barlett, R. T., Rai, V. R., and Khan, F. R. 1994. Extraction of rIL-2 inclusion bodies from *Escherichia coli* using cross-flow filtration. *Biotechnol Bioeng*. **43**: 969-977.

Melbourne, J.D. and Zabel, T.F. 1977. *Flotation for water and waste treatment.* Morlow, UK: Water Reserach.

Meyer, H.P., Leist, C., and Fiechter, A. 1984. Acetate formation in continuous culture of *Escherichia coli* K12 D1 on defined and complex media. *J. Biotechnol*. **1**: 355-358.

Middelberg, A.P.J., Bogle, I.D.L. and Snoswell, M.A. 1990. Sizing biological samples by photosedimentation technique. *Biotechnol. Prog*. **6**: 255-261.

Middelberg, A.P.J. 1996. Large-scale Recovery of Recombinant Protein Inclusion Bodies Expressed in *Escherichia coli. J Microbiol Biotechnol.* **6**: 225-231.

Milner, S. 1999 CRC for Tissue Growth and Repair, the University of Adelaide. *personal communication.*

Miranda, E.A. and Berglund, K.A. 1993. Evaluation of column flotation in the downstream processing of fermentation products: recovery of a genetically engineered α-amylase. *Biotechnol Prog*. **9**: 411-420.

Miyazu, Y. and Yano, T. 1974. Surface character and absorbability to air bubbles of a hydrocarbon-grown yeast. *Agri Biol Chem.* **38**(1): 183-188.

Mori, H., Yano, T., Kobayashi, T., and Shimizu, S. 1979. High density cultivation of biomass in fed-batch system with DO-Stat. *J. Chem. Eng. Jap.* **12**: 313-319.

Moy, V. T., Florin, E-L. and Gaub, H. E. 1994a. Adhesive forces between ligand and receptor measured by AFM. *Colloids Surfaces A: Physicochem Eng Aspects*. **93**: 343-348.

Moy, V.T., Florin, E-L., and Gaub, H.E. 1994b. Intermolecular Force and Energies Between Ligands and Receptors. *Science.* **226**: 257-259.

Mukhopadhyay, A. 1997. Inclusion bodies and purification of proteins in biollogically active forms. *Adv Biochem Eng Biotechnol.* **56**:61-109.

Mulvaney, P., Perera, J. M., Biggs, S., Grieser, F., and Stevens, G. W. 1996. The direct measurement of the forces of interaction between a colloid particle and oil droplet. *J Colloid Interface Sci.* **183**: 614-616.

Nicol, S. K., Engel, M. D., and The, K C. 1986. Fine particle flotation in an acoustic field. *Inter J Mineral Processing.* **17**: 143-150.

Noy, A., Frisbie, C.D., Rosznyai, L.F. and Lieber, C.M. 1995. Chemical force microscopy: Exploiting chemically-modified tips to quantify adhesion, friction and functional group distributions in molecular assemblies. *J Am Chem Soc.* **117**: 7943.

Okada, K., Akagi, Y. 1987. Method and apparatus to measure the ζ-potential of bubbles. *J Chem Eng Jap.* **20**(1): 11-15.

Okada, K., Akagi, Y. 1988. Effect of zeta potential of oil droplets and bubbles on flotation of oil-in-water mixtures. *Can J Chem Eng.* **66**: 276-281.

Okada, K., Akagi, Y., Kogure, M., and Yoshioka, N. 1990. Effect of surface charge of bubbles and fine particles on air flotation process. Pal, R. and Masliyah, J. 1989. Flow characteristic of a flotation column. *Can J Chem Eng.* **67**: 916-923.

Olbrich, R. 1989. The characterisation and recovery of protein inclusion bodies from recombinant *Escherichia coli.* PhD thesis. The University of London. London, UK.

O'Melia, C.R. 1980. Aquasols: The behaviour of small particles in aquatic systems. *Environ Sci Technol.* **14**: 1052-1060.

O'Melia, C.R. 1985. Particles, pretreatment and performance in water filtration. *J Environ Eng.* **111**(6): 874-890.

Paalme, T., Tilsma, K., Kahru, A. Vanatalu, K., and Vilu, R. 1990. Glucose-limited fed-batch cultivation of *Escherichia coli* with computer-controlled fixed growth rate. *Biotechnol. Bioeng.* **35**: 312-319.

Pan, J. G., Rhee, J. S., and Lebeault, J. M.. 1987. Physiological constraints in increasing biomass concentration of *Escherichia coli* B in fed-batch culture. *Biotechnol. Lett.* **9**: 89-94.

Paul, D. C., Van-Frank, R. M, Muth, W. L., Ross, J. W., and Williams, D. C. 1983. Immunocytochemical demonstration of human proinsulin chimeric polypeptide within cytoplasmic inclusion bodies of *Escherichia coli. Eur J Cell Biol.* **31**: 171-174.

Paulson, O. and Pugh, R. J. 1996. Flotation of hydrophobic particles in aqueous solutions of inorganic electrolytes. *Langmuir.* **12**: 4808-4813.

Prater, C.B., Maivald, P.G., Kjoller, K.J. and Heaton, M.G. -. Application Notes: *Probing nano-scale forces with the atomic force microscope.* Digital Instruments, Inc. Santa Barbara, CA, USA.

Quirk, A.V. and Woodrow, J.R. 1984. Investigation of the parameters affection separation of bacterial enzymes from cell debris by tangential flow filtration. *Enzyme Microb Technol.* **6**: 201-206.

Raab, A., Han, W., Badt, D., Smith-Gill, S.J., Lindsay, S.M., Schindler, H. and Hinterdorfer, P. 1999. Antibody recognition imaging by force microscopy. *Nature Biotechnol.* **17**: 902-905.

Rabinovich, Y.I., and Yoon, R.-H. 1994. Use of atomic Force Microscope for the Measurements of Hydrophobic Forces between Silanated Silica Plate and Glass Sphere. *J Am Chem Soc.* **10**(6): 1903-1909.

Radmacher, M., Fritz, M., Cleveland, J.P., Walters, D.A. and Hansma, P.K. 1994. Imaging Adhesion Force and Elasticity of Lysozyme Adsorbed on Mica with the Atomic Force Microscope. *Langmuir.* **10**(10): 3809-3814.

Reay, D. and Ratcliffe, G.A. 1973. Removal of fine particles from water by dispersed air flotation: Effects of bubble size and particle size on collection efficiency. *Can J Chem Eng.* **51**: 178-185.

Rees, A.J., Rodman, D.J. and Zabel, T.F. 1979. *Water clarification by flotation-5.* Technical Report TR 114. Water Research Centre. Medmenham, UK.

Riesenberg, D. 1991a. High cell density cultivation of *Escherichia coli. Curr Opin Biotechnol.* **2**: 380-384.

Riesenberg, D. et al. 1991b. High cell density cultivation of *Escherichia coli* at controlled specific growth rate. *J Biotechnol.* **20**: 17-28.

Rubin, A. J. 1968. Microflotation: coagulation and foam separation of *Aerobacter aerogenes. Biotechnol Bioeng.* **10**: 89-98.

Ryan, W. L. and Hemmingsen, E. A. 1993. Bubble formation in water at smooth hydrophobic surfaces. *J Colloid and Interface Sci.* **157**: 312-317.

Sader, J.E., Larson, I., Mulvaney, P., and White, L.R. 1995. Method for the calibration of atomic force microscope cantilevers. *Rev Sci Instrum.* **66**(7): 3789-3798.

Sader, J.E., Chon, J.W.M. and Mulvaney, P. 1999. Calibration of rectangular atomic force microscope cantilevers. *Rev Sci Intrum.* 70(10):3967-3969.

Sarid, D. 1994. *Scanning Force Microscopy, with applications to electric, magnetic and atomic forces.* Revised Edition. Oxford University Press. New York. pp. 181-232.

Schwarz, U.D., Haefke, H., Reimann, P. and Guntherodt, H.-J. Tip artefacts in scanning force microscopy. *J Microscopy.* **173**: 182-197.

Sceludko, A. D., Toshev, B. V., and Bojadiev, D. T. 1976. Attachment of particles to a liquid surface (capilary theory of flotation). *J Chem Soc Faraday Trans I.* **72**: 2815.

Schulze, H J. 1983. *Physico-chemical elementary processes in flotation.* Elsevier. Amsterdam.

Schulze, H J. 1989. Hydrodynamics of bubble-mineral particle collisions. *Mineral Processing and Extractive Metallurgy Rev.* **5**: 43-76.

Senden, T. J. and Ducker, W. A. 1994. Experimental determination of spring constants in atomic force microscopy. *Langmuir.* **10**: 1003-1004.

Senden, T.J. and Drummond, C.J. 1995. Surface chemistry and tip-sample interactions in atomic force microscopy. *Colloids Surfaces A: Physicochem Eng Aspects.* **94**: 29-51.

Sheppard, C.J.R. 1993. Confocal microscopy - principles, practice and options. In *Fluorescent and Luminescent Probes for Biological Activity* (Mason, W.T., ed.). Academic Press. San Diego. pp. 229-236.

Shimizu, M., Iijima, S., and Kobayashi, T. 1992. Production of insecticidal protein of Bacillus thuringiensis by cultivation of recombinant *Escherichia coli. J. Fermen. Bioeng.* **74**: 163-168.

Smith, S.T., and Howard, L.P. 1994. A precision, Low-force balance and its application to atomic force microscope probe calibration. *Rev Sci Instrum.* **65**(4): 903-909.

Suffman, P.G. and Turner, J.S. 1956. On the collision of drops in turbulent clouds. *J. Fluid Mech.* **1**: 16-30.

Synder, B.A., Aston, D.E. and Berg, J.C. 1997. Particle-drop interactions examined with an atomic force microscope. *Langmuir.* **13**: 590-593.

Strandberg, L and Enfors, S-O. 1991. Batch and fed batch cultivations for the temperature induced production of a recombinant protein in *Escherichia coli. Biotechnol Lett.* **13**: 609-614.

Takahashi, T., Miyahara, T. and Michizuki, H. 1979. Fundamental study of bubble formation in dissolved air pressure flotation. *J Chem Eng Jap.* **12**: 275-280.

Tao, N. J., Lindsay, S. M., and Lees, S. 1992. Measuring the microelastic properties of biological material. *Biophys J.* **63**: 1165-1169.

Tambo, N and Watanabe, Y. 1979. Physical characteristics of flocs: I. The floc density function and aluminium floc. *Wat Res.* **13**: 409-419.

Tambo, N., Hozumi, H. and Watanabe, Y. 1981. A rational design of flocculator. *J Jap Wat Works* Assoc. **50**(6): 20-27.

Tambo, N., Matsui, Y. and Fukushi, K. 1986. A kinetic study of dissolved air flotation. *Proc. 3rd World Congress Chem. Eng.* Tokyo. **Vol. 3**: 200-203.

Taylor, G., Hoare, M., Gray, D. R., and Marston, F. A. O. 1986. Size and density of protein inclusion bodies. *Bio/Techonol.* **4**: 553-557.

Tien, C. 1989. *Granular filtration of aerosols and hydrosols*. Butterworths. Boston.

Thundat, T., et al. 1993a. Role of relative humidity in atomic force microscopy imaging. *Surf Sci.* **294**: L939-L943.

Thundat, T., Zheng, X-Y., Chen, G.Y., Sharp, S.L., Warmack, R.J., and Schowalter, L.J. 1993b. Characterization of atomic force microscope tips by adhension force measurements. *Appl Phys Lett.* **63**(15): 2150-2152.

Toikka, G., Hayes, R.A., and Ralston, J. 1996. Adhesion of iron oxide to silica studies by atomic force microscopy. *J Colloid Interface Sci.* **180**: 329-338.

Toikka, G. and Hayes, R.A. 1997. Direct measurement of colloidal forces between mica and silica in aqueous electrolyte. *J Colloid Interface Sci.* **191**: 102-109.

Torii, A., Sasaki, M., Hane, K., and Okuma, S. 1994. Adhension of microstructures investigated by atomic force microscopy. *Sensors and Actuators A.* **40**: 71-76.

Torii, A., Sasaki, M., Hane, K., and Okuma, S. 1996. A method for determining the spring constant of cantilevers for atomic force microscopy. *Meas Sci Technol.* **7**: 179-184.

Topometrix. 1994-1996. *Acurex™ /Explorer™ Technical Briefs*. Santa Clara.

Tsao, Y. -H., Yang, S. X., and Evans, D. F. 1992. A reevaluation of temperature-dependant bilayer interaction forces as determined by surface forces and atomic force microscopy measurements. *Langmuir.* **8**: 1188-1194.

Tsukruk, V.V. and Bliznyuk, V.N. 1998. Adhesive and friction forces between chemically modified silicon and silicon nitride surfaces. *Langmuir.* **14**: 446-455.

Upton, F Z, Francis, G L, Ross, M, Wallace, J C, and Ballard, F J. 1992. Production and characterization of recombinant chicken insulin-like growth factor-I from *Escherichia coli. J Mole Endocrinol.* **9**:83-92.

Valax, P. and Georgiou, G. 1993. Molecular characteristics of β-lactamase inclusion bodies in E coli. 1 Composition., *Biotechnol Prog.* **9**: 539-547.

Van den Werf, K.O., Putman, C.A.J., de Grooth, B.G. and Greve, J. 1994. Adhesion force imaging in air and liquid by adhesion mode atomic force microscopy. *Appl Phys Lett* **65**(9): 1195-1197.

Van der Brande, J L. 1992. Structure of the human insuline-like growth factors: relationship to function. *In The Insuline-like Growth Factors: Structure and Biological Functions* (P.N. Schofield, ed.). Oxford Medical Publications. New York.

Van der Vegte, E.W. and Hadziioannou, G. 1997. Scanning force microscopy with chemical specificity: An extensive study of chemically specific tip-surface interactions and the chemical imaging of surfaces functional groups. *Langmuir.* **13**: 4357-4368.

Van der Wal, A., Minor, M., Norde, W., Zehnder, A.J.B., Lyklema, J. 1997. Electrokinetic Potential of Bacterial Cells. *Langmuir* **13**: 165-171.

Van Oss, C. J., Good, R. J., and Chaudhury, M. K. 1986. The role of van der Waals forces and hydrogen bonds in hydrophobic interactions between biopolymers and low energy surfaces. *J Colloid Interface Sci.* **111**(2): 378-390.

Vasudevan, V. and wiencek, J. M. 1997. Role of the interface in protein extractions using nonionic microemulsions. *J Colloid Interface Sci.* **186**: 185-192.

Veeramasuneni, S., Yalamanchili, M. R., and Miller, J. D. 1996. Measurement of interaction forces between silica and α-alumina by atomic force microscopy. *J Colloid Interface Sci.* **184**: 594-600.

Walker, S.G. and Lyddiatt, A. 1996. An investigation of the role for aqueous two phase sytems in the processing of α-glucosidase PI inclusion bodies expressed in recombinant *E. coli.* In Proceeding of 1996 IChemE Research Event (Leeds, UK). Institution of Chemical Engineers. Rugby, UK. 55-57.

Watt, I.A. 1985. *The principles and practice of electron microscopy.* University Press Cambridge. New York.

Wei, G. and Tang, J.G. 1995. Formation of inclusion bodies may be the key factor for the stability of expressed product in *E. coli. Biochem Mole Biol Inter.* **37**(5): 895-901.

Weisenhorn, A.L., Hansma, P.K., Albrecht, T.R., and Quate, C.F. 1989. Forces in atomic force microscopy in air and water. *Appl Phys Lett.* **54**(26): 2651-2653.

Weisenhorn, A.L., Maivald, P., Butt, H.J., and Hansma, P.K. 1992. Measuring adhension, attraction, and repulsion between surfaces in liquids with an atomic-force microscope. *Phys Rev B.* **45**(19): 11226-11232.

Weisenhorn, A.L, et al. 1993. Deformation and height anomaly of soft surfaces studied with an AFM. *Nanotechnology.*. **4**(2): 106-113.

Weissenborn, P. K. and Pugh, R. J. 1995. Surface tension and bubble coalescence phenomena of aqueous solutions of electrolytes. *Langmuir*. **11**: 1422-1426.

Wetzel R and Goeddel, D V. 1983. *Peptides*. **5**: 1-64.

Weyl, W A. 1951. Surface structure of water and some of its physical and chemical manifestations. *J Colloid Sci*. **6**: 389-405.

Wickramasinghe, K.H. 1991. *Scanned probe microscopy*. American Institute of Physics. Santa Barbara, CA.

Wiese, G.R. and Healy, T.W. 1975. Coagulation and electrokinetic behaviour of TiO_2 and Al_2O_3 colloidal dispersions. *J Colloid Interface Sci*. **51**: 427-433

Williams, D.C., van Frank, R.M., Muth, W.L., and Burnet, J.P. 1982. Cytoplasmic inclusion bodies in *Escherichia coli* producing biosynthetic human insulin proteins. *Science*. **215**: 687-688.

Wong, T.M.H. and Descouts, P. 1995. Atomic force microscopy under liquid: A comparative study of three different AC mode operations. *J Microsc*. **178**: 7-13.

Wong, H H, O'Neill, B K, Middelberg, A P J. 1997. Cumulative sedimentation analysis of *Escherichia coli* debris size. *Biotechnol Bioeng*. **55**(3): 556-564.

Yamane, T. and Shimizu, S. 1984. Fed-batch techniques in microbial processes. In *Advances in Biochemical Engineering/Biotechnology*. (A. Fiechter, ed.). **vol 30**: 147-194. New York. Spinger-Verlag.

Yao, K.M., Habibian, H.T. and O'Melia. 1971. Water and wastewater filtration: Concepts and applications. *Eviron Sci Technol*. **5**:1105-1112.

Yang, X-M., Xu, L., and Eppstein, L. 1992. Production of recombinant human interferon-alpha-1 by Escherichia coli using a computer-controlled cultivation process. *J Biotechnol*. **23**: 291-230.

Yarar, B and Alvarez, J. 1985. Separation of sulfide minerals by the gamma flotation method. *In Proceedings XVIth International Mineral Processing Congress* (K.S.E. Forssberg, ed.). Elsevier. Amsterdam.

Yee, L. and Blanch, H.W. 1992. Recombinant protein expression in high cell density fed-batch cultures of *Escherichia coli*. *Bio/Technol*. **10**: 1550-1556.

Yoon, R.-H., Flinn, D. H., and Rabinovich, Y. I. 1997. Hydrophobic interactions between dissimilar surfaces. *J Colloid Interface Sci*. **185**: 363-370.

Yoon, R. H. and Luttrell, G. H. 1989. The effect of bubble size on fine particle flotation. *Mineral Processing and Extractive Metallurgical Rev.* **5**:101.

Yoon, R H and Yordan, J L. 1986. Zeta potential measurement on microbubbles generated using various surfactants. *J Colloid Interface Sci.* **113**(2): 430-438.

Zabel, T. 1984. Flotation in water treatment. In *The Scientific Basis of Flotation.* (K.J. Ives, ed.). NATO ASI Series. Martinus Nijhoff Publisher. Boston. pp. 349-377.

Zabel, Th.F. 1992. Flotation in water treatment. In *Innovations in Flotation Technology* (P. Mavros and K.A. Matis, eds.). Kluwer Academic Publisher. Dordrecht. pp. 431-454.

Zhong, Q., Inniss, D., Kjoller, K. and Elings, V.B. 1993. Fractured polymer silica fiber surface stidied by tapping mode atomic force microscopy. *Surf Sci.* **290**: L688.

Zhou, Z. A., Xu, Z., and Finch, J. A. 1994. On the role of cavitation in particle collection during flotation - a critical review. *Mineral Eng.* **7**(9): 1073-1084.

Zhou, Z. A., Xu, Z., and Finch, J. A. 1995. Effect of gas nuclei on hydrophobic coagulation. *J Colloid Interface Sci.* **179**: 311-314.

APPENDIX A

AFM FORCE CURVES AND DATA

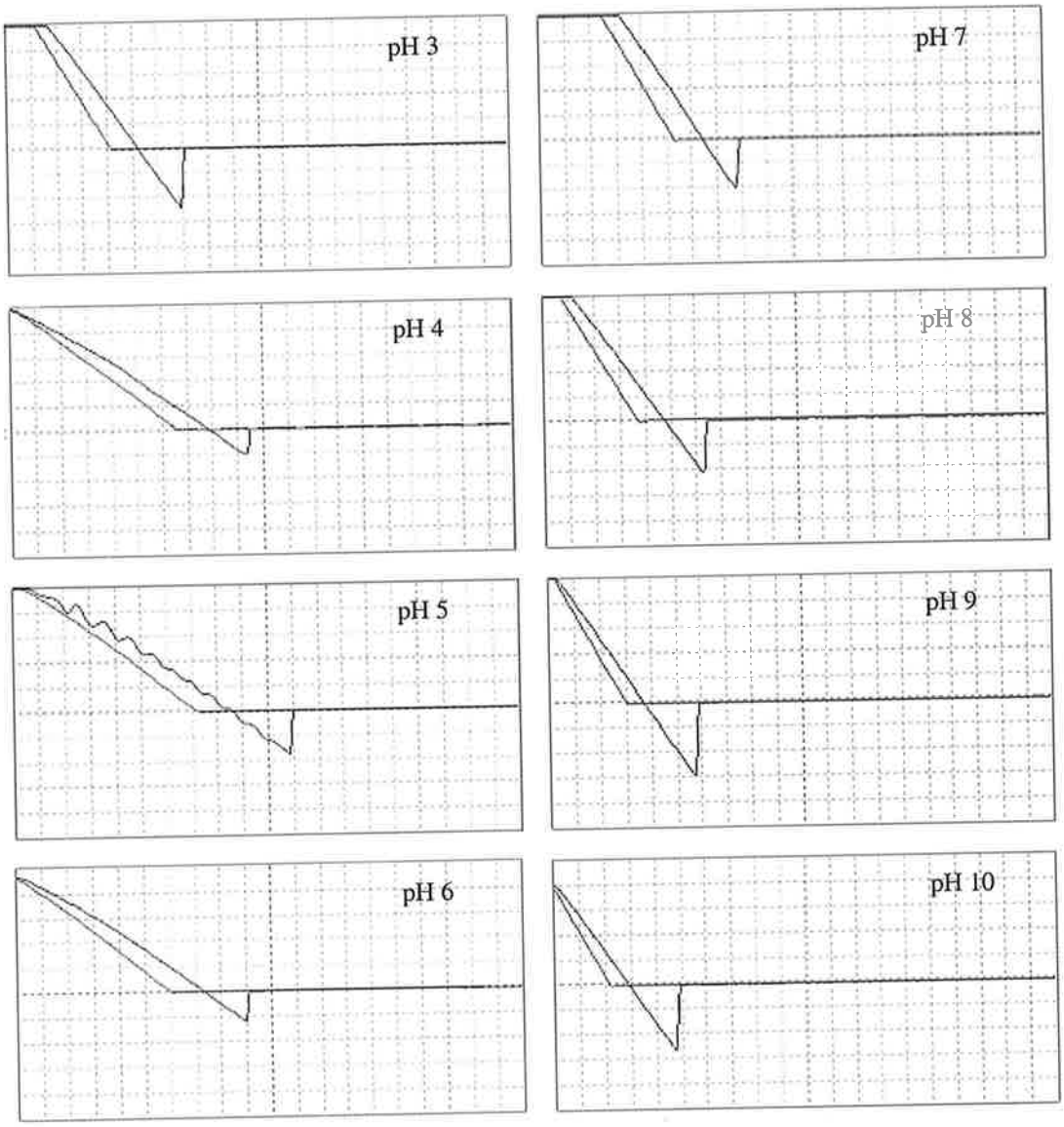

Figure A.1 AFM force curve of interactions between inclusion body and an air bubble as plots of z position versus tip deflection. The measurements were conducted in 0.05 M buffer solution at various pH values. The unit of z position (x axis) is 0.15 μm/division. The unit of tip deflection (y axis) is 0.1 μm/division for pH 3 and 7 to 10, and 0.2 μm/division for pH 4 to 6. For all pH, the z range and scan rate are 1 μm (except pH = 4 - 6, 2 μm) and 0.5 Hz respectively.

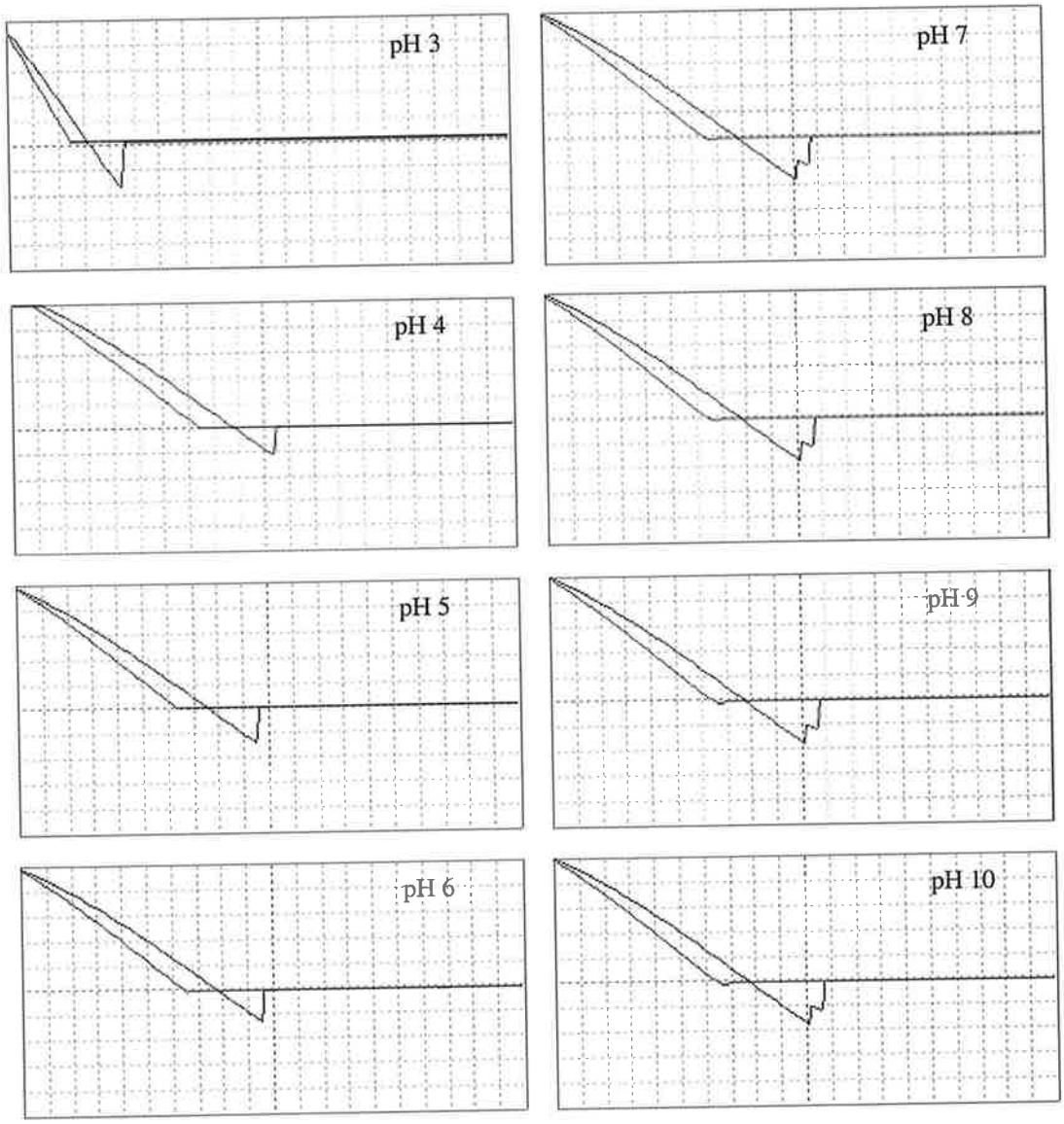

Figure A.2 AFM force curve of interactions between inclusion body and an air bubble as plots of z position versus tip deflection. The measurements were conducted in 0.2 M buffer solution at various pH values. The unit of z position (x axis) is 0.15 μm/division. The unit of tip deflection (y axis) is 0.1 μm/division for pH 3 and 0.2 μm/division for pH 4 to 10. For all pH, the z range, scan size and scan rate are 2 μm (except pH = 3, 1 μm) and 0.5 Hz respectively.

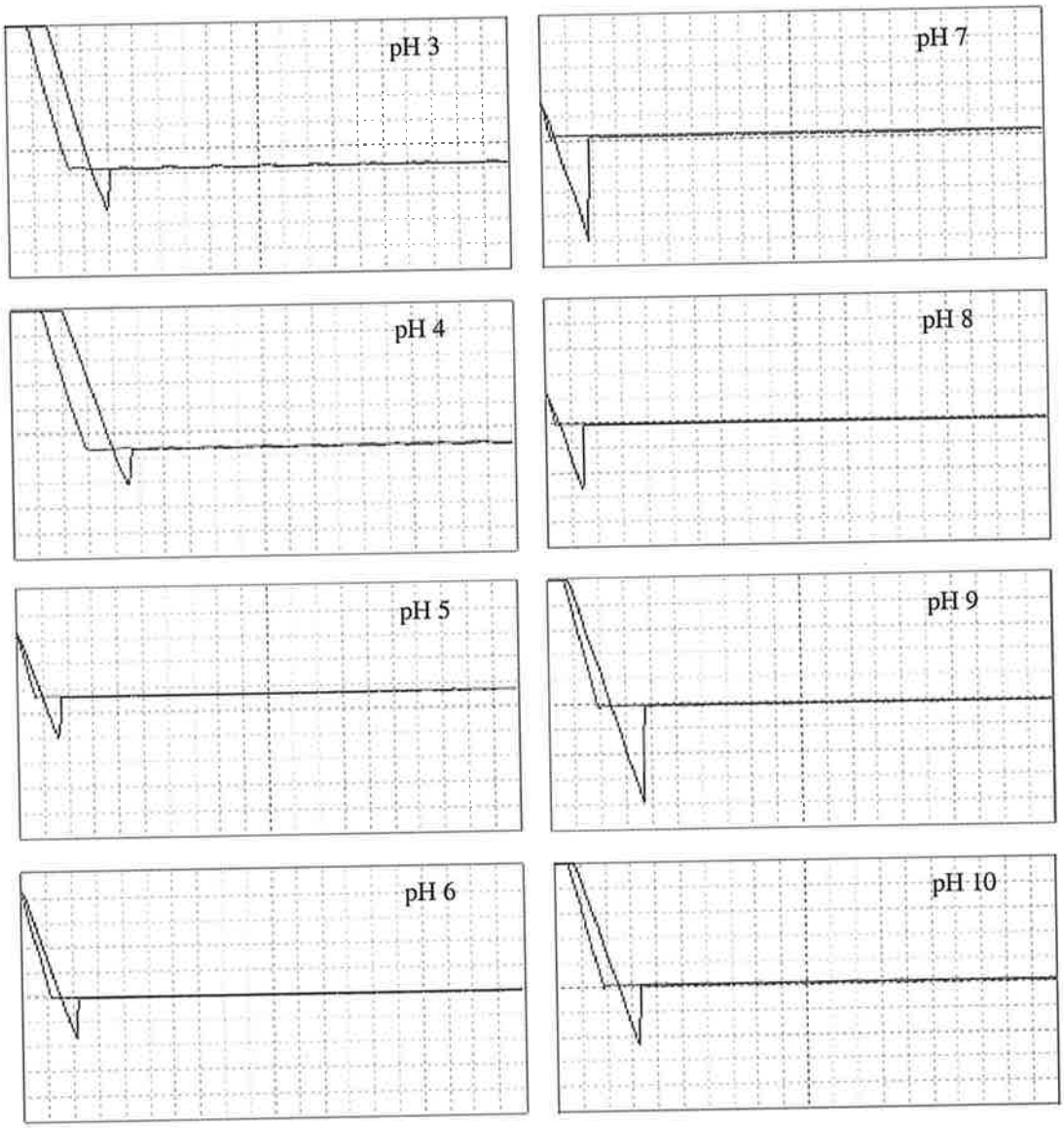

Figure A.3 AFM force curve of interactions between bare tip and an air bubble as plots of z position versus tip deflection. The measurements were conducted in 0.2 M buffer solution at various pH values. The unit of z position (x axis) is 0.15 μm/division. The unit of tip deflection (y axis) is 50 nm/division (except for pH 10, 51.45 nm/division). For all pH values, the z range, scan size and scan rate are 500 nm (except for pH = 10, 514 nm) and 0.54 Hz respectively.

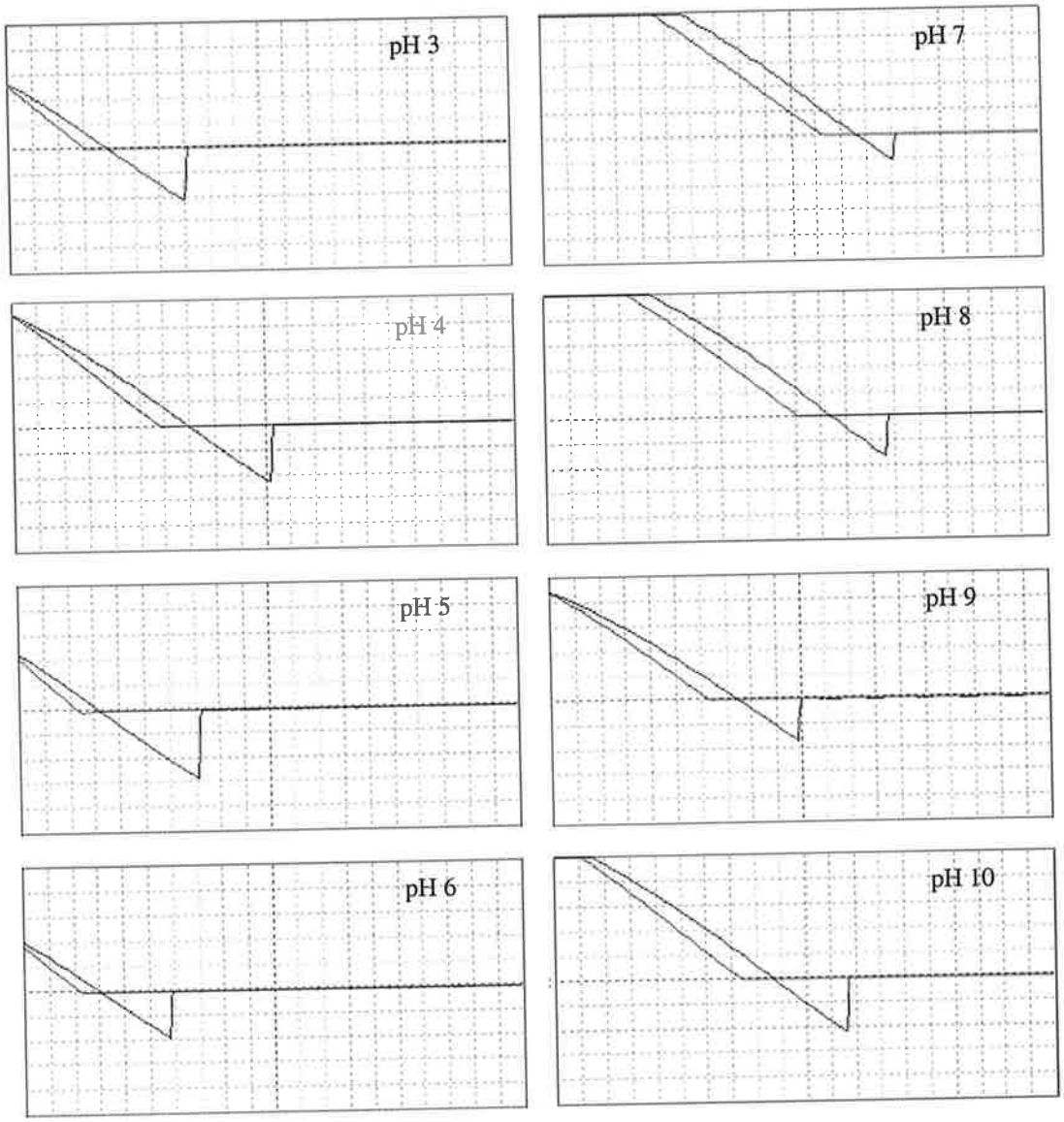

Figure A.4 AFM force curve of interactions between SPDP-modified tip and an air bubble as plots of z position versus tip deflection. The measurements were conducted in 0.2 M buffer solution at various pH values. The units of z position (x axis) and tip deflection (y axis) are 0.15 and 0.2 μm/division respectively. For all pH values, the z range, scan size and scan rate are 2 μm and 0.5 Hz respectively.

Table A.1 AFM data of interactions forces between inclusion body and an air bubble measured in various buffer concentration and pH. Each interactions force data presented in the table is a mean value of approximately 100 (Exp. 1, 2 and 3) and 300 (Overall) AFM force measurements.

Buffer Concentration: 0.05 M

	Exp. 1		Exp.2		Exp.3		Overall	
pH	F_{ad} (nN)	Std. dev.	F_{ad} (nN)	Std. dev.	F_{ad} (nN)	Std. dev.	F_{ad} (nN)	Std. dev.
3	10.71	1.17	10.78	1.13	10.51	0.95	10.67	1.15
4	10.10	0.66	10.06	0.59	10.26	0.60	10.14	0.63
5	13.88	0.78	13.91	0.82	13.66	0.52	13.82	0.80
6	10.67	0.51	10.66	0.51	10.64	0.41	10.66	0.51
7	9.58	0.41	9.69	0.45	9.73	0.40	9.67	0.43
8	9.68	0.51	9.49	0.49	9.86	0.59	9.68	0.61
9	10.20	0.83	10.32	1.05	9.98	0.95	10.16	1.03
10	9.82	0.68	9.60	0.59	9.62	0.71	9.68	0.78

Buffer Concentration: 0.10 M

	Exp. 1		Exp.2		Exp.3		Overall	
pH	F_{ad} (nN)	Std. dev.	F_{ad} (nN)	Std. dev.	F_{ad} (nN)	Std. dev.	F_{ad} (nN)	Std. dev.
3	15.68	0.86	15.53	0.78	15.58	0.65	15.60	0.82
4	20.06	1.36	17.86	0.82	18.24	0.83	18.70	1.30
5	25.16	0.66	25.90	0.48	24.89	0.49	25.33	0.65
6	19.49	0.52	19.56	0.36	20.20	0.90	19.75	0.69
7	14.75	0.86	14.77	0.89	15.09	0.72	14.80	0.85
8	17.01	0.87	16.83	0.61	16.70	0.46	17.11	0.71
9	16.63	1.16	17.53	0.78	18.47	0.96	17.69	1.13
10	10.83	0.68	12.20	0.66	11.10	0.67	11.36	0.84

Buffer Concentration: 0.20 M

	Exp. 1		Exp.2		Exp.3		Overall	
pH	F_{ad} (nN)	Std. dev.	F_{ad} (nN)	Std. dev.	F_{ad} (nN)	Std. dev.	F_{ad} (nN)	Std. dev.
3	12.03	0.85	11.69	0.69	11.54	0.76	11.76	0.95
4	12.54	0.86	13.45	0.98	12.32	1.06	12.77	1.12
5	15.37	0.65	16.09	0.55	16.29	0.61	15.92	0.79
6	12.26	0.55	12.53	0.65	12.78	0.71	12.52	0.90
7	10.36	0.96	10.67	0.92	11.15	1.01	10.72	0.99
8	11.87	0.93	12.22	1.24	12.30	0.98	12.02	0.98
9	11.15	0.72	11.65	0.84	11.60	0.81	11.47	0.81
10	10.83	0.71	9.16	0.54	9.62	0.71	9.90	0.89

Table A.2 Interactions forces between bare tip and an air bubble measured by AFM in various buffer concentration and pH. Each interactions force data presented in the table is a mean value of approximately 100 (Exp. 1, 2 and 3) and 300 (Overall) AFM force measurements.

Buffer Concentration: 0.05 M

	Exp. 1		Exp.2		Exp.3		Overall	
pH	F_{ad} (nN)	Std. dev.	F_{ad} (nN)	Std. dev.	F_{ad} (nN)	Std. dev.	F_{ad} (nN)	Std. dev.
3	6.42	0.57	7.25	0.90	6.90	0.72	6.86	0.81
4	6.83	0.71	7.01	0.59	7.37	0.83	7.07	0.74
5	6.01	0.57	6.28	0.57	6.34	0.75	6.21	0.65
6	5.21	0.45	5.49	0.55	5.19	0.83	5.29	0.64
7	4.69	1.74	4.41	0.71	4.30	0.83	4.47	1.20
8	4.07	1.09	5.03	1.42	3.74	1.06	4.28	1.41
9	4.12	1.00	3.88	1.07	4.15	1.08	4.05	1.08
10	1.72	0.60	1.50	0.61	1.64	0.73	1.62	0.65

Buffer Concentration: 0.10 M

	Exp. 1		Exp.2		Exp.3		Overall	
pH	F_{ad} (nN)	Std. dev.	F_{ad} (nN)	Std. dev.	F_{ad} (nN)	Std. dev.	F_{ad} (nN)	Std. dev.
3	9.22	0.98	8.48	0.81	8.38	0.68	8.69	0.91
4	9.42	0.53	8.68	0.57	8.16	0.55	8.75	0.75
5	10.39	0.63	9.85	0.63	9.87	0.69	10.03	0.69
6	8.95	0.39	9.21	0.54	8.82	0.50	8.99	0.50
7	8.78	1.59	9.21	1.58	8.43	0.95	8.81	1.91
8	5.97	0.81	5.50	1.00	6.03	0.71	5.83	0.89
9	9.34	0.78	9.50	1.11	11.39	1.61	10.06	1.52
10	10.24	0.75	10.37	1.04	10.42	0.98	10.34	0.98

Buffer Concentration: 0.20 M

	Exp. 1		Exp.2		Exp.3		Overall	
pH	F_{ad} (nN)	Std. dev.	F_{ad} (nN)	Std. dev.	F_{ad} (nN)	Std. dev.	F_{ad} (nN)	Std. dev.
3	3.53	0.66	3.65	0.45	3.42	0.44	3.53	0.46
4	4.70	0.54	4.65	0.47	4.70	0.54	4.67	0.50
5	6.04	0.47	6.32	0.68	6.04	0.47	6.18	0.60
6	5.79	0.51	5.94	0.51	5.79	0.51	6.01	0.62
7	9.73	3.34	12.11	0.94	9.73	3.34	11.39	2.37
8	9.17	0.72	9.06	0.94	9.17	0.72	9.66	0.96
9	10.39	1.11	10.16	0.83	10.39	1.11	10.29	1.09
10	8.47	0.78	7.64	0.83	8.47	0.78	8.05	0.90

Table A.3 AFM data of interactions forces between silanised tip and an air bubble measured in various buffer concentration and pH. Each interactions force data presented in the table is a mean value of approximately 100 (Exp. 1, 2 and 3) and 300 (Overall) AFM force measurements.

Buffer Concentration: 0.05 M

	Exp. 1		Exp.2		Exp.3		Overall	
pH	F_{ad} (nN)	Std. dev.	F_{ad} (nN)	Std. dev.	F_{ad} (nN)	Std. dev.	F_{ad} (nN)	Std. dev.
3	27.83	3.28	29.25	2.61	27.65	2.29	27.95	3.10
4	34.30	5.29	34.09	4.13	37.37	5.01	34.69	5.16
5	30.53	3.39	28.99	4.66	32.63	3.54	30.64	3.72
6	32.88	3.18	28.65	3.03	37.40	2.78	32.93	3.90
7	75.40	1.59	80.33	1.88	74.51	1.65	75.58	2.68
8	64.32	1.95	65.53	2.16	63.50	1.69	64.39	2.01
9	56.11	1.89	55.94	4.71	57.49	2.41	56.29	2.58
10	46.88	3.70	44.17	1.71	47.01	2.08	46.50	3.40

Buffer Concentration: 0.10 M

	Exp. 1		Exp.2		Exp.3		Overall	
pH	F_{ad} (nN)	Std. dev.	F_{ad} (nN)	Std. dev.	F_{ad} (nN)	Std. dev.	F_{ad} (nN)	Std. dev.
3	72.33	0.50	75.74	0.52	73.10	0.50	73.72	0.61
4	68.62	0.51	67.78	0.67	68.02	0.73	68.14	0.81
5	70.12	0.34	67.14	0.48	67.46	0.24	68.24	1.73
6	68.69	0.23	65.83	0.88	65.92	0.41	66.81	2.31
7	67.88	0.81	68.78	1.05	70.10	0.89	68.92	1.61
8	84.03	0.24	82.20	0.34	80.67	0.35	82.24	0.89
9	81.78	0.35	81.48	0.51	81.64	0.38	81.53	0.48
10	77.55	0.70	76.55	0.82	68.66	0.49	75.69	2.80

Buffer Concentration: 0.20 M

	Exp. 1		Exp.2		Exp.3		Overall	
pH	F_{ad} (nN)	Std. dev.	F_{ad} (nN)	Std. dev.	F_{ad} (nN)	Std. dev.	F_{ad} (nN)	Std. dev.
3	30.51	0.77	27.78	2.30	27.37	2.02	27.64	2.17
4	31.04	1.99	31.29	2.62	30.10	1.62	30.81	2.32
5	42.11	1.93	42.24	2.61	41.69	0.80	42.01	2.32
6	32.85	2.18	32.93	2.79	32.62	1.14	32.80	2.46
7	33.64	1.86	41.80	1.51	40.01	1.69	37.99	2.55
8	35.82	2.29	38.28	3.02	35.58	1.31	37.31	2.64
9	22.18	1.93	35.32	2.29	35.03	2.47	32.78	2.29
10	33.69	2.32	32.09	1.79	29.99	1.94	31.96	2.25

Table A.4 AFM data of interactions forces between SPDP-modified tip and an air bubble measured in various buffer concentration and pH. Each interactions force data presented in the table is a mean value of approximately 100 (Exp. 1, 2 and 3) and 300 (Overall) AFM force measurements.

Buffer Concentration: 0.05 M

	Exp. 1		Exp.2		Exp.3		Overall	
pH	F_{ad} (nN)	Std. dev.	F_{ad} (nN)	Std. dev.	F_{ad} (nN)	Std. dev.	F_{ad} (nN)	Std. dev.
3	13.82	0.88	13.31	0.91	15.36	1.24	14.16	2.11
4	22.63	0.81	23.40	0.90	25.10	0.98	23.71	1.39
5	28.05	1.34	26.67	0.84	28.25	0.67	27.66	1.14
6	20.37	0.82	20.44	0.50	19.63	0.27	20.36	0.68
7	17.09	2.07	18.29	1.27	16.70	0.68	17.59	2.14
8	26.91	1.97	25.95	1.63	28.89	2.01	27.26	2.24
9	21.06	1.11	19.17	0.50	21.99	1.24	21.35	1.36
10	17.31	0.99	18.23	0.91	18.26	1.17	17.93	1.11

Buffer Concentration: 0.10 M

	Exp. 1		Exp.2		Exp.3		Overall	
pH	F_{ad} (nN)	Std. dev.	F_{ad} (nN)	Std. dev.	F_{ad} (nN)	Std. dev.	F_{ad} (nN)	Std. dev.
3	30.10	1.04	27.43	1.35	28.66	1.54	28.73	1.88
4	32.57	1.23	27.04	0.99	28.00	0.95	29.06	2.70
5	28.91	1.19	29.56	0.68	29.26	0.95	29.24	1.08
6	28.18	0.84	28.62	0.79	28.66	0.56	28.49	0.77
7	33.30	1.24	34.41	1.16	32.65	0.89	33.34	1.30
8	28.39	1.28	26.36	0.71	25.04	0.50	26.51	1.66
9	30.59	0.63	33.09	0.86	31.87	1.28	31.78	1.46
10	25.89	0.72	26.48	0.57	27.67	0.77	26.73	1.00

Buffer Concentration: 0.20 M

	Exp. 1		Exp.2		Exp.3		Overall	
pH	F_{ad} (nN)	Std. dev.	F_{ad} (nN)	Std. dev.	F_{ad} (nN)	Std. dev.	F_{ad} (nN)	Std. dev.
3	21.79	1.58	21.10	1.44	21.44	0.97	21.44	1.54
4	23.15	1.35	23.44	0.56	23.83	1.09	23.47	1.18
5	28.25	1.28	27.18	1.08	27.76	1.00	27.73	1.30
6	19.70	1.50	19.26	0.79	20.26	0.99	19.74	1.29
7	17.71	1.08	18.68	0.96	19.25	0.92	18.55	0.98
8	17.93	1.29	17.44	0.85	18.39	0.77	17.92	1.10
9	16.64	2.16	17.42	1.49	17.69	1.79	17.25	1.97
10	20.71	2.25	20.50	2.52	20.27	1.90	20.49	2.38

APPENDIX B

LIST OF PUBLICATIONS

Refereed Journal Articles

Wangsa-Wirawan, N.D., Lee, Y.S., Falconer, R.J., Mansell, C.J., O'Neill, B.K. and Middelberg, A.P.J. 1997. Novel Fed-batch Strategy for the Production of Insulin-like Growth Factor 1 (IGF1). *Biotechnology Letters*. **19**(11): 1079-1082.

Wangsa-Wirawan, N.D., Middelberg, A.P.J. and O'Neill, B.K. 1999. Physicochemical Characteristics of LR3-IGF-1 Protein Inclusion Bodies: Electrophoretic Mobility Studies. *Biotechnology Progres*. ***submitted***.

Wangsa-Wirawan, N.D., Ikai, A., Middelberg, A.P.J. and O'Neill, B.K. 1999 Measuring the Interaction Forces Between Protein Inclusion Bodies and an Air Bubble using Atomic Force Microscope. *Biochemical Engineering Journal*. ***submitted***.

Conference Papers

Wangsa-Wirawan, N.D., Lee, Y.S., Falconer, R.J., Jorgensen, L., Mansell, C.J., O'Neill, B.K. and Middelberg, A.P.J. Fermentation Studies for the Production of an Insulin-like Growth Factor Analog (Long-R^3-IGF-I). Presented at *the Asia-Pacific Biochemical Engineering Conference*, Beijing, China. 1997.

Wangsa-Wiwaran, N.D., O'Neill, B.K. and Middelberg, A.P.J. The characteristics of protein inclusion bodies: physicochemical properties of an insulin like growth factor analog Long R^3-IGF-1. Accepted for presentation at *CHEMECA - the 27th Australian Chemical Engineering Conference*. Perth. 2000.